International Conference

Condensed Matter Research at the IBR-2 Reactor

devoted to the 90th anniversary of Yuri M. Ostanevich

CMR@IBR2-2026

JUNE 15-19
JINR, Dubna

JINR 70

FLNP

Joint Institute for Nuclear Research

CONDENSED MATTER RESEARCH AT THE IBR-2 REACTOR

International Conference

Dubna, June 15–19, 2026

Book of Abstracts

Electronic edition

Dubna • 2026

Condensed Matter Research at the IBR-2 Reactor: Book of Abstracts of the
C74 International Conference, Dubna, June 15–19, 2026. — [Electronic edition]. —
Dubna: JINR, 2026. — 179 p.
ISBN 978-5-9530-0672-9

ISBN 978-5-9530-0672-9

Organized By

Frank Laboratory of Neutron Physics, Joint Institute for Nuclear Research (Russia)

Organizing Committee

Dr. Alexander Kuklin - Chairman
Dr. Norbert Kučerka - Vice-chairman
Dr. Bagdaulet Mukhametuly - Vice-chairman
Dr. Tatiana Murugova - Scientific secretary
Dr. Ahmed Elmekawy
Dr. Alexander Ivankov
Dr. Alexander Nezvanov
Ms. Evgeniya Melezhik
Ms. Anna Kapitonova
Mr. Sergey Kozenkov
Dr. Denis Kozlenko
Ms. Yulia Polyakova
Ms. Veronika Smirnova
Ms. Zhanna Sorokina
Dr. Inga Zinicovscaia

International Program Committee

Prof. Pavel Alexeev (National Research Centre "Kurchatov Institute", Russia)
Dr. Eugen Anitas (Joint Institute for Nuclear Research)
Prof. Mira Aničić Urošević (The Institute of Physics Belgrade, Serbia)
Prof. Lambe Barandovski (Ss. Cyril and Methodius University in Skopje, North Macedonia)
Prof. Alexander Belushkin (Joint Institute for Nuclear Research, National Research Centre "Kurchatov Institute")
Assoc. Prof. Dang Ngoc Toan (Duy Tan University, Vietnam)
Prof. Valentin Gordeliy (University Grenoble Alpes, CEA, CNRS, Institut de Biologie Structurale, France)
Prof. Ho Manh Dung (Center for Nuclear Technologies, Vietnam)
Dr. Alexander Ioffe (Russia)
Dr. Alexandre Ivanov (Institut Laue-Langevin, France)
Prof. Alexei Khokhlov (Lomonosov Moscow State University, Russia)
Prof. Ravi Kumar (Indian Institute of Technology Madras, India)
Prof. Tianjiao Liang (China Spallation Neutron Source, China)
Dr. Alfredo Raya Montaño (Michoacana University of San Nicolás de Hidalgo, Mexico)
Prof. Aziz Muzafarov (Enikolopov Institute of Synthetic Polymeric Materials, Russian Academy of Sciences, Russia)
Prof. Dénes Lajos Nagy (Wigner Research Centre for Physics, Hungary)
Prof. Alexander Ozerin (Enikolopov Institute of Synthetic Polymeric Materials, Russian Academy of Sciences, Russia)
Dr. Andrey Rogachev (Moscow Institute of Physics and Technology, Landau Phystech School of Physics and Research, Russia)
Dr. Nurzhan Saduyev (Institute of Nuclear Physics the Atomic Energy Agency of the Republic of Kazakhstan, Kazakhstan)
Prof. Deleg Sangaa (Institute of Physics and Technology of the Mongolian Academy of Sciences, Mongolia)
Prof. Mannab Tashmetov (Institute of Nuclear Physics, Uzbekistan Academy of Sciences, Uzbekistan)
Dr. Yan Zubavichus (Synchrotron Radiation Facility SKIF, Russia)

TABLE OF CONTENTS

TABLE OF CONTENTS **5**

PREFACE **14**

ORAL SESSION **16**

Alruqeishi M.
GRAPHENE OXIDE AS AN EFFICIENT ADSORBENT FOR RADIOACTIVE MATERIAL REMOVAL IN AL-KHATMYAIN FALAJ 17

Aničić Urošević M.
APPLICATION OF NEUTRON ACTIVATION ANALYSIS FOR NON-DESTRUCTIVE ELEMENTAL CHARACTERIZATION OF VARIOUS SAMPLES (MOSS, LICHENS, PLANT LEAVES, SOIL, ROAD DUST, FILTERS, LEAF LITTER, CENTIPEDES) INDICATING ENVIRONMENTAL POLLUTION – 20 YEARS OF COLLABORATION BETWEEN EPL INSTITUTE OF PHYSICS BELGRADE AND FLNP JINR DUBNA 18

Arslanov T.R.
MnAs UNDER HIGH PRESSURE: SPIN DENSITY WAVES AND THREE-DIMENSIONALLY MODULATED STRUCTURE 20

Asadov A.G.
PRESSURE-INDUCED STACKING DISORDER AND TRIGONAL DISTORTION IN $PbFe_{12}O_{19}$ HEXAFERRITE 21

Azarova L.A.
STUDY OF THE EFFECT OF RANDOM LOCAL ANISOTROPY ON THE PROPERTIES OF AMORPHOUS FERROMAGNETS 22

Bakirov A.V.
ORDERING OF SOFT NANOMATERIALS: FROM SPACE FILLING TO CLOSE PACKING 23

Bakirov B.A.
ACCELERATED NEUTRON TOMOGRAPHY AND AI-ASSISTED RECONSTRUCTION FOR THE STUDY OF ARCHAEOLOGICAL ARTIFACTS FROM THE VOLNA 1 NECROPOLIS 25

Balasoiu M.
STUDY OF SMALL-ANGLE NEUTRON SCATTERING IN CARBON FIBERS MODIFIED WITH BOEHMITE AND MAGNETIC PARTICLES 27

Belozerova N.M.
MORPHOLOGY-DEPENDENT PLASMON-FREE SERS ENHANCEMENT IN CRYSTALLINE WSE_2 AND WTE_2 29

Borshchevskiy V.
TOWARDS NEUTRON CRYSTALLOGRAPHY OF MICROBIAL RHODOPSINS 31

Elmekawy A.H.A.
INVESTIGATING STRUCTURAL PERIODICITY OF SEGMENTED/NONSEGMENTED MAGNETIC NANOWIRE ARRAYS BY SANS METHOD 32

Harutyunyan V.V.
RADIATION EFFECTS IN CONDENSED MATTER PHYSICS 33

Grigoriev S.V.
MAGNETIC PHASE TRANSITION IN $Y_{1-x}Tb_xMn_6Sn_6$ COMPOUNDS 35

Ivankov O.I.
ON THE SHOULDERS OF GIANTS: FROM YuMO'S BRILLIANT PAST TO ITS BRIGHT FUTURE 36

Ivashchenko S.D.
COMPARISON OF STRUCTURAL FEATURES OF OLIGOMERIC AND MONOMERIC TISSUE TRANSGLUTAMINASE 38

Kichanov S.E.
CRYSTAL AND MAGNETIC STRUCTURE OF COBALT OXIDES AT HIGH PRESSURE AND TEMPERATURE 39

Karavaeva I.A.
DEVELOPMENT OF A FILTER PROTOTYPE BASED ON TUBULAR CERAMIC MEMBRANES WITH A SELECTIVE LAYER OF MXENE $Ti_3C_2T_x$ 40

Kolupaev E.D.
DEVELOPMENT OF REFLECTOMETRIC STUDIES IN OSCILLATING MAGNETIC FIELDS AT THE IBR-2 REACTOR 42

Kozhevnikov S.V.
INVESTIGATIONS OF MAGNETIC WAVEGUIDES AT REFLECTOMETER REMUR 44

Kravtsov E.A.
POLARIZED NEUTRON REFLECTOMETRY IN STYDY OF RARE-EARTH MULTILAYERS 46

Kurilkin A.K.
DEVELOPMENT OF THERMAL NEUTRON DETECTORS BASED ON STRAW TUBES 47

Kurkin T.S.
ENHANCED ADHESION STRENGTH IN POLYMER COMPOSITES MODIFIED WITH HYBRID NANODIAMOND/GRAPHITE PARTICLES 48

Kwiatkowski A.L.
STRUCTURAL TRANSITIONS OF HYBRID MICELLES OF IONIC SURFACTANT WITH EMBEDDED HYDROPHOBIC POLYMER INDUCED BY SALT AND HYDROCARBON 49

Lebedev O.V.
DETONATION NANODIAMOND SOOT AS A PROMISING HYBRID GRAPHITE/NANODIAMOND MATERIAL WITH A TAILORABLE STRUCTURE 50

Litvinenko E.I.
DATA ACQUISITION SYSTEM BASED ON THE R5560 DIGITIZER WITH OPEN FPGA FOR THE WIDE-APERTURE DETECTOR OF THE HIGH-RESOLUTION NEUTRON FOURIER DIFFRACTOMETER HRFD 51

Lychagina T.A.
CRYSTALLOGRAPHIC TEXTURE OF NUCLEAR REACTOR CLADDING TUBES 52

Maksimov P.A.
KITAEV AND ISING COBALT-BASED MAGNETS: INSIGHTS FROM NEUTRON SCATTERING 54

Manukovskaya D.V.
DETERMINATION OF THE LOCALIZATION OF BORON CATIONS IN THE STRUCTURE OF NONLINEAR OPTICAL LITHIUM NIOBATE CRYSTALS $LiNbO_3$:B AND $LiNbO_3$:Me:B (Me - Zn, Mg, Gd) 55

Manukovskaya D.V.
HYDROGEN BONDS IN LITHIUM NIOBATE CRYSTALS OF DIFFERENT COMPOSITIONS AND GENESIS 57

Martyanov D.E.
STRUCTURAL STUDIES OF NANODIAMONDS MODIFIED WITH SURFACTANT IN DIMETHYL SULFOXIDE 58

Minaeva A.V.
ASSEMBLED RECOMBINANT CHLOROPLAST C-RING IN *ESCHERICHIA COLI* 60

Molchanov V.S.
MORPHOLOGICAL PERFORMANCE OF SELF-ASSEMBLED COMPLEX NETWORKS 61

Nashaat M.
HYBRID φ_0 JOSEPHSON JUNCTION AS A POSSIBLE HOST FOR SPACE-TIME CRYSTALLINE-LIKE PATTERN 62

Nguyen N.T.
STUDY ON STRUCTURAL AND MAGNETIC PROPERTIES OF HIGH-ENERGY BALL-MILLED NANOPARTICLES $CoFe_2O_4$ BY NEUTRON DIFFRACTION 63

Nikolayev D.I.
DEVELOPMENT OF THE SKAT TEXTURE DIFFRACTOMETER 64

Pakhnevich A.V.
CRYSTALLOGRAPHIC TEXTURE OF CALCITE IN THE SHELLS OF RECENT BRACHIOPODS 66

Petrova M.O.
2D ^{10}B-RPC FOR SLOW NEUTRONS 68

Ryazanov V.V.
PROXIMITY EFFECTS AND COHERENT TRANSPORT IN JOSEPHSON JUNCTIONS WITH FERROMAGNETS 69

Ryzhykau Yu.L.
STOICHIOMETRIC CONSTRAINTS AS A ROUTE TO MORE RELIABLE SAXS ANALYSIS OF MEMBRANE PROTEINS IN DETERGENT 71

Saprykina I.
NEW DISCOVERIES IN THE STUDY OF ARCHAEOLOGICAL SITES USING METHODS OF NATURAL AND FUNDAMENTAL SCIENCES 73

Shvetsova M.
ELEMENTAL COMPOSITION OF FIFTEEN MEDICINAL SPECIES OF ASTERACEAE FAMILY OF MOLDOVAN ORIGIN DETERMINED BY NEUTRON ACTIVATION ANALYSIS 74

Sterkhov E.V.
LAYERED RARE EARTH MANGANITES UNDER EXTREME CONDITIONS 75

Tilinova O.M.
STRUCTURAL STUDIES OF APOFERRITIN-LIPID SYSTEMS 76

Ushkov A.A.
EMERGENT FUNCTIONALITIES IN VAN DER WAALS NANOPARTICLES SYNTHESIZED VIA FEMTOSECOND LASER ABLATION 77

Vershinina T.N.
SPINODAL DECOMPOSITION IN Fe-Ga ALLOYS 79

Vlasov A.V.
FERRITIN-BASED HYBRIDS FOR VACCINES, DRUG DELIVERY AND IMAGING PLATFORMS 81

Volkov V.V.
FUNDAMENTALS OF SMALL-ANGLE SCATTERING IN THE STUDY OF THE STRUCTURE OF DISORDERED SYSTEMS 83

Zaky I.
NEUTRON OPTICS INSPIRED BY PHOTONIC AND PHONONIC CRYSTALS: BRAGG FILTERING, DEFECT MODES AND TOPOLOGICAL EDGE STATES IN PERIODIC AND QUASI PERIODIC MULTILAYERS 84

Zhaketov V.D.
FERROMAGNETIC-SUPERCONDUCTING FIBONACCI LAYERED QUASICRYSTALS: NEUTRON-OPTICAL MODELING AND PROSPECTS FOR STUDYING STRONGLY CORRELATED STATES 85

Zhurenko S.V.
MAGNETIC ORDER AND DYNAMICS IN FRUSTRATED MAGNETS: THE INDISPENSABLE ROLE OF LOCAL NMR MEASUREMENTS IN COMBINATION WITH NEUTRON SCATTERING 86

Zinicovscaia I.
NEUTRON ACTIVATION ANALYSIS AT THE IBR-2 REACTOR 88

Zubavichus Y.V.
SYNCHROTRON RADIATION FACILITY SKIF: A NEW-BORN MEMBER IN THE RUSSIAN MEGASCIENCE FAMILY 89

POSTER SESSION **90**

Abdurakhimov B.A.
CRYSTAL STRUCTURE OF Bi/Mn CO-DOPED STRONTIUM ALUMINATE PHOSPHORS 91

Abiyev A.S.
NEUTRON DIFFRACTION STUDY OF GAMMA- AND NEUTRON-IRRADIATED W-Ni HEAVY ALLOY 92

Andjelković Lj.
THERMAL DECOMPOSITION OF ACETYLACETONATE PRECURSORS AS A ROUTE TO MONODISPERSE SUPERPARAMAGNETIC $NiFe_2O_4$ NANOCRYSTALS 94

Aničić Urošević M.
NEUTRON ACTIVATION ANALYSIS FOR ELEMENTAL CHARACTERISATION OF COLLOCATED SOIL, LEAF LITTER AND CENTIPEDE SAMPLES 95

Astaf'eva S.A.
FROM STRUCTURE TO STRENGTH: ANALYSIS OF POLYMER COMPOSITES FILLED WITH HYBRID FILLERS 97

Avdeev M.M.
STRUCTURAL STUDIES OF SURFACTANT MICELLES INTERACTING WITH POLYMERS IN BULK AND AT INTERFACES BY NEUTRON SCATTERING 99

Belozerova N.M.
PRESSURE-INDUCED PHASE TRANSITION IN NANOSTRUCTURED CATION-DEFICIENT $ZN_{0.34}FE_{2.53}\square_{0.13}O_4$ FERRITE 101

Berestneva Yu.V.
CHEMICAL ACTIVATION OF *tert*-BUTYL HYDROPEROXIDE BY Et_4NBr. NOTE ON INTRAMOLECULAR DYNAMICS 102

Bezruchko I.O.
SANS STUDY OF NATIVE HORSE SPLEEN FERRITIN AT DIFFERENT CONTRAST VARIATION 103

Borisov R.D.
MODERNISATION OF DATA REDUCTION ALGORITHMS FOR SMALL-ANGLE NEUTRON SCATTERING USING NUMERICAL SIMULATION 104

Chausova V.A.
STUDY OF PHOSPHOLIPID LAYERS ADSORPTION ON PLANAR SOLID INTERFACES BY SPECULAR NEUTRON REFLECTOMETRY 105

Chen J.
NEUTRON DIFFRACTION STUDIES OF AL-SUBSTITUTED HEXAFERRITES WITH GIANT COERCIVITY 107

Culicov O.-A.
ANTIBIOTIC-DRIVEN CHANGES IN THE ELEMENTAL STATUS OF CULTIVATED SOILS 108

Cuong T.V.
MEASUREMENT OF NEUTRON TRANSMISSION FACTOR AND TOTAL CROSS SECTION OF VANADIUM IN THE WAVELENGTH RANGE 0.5–10 Å AT THE YuMO FACILITY 109

Devyaterikov D.I.
INVESTIGATION OF CRYSTAL STRUCTURE OF EPITAXIAL THIN FeRh FILMS DURING AFM-FM PHASE TRANSITION 110

Egorov V.V.
ALBUMIN COMPLEXES WITH AMYLOIDOGENIC PROTEINS: A SANS STUDY 111

Elnikova L.V.
NANOPARTICLES OF REDUCED GRAPHENE OXIDE AND GRAPHENE NANOPLATELET – HOW AND THEY ORGANIZED IN POLYLACTIDE MATRIX? 112

Fedoseev M.L.
PHASE COMPOSITION ANALYSIS OF WELDS IN AUSTENITIC STAINLESS STEELS 114

Gavrilicheva K.A.
CRYSTAL AND MAGNETIC STRUCTURE OF OXYGEN-DEFICIENT $La_{0.5}Sr_{0.5}FeO_{3-\delta}$ FERRITE AT ROOM AND LOW TEMPERATURE 116

Genov I.G.
STRUCTURE AND PROPERTIES OF MATERIALS FROM BiOX (X=Br, Cl, I, BrO3), WITH APPLICATION FOR PHOTOCATALYTIC WATER PURIFICATION AND NO2 GAS SENSORS 118

Gergelezhiu P.A.
STUDY OF NSAIDS MOLECULAR DYNAMICS BY INELASTIC NEUTRON SCATTERING AND COMPLEMENTARY METHODS 119

Gudkov E.L.
THEORETICAL DESCRIPTION OF NEW EFFECT SPACE OSCILLATION OF CORRELATION FUNCTION FOR ULTRA-THIN FERROMAGNETIC FILM IN ALGEBRAIC THEORY OF SYMMETRY BREAKING AND SUGGESTION OF ITS EXPERIMENTAL VERIFICATION 120

Harutyunyan V.V.
STUDY OF RADIATION-THERMOSTIMULATED PROPERTIES IN MODIFIED COMPOSITE THERMOREGULATING COATINGS 122

Ivankina T.I.
MINERAL PREFERRED ORIENTATION AND PROPERTIES OF ROCKS FROM SOURCE AREA OF EARTHQUAKES: COMPREHENSIVE STUDY BY NEUTRON DIFFRACTION AND ULTRASONIC ANALYSIS 124

Kamalieva L.A.
COMPARATIVE ANALYSIS OF LIGAND AFFINITY TO THE C-RING OF ATP SYNTHASE 126

Khongorzul B.
EFFECTS OF MN^{2+} DOPING ON MAGNETIC AND ELECTRONIC PROPERTIES OF $ZNFE_2O_4$: A FIRST-PRINCIPLES STUDY 127

Kopitsa G.P.
STRUCTURE OF IONOGELS BASED ON POLYMER AEROGELS OBTANIED FROM POLYAMIDE 6,6 129

Korshikov Y.S.
CRYOGENIC INSERT FOR STUDYING KAPITZA JUMP AND TURBULENT HEAT TRANSFER IN SUPERFLUID HELIUM AT TEMPERATURES BELOW 1 K 131

Kuklin A.I.
MAIN DIRECTIONS OF YUMO SPECTROMETER DEVELOPMENT 132

Kurbonov S.
SPACER-DEPENDENT SELF-ASSEMBLY OF UREA-BASED GEMINI SURFACTANTS AND THEIR APPLICATION IN TEMPLATING ORDERED MESOPOROUS SILICA 133

Lebedev D.V.
STRUCTURE OF THE COMPLEXES OF RecA AND DprA PROTEINS WITH SHORT SINGLE STRANDED DNA 135

Lis O.N.
PRESSURE EFFECT ON CRYSTAL, MAGNETIC STRUCTURE AND VIBRATIONAL PROPERTIES OF VAN DER WAALS MATERIALS 136

Litvinenko E.I.
ARCHITECTURE AND FEATURES OF THE DATA ACQUISITION SYSTEM BASED ON THE DT5560 DIGITIZER FROM CAEN FOR THE DETECTOR SYSTEM OF THE FOURIER STRESS DIFFRACTOMETER FSD 137

Lukin E.V.
AT FLNP JINR: CAPABILITIES AND APPLICATIONS 138

Makarova M.V.
STUDY OF THE HYDROGEN-INDUCED MAGNETIC PROPERTIES OF THE FE/GD SUPERLATTICE USING POLARIZED NEUTRON REFLECTOMETRY 139

Manko I.D.
NEUTRON SCATTERING IN SOLID SOLUTIONS $Mn_{1-x}Rh_xSi$ WITH TEMPERATURE-BLURRED PHASE TRANSITION 141

Matyukhov V.V.
CHANGES IN THE STRUCTURAL PROPERTIES OF THIN FILMS OF RARE-EARTH METALS DURING HYDRATION 142

Meshkov I.V.
SIMULATION OF EPITHERMAL NEUTRON FLUX SPATIAL DISTRIBUTION FROM 1 TO 200 EV AT PHOTONEUTRON SOURCE 143

Nabiyev A.A.
STRUCTURE AND CRYSTALLIZATION KINETICS IN SODIUM MONTMORILLONITE-CONTAINING POLYPROPYLENE NANOCOMPOSITES: INTEGRATION OF SAXS AND DSC ANALYSES OF DISPERSION, FRACTAL STRUCTURE, AND INTERFACIAL PROPERTIES 144

Nabiyev A.A.
HIGH-DOSE GAMMA IRRADIATION EFFECTS ON HDPE/SiO_2 NANOCOMPOSITE FILMS: STRUCTURE, CRYSTALLINITY, AND INTERFACIAL BEHAVIOR 146

Nabiyev A.A.
EFFECT OF HIGH-DOSE GAMMA RADIATION AND WS_2 NANOSHEETS ON THE SUPRAMOLECULAR STRUCTURE, FRACTAL MORPHOLOGY, AND INTERFACIAL BEHAVIOR OF PVDF BY SAXS 148

Nikova E.S.
PHASE RECOVERY IN POLARIZED NEUTRON REFLECTOMETRY USING DY AND ITS HYDRIDES AS REFERENCE LAYERS 150

Norov D.A.
PROXIMITY EFFECTS IN HETEROSTRUCTURES OF SUPERCONDUCTING NIOBIUM AND RARE EARTH METALS WITH HELIMAGNETIC ORDERING 152

Nurulin R.
CHARACTERIZATION OF INTERLAYER CORRELATIONS IN SPECIAL PLANAR STRUCTURES BY SPECULAR NEUTRON REFLECTOMETRY 153

Petrova E.A.
STUDY AND OPTIMIZATION OF VIRAL RHODOPSINES 1 154

Ponomarev V.N.
EPITHERMAL NEUTRON FLUX MEASUREMENTS AT PHOTONEUTRON SOURCE USING POSITION-SENSITIVE DETECTOR WITH DOUBLE-LAYER ^{10}B 155

Popov A.I.
DESIGN AND ANALYSIS OF THE LATENT SPACE FOR VAE-BASED NEUTRON DIFFRACTION DATA 156

Popov A.I.
A MULTIMODAL DUAL-BRANCH SWIN TRANSFORMER NETWORK FOR NEUTRON 2D DIFFRACTION POST-PROCESSING 157

Popović M.
NONLINEAR LASER SCANNING MICROSCOPY FOR LABEL-FREE POLYMER (MICROPLASTIC) DETECTION IN A BIOLOGICAL MATRIX 158

Raksha E.V.
INTRA- AND INTERMOLECULAR DYNAMICS OF AZA-AROMATIC SYNTHONS: A CASE STUDY OF THE 4,4′-BIPYRIDINE 159

Rutkauskas A.V.
PRESSURE-INDUCED PHASE TRANSITIONS IN MAGNETITE NANOPARTICLES DOPED WITH Sm AND La IONS 160

Sadradze R.N.
DEVELOPMENT OF COMPLEX FIBONACCI SYSTEMS WITH MIXED SUPERCONDUCTIVITY AND ARTIFICIAL ANTIFERROMAGNETISM 161

Savin V.V.
NEUTRON-DIFFRACTION STUDY OF ANISOTROPY IN GAS-ATOMIZED Nd-Fe-B MAGNETS POWDERS 162

Shishkin A.Yu.
INVESTIGATION OF LIPID MEMBRANES AND MEMBRANE-MIMETIC SYSTEMS BY SANS AT YUMO SPECTROMETER 164

Sikolenko V.V.
NEUTRON DIFFRACTION STUDY OF STRUCTURAL DISTORTIONS AND MAGNETIC STRUCTURE OF Bi-Sm-Fe-Ti-O MULTIFERROIC 166

Sudarev V.V.
OPTIMIZATION OF PURIFICATION AND CRYSTALLIZATION CONDITIONS FOR OLPVR2 167

Šuljagić M.
PHASE-PURE COBALT FERRITE NANOPARTICLES WITH TUNABLE MAGNETIC PROPERTIES *VIA* MILD THERMAL TREATMENT AND CONTROLLED PRECIPITATION 168

Trung N.T.H
A NEW MODEL OF PRIMARY RADIATION DAMAGE IN MATERIALS 169

Zhezlyaev G.E.
SOFTWARE FOR TRANSFORMING NEUTRON SCATTERING DATA FROM INSTRUMENTAL COORDINATES INTO Q-SPACE FOR TIME-OF-FLIGHT INSTRUMENTS BASED ON IBR-2 170

Zel I.Yu.
EPSILON AS A TEXTURE DIFFRACTOMETER: FIRST RESULTS 172

Zinicovscaia I.
CONCENTRATION OF METALS IN MOSS SAMPLES FROM FIVE DIFFERENT ENVIRONMENTS IN SERBIA: COMPARISON AND ANALYSIS 173

List of Authors **174**

Oral Session 174
Poster Session 175
Alphabetical Authors List 176

PREFACE

The International Conference on Condensed Matter Research at the IBR-2 Reactor (CMR@IBR2-2026) is a continuation of the long-year scientific tradition of the Frank Laboratory of Neutron Physics, uniting specialists in neutron physics, condensed matter physics, materials science, chemistry, biophysics, and related disciplines. The Conference is held during the period of intensive development of modern neutron technologies and increased interest of the world scientific community in research into the structure and dynamics of matter at the atomic and molecular levels. In 2026, the Conference takes place from June 15 to 19 and is one of the central scientific events of the jubilee year devoted to the 70th anniversary of the Joint Institute for Nuclear Research (JINR).

Founded in 1956, JINR is one of the leading international scientific centers, promoting the development of fundamental and applied science, training highly qualified personnel, and strengthening international cooperation in nuclear physics and related fields. Over the years, JINR has built a unique, world-class research infrastructure that brings together scientists and engineers from dozens of countries. Today, the Institute continues to play a vital role in the development of international scientific cooperation, serving as a platform for implementation of large-scale research projects and introduction of advanced technologies.

A special place in the scientific infrastructure of JINR is occupied by the IBR-2 reactor—one of the largest pulsed neutron sources in the world. Every year, over 200 experiments are carried out at the IBR-2 instruments within the framework of the FLNP User Program, involving researchers from more than 20 countries. This confirms the reactor's high international status as one of the key centers for neutron research and demonstrates the growing demand within the scientific community for neutron methods to address fundamental and applied challenges. Neutron scattering and neutron imaging are now indispensable tools for studying the structure and properties of functional materials, magnetic systems, polymers, biological objects, residual stresses, geological samples, and engineering structures.

The CMR@IBR2-2026 Conference is dedicated to the 90th anniversary of Yuri M. Ostanevich, an outstanding scientist who made a fundamental contribution to the development of neutron physics and methods of structural research of matter. His scientific work had a significant impact on the establishment of modern methods of small-angle neutron scattering at pulsed sources. The results he obtained formed the basis of numerous papers that remain relevant to this day. The previous small-angle scattering conferences dedicated to Yu.M. Ostanevich, held in 2006, 2011, and 2016, have consistently highlighted his contribution to science.

The scientific program of the Conference covers a wide range of relevant research areas. These include functional and nanostructured materials, magnetic and colloidal systems, layered magnetic nanostructures, carbon nanomaterials, materials under extreme conditions, soft matter, biological nanosystems, lipid membranes, polymers, the dynamics of crystal and molecular structures, texture and property analysis of rocks and industrial materials, residual stresses in structural elements, neutron imaging, applied research, and cultural heritage objects.

The Conference focuses also on the development of the experimental infrastructure of the IBR-2 reactor, modernization of existing instruments, development of new detector systems, improvement of methods for processing experimental data, and integration of modern digital technologies into neutron research. An important part of the scientific program is the discussion of prospects for developing new research instruments and expanding the capabilities of the FLNP User Program. The event features a user roundtable dedicated to increasing the efficiency of experimental research, improving user infrastructure, and defining strategic directions for the development of neutron science.

The Organizing Committee expresses its sincere gratitude to all participants, partners and scientific organizations involved in preparing and hosting the Conference. We are confident that CMR@IBR2-2026 will become an important international platform for exchanging knowledge, strengthening scientific cooperation, forming new research initiatives, and advancing cutting-edge neutron technologies.

We wish all conference participants fruitful work, interesting scientific discussions, inspiration, new professional contacts, and significant scientific achievements.

Organizing Committee of CMR@IBR2-2026

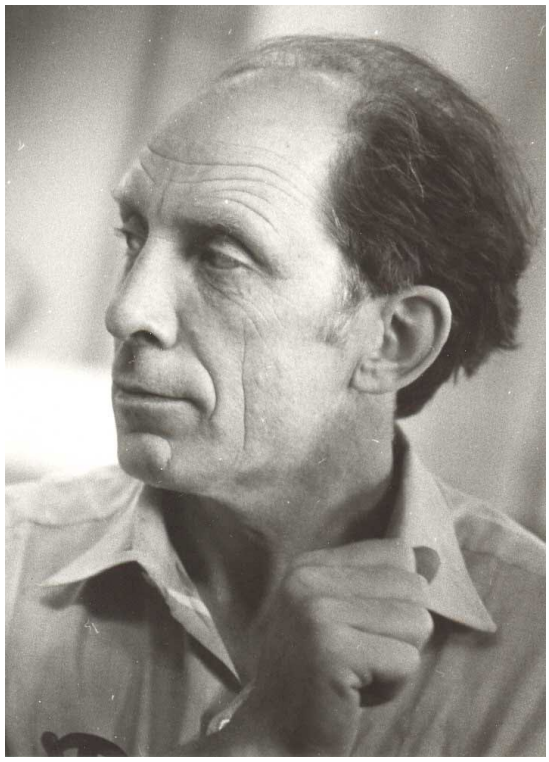

Professor Yuri M. Ostanevich (1936–1992) was one of the organizers of the Frank Laboratory of Neutron Physics and the Condensed Matter Physics Department, which he headed for many years. His contribution was crucial and decisive in selecting scientific directions, creating spectrometers at the IBR-2 pulsed reactor, and developing the time-of-flight small-angle neutron scattering (SANS) technique. To achieve this, unique approaches were developed—detectors with a ring geometry and a central hole for the direct beam, as well as normalization to a vanadium standard, which fundamentally enables obtaining the differential small-angle scattering cross-section in absolute units. His leadership and outstanding scientific achievements in the applications of the Mössbauer effect in physics and chemistry, alongside his SANS studies of polyelectrolytes, small molecules, fractals, metallic glasses, macromolecules, polymers, and other systems, were recognized by a number of awards, including the State Prize of the Russian Federation in 2000. His contribution to introducing neutron scattering methods into molecular biology research is particularly noteworthy. The exceptional scientific insight and expertise of Prof. Yury Ostanevich, along with his generous mentorship, warm friendship, and support are greatly missed.

A.M. Balagurov, Frank Laboratory of Neutron Physics, JINR, Dubna

ORAL SESSION

GRAPHENE OXIDE AS AN EFFICIENT ADSORBENT FOR RADIOACTIVE MATERIAL REMOVAL IN AL-KHATMYAIN FALAJ

M. Alruqeishi[1], N. Alsalmi[1], H. Alshumi[1]

[1] *Physics Section, Department of Mathematical and Physical Sciences, College of Arts and Sciences, University of Nizwa, P.O. Box 33, P.C. 616, Barakit Al-Mouz, Nizwa, Sultanate of Oman.*

E-mail: majiduon@unizwa.edu.om

Graphene oxide (GO) was investigated as a selective adsorbent for the removal of radionuclides from Al-Khatmyain falaj, a traditional groundwater-fed irrigation channel. Radioactivity levels of Ra-226, Am-241, Cs-134, Cs-137, I-131, and K-40 in water samples were measured using a high-purity germanium (HPGe) detector. Initial radiological assessment showed that all radionuclide concentrations were below World Health Organization safety limits, with annual committed effective doses ranging from 5.3×10^{-5} to 4.4×10^{-2} mSv yr^{-1}, well below the reference level of 0.1 mSv yr^{-1}. The removal performance of GO was evaluated under untreated conditions, fixed GO concentration (0.006 g/mL), and variable concentrations (0.012–0.020 g/mL) at constant pH (~7.2). Results demonstrated dose-dependent and selective adsorption, achieving removal efficiencies of ≥96% for K-40, ≥72% for I-131, ≥62% for Ra-226, and ≥40% for Am-241, with optimal performance at 0.016 g/mL. The selective adsorption mechanism is attributed to oxygen-containing functional groups on GO that facilitate electrostatic attraction, ion exchange, and chelation, particularly for divalent cations. Reduced efficiency at higher concentrations was associated with nanosheet aggregation and active-site blocking. These findings highlight GO's strong potential for targeted radionuclide remediation in aqueous systems.

Keywords: Graphene oxide, Radioactive materials, Water contamination.

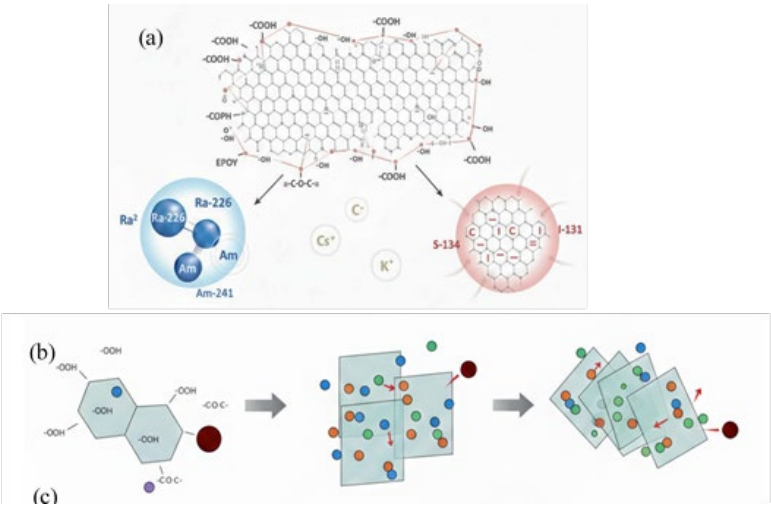

Figure 1.0: (a) Selective adsorption of radionuclides by graphene oxide (GO): divalent cations (Ra^{2+}) are strongly removed via complexation, while monovalent cations (Cs^{+}, K^{+}) and anions (I^{-}) show minimal adsorption. (b) Schematic representation of radionuclide adsorption on graphene oxide (GO) and corresponding activity measurements at different GO concentrations.

APPLICATION OF NEUTRON ACTIVATION ANALYSIS FOR NON-DESTRUCTIVE ELEMENTAL CHARACTERIZATION OF VARIOUS SAMPLES (MOSS, LICHENS, PLANT LEAVES, SOIL, ROAD DUST, FILTERS, LEAF LITTER, CENTIPEDES) INDICATING ENVIRONMENTAL POLLUTION – 20 YEARS OF COLLABORATION BETWEEN EPL INSTITUTE OF PHYSICS BELGRADE AND FLNP JINR DUBNA

M. Aničić Urošević[1], M. Tomašević[1], A. Popović[2], G. Jovanović[1], T. Milićević[1], J. Roganović[2], M. Ilić[3], B. Mitić[4], M. Popović[1], K. Vergel[5], O. Chaligava[5], A. Uzhinskiy[5], N. Yushin[5], L.P. Strelkova[5], T. Ostrovnaya[5], Z. Goryainova[5], S.S. Pavlov[5], I. Zinicovscaia[5], M.V. Frontasyeva[5]

[1] *Institute of Physics Belgrade, University of Belgrade, Belgrade, Serbia*
[2] *Faculty of Chemistry, University of Belgrade, Belgrade, Serbia*
[3] *University of Novi Sad, Faculty of Sciences, Department of Biology and Ecology, Serbia*
[4] *Institute of Zoology, University of Belgrade – Faculty of Biology, Belgrade, Serbia*
[5] *Frank Laboratory of Neutron Physics, Joint Institute for Nuclear Research, Dubna, Russia*

E-mail: mira.anicic@ipb.ac.rs

Since 2005, in the frame of the cooperation between the Environmental Physics Laboratory of the Institute of Physics Belgrade (Serbia) and FLNP (JINR), instrumental neutron activation analysis (INAA) has been used for elemental characterization of different types of environmental samples. Many major, minor, trace, and rare-earth elements, present in excess, proved to be potentially toxic and recommended for monitoring. A non-destructive INAA has often been used in environmental studies, capable of detecting up to 45 elements with minimal sample preparation. The collaborative studies were mainly carried out in Serbia, while the analytical part was performed using the REGATA system at the reactor IBR-2. However, there was a study carried out in parallel over Belgrade and Moscow [1]. Mosses and lichens have been among the most explored samples for the purpose of biomonitoring airborne potentially toxic elements (PTEs), both passive and active approaches. Passive approach considered using naturally growing mosses for biomonitoring purposes mainly in remote and rural areas [2] but sometimes in urban areas, too [3], while active approach implies the use of moss/lichen transplants for exposition in any place of interest – street canyons, tunnels, crossroads, parking garages, etc., mostly within `moss/lichen deserts` such as urban [4-10] or agricultural areas [11, 12]. The moss biomonitoring database has been successfully used in combination with satellite imagery and machine learning for the prediction of air pollution by PTEs [13]. Plant samples (coniferous leaves) were selected for biomonitoring of PTEs in urban areas, and these samples were used for comparative analysis of the non-destructive INAA technique and the conventionally used spectrometric ICP-OES and ICP-MS techniques [14]. Rare-earth elements have been measured in the road dust from the vicinity of coal-fired thermal power plants [15]. Quartz filters used for regulatory collection of particulate matter (PM2.5 and PM10) were analyzed by INAA. Our latest ongoing research focuses on investigating centipedes as bioindicators of anthropogenic pollution impacts on soil ecosystems by measuring PTEs in their different life forms, and in the collocated topsoil and leaf litter samples as well.

[1] Z. Goryainova, G. Vuković, M. Aničić Urošević, K. Vergel, T. Ostrovnaya, M. Frontasyeva, H. Zechmeister (2016). Assessment of vertical element distribution in street canyons using the moss *Sphagnum girgensohnii*: A case study in Belgrade and Moscow cities. Atmospheric Pollution Research 7, 690-697.
[2] M. Aničić Urošević, M. Ilić, D. Radnović, K. Vergel, N. Yushin, O. Chaligava, I. Zinicovscaia (2024). Comparative biomonitoring of airborne potentially toxic elements

using mosses (*Hypnum cupressiforme*, *Brachythecium* spp.) and lichen (*Evernia prunastri*) over remote areas. Environmental Science and Pollution Research 31, 48296-48296.
[3] M. Aničić, M.V. Frontasyeva, M. Tomašević and A. Popović (2007). Assessment of atmospheric deposition of heavy metals and other elements in Belgrade using moss biomonitoring technique and neutron activation analysis. Environmental Monitoring and Assessment 129, 207-219.
[4] M. Aničić Urošević, M. Kuzmanoski, T. Milićević, I. Kodranov, K. Vergel, A. Popović (2022). Moss bag sensitivity for the assessment of airborne elements at suburban background site during spring/summer season characterized by Saharan dust intrusions. Air Quality, Atmosphere & Health 15, 1357.
[5] G. Vuković, M. Aničić Urošević, M. Pergal, M. Janković, Z. Goryainova, M. Tomašević and A. Popović (2015). Residential heating contribution to persistent air pollutants (PAHs, trace and rare earth elements): A moss bag case study. Environmental Science and Pollution Research 22/23, 18956-18966.
[6] G. Vuković, M. Aničić Urošević, Z. Goryainova, M. Pergal, S. Škrivanj, R. Samson and A. Popović (2015) Active moss biomonitoring for extensive screening of urban air pollution: Magnetic and chemical analyses. Science of the Total Environment 521-522, 200-210.
[7] G. Vuković, M. Aničić Urošević, I. Razumenić, Z. Goryainova, M. Frontasyeva, M. Tomašević and A. Popović (2013). Active moss biomonitoring of small-scale spatial distribution of airborne major and trace elements in the Belgrade urban area. Environmental Science and Pollution Research 20, 5461-5470.
[8] M. Aničić, M. Tomašević, M. Tasić, S. Rajšić, A. Popović, M.V. Frontasyeva, S. Lierhagen and E. Steinnes (2009). Monitoring of trace element atmospheric deposition using dry and wet moss bags: Accumulation capacity versus exposure time. Journal of Hazardous Materials 171, 182-188.
[9] M. Aničić, M. Tasić, M.V. Frontasyeva, M. Tomašević, S. Rajšić, Z. Mijić and A. Popović (2009). Active moss biomonitoring of trace elements with *Sphagnum girgensohnii* moss bags in relation to atmospheric bulk deposition in Belgrade, Serbia. Environmental Pollution 157, 673-679.
[10] M. Aničić, M. Tasić, M.V. Frontasyeva, M. Tomašević, S. Rajšić, L.P. Strelkova, A. Popović and E. Steinnes (2009). Active biomonitoring with wet and dry moss: A case study in an urban area. Environmental Chemical Letters 7, 55-60.
[11] T. Milićević, M. Aničić Urošević, G. Vuković, S. Škrivanj, D. Relić, M.V. Frontasyeva, A. Popović (2017) Assessment of species-specific and temporal variations of major, trace and rare earth elements in vineyard ambient using moss bags. Ecotoxicology and Environmental Safety 144, 208-215.
[12] T. Milićević, M. Aničić Urošević, D. Relić, G. Jovanović, D. Nikolić, K. Vergel, A. Popović (2020). Environmental pollution influence to soil–plant–air system in organic vineyard: bioavailability, environmental, and health risk assessment. Environmental Science and Pollution Research 28, 3361-3374.
[13] A. Uzhinskiy, M. Aničić Urošević, M. Frontasyeva (2020). Prediction of Air Pollution by Potentially Toxic Elements over Urban Area by Combining Satellite Imagery, Moss Biomonitoring Data and Machine Learning. Ciencia e Tecnica Vitivinicola 35(12), pp. xx.
[14] J. Orlić, M. Aničić Urošević, K. Vergel, I. Zinicovscaia, S. Stojadinović, I. Gržetić, K. Ilijević (2022). Comparison of non-destructive techniques and conventionally used spectrometric techniques for determination of elements in plant samples (coniferous leaves). Journal of Serbian Chemical Society 87 (1) 69-81.
[15] J. Roganović, D. Relić, M. Zarić, M. Aničić Urošević, I. Zinicovscaia, K. Ilijević, N.M. Zarić (2025). Rare earth elements and health risk assessment of road dust from the vicinity of coal fired thermal power plants. Chemosphere 377, 144329.

MnAs UNDER HIGH PRESSURE: SPIN DENSITY WAVES AND THREE-DIMENSIONALLY MODULATED STRUCTURE

T.R. Arslanov[1], V.A. Sidorov[2], A.I. Ril[3], A.V. Rutkauskas[4], D.P. Kozlenko[4], A.Yu. Likhacheva[5], S.V. Rashchenko[5] and A.P. Zavyalov[6]

[1] *Amirkhanov Institute of Physics, DFSC, RAS, 367003 Makhachkala, Russia*
[2] *Vereshchagin Institute for High Pressure Physics, RAS, 108840 Troitsk, Moscow, Russia*
[3] *P.N. Lebedev Physical Institute of the Russian Academy of Sciences, Moscow 119991, Russia*
[4] *Frank Laboratory of Neutron Physics, JINR, 141980 Dubna, Russia*
[4] *Sobolev Institute of Geology and Mineralogy SB RAS, Novosibirsk 630090, Russia*
[6] *Synchrotron Research Department, Synchrotron Radiation Facility—Siberian Circular Photon Source "SKIF", Boreskov Institute of Catalysis, SB RAS, Koltsovo, Novosibirsk Region, 630559 Russia*

E-mail: arslanovt@gmail.com

Among binary Mn pnictides, MnAs is a historically important and yet in many ways unique system since its discovery more than a century ago. Unlike its counterpart MnP, which has a double-helical structure and develops pressure-induced superconductivity [1], MnAs does not exhibit any noncollinear magnetic order under ambient conditions. The most stable phase of MnAs is the ferromagnetic (FM) hexagonal which under pressure vanishes near 0.44 GPa, and a long-range antiferromagnetic (AFM) phase develops below 230 K at least up to ~1 GPa [2]. Upon further compression above 0.8 GPa, an orthorhombic [Space group *Pnma*] FM phase is stabilized over entire pressures, however, its origin remains unclear.

By combining high-pressure synchrotron x-ray diffraction, neutron scattering, and transport measurements up to 5.5 GPa, we reveal a novel phase sequence in MnAs. Above ~1.1 GPa, a broad FM phase is indeed stabilized. Within this FM state, upon cooling below a temperature T^* that increases with pressure, neutron diffraction reveals the emergence of additional magnetic reflections. These signal the formation of a spin density wave (SDW), coexisting with the FM background, as evidenced by the itinerant character of the transition (absence of a specific heat peak). Furthermore, at 4.6 GPa, x-ray diffraction uncovers a static structural modulation characterized by a tripling of the unit cell and a transition to the noncentrosymmetric space group $Pna2_1$ (the *Pnma* sub-group). The existence of the isomorphic $Pna2_1$ sub-groups tripled in the directions *a*, *b* and *c* substantiates the possibility for modulation in MnAs structure with the vector components close to $a^*/3$, $b^*/3$ and $c^*/3$ or their combination. Our results demonstrate that MnAs under pressure evolves into a system where a lattice instability drives the formation of a pressure-stabilized SDWs within an itinerant ferromagnet, presenting a rare example of intertwined structural and magnetic modulations that are enhanced by compression.

[1] J.-G. Cheng (2015). Pressure Induced Superconductivity on the Border of Magnetic Order in MnP. Phys. Rev. Lett. 114, 117001.
[2] N. Menyuk (1969). Effects of Pressure on the Magnetic Properties of MnAs. Phys. Rev. 177, 942.

PRESSURE-INDUCED STACKING DISORDER AND TRIGONAL DISTORTION IN $PbFe_{12}O_{19}$ HEXAFERRITE

A.G. Asadov[1,2], D.P. Kozlenko[1], E.V. Lukin[1], O. Lis[1], S.E. Kichanov[1]

[1] *Frank Laboratory of Neutron Physics, JINR, 141980 Dubna, Russia*
[2] *Institute of Physics, Ministry of Science and Education of the Republic of Azerbaijan, Baku AZ-1143, Azerbaijan*

E-mail: asifasadov@jinr.ru

High-pressure X-ray diffraction (XRD) experiments on $PbFe_{12}O_{19}$ (M-type lead hexaferrite, ambient $P6_3/mmc$ structure) reveal a structural distortion between 8 and 25 GPa, manifesting as stacking disorder along the c-axis and trigonal symmetry breaking. At ambient conditions and up to ~29 GPa, prior studies report isostructural compression with no phase changes [1].

Here, using diamond anvil cell (DAC) XRD (Cu Kα), a new low-angle peak emerges at 4.8° 2θ (d ≈ 18.38 Å) at 8 GPa, alongside activation of the forbidden (003) reflection (l=3 odd, absent in $P6_3/mmc$). Rietveld refinement (FullProf) of the 8 GPa pattern requires a 1×1×3 supercell (c ≈ 68 Å, multiplicity m=3) with reduced P31m symmetry (157), yielding low R_{wp} ≈ 5–8% and indexing all peaks, including (004) for the new reflection and (003) via trigonal allowance (00l: l=3n).

This distortion arises from extreme c-axis compressibility anisotropy (B_c ≈ 556 GPa vs. B_a ≈ 997 GPa), inducing periodic stacking faults in the R-S-R-S* block sequence and layer tilting [2]. Above 25 GPa, both features revert, restoring $P6_3/mmc$ as cumulative strain anneals faults. No such low-pressure stacking disorder or $P6_3/mmc \rightarrow P31m$ transition is reported in $PbFe_{12}O_{19}$ or hexaferrite analogs, highlighting sample-dependent shear effects (e.g., defects/non-hydrostaticity). Equation-of-state analysis confirms B_0 ≈ 254 GPa. These findings uncover transient pressure-tuned disorder in layered ferrites, with implications for multiferroic tuning [3].

[1] Zhang Q, et al. (2015). Structural Behavior of $PbFe_{12}O_{19}$ under Pressure. Chinese J High Press Phys. 29(5), 363-368.
[2] Abdulvakhidov K, et al. (2024) Structure, electrophysical, optical, and magnetic properties of $PbFe_{12}O_{19}$–$PbTiO_3$ composites. Appl Phys A. 130:532.
[3] Tan G, Wang M. (2011) Multiferroic $PbFe_{12}O_{19}$ ceramics. J Electroceram. 26,170-174

STUDY OF THE EFFECT OF RANDOM LOCAL ANISOTROPY ON THE PROPERTIES OF AMORPHOUS FERROMAGNETS

L.A. Azarova[1,2], K.A. Pschenichniy[1], O.I. Utesov[1,3], R.D. Borisov[1,2], S.V. Grigoriev[1,2]

[1] *Petersburg Nuclear Physics Institute named by B.P. Konstantinov of NRC "Kurchatov Institute", 188300 Gatchina, Russia*
[2] *Saint Petersburg State University, 199034 Saint Petersburg, Russia*
[3] *Center for Theoretical Physics of Complex Systems, Institute for Basic Science, Daejeon 34126, Republic of Korea*

E-mail: loveazarova@gmail.com

Amorphous magnetic materials, valued for their low coercive fields (e.g., in transformer cores), exhibit complex interplay between structural disorder and magnetic behavior. While progress has been made in understanding static spin clusters in these systems, their dynamic properties - particularly magnetic excitations and magnon dispersion - remain poorly explored [1]. The morphology-dependent response of spin clusters to external fields, coupled with unresolved correlations between structural and magnetic disorder, highlights critical gaps in knowledge. To bridge this gap, we employ polarized neutron small-angle scattering (SANS) combined with an inclined magnetic field configuration - an indirect yet precise method - to study spin wave spectra and excitations, enabling detailed characterization of dynamic processes in amorphous magnetic systems.

The dispersion of spin waves in an amorphous ferromagnet can be described through the model of a ferromagnet with random anisotropy: $\epsilon(q) = Aq^2 + g\mu_B H + \delta\omega(q)$, where $\delta\omega(q)$ is a linear in $|q|$ additive [1-3]. In this paper, we investigate the temperature dependence of the energy characteristics in the spin wave spectrum of the amorphous ferromagnetic alloy $Fe_{48}Ni_{34}P_{18}$ and show that it is possible to obtain information not only about the spin-wave stiffness, but also about the characteristic random anisotropy constant that determines the appearance of the additive $\delta\omega(q)$. We use the method of small-angle scattering of polarized neutrons to prove the significance of the additional term $\delta\omega(q)$ in the dispersion. The measurements were carried out at different values of the external magnetic field H and the neutron wavelength λ. The neutron scattering map is a circle of a certain radius centered at the point $q = 0$. The spin-wave stiffness A is extracted directly from the λ-dependence of the radius of this circle. The spin-wave stiffness A of an amorphous alloy decreases slightly from 140 to 110 meV Å^2 with an increase in temperature in the range of 50 to 300 K. The field dependence of the radius demonstrates the presence of an additive δω(q) in the form of an energy gap, which is practically independent of field and temperature. Therefore, the experiments have revealed an internal "effective energy gap" associated with random anisotropy in the spin wave spectrum of the $Fe_{48}Ni_{34}P_{18}$ alloy over a wide range of temperatures and magnetic fields. The "gap" value of 0.015 meV was measured with an accuracy of 0.002 meV, which is a record achievement in terms of its accuracy. The presence of a linear additive in the spectrum of spin waves is experimentally demonstrated, confirming the validity of the "random anisotropy theory" for amorphous ferromagnets [3].

[1] R. S. Iskhakov, S. V. Komogortsev, A. D. Balaev, and L. A. Chekanova, JETP Lett. 72, 304 (2000).
[2] V. A. Ignatchenko and R. S. Iskhakov, Zh. Eksp. Teor. Fiz. 72, 1005 (1977).
[3] S. V. Grigoriev, L. A. Azarova, K. A. Pshenichnyi, and O. I. Utesov, J. Exp. Theor. Phys. 137, 463 (2023)

ORDERING OF SOFT NANOMATERIALS: FROM SPACE FILLING TO CLOSE PACKING

A.V. Bakirov[1,2], A.M. Muzafarov[1,3], S.N. Chvalun[1,2]

[1] *Enikolopov Institute of Synthetic Polymer Materials RAS, 70 Profsoyuznaya str., 117393, Moscow, Russia*
[2] *National Research Centre "Kurchatov Institute", 1 Kurchatov sq., Moscow, 123098, Russia*
[3] *A.N. Nesmeyanov Institute of Organoelement Compounds of Russia Academy of Sciences, 28 Vavilova str., 119991 Moscow, Russia*

E-mail: bakirov.artem@gmail.com

Over the past two decades, as new polymerization methods and high-efficiency chemical synthesis techniques have advanced, it has become possible to create novel macromolecules with narrow molecular weight distributions, defined chemical structures, and specific functionalization. This has provided a platform for rethinking the self-assembly of traditional block copolymers and other specifically designed amphiphilic macromolecules. Recent progress in the field of macromolecular self-assembly sheds new light on the formation mechanisms of novel ordered structures and their relationship with well-established phases. The ordered structures arising from the packing of spherical subunits are particularly diverse; this diversity may be attributed to complex three-dimensional close-packing schemes of "soft" nanospheres and various types of frustration stemming from the flexibility and compressibility of self-assembling spherical motifs.

In particular, highly ordered and complex Frank–Kasper (F–K) phases based on spherical motifs have been discovered in soft matter systems, such as liquid crystals, low-molecular-weight surfactants, dendrimers, block copolymers, colloidal particles, and, most recently, giant molecular tetrahedra. In these systems, organic or hybrid molecules first assemble into spherical motifs, which then organize into ordered supramolecular phases. Frank–Kasper phases represent a family of spherical structures that combine a distorted icosahedron with a coordination number (CN) of 12 and Kasper polyhedra (with higher coordination numbers of 14, 15, and 16). This results in unique spherical structures featuring various combinations of symmetry operations and space groups.

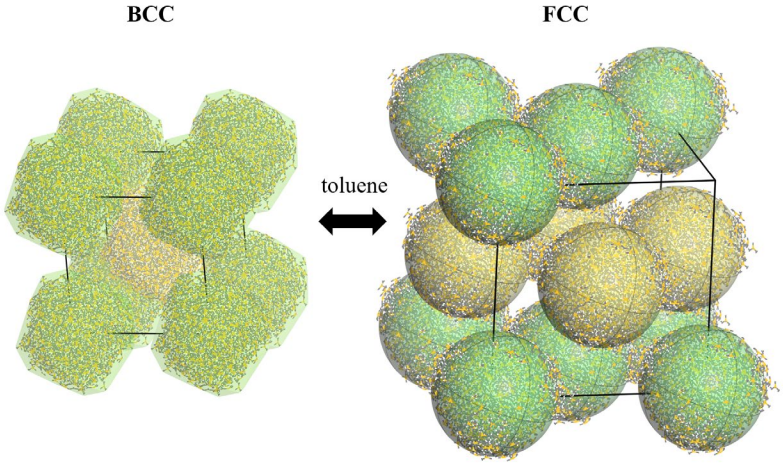

Figure 1. Model of phase transition upon solvent vapor annealing in 6th generation carbosilane dendrimers [2].

The study of F–K phases is linked to the classical problem of 3D hard-sphere packing, which has found widespread application in the crystallography of metal alloys containing metal atoms

of at least two different sizes and electronic states. To fill 3D space with identical metal atoms, it is generally accepted that packing with a coordination number of 12 is the most efficient. In this context, three possible environments for the central atom are distinguished: the cuboctahedron in face-centered cubic (FCC) packing, the twinned cuboctahedron in hexagonal close-packed (HCP) structures, and the icosahedron in so-called topologically close-packed (TCP) structures. Although F–K phases were originally discovered in metal alloys, in recent years they—along with quasicrystals—have unexpectedly been found in a variety of soft matter systems, including surfactant micelles, dendritic liquid crystals, and block copolymers. This report reviews key studies dedicated to Frank–Kasper phases and quasicrystals in macromolecular systems.

[1] Bakirov A.V., Tatarinova E.A., Milenin S.A., Shcherbina M.A., Muzafarov A.M., Chvalun S.N. Soft Matter. 2018. V. 14, № 48. P. 9755–9759.
[2] Bakirov A.V., Shcherbina M.A., Milenin S.A., Tatarinova E.A., Buzin A.I., Muzafarov A.M., Chvalun S.N. Macromolecules 2024 57, 4, 1625–1631

ACCELERATED NEUTRON TOMOGRAPHY AND AI-ASSISTED RECONSTRUCTION FOR THE STUDY OF ARCHAEOLOGICAL ARTIFACTS FROM THE VOLNA 1 NECROPOLIS

B.A. Bakirov[1],

[1] *Frank Laboratory of Neutron Physics, Joint Institute for Nuclear Research, Dubna, Russia*

E-mail: bulatbakirov@jinr.ru

The Volna 1 necropolis on the Taman Peninsula is one of the key archaeological sites associated with Greek colonization in the Northern Black Sea region. Metal artifacts discovered there are of particular importance for the study of ancient craftsmanship, cultural contacts, burial practices, and corrosion processes. At the same time, such objects are often unique and fragile, which makes non-destructive analytical methods essential for their investigation. Previous work has shown that neutron and X-ray tomography complement each other well in the study of archaeological finds from Volna 1: neutron imaging is highly informative for detecting internal corrosion products, hidden voids, and features associated with light elements, whereas X-ray tomography provides high-quality visualization of dense metallic regions. Their combined use makes it possible to characterize both preservation state and technological features of ancient objects without physical intervention.

A major practical limitation of neutron tomography, however, is the long acquisition time required to collect a sufficiently dense set of radiographic projections. This reduces throughput, complicates the study of series of artifacts, and is especially undesirable for valuable archaeological material. In earlier work, convolutional neural networks were explored as a tool for reconstruction of neutron tomography from incomplete projection sets, showing that the number of required projections could be reduced substantially while preserving acceptable reconstruction quality. This direction is especially promising for cultural heritage studies, where measurement time, activation concerns, and access to beam facilities are critical constraints.

In the present study, we develop this approach further by addressing the reconstruction problem in a form that is more suitable for sparse-angle neutron tomography. Instead of treating the task as a classification or segmentation problem, we formulate it as image-to-image completion of the sinogram followed by reconstruction in image space. The input consists of a sparse sinogram acquired on a reduced angular grid, while the target is the full sinogram corresponding to a standard acquisition geometry. To improve physical consistency, the measured angular rows are preserved explicitly, and the neural network predicts only the missing information. This hard data-consistency strategy helps prevent degradation of experimentally measured projections and stabilizes training.

The model combines two stages. In the first stage, a convolutional network reconstructs the missing angular information in the sinogram. In the second stage, a refinement network operates directly in reconstruction space and corrects residual artifacts after filtered backprojection. This dual-domain strategy is motivated by the fact that global consistency is easier to recover in projection space, while local fine details and object morphology are more naturally corrected in image space. To improve the fidelity of internal features, the training procedure includes object-focused supervision in reconstruction space, with increased emphasis on the artifact region and its internal structure rather than on the empty background.

The proposed pipeline is aimed not only at improving visual quality, but also at preserving archaeologically relevant information: internal cavities, corrosion patterns, density heterogeneities, cracks, and technological traces that may reflect manufacturing history or post-depositional alteration. This is especially important for finds from Volna 1, where the interpretation of metal composition, preservation state, and production technology depends

strongly on the reliability of internal structural data. In practical terms, accelerated tomography based on sparse-angle acquisition and neural reconstruction may make it possible to investigate larger numbers of artifacts, shorten beam time, and reduce the burden on unique museum and excavation materials.

The results obtained so far indicate that AI-assisted reconstruction from incomplete projection data can significantly improve the efficiency of neutron tomography while retaining physically meaningful internal structure. In the context of the Volna 1 necropolis, this opens new possibilities for systematic, non-destructive study of ancient metal artifacts and for integrating advanced imaging methods into archaeological research, conservation planning, and the reconstruction of ancient technological traditions. The combination of neutron tomography, X-ray tomography, and neural-network-based reconstruction therefore represents a promising interdisciplinary framework for the investigation of cultural heritage materials from the Classical world.

This study was supported by the Russian Science Foundation, grant No. 23-18-00196.

STUDY OF SMALL-ANGLE NEUTRON SCATTERING IN CARBON FIBERS MODIFIED WITH BOEHMITE AND MAGNETIC PARTICLES

M. Balasoiu[1,2,3], S.A. Astaf'eva[4], E.V. Ivanova[4], E.A. Lebedeva[4], D.K. Trukhinov[4], A.H.A. Elmekawy[1,5], O.I. Ivankov[1], S.E. Kichanov[1]

[1] *Joint Institute of Nuclear Research, Dubna, Moscow Region, 141980, Russia*
[2] *West University of Timisoara, Timisoara, Romania*
[3] *Horia Hulubei National Institute for R&D in Physics and Nuclear Engineering, Bucharest - Magurele, Romania*
[4] *Institute of Technical Chemistry of UB RAS–Affiliation of Perm Federal Research Centre of Ural Branch of Russian Academy of Sciences, Perm, Russia*
[5] *Department of Experimental Nuclear Physics, Nuclear Research Center, Egyptian Atomic Energy Authority, Cairo, Egypt*

E-mail: balas@jinr.int

Application of polyacrylonitrile (PAN) derived carbon fibers (CFs), are of great interest in the field of design and construction of supercapacitors, adsorption of volatile organic compounds, storage and separation of gasses, due to their developed micro-porosity and high specific surface area. Their high mechanical properties in combination with strength-to-weight ratio, allows to use them in the aerospace, defense and energy industries, as well as in other engineering and construction industries [1, 2]. Moreover, the inert nature of carbon fiber, along with the above-mentioned properties, creates favorable conditions for its use in medical purposes.

The complexity of the carbon fiber structure is due to the multistage chemical and structural transformations occurring in the PAN-precursor during the stages of thermostabilization and carbonization. Therefore, its investigation involves multiple characteristic length scales that require specific techniques, for example, from spectroscopic techniques for probing molecular or atomic structures, X-ray diffraction for identifying crystalline or amorphous domains, or both optical and electron microscopy [3].

The microstructure of three types of PAN carbon fibers – virgin, recycled, and functionalized with nitric acid was investigated using the small-angle X-ray scattering (SAXS), and characteristic sizes of elongated nano-objects – fibrils for each type of carbon fiber and features of their surfaces and distribution inside the fiber were determined [3].

This work presents preliminary results of small-angle neutron scattering (SANS) studies of the structure of carbon fibers modified with boehmite and magnetic particles [4, 5], with the aim of obtaining hybrid fillers for polymer-based composite materials.

[1] E.A. Lebedeva, E.V. Ivanova, D.K. Trukhinov, T.S. Istomina, N.S. Knyazev, A.I. Malkin, V.A. Chechetkin, A.N. Korotkov, M. Balasoiu, S.A. Astaf'eva (2024). Electrophysical Characteristics of Acrylonitrile Butadiene Styrene Composites Filled with Magnetite and Carbon Fiber Fillers. Polymers. 16(15), 2153. https://doi.org/10.3390/polym16152153

[2] E.V. Kornilitsina, E.A. Lebedeva, S.A. Astaf'eva, D.K. Trukhinov, N.S. Knyazev, A.I. Malkin, S.T. Knyazev, A.N. Korotkov, M. Balasoiu (2023). Enhanced electrodynamic properties acrylonitrile butadiene styrene composites containing short-chopped recycled carbon fibers and magnetite. Diamond and Related Materials. 135, 109814 https://doi.org/10.1016/j.diamond.2023.109814

[3] M. Bălășoiu, E. Ivanova, E. Lebedeva, S. Astaf'eva, D. Trukhinov, O. Ivankov, O. Lis, A. Rutkauskas (2026). Study of Virgin, Reclaimed and Functionalized Carbon Fibers using Small-Angle X-ray Scattering. Romanian Journal of Physics. 71(1-2), 302(13). https://doi.org/10.59277/RomJPhys.2026.71.601

[4] D.K. Trukhinov, E.A. Lebedeva, S.A. Astaf'eva, A.Sh. Shamsutdinov, E.V. Kornilitsina, M. Balasoiu (2023). Seed-assisted hydrothermal fabrication of nanostructured boehmite coating on carbon fiber. Surface and Coatings Technology. 452, 129083 https://doi.org/10.1016/j.surfcoat.2022.129083
[5] M. Balasoiu, S.A. Astaf'eva, E.V. Ivanova, E.A. Lebedeva, D.K. Trukhinov, A.H.A. Elmekawy, O. Ivankov, S.E. Kichanov (2026). SANS study of polyacrylonitrile - based carbon fibers modified with magnetic nanoparticles. J. Surf. Investig. (accepted)

MORPHOLOGY-DEPENDENT PLASMON-FREE SERS ENHANCEMENT IN CRYSTALLINE WSE_2 AND WTE_2

N.M. Belozerova[1], A.A. Ushkov[1], D.V. Dyubo[1], A.V. Syuy[1], S.M. Novikov[1], G.I. Tselikov[1], A.V. Arsenin[1]

[1] *Center for Photonics and 2D Materials, Moscow Institute of Physics and Technology, 141701, Dolgoprudny, Russia*

E-mail: belozerova.nm@mipt.ru

The development of reproducible and stable plasmon-free substrates for surface-enhanced Raman scattering (SERS) is crucial for advancing practical applications in analytical chemistry. Conventional plasmonic platforms based on noble metals often face fundamental limitations, including a "reproducibility crisis" caused by the stochastic formation of electromagnetic "hot spots," as well as chemical instability and potential cytotoxicity [1,2]. As a reliable alternative, materials implementing the chemical enhancement mechanism (CM), which is based on photoinduced charge-transfer processes, are being actively investigated. Layered transition-metal dichalcogenides (TMDCs) have become a promising platform for studying CM-SERS due to their unique electronic properties and high chemical stability [3–5]. However, their analytical performance is often limited by the chemical inertness of pristine crystalline basal planes featuring coordinatively saturated bonds. The creation of chemisorption-active sites therefore requires targeted defect engineering.

This work presents a comparison between crystalline flakes and nanoparticles of tungsten diselenide (WSe_2) and tungsten ditelluride (WTe_2). The flakes were produced by quasi-equilibrium liquid-phase ultrasonic exfoliation, preserving the low-defect structure of the bulk crystal. In contrast, spherical nanoparticles were synthesized using a nonequilibrium method—femtosecond pulsed laser ablation in liquids.

Structural analysis (TEM and electron diffraction) showed that, despite the extreme conditions of laser ablation, the obtained WSe_2 and WTe_2 nanoparticles retain a high degree of crystallinity in their cores, comparable to that of the exfoliated flakes. This makes it possible to rule out phase transitions or amorphization as confounding factors and to focus on the role of morphology and surface defects.

SERS measurements using the dye crystal violet (CV) demonstrate that nanoparticle-based substrates consistently outperform their flake-based counterparts, achieving enhancement factors in the $\sim 10^4$ range, typical of chemical enhancement, whereas flakes exhibit enhancement factors an order of magnitude lower ($\sim 10^3$). The limit of detection (LOD) for the nanoparticles was 10^{-7} M.

The improved performance of the nanoparticles is attributed to a substantially higher density of structurally induced active sites, including edges, point defects, and high-curvature regions inherent to their morphology. This defect-enriched surface promotes efficient, defect-mediated charge transfer between the substrate and the analyte. Overall, this study demonstrates that morphology engineering via nonequilibrium synthesis is a powerful and universal strategy for designing high-performance SERS platforms, paving the way toward robust and reproducible analytical systems.

This research was funded by the Russian Science Foundation, grant number 25-79-00214.

[1] R. Pilot (2019). A review on surface-enhanced Raman scattering. Biosensors. 9(2), 57
[2] M.A. Tahir (2021). Surface-enhanced Raman spectroscopy for bioanalysis and diagnosis. Nanoscale. 13(27), 11593-11634.

[3] A.A. Ushkov (2025). Femtosecond laser ablation and fragmentation for TMDC nanoparticles synthesis: A comparative study. Applied Surface Science. 707, 163547.
[4] A.A. Ushkov (2024). Tungsten Diselenide Nanoparticles Produced via Femtosecond Ablation for SERS and Theranostics Applications. Nanomaterials. 15(1), 4.
[5] A.A. Ushkov (2025). Laser-Synthesized Amorphous $PdSe_{2-x}$ Nanoparticles: A Defect-Rich Platform for High-Efficiency SERS, Photocatalysis, and Photothermal Conversion. Advanced Materials Interfaces. e00902.

TOWARDS NEUTRON CRYSTALLOGRAPHY OF MICROBIAL RHODOPSINS

V. Borshchevskiy[1,2]

[1] *Moscow Institute of Physics and Technology, Moscow, Russia*
[2] *Frank Laboratory of Neutron Physics, Joint Institute for Nuclear Research, Dubna, Russia*

E-mail: borshchevskiy@gmail.com

Microbial rhodopsins are a large family of seven-helical transmembrane retinal-binding proteins, currently comprising tens of thousands of representatives. Their primary biological functions include light-driven ion transport across biological membranes and photoreception. Owing to their versatile biological roles and relatively simple architecture, microbial rhodopsins have become a major focus of modern biophysical research, particularly in bioenergetics. At the same time, they have found important practical applications, most prominently in optogenetics, where engineered rhodopsins are widely used to control cellular activity with light.

Among the most widespread functions within this protein family is light-driven proton transport across the membrane bilayer. Since proton transfer is fundamentally governed by the positions and dynamics of hydrogen atoms, neutron diffraction represents an especially attractive approach for studying microbial rhodopsins. Unlike X-ray crystallography, neutron diffraction can directly visualize hydrogen/deuterium atoms and protonation states, providing unique information about hydrogen-bond networks, internal water molecules, Schiff base chemistry, and proton-transfer pathways.

In this talk, we will discuss the key requirements for successful neutron diffraction experiments on crystals of microbial rhodopsins, summarize recent progress toward obtaining neutron-diffraction-quality crystals of microbial rhodopsins, outline the methodological advances that make such experiments feasible, and discuss the major unresolved problems that still limit the application of neutron crystallography to this important class of light-driven membrane proteins.

INVESTIGATING STRUCTURAL PERIODICITY OF SEGMENTED/NONSEGMENTED MAGNETIC NANOWIRE ARRAYS BY SANS METHOD

A.H.A. Elmekawy[1,2,3], O.I. Ivankov[1], A. Islamov[1], A.I. Kuklin[1]

[1] *Joint Institute for Nuclear Research, Dubna, Russia.*
[2] *Experimental Nuclear Physics Department, Nuclear Research Centre, Egyptian Atomic Energy Authority, Cairo 13759, Egypt.*
[3] *Cyclotron Facility, Nuclear Research Centre, Egyptian Atomic Energy Authority, Cairo, Egypt.*

E-mail: ahmedalmekawy@ymail.com

The study of nanomagnetic materials is of great importance in scientific and industrial circles due to their use in many applications [1]. Numerous studies have revealed that magnetic properties are strongly correlated with geometrical parameters of used the system. For instance, size or diameters of 2D nanoparticles or the aspect ratio (Length to Diameters) of 3D systems like nanowires and nanorods are considerable parameters.

In the current study we applied small angle neutron scattering method at YuMO spectrometer to investigate structural periodicity of different series of segmented/non segmented magnetic nanowire arrays synthesised with different spatial ordered structure. Results showed that studied systems have 2D hexagonal lattice structure where position of given peaks allow to determine the periodicity for each series by deducing their lattice parameter.

It is quite important to investigate periodicity conservation of studied systems by considering averaging over orientations of porous arrays which is critical factor for application requirements as for information storage and acoustic sensors as well [2,3]. Results also considered very important for users of YuMO spectrometer studying similar systems, like nanoporous membranes or another with periodicity in the range (10 - 110 nm) [4] with reasonable accuracy.

[1] Krishnan KM. Fundamentals and applications of magnetic materials. Oxford University Press; 2016.
[2] Rial J., Proenca M.P. A Novel Design of a 3D Racetrack Memory Based on Functional Segments in Cylindrical Nanowire Arrays // Nanomaterials. 2020. Vol. 10, № 12. P. 403.
[4] McGary P.D. et al. Magnetic nanowires for acoustic sensors (invited) // J. Appl. Phys. 2006. Vol. 99, № 8. P. 08B310.
[5] A.A. Belogorlov, et al, Application of Small-Angle Neutron Scattering to Study the Filling of Nanoporous Material with a Nonwetting Liquid, // Physics of Atomic Nuclei, 2025, Vol. 88, No. 11, pp. 2288–2293.

RADIATION EFFECTS IN CONDENSED MATTER PHYSICS

V.V. Harutyunyan[1], E.M. Aleksanyan[1], N.E. Grigoryan[1], A.A. Sahakyan[1], A.A. Martirosyan[1]

[1] *A.Alikhanyan National Science Laboratory, Yerevan, Armenia*

E-mail: vharut@yerphi.am

Al_2O_3 corundum single crystal irradiated with high-energy particles is one of the most important practical dielectrics used as active elements in lasers, passive shutters frequency tunable over a wide range of the spectrum, and ionizing radiation detectors.

The work is aimed at studying radiation effects in wide-bandgap corundum single crystals under low doses of electron irradiation.

It is known that irradiation of a solid with high-energy particles leads to changes in its electrophysical and optical properties. With respect to electrical properties, semiconductors are particularly sensitive, whereas with respect to optical properties - transparent dielectrics.

This effect, called in [1] “the low-dose effect”, is manifested in imperfect samples that have before irradiation large amounts of loosely bound atoms or defective atomic configurations in the crystal lattice. Although the concentrations of such defects are much lower than the concentrations of normal lattice sites, the energy required to rearrange such defects under the action of fast electrons is much less than the energy required to knocking an atom out of normal lattice sites. Therefore, the efficiency of the rearrangement of loosely bound atoms under the influence of electron irradiation may turn out to be significantly higher than the efficiency of knocking out an atom from normal sites, and at low irradiation doses the radiation-stimulated "ordering" of the crystal lattice prevails over the defect formation. At doses where the "ordering" process is close to saturation, crystal degradation caused by the knocking atoms out of normal sites, becomes dominant.

We have discovered this effect for corundum single crystals. It is considered an established fact that the characteristic additional absorption bands 205 nm (6.05 eV), 230 nm (5.4 eV) and 255 nm (4.8 eV) observed in the UV region of absorption spectrum ***of *C-A1$_2$0$_3$*** irradiated with neutrons, protons and electrons, correspond to ***F*** (oxygen vacancy with two localized electrons) and ***F**** (oxygen vacancy with one localized electron) color centers (IIO), correspondingly [1].

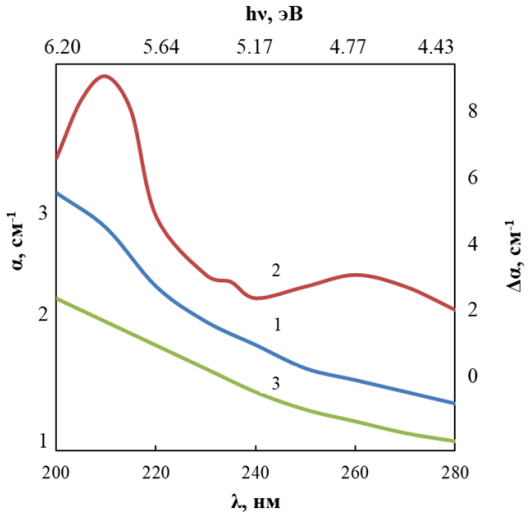

Fig. 1 Absorption spectra of corundum grown by the horizontal crystallization method. 1 - non-irradiated, 2 - irradiated with 50 MeV energy electrons at a dose of $3x10^{17}$ el/cm^2, 3 - irradiated with 50 MeV energy electrons at a dose of $8x10^{10}$ el/cm^2.

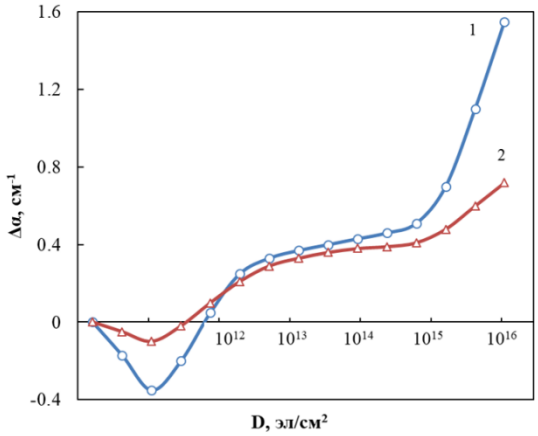

Fig. 2. Dependence of the change in the absorption coefficient of corundum, grown by horizontal crystallization, on the 50 MeV electrons radiation dose. 1 - 205 nm (6.05 eV), 2 - 255 nm (4.8 eV).

The studied samples of non-activated corundum single crystals were grown by the Verneuil method, horizontal crystallization and a modified Kyropoulos method and represented polished 0.05 - 0.1 cm thick plane-parallel plates. The samples were irradiated at temperatures of 77 and 300 K. After each dose of irradiation, absorption spectra were recorded at room temperature. As the wavelength decreases, the degree of enlightenment increases. The transmission of corundum reaches its maximum increase at doses of 10^{11} el/cm^2.A decrease in the absorption of corundum in the UV region was observed for crystals grown by any of the above methods, and also when irradiated with 7.5 MeV electrons. Thermal heating of samples was also studied in the range of 100 - 300°C, however no decrease in corundum absorption was observed. Thus, for the first time, an optical manifestation of the low-dose effect, namely an increase in the transparency of the crystal under the action of irradiation with fast electrons at low doses (10^{11} el/cm^2), was discovered for corundum single crystal.

The following main manifestations of the effect of small doses have been established:

- **Structure ordening:** Radiation exposure can lead to annihilation of defects thus improving the crystal lattice, which is often observed at low doses of radiation.
- **Subsurface effects**: Small doses have the most pronounced effect on the structure of the subsurface layers of crystals.
- **Response nonlinearity:** The effect is not always linear with dose, it may be greatest at certain very low levels of exposure.

Sensitization: Small doses can increase the sensitivity of materials to subsequent loads, making them brittle.

These effects are critical for material science in nuclear power and space applications, where materials are exposed to constant but low-level radiation, which requires assessment of their long-term reliability.

[1] V.V. Harutyunyan, E.M. Aleksanyan, V.V. Arzumanyan, A.O. Badalyan, (2021), Radiation-Induced Phenomena in Wide-Gap Laser Materials Used in High-Radiation Areas, Armenian Journal of Physics, vol.14, issue 3, pp.142-147.

MAGNETIC PHASE TRANSITION IN $Y_{1-x}Tb_xMn_6Sn_6$ COMPOUNDS

S.V. Grigoriev[1], N.A. Grigoryeva[2], A.H.A. Elmekawy[3,4], A.Kh. Islamov[3], A.I. Kuklin[3], A.M. Bartashevich[2], E.G. Gerasimov[2], N.V. Mushnikov[2]

[1] *Petersburg Nuclear Physics Institute, NRC "Kurchatov Institute", Gatchina, Russia*
[2] *M.N. Mikheev Institute of Metal Physics UB RAS, Yekaterinburg, Russia*
[3] *Joint Institute for Nuclear Research, Dubna, Moscow region, Russia*
[4] *Nuclear Research Center, Egyptian Atomic Energy Authority, Cairo, Egypt*

E-mail: grigor@lns.pnpi.spb.ru

The magnetic structure of $Y_{1-x}Tb_xMn_6Sn_6$ compounds (x = 0.0, 0.10, 0.25) was studied using small-angle neutron scattering (SANS) in the temperature range from 260 to 400 K, above and below the critical temperature T_C. The dependences of the SANS intensity on the momentum transfer demonstrate the presence of three contributions to the scattering, which differ in the scattering function (Q-dependence of the intensity) and in the evolution of these dependences with temperature. Scattering by large-scale magnetization domains is observed below T_C and is described by the Porod law Q^n. The Bragg peak from the incommensurate magnetic structure is also observed below T_C in the region of large Q. Ornstein-Zernike scattering by critical magnetization fluctuations is most pronounced at high temperatures. The order-disorder transition temperature, determined from the maximum scattering by critical fluctuations, increases with concentration: T_C = 300 ± 2 K, 325± 2 K, 353±3 K for compounds with concentrations x = 0, 0.1, 0.25. An incommensurate magnetic structure with a complex temperature behavior is observed in all compounds, with the period of the structure increasing with concentration x. The ferromagnetic component of magnetization was detected only in Tb-doped compounds at $T < T_C$. Above T_C, the magnetic structure disintegrates into fluctuating ferromagnetic planes, giving the occurring magnetic phase transition a quasi-two-dimensional character.

Critical fluctuations, according to the Mermin-Wagner theorem [1], demonstrate the instability of ferromagnetic order in two-dimensional systems and can be described by a new, nonmagnetic order parameter along the c-axis [2]. We argue that slowly fluctuating ferromagnetic planes are capable of ordering into a variety of spin structures: a complex double helix (x = 0), a conical helix, and a ferrimagnet (x = 0.1, 0.25). The phase transition from the fluctuating phase to the ordered one in YMn_6Sn_6 occurs in a complex manner through a system of crossovers, implying that on the basis of fluctuating ferromagnetic planes with a decrease in temperature in the range [300 - 340] K, it is possible to form first an antiferromagnetic commensurate (but fluctuating) phase, then a spiral (but fluctuating) phase, and, finally, a stable spiral phase at $T \approx 300$ K. Doping with a rare earth element simplifies the phase transition and the fluctuating Mn planes are immediately ordered into a collinear magnetic (ferrimagnetic for the Mn-Re plane system) structure. The ferromagnetic component of this ferrimagnetic structure increases with decreasing temperature from T_C to $T \approx 300$ K, and then “freezes”, thereby confirming the hypothesis of a phase transition from a two-dimensional magnetic system to its three-dimensional analogue.

[1] N.D. Mermin, et al, (1966). Absence of Ferromagnetism or Antiferromagnetism in One- or Two-Dimensional Isotropic Heisenberg Models. Phys. Rev.Lett. 17(22), 1133-1136.
[2] P. Chandra, et al, (1990). Ising transition in frustrated Heisenberg models. Phys. Rev.Lett. 64, 88–91.

ON THE SHOULDERS OF GIANTS: FROM YuMO'S BRILLIANT PAST TO ITS BRIGHT FUTURE

O.I. Ivankov[1], T.N. Murugova[1], A.Kh. Islamov[1], A.H.A. Elmekawy[1,2], A.A. Nabiyev[1,3], A.V. Rogachev[1,4], T.V. Cuong[1,5], V. Skoi[1], Yu.S. Kovalev[1], M. Balasoiu[1,6,7], A.V. Vlasov[1,4], Yu.L. Ryzhykau[1,4], V. Borshchevskiy[1,4], A.G. Solovjev[1], N. Kučerka[1,8], V.I. Gordeliy[1,4] and A.I. Kuklin[1,4]

[1] *Joint Institute for Nuclear Research, Dubna, Russia*
[2] *Nuclear Research Centre, Egyptian Atomic Energy Authority, Cairo, Egypt.*
[3] *Ministry of Science and Education Republic of Azerbaijan, Institute of Physics, Baku, Azerbaijan*
[4] *Moscow Institute of Physics and Technology, Dolgoprudny, Russia*
[5] *Dalat Nuclear Research Institute, Lam Dong, Viet Nam*
[6] *Horia Hulubei National Institute for R&D in Physics and Nuclear Engineering, Bucharest - Magurele, Romania*
[7] *Institute of Technical Chemistry of UB RAS–Affiliation of Perm Federal Research Centre of Ural Branch of Russian Academy of Sciences, Perm, Russia*
[8] *Department of Physical Chemistry of Drugs, Comenius University Bratislava, Bratislava, Slovakia*

E-mail: ivankov@jinr.ru, alexander.iw.kuklin@gmail.com

YuMO, the time-of-flight small-angle neutron scattering spectrometer at the IBR-2 pulsed reactor, is a rare example of a scientific instrument whose competitiveness has been preserved through continuous conceptual, technical, and software modernization. Emerging from the pioneering Dubna SANS work of Yu.M. Ostanevich, L. Cser, A.B. Kunchenko and their colleagues, YuMO was built around a principle that remains decisive today: to deliver a high useful neutron flux to the sample and convert it into reliable structural information with maximum efficiency. Its “direct-view” geometry, the time-of-flight technique, and the high peak intensity of IBR-2 made the instrument especially powerful for time-dependent soft-matter and biological systems.

One of YuMO’s key breakthroughs was the implementation of a two-detector system with central holes in the detectors. This concept allowed the transmitted beam to pass through the first detector while two detector positions simultaneously covered a broad momentum-transfer range. Combined with the in-beam vanadium calibration scheme, this approach enabled absolute-scale SANS measurements, reduced auxiliary measurements, and helped ensure stable and reproducible results. As a result, YuMO became not only a high-flux instrument, but also a high-throughput instrument, capable of producing interpretable data rapidly during an experiment.

The same philosophy has guided subsequent upgrades. Over the years, YuMO has acquired advanced sample environments, including precise temperature control, high-pressure systems for liquid samples, magnetic-field capabilities, illumination options, and an flexible automated sample-changing area. The standard sample holder evolved from single-sample operation to computer-controlled measurements of up to 25 samples, while the geometry of the sample environment remained compatible with specialized devices. Automation has become an essential part of the instrument: SONIX+ controls experimental parameters and sample-environment devices, while SAS -based data treatment and on-line processing provide rapid feedback to users and allow beam-time strategies to be adjusted during the experiment.

The scientific impact of this development is illustrated by experiments on lipid phase transitions, DNA–lipid complexes, and amyloid-beta peptide interactions with lipid

membranes, where YuMO's flux, dynamic range, absolute calibration, and temperature stability were essential for observing structural transformations and kinetic processes. These examples show that the instrument's technical architecture directly translates into scientific capability.

The future of YuMO is now being shaped by cold-neutron capabilities and detectors modernization. The cold moderator has expanded opportunities at longer wavelengths and so the lower scattering momentum transfer, while the upgraded boron-based direct-beam detector provides stable, efficient transmission monitoring and rapid neutron-absorption measurements. The ongoing commissioning of a position-sensitive detector with a central hole opens the way toward improved studies of anisotropic scattering, kinetic processes, and complex sample environments.

The talk will present selected experiments performed at YuMO and discuss how the ideas laid down by its founders continue to define the instrument's bright future as a modern, automated, high-flux SANS platform for soft matter, materials science, and structural biology.

COMPARISON OF STRUCTURAL FEATURES OF OLIGOMERIC AND MONOMERIC TISSUE TRANSGLUTAMINASE

S.D. Ivashchenko[1], D.V. Sidorov[1] and A.V. Vlasov[1]

[1] *Research Center for Molecular Mechanisms of Aging and Age-Related Diseases, Moscow Institute of Physics and Technology (National Research University), 141701 Dolgoprudny, Russia*

E-mail: ivashchenko.sd@phystech.edu

Human transglutaminase 2 (TG2) is a multifunctional enzyme that plays a major role in tumor progression, metastasis, and resistance to chemotherapy across multiple cancers, including breast, pancreatic, ovarian, and glioblastoma [1]. Elevated TG2 expression correlates with poor prognosis and promotes epithelial-to-mesenchymal transition (EMT), cancer stem-cell survival, extracellular matrix remodeling, and resistance to apoptosis through activation of nuclear factor kappa-light-chain-enhancer of activated B cells (NF-κB) and integrin-mediated signaling pathways. In pancreatic and ovarian cancers, TG2 overexpression has been directly linked to increased metastatic potential and reduced response to standard chemotherapeutics [2]. Importantly, recent studies demonstrated that forced oligomerization of TG2 induces cytotoxicity and therefore promotes death of cancer cells overexpressing TG2; notably, recent research showed that TG2 oligomerization can be pharmacologically controlled using the small-molecule ligand LM11 [3, 4]. However, structural features of oligomeric TG2 still remain unknown, hindering rational design of compounds that enhance therapeutically beneficial oligomerization.

Here, we developed a protocol of recombinant TG2 expression and purification and obtained highly homogeneous monomeric protein. We further established controlled oligomerization of TG2 achieved at 20 °C, 5 mM calcium, and TG2-specific inhibitors: iodoacetamide and LM11. Small-angle X-ray scattering (SAXS) measurements were collected for both monomeric and oligomeric states of TG2, enabling comparative analysis and structural modeling of TG2 oligomers. These results provide structural characterization of TG2 oligomerization and lay the groundwork for structure-based design of next-generation modulators that enhance TG2-mediated cytotoxicity in cancer cells.

The study was supported by the RSF 24-14-00295.

[1] E.Zaltron, F.Vianello, A.Ruzza, A.Palazzo, V.Brillo, I.Celotti, M.Scavezzon, F.Rossin, L.Leanza., F.Severin (2024). The Role of Transglutaminase 2 in Cancer: An Update. International Journal of Molecular Sciences. 25(5), 2797.

[2] K.Mehta, A.Kumar, H.I.Kim (2010). Transglutaminase 2: a multi-tasking protein in the complex circuitry of inflammation and cancer. Biochemical Pharmacology. 80(12), 1921-1929.

[3] N.Kim, W.K.Lee, S.H.Lee, K.S.Jin, K.H.Kim, Y.Lee, M.Song, S.Y.Kim (2017). Inter-molecular crosslinking activity is engendered by the dimeric form of transglutaminase 2. Amino Acids. 49(3), 461-471.

[4] C.Aplin, K.A.Zielinski, S.Pabit (2024). Distinct conformational states enable transglutaminase 2 to promote cancer cell survival versus cell death. Nature Communications Biology. 7, 982.

CRYSTAL AND MAGNETIC STRUCTURE OF COBALT OXIDES AT HIGH PRESSURE AND TEMPERATURE

S.E. Kichanov[1], O.N. Lis[1], D.P. Kozlenko[1], E.V. Lukin[1], and N.T. Dang[2]

[1] *Frank Laboratory of Neutron Physics, Joint Institute for Nuclear Research, Dubna, Russia*
[2] *Institute of Research and Development, Duy Tan University, Danang, Vietnam*

E-mail: ekich@nf.jinr.ru

The study of the crystal and magnetic structure of low-dimensional magnetic compounds is of interest due to their unique physical properties. These include the phenomena of magnetic frustration, ferromagnetism, the formation of exotic magnetic states, etc. From this point of view, $Ca_3Co_2O_6$ is a striking example of a magnetic system with unique magnetic phases due to the geometric topology of its crystal structure [1]. These compounds are interesting model materials for studying the geometry of magnetic interactions along and between one-dimensional structural chains, and on the other hand, there are features in the complex magnetic structure that are highly sensitive to doping and changes in external conditions. The report highlights the results of studies on the effect of manganese doping on the structural and magnetic properties of $Ca_3Co_2O_6$. Detailed studies of the structural and magnetic properties of $Ca_3Co_{2-x}Mn_xO_6$ compounds (x = 0, 0.1, 0.2, and 0.4), using X-ray diffraction and neutron diffraction methods [2]. The magnetic structure of the compound was studied using the DN-12 neutron diffractometer located at the high-flux pulsed reactor IBR-2 (FLNP, Dubna, Russia).

The results of studies on disordered perovskite cobaltites $LaMn_{0.5}Co_{0.5}O_3$ and $YMn_{0.5}Co_{0.5}O_3$ are also presented [3]. In an ideal ordered structure, Co^{2+} and Mn^{4+} ions alternate positions, and superexchange magnetic interactions between cobalt and manganesium ions lead to formation of ferromagnetic ordering. Disordering of cations in perovskite can cause increase of double Mn^{4+}-O-Mn^{4+} or Co^{2+}-O-Co^{2+} exchange interactions, enhancing antiferromagnetic interactions. We present the results of an investigation of the crystal and magnetic structures of orthorhombic $LaMn_{0.5}Co_{0.5}O_3$ and $YMn_{0.5}Co_{0.5}O_3$ compounds using neutron and X-ray diffraction methods in the temperature range 15–300 K and in pressure range up to 30 GPa. The application of high pressures above ~5 GPa leads to a gradual structural phase transition in both materials from an orthorhombic crystal structure with *Pnma* symmetry to *Imma* one, accompanied by anomalies in the behaviour of lattice parameters, unit cell volumes, and some Raman modes under pressure. According to neutron diffraction data at high pressures, the initial ferromagnetic state is suppressed, and there is a noticeable change in Curie temperature from T_C=76 K at ambient pressure down to T_C =38 K at a high pressure of 2.1 GPa.

This work has been supported by the joint grants of the Russian Science Foundation, RSF No:24-42-04002, https://rscf.ru/project/24-42-04002/ and the grant of the Vietnam Academy of Science and Technology, QTRU06.07/24-26.

[1] D.T. Khan, D.P. Kozlenko, S.E. Kichanov, and et al. (2025) Revealing the Electronic Origin of Pressure-Induced Isostructural Transformations in Ca3Co2O6, Journal of Electronic Materials 54:3651–3662.
[2] L.H. Khiem, O.N. Lis, N.T. Nguyen, S.E. Kichanov, et al. (2026) The crystal and magnetic structure of the Ca3Co2O6 manganese-doped compound, Modern Physics Letters B, 40, 2650025.
[3] L.H. Khiem, S.E. Kichanov, O.N. Lis, and et al, (2025) The crystal and magnetic structure of the cation-disordered perovskites, International Journal of Modern Physics B, 39, 25.

DEVELOPMENT OF A FILTER PROTOTYPE BASED ON TUBULAR CERAMIC MEMBRANES WITH A SELECTIVE LAYER OF MXENE $Ti_3C_2T_x$

I.A. Karavaeva[1], D.G. Krotkevich[1], Zh.G. Zabanov[1], E.B. Kashkarov[1]
[1] *National Research Tomsk Polytechnic University, Tomsk, Russia*

E-mail: karavaeva.irishka@gmail.com

Membrane technologies for gas separation and purification are considered promising due to their operational simplicity, high versatility, compactness, scalability, and energy efficiency. Membranes based on two-dimensional carbides (MXenes), such as $Ti_3C_2T_x$, are of particular interest for gas filtration, especially for hydrogen separation [1, 2]. Such thin-film membranes, deposited on tubular porous supports, combine hydrogen selectivity and sufficient mechanical strength [1, 2, 3]. Comprehensive investigation of their gas transport properties over a wide range of temperature (up to 400 °C) and pressure (up to 1 MPa) requires specialized research equipment that ensures gas-tight sealing of tubular samples.

This work focused on three main objectives: 1) obtaining membrane materials from $Ti_3C_2T_x$; 2) developing methods for depositing membrane materials on ceramic tubular supports; 3) development of a filter design using these materials for hydrogen separation and purification. Thus, the aim of this work was to develop and fabricate a prototype filter based on MXene $Ti_3C_2T_x$ on tubular ceramic supports.

In this work, MXene $Ti_3C_2T_x$ was synthesized by selective etching in acid solutions. A typical image of membrane films made from this material is shown in Fig. 1a. It is evident that the resulting films have a layered microstructure formed by the self-assembly of MXene nanoplatelets. The results of X-ray diffraction analysis confirm the formation of MXene nanoplatelets: the diffraction pattern shown in Fig. 1b shows characteristic reflections from the (002), (004), (006), and (008) atomic planes.

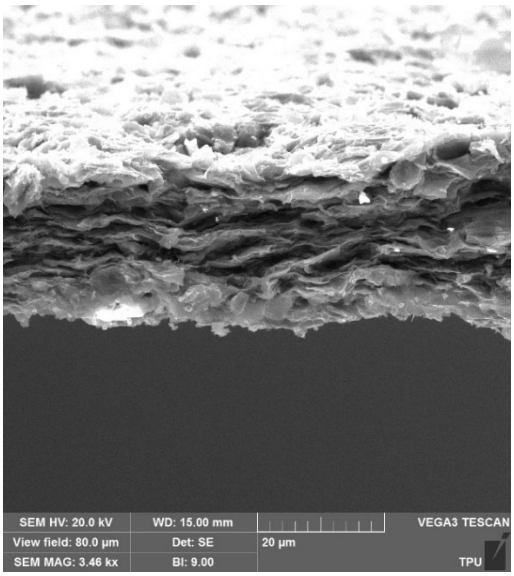

(a)

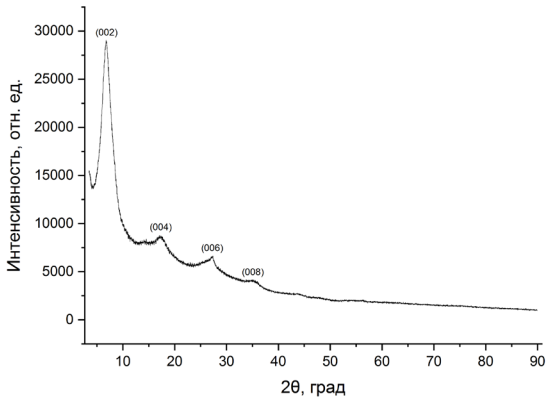

(b)

Figure 1 – SEM image of the microstructure (a) and the corresponding diffraction pattern (b) of a sample of the MXene $Ti_3C_2T_x$ membrane

Studies of the gas permeability of the obtained flat $Ti_3C_2T_x$ membranes showed that hydrogen permeability decreases from $6 \cdot 10^{-12}$ mol/(m·s·$Pa^{0,5}$) at 25 °C to $2.4 \cdot 10^{-12}$ mol/(m·s·$Pa^{0,5}$) at 800 °C, while the selectivity for separating the H_2/N_2 mixture increases from

3.6 to 4.5. The obtained qualitative trends of membrane characteristic changes with increasing temperature are consistent with literature data for a lamellar membrane based on $Ti_3C_2T_x$ with a thickness of 800 nm, formed on a flat porous anodic aluminum oxide support [4]. The results confirm the potential of using MXene $Ti_3C_2T_x$ in membrane gas separation technologies; however, optimization of the interplanar distance (between MXene plates) and the thickness of the selective layer is required to further improve its gas permeability and selectivity.

In this study, membrane elements were formed on tubular porous aluminum oxide supports using vacuum deposition from an aqueous colloidal $Ti_3C_2T_x$ solution. To test the gas permeability and selectivity of the resulting tubular membranes, a prototype filter was designed and manufactured. Its schematic is shown in Figure 2. The cylindrical filter design features high-temperature sealing elements, uniform clamping without damaging the membrane coating, and compatibility with an existing Gas Permeation Machine (GPM) test setup.

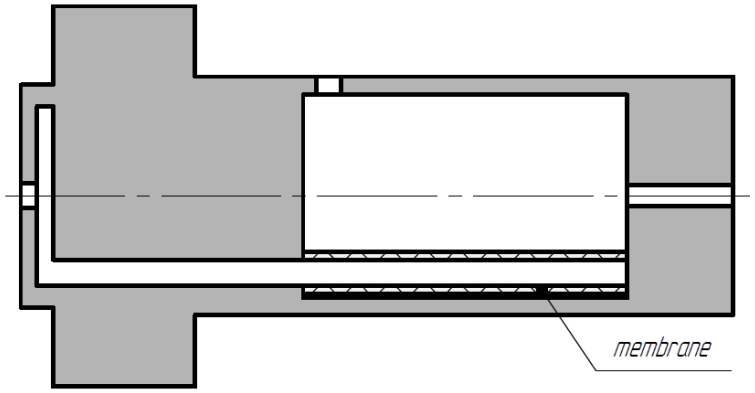

Figure 2 – Schematic of the prototype filter for studying the gas permeability and selectivity of tubular membranes

The developed filter prototype is currently being prepared for testing. The simplicity of the design, scalability, and ability to operate over a wide range of temperatures and pressures allow the proposed solution to be considered as the basis for creating a universal rig for studying the gas separation characteristics of tubular membranes.

The research was funded by the Governmental Program Science, project №FSWW-2024-0001.

[1] Ding L., Wei Y., Li L., Zhang T., Wang H., Xue J., Ding L.-X., Wang S., Caro J., Gogotsi Y. MXene Molecular Sieving Membranes for Highly Efficient Gas Separation // MXenes. — Singapore: Jenny Stanford Publishing, 2023. — P. 1–21.

[2] Luo M., Zhao Y., Wei Y., Wang H. Dual-module integration of large-area tubular 2D MXene membranes for H_2 purification // Chemical Engineering Science. — 2023. — Vol. 281. — P. 119392. — DOI: 10.1016/j.ces.2023.119392.

[3] Zhang Q., Meng X., Yang N. Gas Separation Technologies: MXenes-Based Membrane Systems // MXenes: From Discovery to Applications. — Washington, DC: American Chemical Society, 2023. — Vol. 1443. — P. 107–128. — DOI: 10.1021/bk-2023-1443.ch006.

[4] Jin Y., Fan Y., Meng X., Zhang W., Meng B., Yang N., Liu S. Theoretical and Experimental Insights into the Mechanism for Gas Separation through Nanochannels in 2D Laminar MXene Membranes // Processes. — 2019. — Vol. 7, No. 10. — P. 751. — DOI: 10.3390/pr7100751.

DEVELOPMENT OF REFLECTOMETRIC STUDIES IN OSCILLATING MAGNETIC FIELDS AT THE IBR-2 REACTOR

E.D. Kolupaev[1], V.D. Zhaketov[2] and Yu.V. Nikitenko[1]

[1] *International intergovernmental scientific research organization Joint Institute for Nuclear Research, Frank Laboratory of Neutron Physics, Dubna, Russia*
[2] *National Research University Moscow Institute of Physics and Technology, Moscow, Russia*

E-mail: kolupaev.ed15@physics.msu.ru

Polarized neutron reflectometry (PNR) in an external static magnetic field is one of the principal techniques for investigating thin-film and multilayer magnetic structures. By measuring the four spin-dependent reflection channels, one can separate the nuclear and magnetic contributions to the effective optical potential and thereby reconstruct the depth profile of magnetization along the surface normal. Owing to this depth sensitivity, PNR has become a standard tool for the analysis of artificially structured magnetic materials and spintronic heterostructures [1–4].

Conceptually, RF-PNR retains the central element of magnetic resonance, namely spin reversal in the combined action of a static field and a transverse oscillating magnetic field. However, the physical nature of the measured observable differs fundamentally from that in conventional nuclear magnetic resonance (NMR). In NMR, one detects the collective macroscopic response of the spin subsystem, whereas in polarized neutron reflectometry one measures the reflection probability of an individual neutron in a given spin channel. This probability depends on the depth profile of the nuclear and magnetic potentials, interface-induced interference, the magnitude and orientation of the local magnetic field, and Zeeman corrections to the scattering kinematics. As a consequence, RF-PNR combines resonance selectivity with nanometer-scale depth sensitivity, a capability that is not accessible to conventional NMR techniques [1–6].

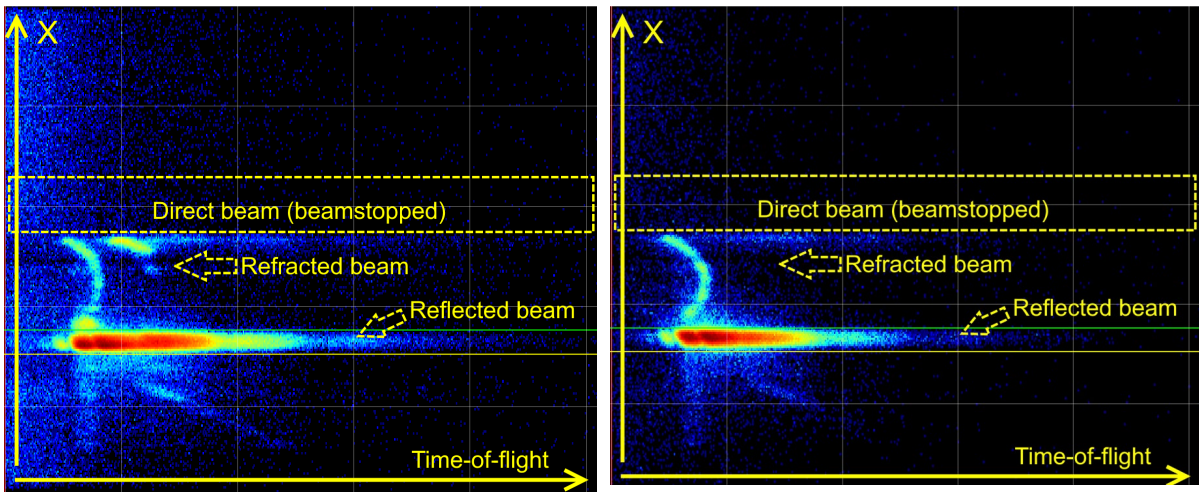

Fig.1: The PSD dependence of the intensity of the reflected neutron beam on the wavelength for the "+-" (left) and "++" (right) components in the oscillating field for sample CaTiO3 // Fe (50nm). H0 = 400 Oe, H1 = 5Oe, θ = 4.8 mrad, λ crit (Fe) = 3A. Larmor frequency ωL = 23.2 MHz

First proof-of-work results (Fig.1) were obtained using a model sample with a simple structure: CaTiO3 // Fe (50nm). A dedicated experimental module for neutron reflectometry in high-frequency oscillating magnetic fields was successfully developed and tested at the REMUR spectrometer. The measurements confirmed the influence of oscillating magnetic fields on polarized neutron reflection. The experiments demonstrated that the system operates

reliably and is suitable for such measurements. A redistribution of the neutron beam intensity was observed as a function of the applied field frequency.

During this experiment we faced a few complications. Firstly, PSD is extremely vulnerable to electromagnetic interference. Therefore, enhanced shielding of the connecting cables and the detector itself is required, along with reliable RF grounding bus. Another limiting factor is sample heating during the experiment. The thermal power when generating an oscillating field of about 5 Oe reaches 140 W. At the same time, the power limit of the assembled module exceeds 2 kW.

The development of polarized neutron reflectometry in an oscillating magnetic field is therefore of considerable importance for the study of modern magnetic and spintronic systems. This approach makes it possible to investigate not only static magnetization profiles in thin films, but also dynamic magnetic processes, spin-flip transitions, resonant phenomena, and effects associated with spatially inhomogeneous internal fields. As a result, the method is particularly promising for the characterization of multilayer nanostructures in which both the depth distribution of magnetic parameters and their high-frequency dynamics are of fundamental importance [2–8].

[1] J. F. Ankner, G. P. Felcher, Polarized-neutron reflectometry, Journal of Magnetism and Magnetic Materials 200 (1999) 741–754.
[2] C. F. Majkrzak, K. V. O'Donovan, N. F. Berk, Polarized Neutron Reflectometry, in: Neutron Scattering from Magnetic Materials (2006).
[3] C. F. Majkrzak, Polarized neutron reflectometry, Physica B: Condensed Matter 221 (1991) 342–356.
[4] H. Zabel, Polarized neutron reflectivity and scattering from magnetic nanostructures and thin films, in: Handbook of Magnetism and Advanced Magnetic Materials (2007).
[5] S. V. Kozhevnikov, F. Radu, Yu. V. Nikitenko, V. L. Aksenov, Reflection of neutrons from a magnetic film placed in static and oscillating magnetic fields, Journal of Surface Investigation: X-ray, Synchrotron and Neutron Techniques 6(5) (2012) 784–789.
[6] B. B. Maranville et al., Measurement and modeling of polarized specular neutron reflectivity in large magnetic fields, Journal of Applied Crystallography 49 (2016) 1121–1129.
[7] D. S. Hussey et al., Simultaneous polarization analysis of Zeeman splitting in polarized neutron reflectometry using a polarized 3He neutron-spin filter, Applied Physics A 74 (2002) s975–s977.
[8] G. P. Felcher et al., Observation of the Zeeman splitting for neutrons reflected from a magnetic film, Physica B: Condensed Matter 221 (1996) 494–497

INVESTIGATIONS OF MAGNETIC WAVEGUIDES AT REFLECTOMETER REMUR

S.V. Kozhevnikov[1], E.D. Kolupaev[1], D.A. Norov[1] and V.D. Zhaketov[1,2]

[1] *Frank Laboratory of Neutron Physics, JINR, Dubna, Russia*
[2] *Moscow Institute of Physics and Technology, Dolgoprudny, Russia*

E-mail: kozhevn@nf.jinr.ru

A neutron beam width defines a spatial resolution at investigations of local microstructures therefore development of neutron focusing devices is an actual task. The existing focusing devices (bent crystal-monochromators, parabolic mirror waveguides, refractive lenses, etc.) have the following restrictions: the minimal microbeam spot 50 μm, high background and inhomogeneous microbeam.

Neutron tri-layer waveguides (Fig. 1) transform a conventional collimated neutron beam into a very narrow but slightly divergent microbeam exiting from the middle layer of the width d [1]. The advantages of the neutron waveguides are "clean" and narrow (about 1 μm of width) microbeam. Its disadvantages are low intensity and slight angular divergence defined by Fraunhofer diffraction on a narrow slit as $\delta\alpha_f \propto \lambda/d$. Here λ is the neutron wavelength. Resonant enhancement of the standing waves and neutron channelling along the middle layer exist in the waveguides simultaneously. Review on investigations and applications of the planar neutron waveguides is done in [2]. For example, the waveguide with magnetic middle layer was used for characterization of weakly magnetic films, the waveguides with external magnetic layers can be applied for a controlled chain reaction with U inside the guiding layer [3] and the non-magnetic waveguide was used for spatial scanning of an amorphous magnetic wire by the polarized neutron microbeam.

As the neutron microbeam intensity is very low, the optimization of the waveguide structure is the important task. In this work, we investigated the microbeam intensity as a function of the neutron scattering length density (SLD).

Experiment was done at the time-of-flight reflectometer REMUR of the reactor IBR-2 in Dubna. The polarized neutron beam was used. The waveguide structures Py(10nm)/Al(140)/Py(50)//glass(substrate) and Fe(10nm)/Al(140)/Fe(50)//glass(substrate) were saturated in the applied magnetic field 1500 Oe. The substrate sizes are 30 × 30 × 5 mm^3. Py (permalloy) is the magnetic alloy Fe (20.6% at.) and Ni (79.4% at.). The SLD is shown in Figs. 1*b* and 1*c*.

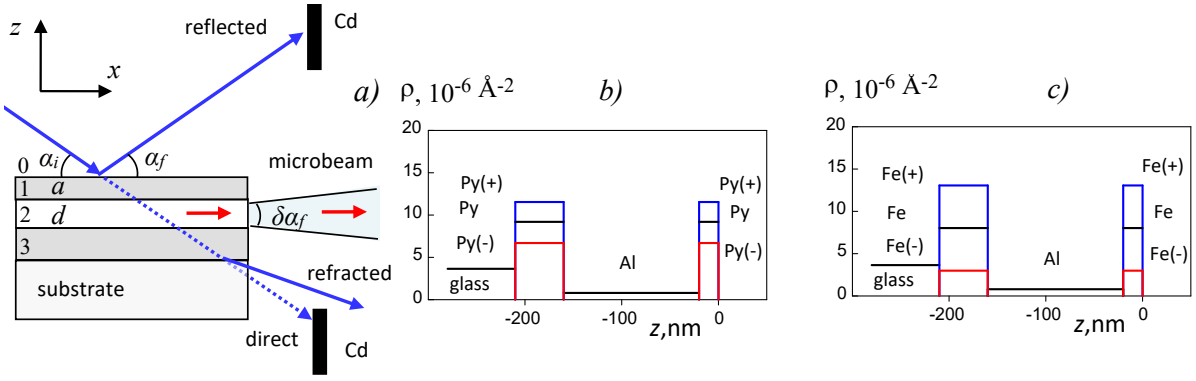

Fig. 1. Neutron planar waveguides: *a)* geometry of experiment; *b)* SLD for Py/Al/Py; *c)* SLD for Fe/Al/Fe.

The grazing angle of the incident beam α_i is equal to 0.236° for Py/Al/Py and 0.228° for Fe/Al/Fe. The angular divergence $\delta\alpha_i$ of the incident beam is 0.009°. Two-dimensional ^{3}He

position-sensitive detector (PSD) with spatial resolution 2.5 mm was used. The distance from the sample to PSD was equal to 5030 mm, the time-of-flight distance from moderator to detector was equal to 34030 mm. The width of the time-of-flight channels was equal to 256 μs, the cold moderator was used and the wavelength resolution was equal to 0.02 Å. The microbeam intensity was registered for the polarization of the incident beam UP (or "+") and DO (or "-") in the region between the direct and the reflected beams partially blocked by Cd plates (see Fig. 1*a*). Indices 0, 1, 2 and 3 corresponds to vacuum, upper, middle and bottom layers.

In Fig. 2 experimental results are presented. The resonant enhancement of the neutron wavefunction density $|\Psi|^2$ takes place in the middle layer 2 at the periodic conditions for the phase of the neutron wavefunction $\Phi(k_{0z}) = 2k_{2z}d + arg(R_{21}) + arg(R_{23}) = 2\pi n$. Here $n = 0, 1, 2 \ldots$ is the order of the resonance, $k_{0z} = \frac{2\pi}{\lambda}\sin\alpha_i$, $k_{1z} = \sqrt{k_{0z}^2 - \rho_1}$, $k_{2z} = \sqrt{k_{0z}^2 - \rho_2}$, $k_{0x} = \frac{2\pi}{\lambda}\cos\alpha_i$, ρ_1 is SLD of the layer 1, and ρ_2 is SLD of the layer 2, R_{21} is the amplitude of the neutron wavefunction in the layer 2 at reflection from the layer 1 and R_{23} is the amplitude of the neutron wavefunction in the layer 2 at reflection from the layer 3. The spectra of the microbeam from the waveguide Py/Al/Py is shown in Fig. 2*a*. One can see the peaks UP and DO of the resonance $n = 0$ at the neutron wavelength 4.95 Å. The spectra of the microbeam from the waveguide Fe/Al/Fe is presented in Fig. 2*b*. One can see the peaks UP and DO of the resonance $n = 0$ at the neutron wavelength 5.15 Å.

In Fig. 3 the integrated microbeam intensity of the resonance $n = 0$ is shown as a function of the SLD depth $\Delta\rho = \rho_1 - \rho_2$. One can see that the neutron microbeam intensity is not changed within the experimental errors about ± 15 %. Calculations by the theory of neutron resonances shows that the changing of the integrated square under the resonance peak of $|\Psi|^2$ consists of about 35 %. It is close to the experimental statistical errors 2·15 = 30 (%).

Thus, for the first time we measured the dependence of the neutron microbeam intensity on the structural parameter of the layered waveguides. Farther, we plan the measurements of the neutron microbeam intensity as a function of the thickness a of the upper layer and the width d of the middle layer.

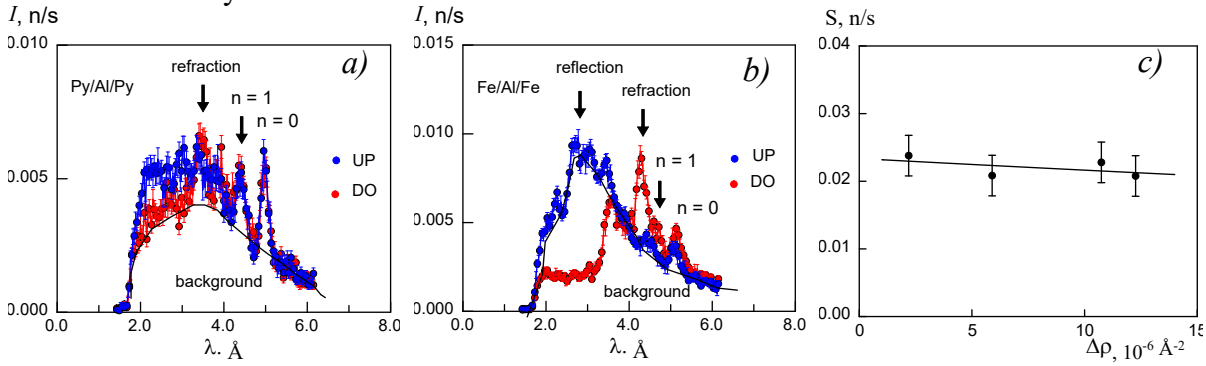

Fig. 2. Experimental results: *a)* neutron microbeam spectrum for UP and DO incident beam polarization for Py/Al/Py; *b)* neutron microbeam spectrum for UP and DO incident beam polarization for Fe/Al/Fe; *c)* integrated microbeam intensity for the resonance n=0 as a function of SLD potential well depth.

[1] F. Pfeiffer et al. (2002). High-resolution Fourier diffractometer at the IBR-2 reactor. Phys. Rev. Lett. 16, 8-12.

[2] S.V. Kozhevnikov (2019). Neutron Planar Waveguides. Physics of Particles and Nuclei. 50, 300-340.

[3] S.P. Pogossian (2007). Enhanced neutron concentration in uranium thin film waveguides. J. Appl. Phys. 102, 104501.

POLARIZED NEUTRON REFLECTOMETRY IN STYDY OF RARE-EARTH MULTILAYERS

D.I. Devyaterikov[1], M.V. Makarova[1], V.V. Matyukhov[1], Yu.A. Salamatov[1], G.E. Zhezlyaev[1], E.A. Kravtsov[1]

[1] *Institute of Metal Physics, Ekaterinburg, Russia*

E-mail: kravtsov@imp.uran.ru

Polarized neutron reflectometry, grazing incidence neutron diffraction, and off-specular scattering are powerful experimental techniques to probe nuclear and magnetic profiles in multilayered nanostructures. By measuring polarized neutron scattered intensity it is possible to determine depth dependence of magnetic moments (two components) throughout the multilayered nanostructure. In my report I give examples of our study of magnetic rare-earth multilayers.

Superlattices Fe/Gd are popular model system displaying a rich magnetic phase diagram depending on temperature and magnetic field. The important feature of this artificial system is strong antiferromagnetic coupling at interface Fe-Gd, in order to initiate spin-flop transition one needs to apply magnet field ca 100 T. By measuring neutron spin-flip scattering we found that it is possible to suppress the field of spin-flop transition by 2-3 orders of magnitude by introducing Pd spacer layer between Fe and Gd. It was shown that spin-flop transition appears in this system without any magnetic anisotropy inside magnetic layers.

Heavy rare-earth metals (Dy, Ho, Tb) are magnetic materials where exist complex magnetic states like helicoidal magnetic ordering. When presented in nanostructures (thin films and multilayers) parameters of magnetic helices are highly dependent on proximity effects from neighboring layers, layer thicknesses, effects order-disorder at interfaces, epitaxial strains, temperature, magnetic field, etc. The helicoidal magnetic order may be detected with neutron diffraction by measuring magnetic satellites arising near fundamental Bragg peaks like (0002), (0004), etc. The position of these satellites provides information on helix period, intensity – information on magnetic moment. Currently there is no way to determine helix parameters in rare-earth multilayers except neutron scattering. However, wide angle neutron diffraction cannot be applied to rare-earth nanostructures because of lack of scattering material. We have shown that magnetic satellites due to helicoidal ordering should appear also around (000) reflection, i.e. near direct neutron beam. These means that magnetic satellite (000)+ can be detected in neutron reflectometry where due to small angle of incidence neutrons pass through significant amount of scattering material. These techniques has been successfully applied to determine magnetic helices in thin Dy & Ho films, Dy/Ho superlattices, and just very recently in ultrathin Tb films.

Support by RSF (project No. 24-12-20024) is acknowledged.

DEVELOPMENT OF THERMAL NEUTRON DETECTORS BASED ON STRAW TUBES

A.K. Kurilkin[1], A.G. Kolesnikov[1,2], V.I. Bodnarchuk[1], A.O. Kolesnikov[1], V.M. Milkov[1], A.A. Bogdzel[1], A.A. Suharev[1,3], V.A. Drozdov[1], O. Daulbayev[4,5]

[1] *Joint Institute for Nuclear Reasearch, Dubna, Moscow region , Russia*
[2] *Dubna State University, Dubna, Moscow region, Russia*
[3] *Moscow State University, Moscow,Russia*
[4] *Kazakhstan Institute of Nuclear Physics, Almaty, 050032 Kazakhstan,*
[5] *Satbayev University, Almaty. Kazakhstan*

E-mail: akurilkin@jinr.ru

A promising direction for the development of neutron detectors at JINR is the construction of detectors based on boron carbide(B_4C), which are widely used in world scientific center as an alternative to ^3He detectors. This paper presents the results of evaluating the theoretical efficiency of a thermal neutron detector based on straw tubes with solid-state converter B_4C. The software package Geant4 was used as a tool for numerical simulation by the Monte Carlo method. The simulation results are compared with experimental measurements of prototype the straw detector by using neutron source ^{252}Cf and the experimental data obtained on the reflectometer REFLEX, 9th channel of the reactor IBR-2.

ENHANCED ADHESION STRENGTH IN POLYMER COMPOSITES MODIFIED WITH HYBRID NANODIAMOND/GRAPHITE PARTICLES

T.S. Kurkin[1], O.V. Lebedev[1], E.K. Golubev[1], V.Yu. Dolmatov[2] and A.N. Ozerin[1]

[1] *Enikolopov Institute of Synthetic Polymer Materials Russian Academy of Sciences (ISPM RAS), Moscow, Russia*

[2] *Federal State Unitary Enterprise, Special Design and Technology Bureau 'Technolog', Saint Petersburg, Russia*

E-mail: kurkints@ispm.ru

The perfomance of composite polymer materials in advanced applications often relies on the optimization of various aspects such as polymer processing regimes and post-processing conditions, which in turn affect mechanical and thermal properties of the resulting material. The role of these optimization aspects become even more decisive in case the nano- and submicronscale particles are introduced into the system, and while such modification can sometimes yield a significant boost in properties for the composite system, it is vital that modification is carried out in a controlled and well-monitored manner. According to a current trend, the effective way to control the properties of matrix-particle interface and enhance the macroscale performance of composite material is to introduce surface-functionalized and often electrostatically charged particles into the polymer matrix.

The presented study is dedicated to evaluation of the effect of two types of hybrid nanodiamond/graphite particles [1] differing in surface charge polarity on the adhesion strength of highly oriented poly(vinyl alcohol) and poly(acrylonitrile) fibers to the epoxy matrix. Several types of cured industrial epoxy matricies were employed, cured by various conventional hardener agents.

The observed results suggest that the most effective approach to enhance the adhesion strength of the fiber-matrix interface is to modify both fiber and the matrix with oppositely charged particles. Such modification proved to be furthermore effective due to the interaction between hybrid nanodiamond/graphite particles and PVA/PAN fibers, resulting in a significant increase of their stress/strain characteristics. One of the most important aspects of this approach is to provide a quantitative assessment of filler particle dispersion in polymer matrix. In the presented study absolute intensity SAXS measurements were used as an effective tool to achieve this goal.

The presented results also suggest that hybrid nanodiamond/graphite particles are indeed an active modifier agent for investigated epoxy-based systems, with filer particles being involved in the genesis of the cross-linked cured structure.

The reported study was conducted with the financial support from Ministry of Science and Higher Education of the Russian Federation (№ FFSM-2024-0002).

[1] T.S. Kurkin, O. V Lebedev, E.K. Golubev, A.K. Gatin, V. V Nepomnyashchikh, V.Y. Dolmatov, A.N. Ozerin (2025). Detonation Nanodiamond Soot—A Structurally Tailorable Hybrid Graphite/Nanodiamond Carbon-Based Material. Nanomaterials. 15, 56.

STRUCTURAL TRANSITIONS OF HYBRID MICELLES OF IONIC SURFACTANT WITH EMBEDDED HYDROPHOBIC POLYMER INDUCED BY SALT AND HYDROCARBON

A.L. Kwiatkowski[1], V.S. Molchanov[1], A.I. Kuklin[2], O.I. Ivankov[2], Yu.M. Chesnokov[3] and O.E. Philippova[1]

[1] *Faculty of Physics, Lomonosov Moscow State University, Moscow, Russia*
[2] *Joint Institute for Nuclear Research, Dubna, Russia*
[3] *National Research Center, Kurchatov Institute, Moscow, Russia*

E-mail: kvyatkovsky@polly.phys.msu.ru

During the last decades, there is an enhanced interest for applying surfactants together with polymers in many industrial areas. Particularly, in oil recovery semidilute solutions of both polymers and surfactants are used as thickeners in hydraulic fracturing fluids. Polymer/surfactant complexes in aqueous medium, also called hybrid micelles, yield a variety of objects with form and structure governed by the environment. Rheological experiments demonstrate, that viscoelastic properties of the solutions of hybrid micelles are sufficiently sensitive to such conditions as salinity and presence of hydrophobic species. Therefore small-angle neutron scattering (SANS) and X-ray scattering (SAXS) are essential experimental techniques to provide the data on the form and structural transitions of hybrid micelles induced by addition of inorganic salt and hydrocarbon. Furthermore, contrast variation in SANS allows to obtain the scattering profiles separately from polymer and surfactant molecules in hybrid complexes.

The present study is devoted to the influence of KCl and decane concentrations on the hybrid micelles of anionic surfactant potassium oleate with embedded hydrophobic polymer poly(4-vinylpyridine). Several complimentary experimental methods, including cryo-transmission electron microscopy, 2D NMR, dynamic-light scattering and florescent spectroscopy, beyond SANS and SAXS, were applied to represent the transition from beads-on-string complexes to wormlike hybrid micelles induced by salt and vice versa upon solubilization of hydrocarbon.

The SANS and SAXS experiments were carried out at the Frank Laboratory of Neutron Physics (Joint Institute for Nuclear Research, Dubna, Russia). The SANS measurements were performed with the YuMO instrument at the high-flux pulsed reactor IBR-2. Xeuss 3.0 SAXS/WAXS System was used for SAXS.

Acknowledgement: The study was conducted under the state assignment of Lomonosov Moscow State University

DETONATION NANODIAMOND SOOT AS A PROMISING HYBRID GRAPHITE/NANODIAMOND MATERIAL WITH A TAILORABLE STRUCTURE

O.V. Lebedev[1], T.S. Kurkin[1], E.K. Golubev[1], V.Yu. Dolmatov[2] and A.N. Ozerin[1]

[1] *Enikolopov Institute of Synthetic Polymer Materials Russian Academy of Sciences (ISPM RAS), Moscow, Russia*

[2] *Federal State Unitary Enterprise, Special Design and Technology Bureau 'Technolog', Saint Petersburg, Russia*

E-mail: oleg.lebedev@phystech.edu

This work presents the results of a systematic investigation of the structural and functional characteristics of nanodiamond soot (NDS) as a promising nanoscale filler in polymer composite systems. The studied NDS powders were synthesized via detonation of different explosive precursors: trinitrotoluene (TNT), TNT–hexogen mixtures, and tetryl [1].

The colloidal stability and dispersion behavior of NDS in various liquid media were assessed to understand their compatibility with various polymer matrices and processing methods. Morphological analysis using scanning electron microscopy, complemented by dynamic light scattering, zeta potential measurements, and laser diffraction, indicated that NDS forms hierarchical aggregates and agglomerates with comparable structural features across the samples.

The phase composition and crystallographic structure of the nanoparticles were characterized using X-ray diffraction, Raman spectroscopy, electron diffraction, transmission electron microscopy, atomic force microscopy, and scanning tunneling microscopy. The analysis of the results confirmed the coexistence of sp^3-bonded diamond and sp^2-bonded graphitic phases within the NDS. The relative phase fraction was found to depend strongly on the explosive precursor, with the graphitic component contributing significantly to the electrical conductivity of the material due to its partial presence in the form of graphene nanoribbons.

The reinforcing efficiency of NDS as a nanofiller was further evaluated through its incorporation into polymer matrices, with emphasis on mechanical, tribological, and functional performance. The resulting nanocomposite properties were shown to be highly sensitive to filler characteristics, matrix type, and processing conditions. These findings demonstrate that NDS can serve as a model nanofiller system for elucidating structure–property relationships in polymer nanocomposites, enabling direct correlation between nanoscale filler architecture and macroscopic composite performance.

The reported study was conducted with the financial support from Ministry of Science and Higher Education of the Russian Federation (№ FFSM-2024-0002).

[1] T.S. Kurkin, O. V Lebedev, E.K. Golubev, A.K. Gatin, V. V Nepomnyashchikh, V.Y. Dolmatov, A.N. Ozerin (2025). Detonation Nanodiamond Soot—A Structurally Tailorable Hybrid Graphite/Nanodiamond Carbon-Based Material. Nanomaterials. 15, 56.

DATA ACQUISITION SYSTEM BASED ON THE R5560 DIGITIZER WITH OPEN FPGA FOR THE WIDE-APERTURE DETECTOR OF THE HIGH-RESOLUTION NEUTRON FOURIER DIFFRACTOMETER HRFD

E.I. Litvinenko[1], A.A. Bogdzel[1], V.M. Milkov[1] and S.V. Sumnikov[1]

[1] *Joint Institute for Nuclear Research, Dubna, Russia*

E-mail: litvin@nf.jinr.ru

During the commissioning of a large-scale scintillation detector with a total sensitive elements area of approximately 13 m^2 at the HRFD diffractometer of the IBR-2 reactor in 2025 [1], three variants of data acquisition systems were tested. Better results in terms of performance and reliability were demonstrated by the new data acquisition system based on a 128-channel R5560SE digitizer from CAEN, which allows the user to write his own pulse processing algorithm on an open FPGA. Unlike the other two acquisition systems [2], the digitizer-based system includes a pulse shape discrimination algorithm, which is crucial for neutron-gamma separation and is optimized for the timing characteristics of ZnS(Ag)/^{6}LiF scintillator signals. The article presents the digitizer-based system, signal processing algorithms implemented as the digitizer's firmware, as well as the software of the data acquisition system and some results of the analysis of the measured data.

[1] Sumnikov, S. V. et al. (2026) “High-resolution neutron Fourier diffractometer with wide-aperture detector,” Journal of Applied Crystallography, 59(2), pp. 426–439. Available at: https://doi.org/10.1107/S1600576726001986.

[2] Bogdzel, A. A., et al. (2019) “The New Data Acquisition System MPD-32 for the High-Resolution Fourier Diffractometer at the IBR-2 Pulsed Reactor”, Proceedings of the 27th International Symposium on Nuclear Electronics and Computing, pp. 142–146. Available at: https://ceur-ws.org/Vol-2507/142-146-paper-24.pdf.

CRYSTALLOGRAPHIC TEXTURE OF NUCLEAR REACTOR CLADDING TUBES

T.A. Lychagina[1], D.I. Nikolayev[1]

[1] *Joint Institute for Nuclear Research, Dubna, Russia*

E-mail: lychagina@jinr.ru

Crystallographic texture is one of parameter that plays a crucial role in the performance of nuclear reactor cladding tubes, as it directly determines the anisotropy of their physical and mechanical properties upon irradiation. In zirconium alloys used to produce VVER-1000 reactor cladding tubes with a hexagonal close-packed (HCP) lattice, texture control is crucial to minimize radiation growth, creep, and preventing failure due to hydride embrittlement [1]. An error in texture can cause the cladding tube to bend in an "arc".

Texture is also important for steel cladding tubes of fast neutron reactors, although steel with a cubic lattice (BCC or FCC) is often considered more isotropic on a macroscale. The texture created during the rolling process influences microstructural stability and the balance of strength and ductility, which is important for fast reactors cladding tubes. Texture determines how the tube will perform under extreme loads in the reactor core [2]. It affects how much the tube deforms under the pressure of the coolant and gases inside. Controlling the crystal orientation makes the cladding tubes more rigid and resistant to deformation. Unlike zirconium, where texture controls the orientation of hydrides, in steels the main challenge is dimensional stability (swelling minimizing) under high irradiation doses. Not optimal crystallographic texture of the cladding tubes could lead to worse sodium flow.

Information about texture of cladding tubes can be obtained from experimentally measured pole figures. Pole figures characterize the relative volume of specific crystallographic direction measured in a sample coordinate system on the unit sphere. The most common method to measure pole figures is X-ray diffraction. However, due to the small X-rays penetration depth into substance, pole figures can only be measured in reflection mode. This makes impossible direct measurements of complete pole figures. The EBSD (electron backscatter diffraction) method is implemented in a scanning electron microscope (SEM). This method allows one to construct orientation maps of the microstructure, see the texture distribution in specific zones and analyze grain boundaries. However, in the case of X-ray diffraction, the penetration depth is approximately 100 μm; the EBSD technique provides information for only a few atomic layers. So, X-ray and EBSD can characterize the sample only locally (typical gauge volume is 0,01 cm^3 and 0,01 mm^3 respectively). Due to the high penetrating power of neutrons, texture can be examined in bulk samples (up to 100 cm^3) or entire tube fragments in transmission mode without destruction or any special sample preparation.

The complete pole figures of the Zr-1%Nb alloy and austenitic steel samples were extracted from the time-of-flight patterns measured at the SKAT spectrometer (Spectrometer for the Quantitative Analysis of Textures). SKAT is situated at the 7A-2 beamline of the high flux pulsed nuclear reactor IBR-2 (FLNP, JINR). The samples were glued together from seven sections of the original cladding tubes. Since the complete pole figures are measured, they can be normalized by integrating the pole density over the sphere. The complete normalized pole figures (0002), (10-10), (11-20), and (10-11) were obtained for cladding tubes made of the Zr-1%Nb alloy and pole figures (111), (200), (220), (311) for cladding tubes made of the austenitic steel. Some of the pole figures are shown in the figs. 1, 2. The Zr-1%Nb alloy texture is axial, with the texture axis coinciding with the tube axis. The crystallographic direction [0002] lies in the plane perpendicular to the tube axis. The maximum of normalized basal pole figure (0002) is 3.78 mrd.

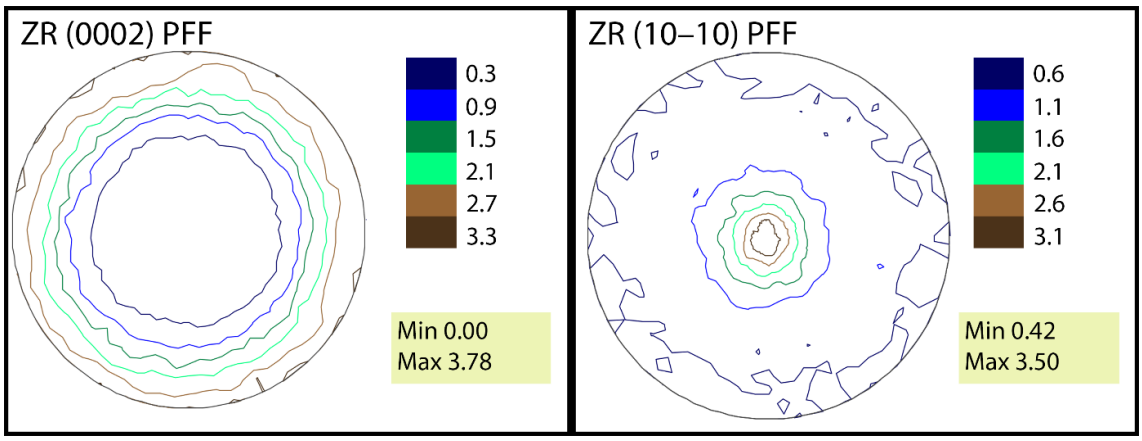

Fig.1 The complete normalized pole figures for the Zr1%Nb alloy cladding tube

During operation, zirconium absorbs hydrogen that leads to hydrides formation. This texture ensures that the hydrides will be oriented tangentially (along the tube's circumference), without creating dangerous "notches" in the wall.

The steel tube has two component axial texture with texture axis coinciding with the tube axis.

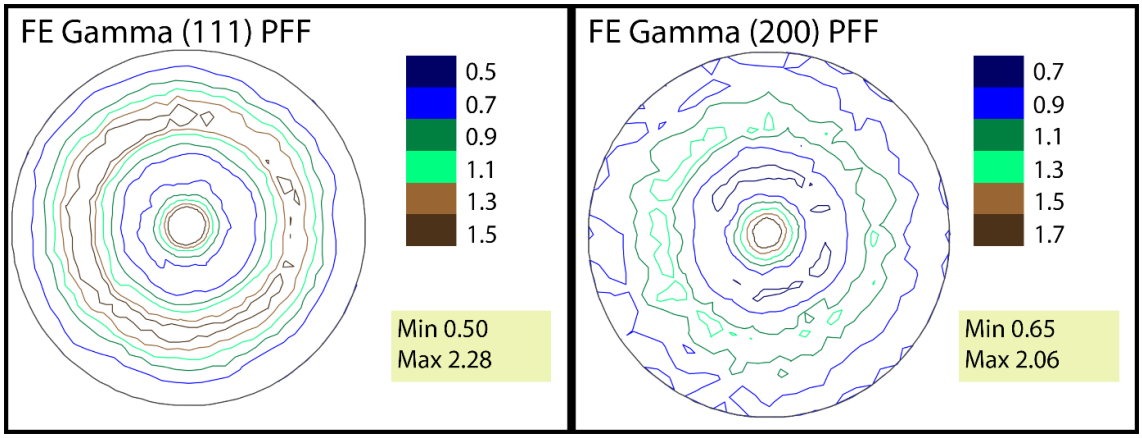

Fig.2 The complete normalized pole figures for the austenitic steel cladding tube

In this case the normal to (111) and (200) planes coincide with tube axis. The maximum pole density 2.28 mrd at the pole figure (111), whereas one is 2.06 mrd at the pole figure (200).

The optimization of texture of the steel cladding tubes to improve resistance to radiation swelling need further investigations.

[1] E. Tenckhoff (1988) Deformation Mechanisms, Texture, and Anisotropy in Zirconium and Zircaloy, ASTM International.

[2] K. Linga Murty, Indrajit Charit (2006) Texture development and anisotropic deformation of zircaloys. Progress in Nuclear Energy, 48 (4), 325-359.

KITAEV AND ISING COBALT-BASED MAGNETS: INSIGHTS FROM NEUTRON SCATTERING

P.A. Maksimov[1]

[1] *Bogolyubov Laboratory for Theoretical Physics, Joint Institute for Nuclear Research, Dubna, Russia*

E-mail: maksimov@theor.jinr.ru

Cobalt-based materials were recently proposed to host strongly anisotropic interactions due to the presence of spin-orbit coupling [1], including the long-sought Kitaev interaction [2]. We use inelastic neutron scattering data to establish exchange Hamiltonian of several materials with magnetic Co^{2+} ions.

First, we show that high-field spin-wave dispersion of quasi-two-dimensional honeycomb material $BaCo_2(AsO_4)_2$ unequivocally points to the presence of strong Kitaev interaction [3]. Fitting neutron scattering data yields full magnetic Hamiltonian. We also establish its phase diagram and present evidence for its unique "double-zigzag" ground state.

Second, we also studied two members of the pyroxene mineral group. Using inelastic neutron scattering data, we showed that these cobalt-based pyroxenes are a platform for realization of strongly anisotropic exchange interactions. As we show, $SrCoGe_2O_6$ is proposed to host one-dimensional version of the Kitaev model [4]. The ground state and magnetic spectrum of orthopyroxene $CoGeO_3$ are a result of bond-dependent Ising interactions [5].

This work is supported by Russian Science Foundation Grant 23-12-00159.

[1] H. Liu, J. Chaloupka, and G. Khaliullin (2020). Kitaev Spin Liquid in 3d Transition Metal Compounds, Phys. Rev. Lett. 125, 047201.

[2] A. Kitaev (2006). Anyons in an exactly solved model and beyond, Annals of Physics 321, 2.

[3] P.A.Maksimov, S. Jiang, L.P. Regnault, A.L. Chernyshev (2025). Strong Kitaev Interaction in $BaCo_2(AsO_4)_2$, Phys. Rev. Lett. 135, 066703

[4] P.A. Maksimov, A.V. Ushakov, A.F. Gubkin, G.J. Redhammer, S.M. Winter, A.I. Kolesnikov, A.M. Dos Santos, Z. Gai, M.A. McGuire, A. Podlesnyak, S.V. Streltsov (2024). Cobalt-based pyroxenes: A new playground for Kitaev physics, Proc. Natl. Acad. Sci. U.S.A. 121 (43) e2409154121.

[5] P.A. Maksimov, A.F. Gubkin, A.V. Ushakov, A.I. Kolesnikov, M.S. Cook, M.A. McGuire, G.J. Redhammer, A. Podlesnyak, S.V. Streltsov (2025). Ising spin ladders of orthopyroxene $CoGeO_3$, Phys. Rev. B 112, L220407.

DETERMINATION OF THE LOCALIZATION OF BORON CATIONS IN THE STRUCTURE OF NONLINEAR OPTICAL LITHIUM NIOBATE CRYSTALS $LiNbO_3$:B AND $LiNbO_3$:Me:B (Me - Zn, Mg, Gd)

D.V. Manukovskaya[1], R.A. Titov[1], N.V. Sidorov[1], M.N. Palatnikov[1]

[1] *Tananaev Institute of Chemistry–Subdivision of the Federal Research Centre "Kola Science Centre of the Russian Academy of Sciences" (ICT KSC RAS), Apatity, Russia*

E-mail: d.manukovskaia@ksc.ru

Lithium niobate ($LiNbO_3$, LN) is one of the most sought-after single-crystal materials in modern materials science. Numerous studies have shown that improving several stages of LN crystal production technology can significantly improve a number of its practically significant properties in order of magnitude. A significant technological step is doping. Doping determines the characteristics of the secondary (defect) structure of LN crystals. This secondary structure, in turn, determines the crystals' target properties. Therefore, the secondary structure in LN requires detailed and meticulous research.

The main point antisite defects of LN are niobium cations localized in the lithium octahedra of the crystal structure (Nb_{Li}). Nb_{Li} form because of the non-stoichiometric composition of the congruent charge (R = [Li] / [Nb] = 0.946). This charge forms the basis for producing nominally pure congruent (CLN) and doped (LN:Me, where Me is the dopant) crystals. Stoichiometric (SLN) crystals are grown from a melt with an excess Li_2O content (58.6 mol%), from a congruent melt with the addition of 6 wt% K_2O flux, or using technological approaches such as the double crucible method and others.

Doping LN with non-photorefractive metal cations (Me - Zn^{2+}, Mg^{2+}, Gd^{3+}, etc.) reduces the concentration of Nb_{Li} defects by replacing them with new point defects, such as Zn_{Li}^{+}. With the introduction of high concentrations of such cations, they begin to localize additionally in vacant and niobium oxygen octahedra, such as Zn_V^{2+} and Zn_{Nb}^{3-}. The increased variability of point defect types in LN:Me crystals causes the evolution of the secondary (defect) structure.

The doping method also influences the structural properties of LN:Me crystals. It has been reliably established that homogeneous doping can introduce a higher concentration of dopant into the crystal structure than direct doping [1]. On the other hand, introducing high concentrations of metal cations into the crystal, close to the threshold, leads to a decrease in compositional homogeneity, as observed, for example, in LN:Mg crystals.

Problems arising during LN doping can be avoided by introducing the non-metallic element boron into the crystal structure. The technology for single doping of LN crystals with boron cations was developed at ICT KSC RAS (a comprehensive review is given in [2]). To date, we have already implemented an approach to producing boron-containing lithium niobate crystals doubly doped: LN:Mg:B [3, 4], LN:Zn:B [5], LN:Gd:B [6].

The addition of boron-containing alloying components (B_2O_3, H_3BO_3) to a congruent charge has a complex effect on the structure of the melt and crystal. In such a melt, boron complexes the regulated cations of impurity metals, partially preventing their transition into the crystal structure [7], and also binds excess niobium [2]. The physicochemical processes occurring in such a melt reduce the concentration of Nb_{Li} point structural defects in LN:B crystals compared to CLN crystals [2].

The addition of boron has a positive effect on the crystal-melt system even in the case of double doping. LN:Gd:B crystals are characterized by a high Curie temperature (≈ 1210-1213°C). This indicates structural ordering and the detection of a synergistic effect of a combination of these dopants [6]. For LN:Zn:B crystals, the dependence of the Zn concentration in the crystal and the distribution coefficient on the concentration of the metal dopant in the

melt does not exhibit the kinks typical for LN:Zn crystals [5]. In LN:Mg:B crystals, the photorefraction effect decreases at a much lower concentration of magnesium cations, compared to LN:Mg crystals [3]. In this case, the homogeneous doping method is preferable for the synthesis of LN:B crystals, and the direct solid-phase doping method is preferable for the synthesis of LN:Mg:B crystals [4].

A crucial aspect of LN:B synthesis is the fact that boron is present in the crystal structure in trace amounts (≈ 10^{-4} mol%) [2]. Model calculations were performed to localize trace amounts of boron cations in the faces of vacant tetrahedral voids. The most probable localization of boron cations is the faces of vacant tetrahedral voids O_4, shared with vacant niobium oxygen octahedra V_{Nb}^{5-} [4]. This localization is due to the increased stoichiometry of boron-containing crystals (≈1) grown from a batch of congruent composition (R=0.946), the charge difference (B^{3+} and V_{Nb}^{5-}), and the steric factor [4].

Unfortunately, we have not been able to determine a more precise localization of boron cations in the structure of LN:B and LN:Me:B crystals to date. In this regard, the use of the neutron scattering method will make it possible to accurately determine the localization of trace amounts of boron cations in the structure of boron-containing crystals, which is extremely important for modern materials science.

The work is performed with the financial support of the Ministry of Science and Higher Education Russian Federation (Kola Science Centre) scientific topic FMEZ-2025-0055 and the Ministry of Science and Higher Education Russian Federation grant agreement No. 075-15-2025-585.

[1] M.N.Palatnikov (2017). Fundamental aspects of the technology of heavily doped lithium niobate crystals, Apatity: KSC RAS.
[2] N.V. Sidorov N.V. (2022). Single crystals of lithium niobate and tantalate of different composition and genesis. Moscow: RAS.
[3] M.N.Palatnikov (2023). Structure, Optical Properties and Physicochemical Features of $LiNbO_3$:Mg,B Crystals Grown in a Single Technological Cycle: An Optical Material for Converting Laser Radiation. Materials. 16. 4541.
[4] R.A.Titov (2025). Features of the Defect Structure of $LiNbO_3$:Mg:B Crystals of Different Composition and Genesis. Materials. 18. 436.
[5] M.N.Palatnikov (2025). Preparation and features of defective structure and optical properties of $LiNbO_3$:Zn:B crystals. Optical and Quantum Electronics. 57. 491.
[6] I.V.Biryukova (2025). Defect structure, optical and photorefractive properties of $LiNbO_3$:B:Gd single crystals. Technical Physics. 70. 2064-2079.
[7] M.N.Palatnikov (2023). Growing, structure and optical properties of $LiNbO_3$:B crystals, a material for laser radiation transformation. Materials. 16. 732.

HYDROGEN BONDS IN LITHIUM NIOBATE CRYSTALS OF DIFFERENT COMPOSITIONS AND GENESIS

D.V.Manukovskaya[1], L.A. Bobreva[1]

[1] *Tananaev Institute of Chemistry–Subdivision of the Federal Research Centre "Kola Science Centre of the Russian Academy of Sciences" (ICT KSC RAS), Apatity, Russia*

E-mail: d.manukovskaia@ksc.ru

Functional materials based on nonlinear optical lithium niobate single crystal ($LiNbO_3$) are widely used in the modern electronics industry for actively nonlinear laser media, for the conversion and parametric generation of laser radiation frequencies, for optical sensors, deflectors, etc. [1]. An important advantage of lithium niobate is the ability to control the physical characteristics of the crystal over a wide range by varying the state of its defect structure. One of the features of $LiNbO_3$ crystals grown in an air atmosphere is the presence of defects in the structure in the form of hydroxyl groups (OH^-) [1-3]. The mechanism of hydrogen atom incorporation into the crystal lattice of $LiNbO_3$ crystals is not entirely clear. It is believed that it enters the lattice from the air atmosphere during the growth of the $LiNbO_3$ crystal [1, 2]. Due to its small size and relatively weak hydrogen bond, the hydrogen atom is highly sensitive to changes in the crystal field that occur with changes in the Li/Nb ratio and doping of the crystal, which leads to changes in the main parameters of the band in the IR absorption spectrum in the region of stretching vibrations of OH^--groups. This fact is used to study the defect structure of the crystal. The position of hydrogen atoms linked to the oxygen atom by a hydrogen bond in the structure of non-stoichiometric crystals varies depending on the type and concentration of the dopant. The presence of hydrogen atoms in the structure of the $LiNbO_3$ crystal leads to the formation of complex defects with the main (Nb^{5+} and Li^+) and doping cations (Me): V_{Li}-OH, Nb_{Li}-OH,Me-OH,Me-OH-Me [1-4]. The presence of OH groups plays an important role in the formation of the secondary structure and physical characteristics of the crystal: it increases low-temperature conductivity, reduces the photorefraction effect and the magnitude of the coercive field [1,2]. $LiNbO_3$ crystals grown under different atmospheric conditions using different technologies contain varying concentrations of OH^--groups. IR spectroscopy, based on the intensity of lines corresponding to the stretching vibrations of O–H bonds, allows one to calculate the concentration of OH^--groups in the crystal structure [4]. The method of IR absorption spectroscopy in the region of hydrogen bond stretching vibrations can be an identifier not only for determining the change in the stoichiometry of the $LiNbO_3$ crystal, but also for determining whether the dopant reaches its concentration threshold.

Neutron scattering is one of the most effective methods for studying light elements, such as hydrogen, in crystal structures $LiNbO_3$. Is it possible to use neutron scattering to conduct a comprehensive study of hydrogen in lithium niobate crystals, from precisely determining its position and quantity to analyzing its dynamics and interactions with the environment?

The work is performed with the financial support of the Ministry of Science and Higher Education Russian Federation (Kola Science Centre) scientific topic FMEZ-2025-0055 and the Ministry of Science and Higher Education Russian Federation grant agreement No. 075-15-2025-585.

[1] K. Lengyel (2015) Growth, defect structure, and THz application of stoichiometric lithium niobate. Appl. Phys. Rev. 2, 040601-1 040601-28.
[2] J. M. Cabrera (1996) Hydrogen in lithium niobate. Adv. Phys. 45, 349-392.
[3] L. Kovacs (2014) Hydroxyl ions in stoichiometric $LiNbO_3$ crystals doped with optical damage resistant ions. Opt. Mat. 20, 55-58.
[4] S. Klauer,. (1992) Influence of H-D isotopic substitution on the protonic conductivity of $LiNbO_3$. Phys. Rev. B. 45 (6), 2786–2799

STRUCTURAL STUDIES OF NANODIAMONDS MODIFIED WITH SURFACTANT IN DIMETHYL SULFOXIDE

D.E. Martyanov[1], V.T. Lebedev[2], V.V. Skoi[3], A.I. Kuklin[3], A.Ya. Vul[1]

[1] *Ioffe Insitute, 194021 Saint-Petersburg, Russia*
[2] *Petersburg Nuclear Physics Institute National Research Center "Kurchatov Institute", 188300 Gatchina, Leningradskaya distr., Russia*
[3] *Frank Laboratory of Neutron Physics, Joint Institute for Nuclear Research, 141980 Dubna, Russia*

E-mail: molibdenchik@mail.ioffe.ru

The applications of detonation nanodiamonds (DND, size ~4.5 nm) have not yet been fully defined. Recent publications consider DND as a promising filler in polymer composites [1], a slow-neutron reflector [2], a carrier for targeted drug delivery [3], and a contrast agent for magnetic resonance imaging [4]. For most applications, it is necessary to obtain stable DND sols in organic solvents and, as demonstrated by the complex fractal structure of electrostatically stabilized hydrosols, to conduct systematic studies of such systems using small-angle neutron scattering (SANS) [5,6]. Of particular interest for organic synthesis and medicine is dimethyl sulfoxide (DMSO), a solvent with unique dissolving power and the lowest toxicity among polar aprotic solvents.

Previously [7], we proposed a method for the steric stabilization of diamond nanoparticles in DMSO by binding the surface carboxyl groups of DND with the cationic surfactant cetyltrimethylammonium bromide (CTAB). The systems obtained in this way were shown to have an average size of diamond aggregates of ~27 nm.

In this work, SANS was used to study sols of diamond nanoparticles modified with both CTAB micelles and free CTAB molecules. The measurements were performed on the YuMO spectrometer (IBR-2 reactor, JINR) using protonated and deuterated DMSO for isotopic contrast variation. Sols of carboxylated DND in light and heavy water served as reference samples.

It is shown that the structure of the formed particles does not depend on the modification method. According to the Guinier approximation, the radii of gyration of diamond aggregates in all the samples are ~14−15 nm. DND-CTAB particles in DMSO form fractal structures, but with a lower fractal dimension (D_f = 2.2) than that of hydrosols (D_f = 2.5), which indicates their greater branching.

The obtained results complement the understanding of the internal structure of systems formed by diamond nanoparticles in DMSO and water. This finding is important for the development of new colloidal materials for biomedical applications.

[1] P.Karami, S.Salkhi Khasraghi, M.Hashemi, S.Rabiei, A.Shojaei (2019). Polymer/nanodiamond composites - a comprehensive review from synthesis and fabrication to properties and applications. Advances in Colloid and Interface Science. 269, 122-151. DOI: 10.1016/j.cis.2019.04.006.
[2] V.Nesvizhevsky, U.Köster, M.Dubois, N.Batisse, L.Frezet, A.Bosak, L.Gines, O.Williams (2018). Fluorinated nanodiamonds as unique neutron reflector. Carbon. 130, 799-805. DOI: 10.1016/j.carbon.2018.01.086.
[3] S.Chauhan, N.Jain, U.Nagaich (2020). Nanodiamonds with powerful ability for drug delivery and biomedical applications: Recent updates on in vivo study and patents. Journal of Pharmaceutical Analysis. 10, 1-12. DOI: 10.1016/j.jpha.2019.09.003.
[4] A.S.Chizhikova, E.B.Yudina, A.M.Panich, M.Salti, Yu.V.Kulvelis, A.I.Shames, O.Prager, E.Swissa, A.E.Aleksenskii, A.Ya.Vul' (2024). Diamond nanoparticles as a

contrast agent for MRI. Technical Physics. 69, 1365. DOI: 10.61011/TP.2024.09.59283.70-24.
[5] A.Ya.Vul, E.D.Eidelman, A.E.Aleksenskiy, A.V.Shvidchenko, A.T.Dideikin, V.S.Yuferev, V.T.Lebedev, Yu.V.Kul'velis, M.V.Avdeev (2017). Transition sol-gel in nanodiamond hydrosols. Carbon. 114, 242-249. DOI: 10.1016/j.carbon.2016.12.007.
[6] V.Lebedev, Y.Kulvelis, A.Kuklin, A.Vul (2016). Neutron Study of Multilevel Structures of Diamond Gels. Condensed Matter. 1, 10. DOI: 10.3390/condmat1010010.
[7] D.E.Martyanov, A.T.Dideikin, A.D.Trofimuk, A.Ya.Vul' (2025). Stable sols of carboxylated diamond nanoparticles in dimethyl sulfoxide. Technical Physics. 70, 348-358. DOI: 10.61011/TP.2025.02.60837.369-24.

ASSEMBLED RECOMBINANT CHLOROPLAST C-RING IN *ESCHERICHIA COLI*

A.V. Minaeva[1], S.D. Osipov[1], M.A. Semeno[1], L.A. Kamalieva[1], A.V. Vlasov[1,2]

[1] *Research Center for Molecular Mechanisms of Aging and Age-Related Diseases, Moscow Institute of Physics and Technology, 141700 Dolgoprudny, Russia*
[2] *Joint Institute for Nuclear Research, 141980 Dubna, Russia*

ATP synthase is a protein that provides cells with adenosine triphosphate (ATP), which is the main source of energy for the majority of biochemical processes in living organisms. ATP synthase converts transmembrane electrochemical potential into mechanical rotation of the c-ring rotor in the membrane part (F_o) and the central stalk (γ/ε) of the protein complex, triggering corresponding conformational changes in ATP catalytic centers [1].

The key element of ATP synthase is its membrane rotor domain c-ring, consisting of n protomers (c_1 subunits). The number of protons requiring to pass through the c-ring for the synthesis of a single ATP molecule is determined by the stoichiometry of the c-ring. The stoichiometry is constant within each specie, but can significantly vary between distant lineages. Target mutations allow to change c-ring stoichiometry and are described in literature [2]. However, the role of the surrounding environment is not sufficiently studied yet. For instance, it is not proven that c-rings with identical amino acid sequences, assembled in different species, will have the same stoichiometry.

In this work, a recombinant c-ring from ATP synthase from spinach chloroplasts, expressed in *Escherichia coli*, was studied. Optimal expression parameters for providing assembly of the complex were selected. It was shown that polyhistidine tag (His-tag) interferes with assembly, thus a genetic construction without His-tag was used. The protein was isolated and purified via the following biochemical methods: centrifugation, precipitation at the step of ammonium sulfate, and anion-exchange chromatography. The sample of purified c-ring was then biochemically and structurally characterized and shown to most likely consist of 14 subunits, which corresponds with the stoichiometry of the native chloroplast c-ring. It is notable that the completed c-ring was located exclusively in the water-soluble fraction of the cell lysate, while the membrane hydrophobic fraction mostly contained c_1 subunits. The acquired sample was studied by electron microscopy with negative contrast.

We acknowledge the support from the Russian Science Foundation (RSF) Project 24-74-00053. Protein expression and purification infrastructure were supported by the Ministry of Science and Higher Education of the Russian Federation (agreement 075 03-2026-305, project FSMG-2025-0003).

[1] Vlasov, A. V., et al. "Unusual features of the c-ring of F 1 FO ATP synthases." Scientific reports 9.1 (2019): 1-11.
[2] Pogoryelov, Denys, et al. "Engineering rotor ring stoichiometries in the ATP synthase." Proceedings of the National Academy of Sciences 109.25 (2012): E1599-E1608.

MORPHOLOGICAL PERFORMANCE OF SELF-ASSEMBLED COMPLEX NETWORKS

V.S. Molchanov[1], A.I. Kuklin[2], A.L. Kwiatkowski[1], K.B. Shishkhanova[1], M.M. Avdeev[1] and O.E. Philippova[1]

[1] *Physics Department, Lomonosov Moscow State University, Moscow, Russia*
[2] *Frank Laboratory of Neutron Physics, Joint Institute for Nuclear Research, Dubna, Russia*

E-mail: molchan@polly.phys.msu.ru

Modern soft network structures based on polymer chains, self-assembled surfactant chains, and anisotropic particles attract the attention of researchers as adaptive or stimuli-responsive systems. They are capable of recovering the structure and changing properties under the influence of external factors or small changes in the composition of the system. The mechanism of structure change is usually realized through the influence on physical interactions: hydrophobic, electrostatic, magnetic, etc. This explains the complete reversibility of the processes of rearrangement of nanostructures. Small-angle neutron scattering (SANS) is one of the most important methods for carrying out non-destructive experiments and independently obtaining information about individual components of the system.

An example of the use of the SANS method for nanostructured systems is the study of solutions based on aggregates of surfactants. The main aggregates of surfactants described in the literature are a sphere, a cylinder and a vesicle (bilayer). In our work, we studied the transformation of the structure from cylindrical micelles to vesicles through the formation of saturated networks of branched cylindrical aggregates and perforated vesicles [1]. The latter can be used as nanocontainers with adjustable nanopores.

In another part of the work, we combined worm-like micelles and cellulose nanocrystals to produce novel networks with unique stimulus-responsive viscoelastic properties due to wormlike micelles to vesicles transition [2]. Polymer-like self-organizing chains, worm-like micelles are flexible cylindrical micelles reaching tens of microns in length with a transverse dimension of 4-6 nm. Such micellar chains, like polymer chains, are able to entangle in solution to form a three-dimensional network and impact unique viscoelastic properties. SANS was used to determine the persistent length of wormlike micelles [3]. They are used as thickeners in the oil industry and household chemicals. The structure of such complex networks was studied for the first time using the method of contrast variation by the MRN method.

The study was conducted under the state assignment of Lomonosov Moscow State University.

[1] W.Hao, Y.M.Chesnokov, V.S.Molchanov, P.R.Podlesniy, A.I.Kuklin, V.V.Skoi, and O. E. Philippova (2024). Cryo-electron tomography study of the evolution of wormlike micelles to saturated networks and perforated vesicles. Journal of Colloid and Interface Science. 672, 431–445.

[2] M.M.Avdeev , V.S.Molchanov, A.I.Kuklin, O. E.Philippova (2026). Cellulose Nanocrystals Enhance the Rheological Properties and pH-Responsiveness of Potassium Oleate Solutions. Polysaccharides. 7.

[3] V.S.Molchanov, A.V.Rogachev, O.E.Philippova (2021). Determination of the local structure and the persistence length of wormlike micelles of potassium oleate by small-angle neutron scattering. Journal of Surface Investigation: X-ray, Synchrotron and Neutron Techniques. 15, 1015–1019.

HYBRID φ_0 JOSEPHSON JUNCTION AS A POSSIBLE HOST FOR SPACE-TIME CRYSTALLINE-LIKE PATTERN

M. Nashaat[1,2], J. Tekić[3] and Yu.M. Shukrinov[1,4]

[1] *BLTP, JINR, Dubna, Moscow Region 141980, Russia*
[2] *Department of Physics, Faculty of Science, Cairo University, 12613 Giza, Egypt*
[3] *"Vinča" Institute of Nuclear Sciences, Laboratory for Theoretical and Condensed Matter Physics–020, University of Belgrade, P. O. Box 522, 11001 Belgrade, Republic of Serbia*
[4] *Dubna State University, Dubna, Russia*

E-mail: majed@sci.cu.edu.eg

We report the possibility of emergence of an intrinsic space-time crystalline order in a long ferromagnetic φ_0 Josephson junction on a topological insulator, achieved without external periodic modulation of the critical current [1,2]. The proposed system assumes ferromagnetic layer with broken inversion symmetry. In the presence of the exchange and Dzyaloshinskii-Moriya interactions, the critical current is internally modulated through the coupling between the magnetic moment and the Josephson phase. This internal modulation breaks time translation symmetry, giving rise to a space-time crystalline pattern in the spatiotemporal distribution of the in-plane current, which oscillates at nearly twice the ferromagnetic resonance frequency.

We demonstrate also, in the absence of such internal modulation of the critical current, the space-time crystalline order appears only when an external parametric modulation is applied. In this case, the system exhibits a classical discrete space-time crystalline order, oscillating at half the modulation frequency.

M. Nashaat and Yu. M. Shukrinov acknowledge the financial support of the Russian Science Foundation in the framework of Project No. 22-71- 10022 of the Russian Scientific Fund. J. Tekić. acknowledges the support from the Ministry of Education, Science, and Technological Development of the Republic of Serbia, Grant No. 451-03-1F36/2025-03/200017 ("Vinca" Institute of Nuclear ˇ Sciences, University of Belgrade) and the Projects within the Cooperation Agreement between the JINR, Dubna, Russian Federation and the Republic of Serbia (P02 and P12).

[1] M. Nashaat, J. Tekić, and Yu. M. Shukrinov, Phys. Rev. B **112**, 184507**, (2025).**
[2] R. Kleiner, X. Zhou, E. Dorsch, X. Zhang, D. Koelle, and D. Jin Nat. Commun. **12**, 6038 (2021).

STUDY ON STRUCTURAL AND MAGNETIC PROPERTIES OF HIGH-ENERGY BALL-MILLED NANOPARTICLES $CoFe_2O_4$ BY NEUTRON DIFFRACTION

N.T. Nguyen[1,2], N. Truong-Tho[2], N.T. Dang[3,4], S.E. Kichanov[5], A.V. Rutkaukas[5], D.T. Khan[6], L.V.T. Son[6], T.N. Dat[6], D.P.T. Tien[1], P.D. Thinh[1]

[1] *Institute of Oceanography, Vietnam Academy of Science and Technology, Nha Trang 650000, Vietnam*
[2] *Faculty of Electronics, Electrical Engineering and Material Technology, University of Sciences, Hue University, 530000 Hue, Vietnam*
[3] *Institute of Research and Development, Duy Tan University, 550000 Danang, Viet Nam*
[4] *Faculty of Environmental and Natural Sciences, Duy Tan University, 550000 Danang, Viet Nam*
[5] *Frank Laboratory of Neutron Physics, Joint Institute for Nuclear Research, 141980 Dubna, Russia*
[6] *University of Science and Education, The University of Danang, 550000 Danang, Vietnam*

E-mail: ntnghiem@io.vast.vn

Among spinel-structured materials, cobalt ferrite ($CoFe_2O_4$) has been extensively studied due to its numerous potential technological applications, including outstanding hard magnets, ultra-dense information storage, catalysts, sensors, ferromagnetic fluids, cancer therapy, drug delivery, and biomedical imaging. Furthermore, this material is also a subject of great interest from a fundamental science perspective due to the magnetic attraction phenomena arising from the interaction between geometrically frustrated lattice arrangements and complex cation distribution at crystal sites [1]. Meanwhile, neutron diffraction is a powerful experimental technique for the simultaneous investigation of crystal structures and magnetic ordering in solid-state materials. Due to their electrical neutrality, neutrons are only scattered by atomic nuclei. This characteristic enables the precise localization of atomic positions within the unit cell and grants neutrons a significantly greater penetration depth compared to X-rays [2]. In this study, nanoparticles were synthesized from the initial bulk $CoFe_2O_4$ using high-energy ball milling. Neutron diffraction analysis confirmed that the resulting nanoparticles maintain a stable, single-phase spinel structure with space group $Fd\bar{3}m$ throughout the milling process. Furthermore, neutron diffraction analysis revealed ferrimagnetic behavior as milling time increased, significantly influencing the magnetic ordering of the system.

Nguyen Thanh Nghiem (N.T. Nguyen) was funded by the PhD Scholarship Programme of Vingroup Innovation Foundation (VINIF), VinUniversity, code VINIF.2025.TS26. The neutron diffraction experiment has been supported by the joint grants the Russian Science Foundation, RSF 24-42-10003, https://rscf.ru/project/24-42-10003/ and the Belarusian Foundation for Basic Research, BFBR T23RNFM-023.

[1] R. Sato Turtelli, M. Atif, N. Mehmood, F. Kubel, K. Biernacka, W. Linert, R. Grössinger, Cz. Kapusta, M. Sikora (2012). Interplay between the cation distribution and production methods in cobalt ferrite. Materials Chemistry and Physics, 132(2–3), 832-838.
[2] G.E. Bacon, K. Lonsdale (1953). Neutron diffraction. Reports Progress Physics, 16(1), 1-61.

DEVELOPMENT OF THE SKAT TEXTURE DIFFRACTOMETER

D.I. Nikolayev[1], T.A. Lychagina[1], B. Altangerel[1], O. Daulbaev[1], V.V. Shvetsov[1], V.M. Milkov[1], D.P. Kozlenko[1], S.E. Kichanov[1], E.V. Lukin[1], G.M. Aydanov[1], I.Y. Zel[1], B.N. Savenko[1], T.B. Petukhova[1], S.M. Murashkevich[1], A.S. Kirilov[1]

[1] *Frank Laboratory of Neutron Physics, Joint Institute for Nuclear Research, 141980 Dubna, Russia*

E-mail: dmitry@nf.jinr.ru

Texture diffractometer SKAT is fruitfully exploited since 1997 [1-3]. The present development of the instrument was motivated by a need to increase a number of samples to be measured. The main objective of the instrument to measure crystallographic texture of alloys, geological, biological samples and ceramics. The number of samples that were measured before reactor modernization exceeds the user demand. The diffractometer situated at the IBR-2M beam line 7A-2. The beam cross section it this beam line is 50 by 95 mm. Typical sample size is from 30 to 50 mm in all dimensions, so it can be effectively split into two parts. Fortunately, large beam cross section allows to install the second ring for simultaneous measurements of two samples. A compact system for neutron radiography was used to obtain a neutron image of the profile of 7A-2 beam line. The scintillator 6LiF/ZnS converted the neutron image into an optical one, which was detected by a highly sensitive CCD cameraVIDEOSCAN-11002-2001. The dimensions of the scintillator up to 200 mm make it possible to obtain a complete image of the neutron beam and detect the position of the sample in it. Figure 1 illustrates the possibility of a sample positioning in the instrument.

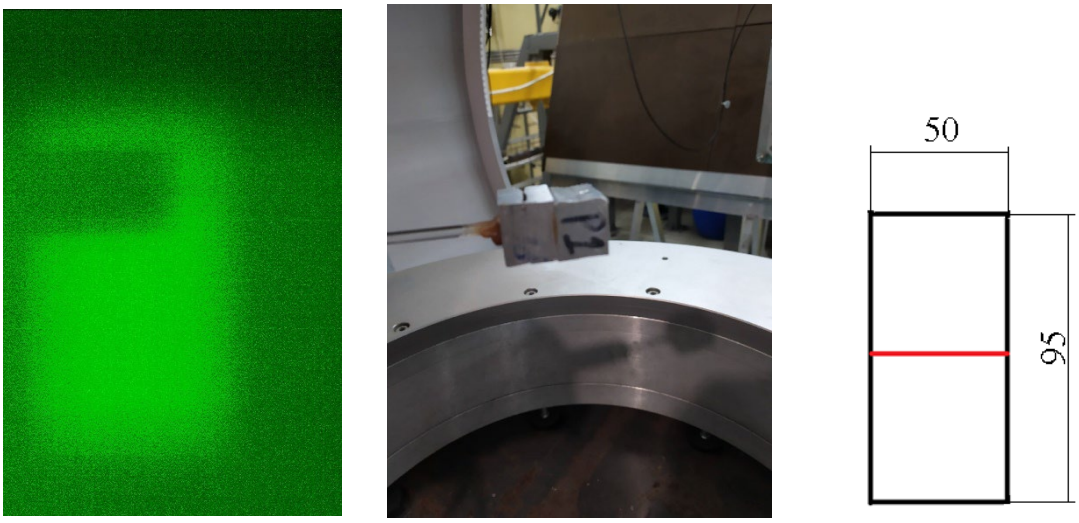

Figure 1 a) shadow of the Al with Gd sample placed at the first ring shown in b). c) The neutron beam cross section.

Neutrons scattered at a sample are registrated by detectors situated at the same angle of 90º. Detectors are positioned in a way to have regular 5 by 5-degree greed on a sphere. The distance from a sample to detector is one meter. The distance between samples is about 60 centimeters. There are 19 detectors based of ^{3}He counters with soller collimators at each ring. One ring is equipped with 29′ angular divergence collimators, another ring with 43′ angular divergence collimators. During the modernization of the spectrometer, new ^{3}He counters and preamps were installed. Compared to the old set of detectors, this significantly increased the efficiency of the

spectrometer. For independent operation of the two detector systems, each is equipped with its own MPD-240 data acquisition system [4] and has its own control computer. The MPD-240 DAQ systems are clocked by a common reactor start signal corresponding to the periodic neutron pulse at the output of the IBR-2 reactor cold moderator, with a frequency of 5 Hz and a duration of 2 μs. Therefore, the time counting for each event in both detectors starts at the same moment with a time resolution of 16 ns.

Important question is connected with mutual influence of the samples on the measured spectra. To assure the absence of the mutual influence, two powder samples of different materials were measured simultaneously at different positions and rings. One sample was aluminum with cerium and another was mixture of calcite and aragonite. Figure 2 displays the results of such measurements. One can clearly see that each spectrum is not affected by the other one. This becomes possible due to presence of the soller collimators in front of detectors. They effectively transmit just those scattered neutrons that are at the angle of 90º.

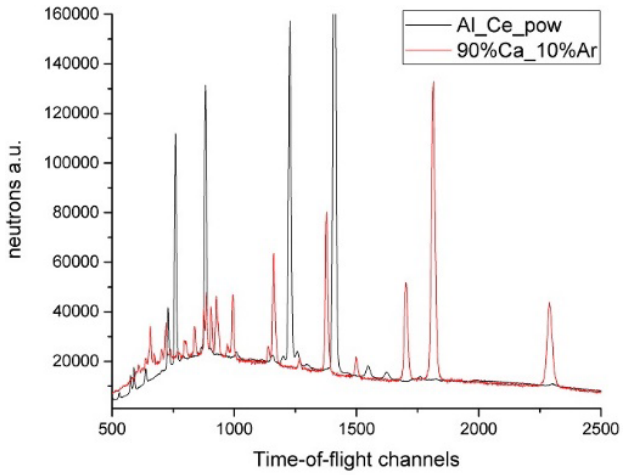

Figure 2 Two simultaneously measured powder samples.

It is necessary to mention that new preamplifiers as well as other electronics was updated. Sonix+ software package [4] is used for data acquisition and data storage for both rings independently. Measurements of the same samples at different rings to be presented and discussed. Besides, the present development of the instrument allows increase almost four times the output of the instrument.

[1] Feldmann, K. (1991). Texture Investigations by neutron Time-of-Flight Diffraction. Textures and Microstructures, 59-64.
[2] Feldmann, K., Betzl, M., KLeinsteuber, W., Walther K. (1991). Neutron Time-of-flight Texture Analysis. Textures and Microstructures, 59-64.
[3] Keppler, R., Ullemeyer, K., Behrmann, J., Stipp, M. (2014). Potential of full pattern fit methods for the texture analysis of geological materials: implications from texture measurements at the recently upgraded neutron time-of-flight diffractometer SKAT. J. Appl. Cryst., 1520-1534;
[4] S. A. Kulikov and V. I. Prikhodko «A New Generation of Data Acquisition and Data Storage Systems of the IBR-2 Reactor Spectrometers Complex» ISSN 1063-7796, Physics of Particles and Nuclei, 2016, Vol. 47, No. 4, pp. 702–710.

CRYSTALLOGRAPHIC TEXTURE OF CALCITE IN THE SHELLS OF RECENT BRACHIOPODS

A.V. Pakhnevich[1,2], D.I. Nikolayev[2] and T.A. Lychagina[2]

[1] *Borissiak Paleontological Institute of RAS, Moscow, Russia*
[2] *Joint Institute for Nuclear Research, Dubna, Russia*

E-mail: alvpb@mail.ru

Brachiopods are invertebrates whose bodies are enclosed in a bivalve shell. However, they do not belong to the Phylum Mollusca. The bivalve shell's protection arose as a result of convergent evolution, an adaptation to similar habitats. Brachiopods have been known since the early Cambrian, approximately 535 million years ago, and live in recent seas. They are filter feeders. Over millions of years of evolution, brachiopods often competed with bivalves as part of the ocean's bottom biofilter. While they were numerous in the Paleozoic era, today only about 400 species remain.

The microstructure and crystallographic texture of minerals in bivalve shells are actively studied [1], [2], [3]. However, the crystallographic texture of minerals in brachiopod shells is investigated fragmentary [4], [5]. Mostly, only data obtained using EBSD and X-ray diffraction for individual species are available. Brachiopod shells are composed of fluorapatite or calcite. Most species of brachiopods have shells made of calcite. This same mineral is also common in the shells of many bivalves.

We studied the crystallographic texture of calcite in brachiopod shells using several species of recent brachiopods. Measurements were conducted at the Frank Neutron Physics Laboratory of the Joint Institute for Nuclear Research (Dubna, Moscow Region) using the SKAT instrument situated at the beamline 7A-2 at the IBR-2 pulsed reactor. We analyzed valves of the recent brachiopod *Neothyris lenticularis* from empty shells collected off the coast of New Zealand, *Coptothyris adamsi* from Peter the Great Bay (Russia), and *Liothyrella neozelanica* and *Terebratella sanguinea* from the coast of New Zealand, South Island, and the Doubtful Sound Biological Station (New Zealand). All studied brachiopods belong to the order Terebratulida. Multiple brachiopod valves were glued together.

Our study confirmed that all valves are composed of calcite. The global crystallographic texture of calcite in brachiopod shells was measured for the first time. The obtained calcite pole figures differed from those measured using EBSD in all previously studied brachiopods [6]. The contour pattern of the pole figures (0006) and (10–14) replicates the shell shape, as previously observed in the pole figures of aragonite in the nacreous layer of bivalve valves or in the case of foliated calcite in the fossil Jurassic bivalve *Gryphaea dilatata*. This is the first time that similarity in the contour patterns of pole figures corresponding to different crystallographic directions has been noted. The pole figure (0006) easily distinguishes between the ventral and dorsal valves. The pole density in this figure is low, ranging from 1.95 to 5.10 mrd. This parameter in the pole figure (10-14) is also low, at 1.37 to 1.63 mrd. Peaks in the pole density are located in the center of the pole figures or can be extended in various directions. Example of the pole figures is presented in figure 1.

The crystallographic texture of calcite in brachiopod shells belonging to the same family varies and depends on the shell shape.

Thus, calcite crystals in the shells of recent brachiopods are characterized by a weak ordering. The isoline pattern follows the shape of the valves. Crystallographic texture features do not depend on the family of studied brachiopods.

[1] C.Hedegaard, H.R.Wenk (1998). Microstructure and texture patterns of mollusc shells. Journal of Molluscan Studies. 64. 1. 133-136.

[2] D.Chateigner, S.Ouhenia, C.Krauss, M.Belkhir, M.Morales (2010). Structural distortion of biogenic aragonite in strongly textured mollusc shell layers. Nuclear Instruments and Methods in Physics Research Section B: Beam Interactions with Materials and Atoms. 268(3-4). 341-345.
[3] A.G.Checa, C.M.Pina, A.J.Osuna-Mascaró, A.B.Rodríguez-Navarro, E.M.Harper (2014). Crystalline organization of the fibrous prismatic calcitic layer of the Mediterranean mussel Mytilus galloprovincialis. European Journal of Mineralogy. 26(4). 495-505.
[4] A.J.Goetz, D.R.Steinmetz, E.Griesshaber, S.Zaefferer, D.Raabe, K.Kelm, S.Irsen, A.Sehrbrock, W.W.Schmahl (2011). Interdigitating biocalcite dendrites form a 3-D jigsaw structure in brachiopod shells. Acta biomaterialia. 7(5). 2237-2243.
[5] M.Cusack (2016). Biomineral electron backscatter diffraction for palaeontology. Palaeontology. 59. 2. 171-179.
[6] M.Simonet Roda, E.Griesshaber, L.Angiolini, C.Rollion-Bard, E.M.Harper, M.A.Bitner, S.M.Garcia, F.Ye, D.Henkel, V.Häussermann,·A.Eisenhauer, H.Gnägi, U.Brand, A.Logan, W.W.Schmahl (2022). The architecture of Recent brachiopod shells: diversity of biocrystal and biopolymer assemblages in rhynchonellide, terebratulide, thecideide and craniide shells. Marine Biology.169(1). 4.

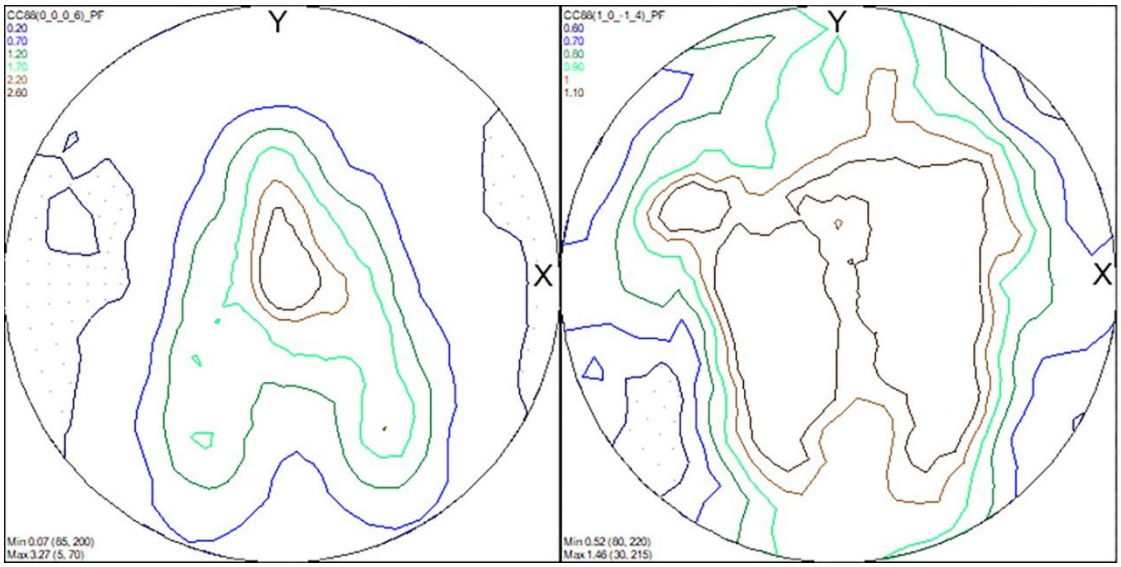

Fig. 1. Calcite pole figures in the dorsal valves of the brachiopod *Neothyris lenticularis*, New Zealand coast.

2D ^{10}B-RPC FOR SLOW NEUTRONS

M.O. Petrova[1,2],V.I. Bodnarchuk[1,2,3], E.I. Litvinenko[1], A.A. Bogdzel[1], V.V. Sadilov[1]

[1] *Joint Institute for Nuclear Research, Dubna, Russia*
[2] *Dubna State University, Dubna, Russia*
[3] *NRC "Kurchatov Institute", Moscow, Russia*

E-mail: mbelova@jinr.ru

The shortage of ^{3}He gas and limitations of spatial resolution and rate capability of ^{3}He-based detectors stimulate development of a new generation of detector systems for registration of slow neutrons. Resistive plate chambers (RPC) have design features that can reduce the uncertainty in measuring the position and time of a neutron's interaction with the detector. RPC also have a higher rate capability compared to wire detectors. The report will present a two-coordinate position-sensitive detector based on RPC with $^{10}B_4C$ thin film converter and the measurement results obtained with different radiation sources.

PROXIMITY EFFECTS AND COHERENT TRANSPORT IN JOSEPHSON JUNCTIONS WITH FERROMAGNETS

V.V. Ryazanov[1]

[1] *Moscow Institute of Physics and Technology, Dolgoprudny, 141700, Russia*

E-mail: valery.ryazanov@gmail.com

Currently, there is a great interest in hybrid nanostructures with coherent transport through various Josephson barriers made of normal metals, ferromagnets, topological insulators, etc. Our group has carried out pioneering experiments with the flow of superconducting current through layers of weak ferromagnets [1,2] and layers of normal metals in contact with ferromagnets [3,4]. The presence of ferromagnets significantly changes the relation between the superconducting current and the superconducting phase difference at a Josephson barrier, up to the transition of the Josephson structure to a state with an inverse current-phase relation, the π-state. Josephson hybrid structures based on ferromagnetic layers (SFS π-junctions) have prospects for use in digital and quantum electronics [5].

Coexistence of superconductivity (S) and ferromagnetism (F) is one of the most actively progressing fields in the condensed matter physics. Undoubtedly the most impressive phenomena observed in this field recently are related to spatial nonuniform superconductivity in a ferromagnet close to superconductor/ferromagnet interface. Antagonism of superconductivity and ferromagnetism differing in spin ordering is a cause of the strong suppression of superconductivity in the contact area of the S- and F -materials. The superconducting order parameter decay length ξ_{F1} is as small as 1 nm if typical strong ferromagnets such as Fe, Co, and Ni are used like F-interlayers in *SFS* junctions. The only approach is to fabricate Josephson *SFS* junctions with weak ferromagnets. The experimental studies of the π-state were carried out by us on thin-film sandwiches Nb-$Cu_{1-x}Ni_x$-Nb, with x in the range 0.52–0.57 and the Curie temperature, T_{Curie}, of the copper-nickel layers in the range 30–150K. Because the weak ferromagnet is alloy, the role of magnetic scattering in the Josephson junction F-barrier is important. We deal with spin-flip scattering due to magnetic inhomogeneity that could be multidomain structure, domain walls, and above all Ni-rich clusters arising in $Cu_{1-x}Ni_x$ ferromagnet for x close to 0.5.

The non-uniform magnetic properties of the Pd/Fe alloy which was used by us for implementation of Josephson SFS magnetic memory [6] are also of great interest. The $Pd_{1-x}Fe_x$ thin layer containing less than 4 at % of iron is a suitable challenger for the implementation in such devises. However, the properties of thin films and nanostructures based on $Pd_{1-x}Fe_x$ differ from those of bulk materials. The decrease in the ferromagnet size leads to the changes in crystallographic anisotropy, to decrease in the spontaneous magnetization, and to lowering of T_{Curie}. For example, for $Pd_{99}Fe_{01}$ alloy, the value of T_{Curie} varies from 40 K for bulk samples down to zero for a film of 10 nm thick. In addition, the magnetic characteristics of the films depend on the properties of adjacent layers and the substrates: interface roughness, stresses and other factors. In the work [7] it was also shown that a cluster structure of the $Pd_{99}Fe_{01}$ ferromagnetic layer causes an appreciable enhancement of the screening supercurrent density in the adjacent superconducting layer.

We believe that the use of neutron methods will be very useful for studying magnetic inhomogeneities and magnetic characteristics of layered hybrid structures.

[1] V.V. Ryazanov, V.A. Oboznov, A.Yu. Rusanov et al (2001). Coupling of two superconductors through a ferromagnet: evidence of a pi-junction. Phys. Rev. Lett. 86, 2427.

[2] V. A. Oboznov, V.V. Bol'ginov, A.K. Feofanov et al (2006). Thickness dependence of the Josephson ground states of superconductor-ferromagnet-superconductor junctions. Phys. Rev. Lett. 96, 197003 (2006).
[3] T.E. Golikova, F. Hübler, D. Beckmann et al (2012). Double proximity effect in hybrid planar superconductor-(normal metal/ferromagnet)-superconductor structures. Phys. Rev. B 86, 064416.
[4] T.A. Golikova, M.J. Wolf, D. Beckmann et al (2021). Controllable supercurrent in mesoscopic superconductor-normal metal-ferromagnet crosslike Josephson structures Supercond. Sci. Technol. 34**,** 095001.
[5] A.K. Feofanov, V.A. Oboznov, V.V. Bol'ginov et al (2010). Implementation of superconductor/ferromagnet/superconductor pi-shifters in superconducting digital and quantum circuits. Nature Physics 6**,** 593.
[6] V.V. Bol'ginov, V.S. Stolyarov, D.S. Sobanin, A.L. Karpovich, V.V. Ryazanov (2012). Magnetic switches based on Nb–PdFe–Nb Josephson junctions with a magnetically soft ferromagnetic interlayer. JETP Lett. 95, 366.
[7] L.S. Uspenskaya*a*,, A.L. Rakhmanov, L.A. Dorosinskii et al (2013). Magnetic Patterns and Flux Pinning in $Pd_{99}Fe_{01}$–Nb Hybrid Structures. JETP Lett. 93, 176.

STOICHIOMETRIC CONSTRAINTS AS A ROUTE TO MORE RELIABLE SAXS ANALYSIS OF MEMBRANE PROTEINS IN DETERGENT

Yu.L. Ryzhykau[1,2], D.D. Kuklina[1], D.V. Sidorov[1], A.Yu. Shishkin[1], I.O. Bezruchko[1], S.M. Bukhalovich[1], E.A. Dronova[1], A.E. Mikhailov[1], Yu.S. Semenov[1], O.I. Ivankov[2], A.I. Kuklin[1,2]

[1] *Research Center for Molecular Mechanisms of Aging and Age-Related Diseases, Moscow Institute of Physics and Technology, MIPT, Dolgoprudny, 141701, Russia*

[2] *Frank Laboratory of Neutron Physics, Joint Institute for Nuclear Research, Dubna, 141980, Russia*

E-mail: rizhikov@phystech.edu

Membrane proteins are central to signal transduction, transport and bioenergetics, yet their quaternary structure in solution is often difficult to establish by high-resolution methods alone. Crystallography and cryo-EM provide indispensable structural detail, but they do not always report the oligomeric organization that is most relevant in detergent or membrane-mimetic environments. Small-angle X-ray scattering is therefore an important complementary approach, since it probes membrane-protein assemblies directly in solution and can be highly informative with respect to their oligomeric state and overall architecture. This point is illustrated by the cyanobacterial rhodopsin ASR: although it forms dimers in the crystal, SAXS and NMR studies indicated predominantly trimeric species, showing that the crystal structure alone did not fully capture the relevant oligomeric state [1]. For oligomeric microbial rhodopsins, SAXS-type solution analysis is therefore not merely supportive but can address a structurally important question that may remain unresolved by a high-resolution structure alone.

At the same time, SAXS analysis of detergent-solubilized membrane proteins is intrinsically complicated by two factors: the detergent corona surrounding the hydrophobic part of the protein and, in many cases, oligomeric polydispersity. Our previous study showed that both effects can strongly bias data interpretation and may even produce misleading low-resolution models if not treated explicitly [2]. Hybrid approaches such as MEMPROT substantially improve this situation by describing the detergent corona with pseudo-atoms representing hydrophobic and hydrophilic regions and fitting the resulting protein-detergent models against the SAXS curve [3,4]. However, more recent work also makes clear that such SAXS-guided modeling remains intrinsically non-unique: several detergent-corona geometries may fit the same data nearly equally well, and physically implausible solutions may survive if model selection is guided only by fit quality. In practice, this means that even an incorrect oligomeric hypothesis can sometimes be artificially compensated by an alternative detergent-belt geometry.

We suggest that this ambiguity can be reduced by introducing stoichiometric constraints, namely the detergent-to-protein ratio in the protein-detergent complex. Such information may be obtained by orthogonal biophysical methods, for example from UV and differential refractive index measurements or from infrared spectroscopy. These approaches are useful, but their accuracy depends on external parameters such as extinction coefficients, dn/dc values and the quantitative calibration of the spectroscopic method. An attractive complementary route is SANS contrast variation, which provides access to the relative volume fractions of the protein and detergent components in scattering terms by comparing the contrast-matching point of the whole complex with those of the individual components. In this way, the detergent-to-protein ratio can be estimated in a form directly relevant to scattering-based modeling and then used as an a priori restriction in SAXS analysis, or later in joint SAXS/SANS refinement.

We are currently testing this concept on DDM-solubilized microbial rhodopsins. In particular, SANS contrast-variation experiments have been performed for KR2, a sodium-pumping rhodopsin whose functional form is pentameric and whose oligomerization is directly important for activity [5]. The ongoing analysis addresses whether stoichiometric information extracted from SANS can help to reduce the effective parameter space of detergent-corona models and thereby improve the uniqueness and physical plausibility of SAXS-based structural interpretation of protein-detergent complexes.

Yu.R. Ryzhykau and D.D. Kuklina acknowledges the Ministry of Science and Higher Education of the Russian Federation (agreement 075-03-2026-305, project FSMG-2025-0003).

[1] S. Milikisiyants , S. Wang , R. A. Munro , M. Donohue, M. E. Ward, D. Bolton , L. S. Brown , T. I. Smirnova , V. Ladizhansky , A. I. Smirnov, Oligomeric structure of Anabaena sensory rhodopsin in a lipid bilayer environment by combining solid-state NMR and long-range DEER constraints, J. Mol. Biol. 429 (2017) 1903–1920. https://doi.org/10.1016/j.jmb.2017.05.005.

[2] Y.L. Ryzhykau, A. V. Vlasov, P.S. Orekhov, M.I. Rulev, A. V. Rogachev, A.D. Vlasova, A.S. Kazantsev, D.P. Verteletskiy, V. V. Skoi, M.E. Brennich, P. Pernot, T.N. Murugova, V.I. Gordeliy, A.I. Kuklin, Ambiguities in and completeness of SAS data analysis of membrane proteins: the case of the sensory rhodopsin II–transducer complex, Acta Crystallogr. D Struct. Biol. 77 (2021) 1386–1400. https://doi.org/10.1107/s2059798321009542.

[3] J. Pérez, A. Koutsioubas, Memprot: a program to model the detergent corona around a membrane protein based on SEC–SAXS data, Acta Crystallographica Section D 71 (2015) 86–93. https://doi.org/10.1107/S1399004714016678.

[4] F. De Pol, M. Baranowski, C. Neumann, S. Trampari, P. Nissen, J. Pérez, Simulation and modelling of the detergent corona around the membrane protein MhsT based on SAXS data, J. Appl. Crystallogr. 57 (2024) 1415–1425. https://doi.org/10.1107/S1600576724006721.

[5] K. Kovalev, V. Polovinkin, I. Gushchin, A. Alekseev, V. Shevchenko, V. Borshchevskiy, R. Astashkin, T. Balandin, D. Bratanov, S. Vaganova, A. Popov, V. Chupin, G. Büldt, E. Bamberg, V. Gordeliy, Structure and mechanisms of sodium-pumping KR2 rhodopsin, Sci. Adv. 5 (2019) eaav2671. https://doi.org/10.1126/sciadv.aav2671.

NEW DISCOVERIES IN THE STUDY OF ARCHAEOLOGICAL SITES USING METHODS OF NATURAL AND FUNDAMENTAL SCIENCES

I. Saprykina[1]

[1] *Institute of Archaeology RAS, Moscow*

The method of neutron tomography, radiography and diffraction, applied to the study of the composition, preservation, and manufacturing technology of archaeological objects, is an already established analytical method for archaeological research, significantly increasing our possibilities of obtaining new scientific data (Kichanov et al., 2017; Abramzon et al., 2018; Kichanov et al., 2018; Saprykina et al., 2019; etc.). This method is applied to determine the factors responsible for corrosion processes, identify compositional heterogeneities, structural features, variations in phase composition, hidden traces of technological operations, etc. Over 10 years of joint research of archaeological objects with the FLnP JINR, new unique data have been successfully obtained on the composition of ancient and Old Russian jewelry, complex technological aspects of minting ancient and medieval coins, and even on unexpected health practices of the population of the ancient Bosporus.

We now have the ability to utilize additional analytical methods (SEM, micro-Raman spectroscopy, mass spectrometry, etc.) in our arsenal. When combined with neutron tomography, radiography, and diffraction, this approach allows us to extract valuable scientific information, regardless of the state of preservation of archaeological objects.

One of the most comprehensively and thoroughly studied archaeological finds to date, using methods of the natural and fundamental sciences, is the collection of archaeological finds from the excavations of the ancient necropolis Volna 1, dating from the last third of the 6th to the 3rd centuries BC (Taman Peninsula). This monument is, in a sense, a unique archaeological site not only due to the scale of the fieldwork conducted. First and foremost, the collection—objects made of ferrous, non-ferrous, and precious metals, ceramic vessels, alabaster, and glass—was systematically studied using modern methods of the natural and fundamental sciences. This approach yielded valuable scientific data characterizing the material component of the Greek colonization of the Northern Black Sea region.

This study was supported by the Russian Science Foundation grant No. 23-18-00196-P “Integrated studies of the new urban necropolis of archaic and classical time Volna 1 in the Asian Bosporus”.

[1] Kichanov S.E., Kozlenko D.P., Saprykina I.A., Lukin E.V., Rutkauskas A.V., Nazarov K., Savenko B.N. Study of archaeological objects by neutron tomography // JINR NEWS, 1, pp. 20–23 (2017). (*In Russian*).

[2] Abramzon M.G., Saprykina I.A., Kichanov S.E., Kozlenko D.P., Nazarov K.M. Study of the chemical composition of the alloy of Bosporan billon staters of the 3rd century AD by X-ray spectroscopy, neutron tomography and diffraction methods // Surface. X-ray, Neutron, Synchrotron radiation, 2, pp. 24–28 (2018). (*In Russian*).

[3] Kichanov S.E., Saprykina I.A., Kozlenko D.P., Nazarov K., Lukin E.V., Rutkauskas A.V., Savenko B.N. “Studies of Ancient Russian Cultural Objects Using the Neutron Tomography Method”, Journal of Imaging, 4(2), pp. 25-34 (2018).

[4] Saprykina I.A., Kichanov S. E., Kozlenko D. P. Possibilities, Limitations, and Prospects of Using Neutron Tomography and Radiography for Preservation of Archaeological Heritage Objects // Crystallography Reports. Pleiades Publishing, 61(1), pp. 177–180 (2019).

ELEMENTAL COMPOSITION OF FIFTEEN MEDICINAL SPECIES OF ASTERACEAE FAMILY OF MOLDOVAN ORIGIN DETERMINED BY NEUTRON ACTIVATION ANALYSIS

A. Ciocarlan[1], M. Shvetsova[2], I. Zinicovscaia[2,3], O. Chaligava[2,4], D. Grozdov[2], A. Aricu[1], N. Ciocarlan[5]

[1] *The Institute of Chemistry, Moldova State University, Chisinau, Moldova*
[2] *Joint Institute for Nuclear Research, Dubna, Russia*
[3] *Horia Hulubei National Institute for R&D in Physics and Nuclear Engineering, Magurele, Romania*
[4] *Faculty of Exact and Natural Science, Georgian Technical University, Tbilisi, Georgia*
[5] *National Botanical Garden (Institute) "A. Ciubotaru", Moldova State University, Chisinau, Moldova*

E-mail: mks@nf.jinr.ru

The content of major- and microelements (Na, Mg, Al, Cl, K, Ca, Sc, V, Cr, Mn, Fe, Co, Ni, Zn, As, Se, Br, Rb, Sr, Mo, Sb, Cs, Ba, La, Ce, Sm, Tb, Hf, Ta, Th and U) in 15 medicinal species of the Asteraceae family collected from the experimental field of the National Botanical Garden of the Republic of Moldova was determined by neutron activation analysis at the IBR-2 reactor. Potassium was found to be the most abundant major element; its content in plants ranged from 20,700 mg/kg in *Artemisia lerchiana* to 58,000 mg/kg in *Matricaria recutita*. The content of other major elements existed in the following ranges: Ca from 4700 to 14,200 mg/kg and Mg from 1710 to 3870 mg/kg. The maximum content of Mg, K and Ca in analyzed plants was higher compared to data presented in the literature. Among essential microelements the most abundant were Fe (83–910 mg/kg), Mn (23–150 mg/kg) and Zn (27–76 mg/kg). The health risk index (HRI) and the daily intake of metal (DIM) were calculated for As, Ni, Sb, V, Mn, Cr, Co, U, Sr, Al, Fe and Zn. DIM values above the oral reference dose (RfD) for Co (0.0003 mg/kg/day) were identified in *Calendula officinalis* (3.12×10^{-4} mg/kg) and *Tanacetum balsamita* (7.47×10^{-4} mg/kg), and above RfD for V (0.00007 mg/kg/day) in *Achillea clypeolata* (4.84×10^{-4} mg/kg), *Artemisia balchanorum* (4.04×10^{-4} mg/kg), *Artemisia lerchiana* (1.11×10^{-3} mg/kg), *Tanacetum balsamita* (3.31×10^{-4} mg/kg), *Helichrysum arenarium* (4.53×10^{-4} mg/kg) and *Matricaria recutita* (3.61×10^{-4} mg/kg). HRI values exceeding threshold were identify in *Calendula officinalis* (1.04 mg/kg) and *Tanacetum balsamita* (2.4 mg/kg) for Co and in all herbal samples for V. The high concentrations of these elements can have a negative impact on the cardiovascular, respiratory and endocrine systems. In herbal plants samples (*Achillea filipendulina*, *Achillea millefolium*, *Artemisia absinthium*, *Centaurea cyanus*, *Tanacetum parthenium*, *Cichorium intybus*, *Echinops ritro* and *Helichrysum italicum*) HRI values for all elements were below the threshold which means insignificant carcinogenic health risk when using infusions from studied plants.

LAYERED RARE EARTH MANGANITES UNDER EXTREME CONDITIONS

E.V. Sterkhov[1], V.A. Sidorov[2], A.Yu. Likhacheva[3], E.V. Lukin[4], S.E. Kichanov[4], S.G. Titova[1]

[1] *Vatolin Institute of Metallurgy of Ural Branch of Russian Academy of Sciences, 620016, Ekaterinburg, Russia*
[2] *Vereshchagin Institute of High Pressure Physics, Russian Academy of Sciences, 108840, Troitsk, Moscow, Russia*
[3] *Sobolev Institute of Geology and Mineralogy, Siberian Branch of Russian Academy of Sciences, 630090, Novosibirsk, Russia*
[4] *Frank Laboratory of Neutron Physics, Joint Institute for Nuclear Research, 141980, Dubna, Russia*

E-mail: ev.sterhov@mail.ru

Due to the strong interaction between different degrees of freedom (spin, charge, orbital, and phonon subsystems), layered manganites have attracted much attention last decades. Under external conditions (temperature, pressure, mechanical stress, electric and magnetic fields), strong correlated materials exhibit unusual optical, electronic, and magnetic properties. A-site ordering in layered $LnBaMn_2O_6$ manganites leads to a significant change in the phase state: materials with large lanthanide ions Ln = La, Pr exhibit ferromagnetic behavior above $T_C > 300$ K, while oxides with small elements Ln = Y – Sm are charge- and/or orbital-ordered insulators with a transition temperature to the "bad metal" state above 350 K. The size of the ion also determines the sequence and type of structural transitions. In particular, for $SmBaMn_2O_6$, the structure is orthorhombic, space group *Cmmm*, $2a_p \times 2b_p \times 2c_p$, where $a_p \sim c_p$ denotes to simple cubic perovskite. Propagation vector $\mathbf{k_1}$ (00½) is connected with the ordering of the simple perovskite cells of $LnMnO_3$ and $BaMnO_3$, while $\mathbf{k_2}$ (½½0) is caused by the tilting of the MnO_6 octahedra. The metal-insulator transition (T_{MI}) is caused by charge ordering ($T_{CO1} = T_{MI} \sim 380$ K) of Mn^{3+} and Mn^{4+} ions, which leads to a new superstructure of $2\sqrt{2}a_p \times 2\sqrt{2}b_p \times 4c_p$ (space group *Pnam*) [1]. In this case manganese ions are ordered in an AABB-type manner along the c-axis, resulting in a 4-fold period along the c-axis. A further cooling leads to a change in the type of charge ordering from AABB to AAAA at $T_{CO2} \sim 200$ K, respectively, and a 4-fold increase in the parameter along the c-axis disappears. Below T_{CO2}, the structure is described as $2\sqrt{2}a_p \times 2\sqrt{2}b_p \times 2c_p$, space group $P2_1am$. In the case of $LaBaMn_2O_6$, there is almost no distortion of the MnO_6 octahedra at low temperatures, so the structure remains tetragonal, $a_p \times a_p \times 2c_p$, space group *P4/mmm*. The result of the competition of different phases and, as a consequence, structural states under the influence of external pressure and temperature of layered manganites is quite unpredictable [2]. Thus, for La- and Nd-based oxides, we have discovered for the first time superstructure reflexes with d ~ 23 Å, which indicates new phase and structural states of oxides under extreme conditions.

[1] Morikawa D., Tsuda K., Maeda Y., Yamada S., Arima T. Charge and Orbital Order Patterns in an *A*-Site Ordered Perovskite-Type Manganite $SmBaMn_2O_6$ Determined by Convergent-Beam Electron Diffraction // J. Phys. Soc. Jpn., 2012, V. 81, P. 09360
[2] S. Titova, E. Sterkhov, V. Sidorov, N. Chtchelkatchev, F. Alabarse, High pressure - low temperature study on $NdBaMn_2O_6$ double manganites, Journal of Alloys and Compounds, 2025, P. 183151.

The work was supported by Russian Science Foundation, grant № 25-23-00102.

STRUCTURAL STUDIES OF APOFERRITIN-LIPID SYSTEMS

O.M. Tilinova[1], Yu.L. Ryzhykau[1], R.K. Gretskii[1], A.I. Yusova[1], D.A. Galiguzov[1], A.I. Kuklin and A.V. Vlasov[1]

[1] *Moscow institute of physics and technology, Dolgoprudny, Russia*

E-mail: tilinova.om@phystech.edu

Iron deficiency anemia (IDA) remain a global health problem, affecting approximately two billion people. Traditional therapy with iron salts is limited by significant side effects, which drives the search for improved delivery systems. A promising approach is the use of the natural nanocontainer ferritin – a globular protein complex composed of 24 subunits that stores iron in a bioavailable form within a cavity of 8 nm in diameter [1]. In this work, we propose the development of a hybrid lipid-protein system in which ferritin is encapsulated into liposomes. Since methods for loading ferritin into liposomes are currently insufficiently developed, and obtaining a stable loaded form represents a significant challenge on its own [2], at the first stage we focus on the structural study of systems based on apoferritin (the empty protein). Establishing a protocol for its encapsulation and verifying the integrity of the resulting complexes will lay the foundation for subsequent development of a therapeutically active formulation for drug delivery systems.

In this work, we assembled hybrid liposome-apoferritin systems using recombinant apoferritin from *Escherichia coli*, and characterized them with the help of biochemical and structural biology methods. Several trials have already been made. Firstly, apoferritin-based liposomes were obtained by extrusion of DMPC MLVs mixed with apoferritin. Secondly, we used asolectin with sodium cholate with the subsequent removal of the detergent by dialysis. Structural studies were performed using small-angle neutron scattering (SANS). The obtained results and future plans are discussed.

The work was supported by the Russian Science Foundation (project № 24-14-00295).

[1] Sudarev V.V. et al. (2023). Ferritin self-assembly, structure, function, and biotechnological applications. Int. J. Biol. Macromol. 224, 319-343.

[2] De Souza T.P. et al. (2012). Encapsulation of ferritin, ribosomes, and ribo-peptidic complexes inside liposomes: insights into the origin of metabolism. Orig Life Evol Biosph. 42, 421-428.

EMERGENT FUNCTIONALITIES IN VAN DER WAALS NANOPARTICLES SYNTHESIZED VIA FEMTOSECOND LASER ABLATION

A.A. Ushkov[1], N.M. Belozerova[1], D.V. Dyubo[1], S.V. Klimov[1], A.V. Syuy[1], S.M. Novikov[1], G.I. Tselikov[1], A.V. Arsenin[1].

[1] *Center for Photonics and 2D Materials, Moscow Institute of Physics and Technology, 141701, Dolgoprudny, Russia*

E-mail: ushkov.aa@mipt.ru

Layered two-dimensional van der Waals (vdW) materials, particularly transition metal dichalcogenides (TMDCs), represent a highly active interdisciplinary frontier in modern research due to their extraordinary electronic, optical, and chemical properties. While traditionally studied in planar geometries, turning these materials into spherical, sub-100 nm colloidal architectures enlarges their functionality in nanophotonics, catalysis, and biomedicine. Femtosecond pulsed laser ablation in liquids (fs-PLAL) has recently emerged as a robust, single-step, and ligand-free top-down methodology capable of synthesizing stable, highly pure nanoparticles directly from a single bulk vdW precursor without the need for complex chemical procedures and passivation. In this work we sum up our experimental and theoretical expertise in this field.

Controlling the atomic structure of these nanoparticles - specifically, the conservation of the crystallinity or amorphization enhancing - is important for tailoring their functional performance. The fs-PLAL process is abundant in structural outcomes depending on the thermodynamic stability of the precursor [1]. Ablation of highly stable targets, such as tungsten diselenide WSe_2, produces spherical nanoparticles that preserve the bulk hexagonal 2H crystalline lattice [2,3]. In contrast, the extreme non-equilibrium kinetic quenching of less stable precursors like palladium diselenide $PdSe_2$ drives complete amorphization, forming non-stoichiometric $PdSe_{2-x}$ (Pd:Se ≈ 1:1) nanoparticles inherently enriched with coordinatively unsaturated sites and selenium vacancies [3,4].

Preserving the high refractive index and excitonic resonances of bulk vdW crystals within sub-wavelength nanoparticles is a key towards advanced all-dielectric nanophotonics. Despite the extreme synthesis conditions, we managed to crystallize WSe_2 and MoS_2 nanoparticles with a giant dielectric permittivity of their precursors and demonstrated strong, size-tunable Mie multipole resonances hybridized with pronounced room-temperature excitonic transitions (e.g., the A-exciton at ~770 nm for WSe_2) [2,5]. In contrast, the structural disorder and non-stoichiometric bonding in amorphous $PdSe_{2-x}$ nanoparticles suppress discrete excitonic features, instead providing a smooth, wavelength-independent broadband optical extinction that spans the entire near-infrared (NIR-I) biological transparency window [3].

The development of reliable, plasmon-free surface-enhanced Raman scattering (SERS) platforms with a spatially uniform enhancement relies on defect-mediated chemical mechanism instead of a highly-resonant inhomogeneous amplification observed in traditional noble metal substrates. Nanoparticle morphology significantly amplifies this chemical enhancement compared to planar flakes due to a substantially higher density of structurally induced active sites and surface curvature. Crystalline WSe_2 nanoparticles achieve SERS enhancement factors (EF) of ~10^4 and a limit of detection (LOD) of 10^{-7} M for rhodamine 6G, outperforming crystalline flakes (EF ~10^3) by an order of magnitude [2]. Furthermore, defect-engineered amorphous $PdSe_{2-x}$ nanoparticles yield a record-high plasmon-free EF exceeding 10^6 and LOD of 10^{-9} M for crystal violet, driven by efficient resonant charge transfer at abundant selenium vacancy sites [4].

Efficient conversion of NIR light into localized heat is a fundamental requirement for advanced theranostics, including deep-tissue photothermal tumor ablation. TMDC nanoparticles synthesized via fs-PLAL deliver exceptional, material-dependent photothermal conversion efficiencies (PCE). Crystalline WSe_2 nanoparticles act as narrowband resonant heaters, achieving a peak PCE of 71% when irradiated precisely at their excitonic resonance. In contrast, the intrinsically broadband absorption of amorphous $PdSe_{2-x}$ nanoparticles yields an ultra-high, wavelength-independent PCE of up to 83% at 830 nm, substantially outperforming traditional silicon (10%) and gold (41%) nanoscale photothermal agents.

This research was funded by the Russian Science Foundation, grant number 24-79-00144.

[1] Tselikov, Gleb I., et al. "Tunable nanostructuring for van der Waals materials." ACS nano 19.25 (2025): 22820-22836.
[2] Ushkov, Andrei, et al. "Femtosecond laser ablation and fragmentation for TMDC nanoparticles synthesis: A comparative study." Applied Surface Science 707 (2025): 163547.
[3] Ushkov, Andrei, et al. "Narrowband vs broadband optical absorption: Photothermal behavior of laser-synthesized TMDC nanoparticles." Applied Surface Science (2026): 166095.
[4] Ushkov, Andrei, et al. "Laser-Synthesized Amorphous PdSe2-x Nanoparticles: A Defect-Rich Platform for High-Efficiency SERS, Photocatalysis, and Photothermal Conversion." Advanced Materials Interfaces (2025): e00902.
[5] Tselikov, Gleb I., et al. "Transition metal dichalcogenide nanospheres for high-refractive-index nanophotonics and biomedical theranostics." Proceedings of the National Academy of Sciences 119.39 (2022): e2208830119.

SPINODAL DECOMPOSITION IN Fe-Ga ALLOYS

T.N. Vershinina[1], A.S. Bulaeva[1], B. Yerzhanov[1], S.V. Sumnikov[1], I.S. Golovin[2], A.M. Balagurov[1]

[1] *Joint Institute for Nuclear Research, Dubna, Russia*
[2] *National University of Science and Technology "MISIS", Moscow, Russia*

E-mail: vershinina@nf.jinr.ru

Fe-*x*Ga alloys demonstrate a phenomenon known as giant magnetostriction. What makes them unique is that magnetostriction has two peaks, at $x \approx 19$ and 27 at.%. While the nature of the first peak is more or less understood, there is active debate in the literature regarding the second one. To date, no structural element or set of elements has been reliably identified as the unequivocal cause of the second magnetostriction peak. In Ref. [1], it was found that an ω-like phase, designated by the authors as the X-phase, is observed in the as-cast Fe-27Ga alloy. A detailed analysis of the electron diffraction patterns [2], carried out by A. Leineweber, demonstrated that this phase is the $Fe_{13}Ga_9$ intermetallic compound. The same study also established that the ω-like phases observed by the authors of references [3, 4] in the $Fe_{73.1}Ga_{26.9}$ and $Fe_{73}Ga_{27}$ alloys, respectively, in the quenched and subsequently annealed states, are also the $Fe_{13}Ga_9$ intermetallic compound.

Using transmission electron microscopy, it was found in [4] that the ω-like phase forms via a spinodal decomposition mechanism. A similar conclusion was reached in [5], where a mechanism was proposed to explain the sharp increase in the volume fraction of the metastable $Fe_{13}Ga_9$ intermetallic compound at ~400 °C during continuous heating of alloys with a high gallium content (31–35 at.%). Thus, there arose a need for experimental confirmation of this conclusions.

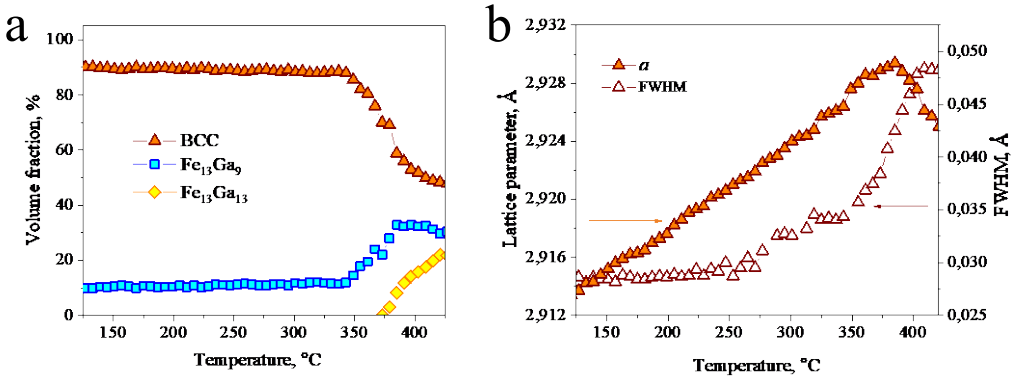

Figure 1. Evolution of the phase composition of the Fe66Ga34 alloy from the initial quenched state upon heating to 420°C (a) and lattice parameter of B2 phase and FWHM of (200) peak (b).

In this study, *in situ* investigations of the $Fe_{66}Ga_{34}$ alloy were carried out using neutron diffraction on a high-resolution Fourier diffractometer (HRFD, IBR-2). This instrument is distinguished by its ability to operate in two modes: high resolution ($\Delta d/d \approx 0.0015$) and high intensity ($\Delta d/d \approx 0.015$).

The initial state of the $Fe_{66}Ga_{34}$ alloy was achieved by quenching it in water at 900 °C. This heat treatment resulted in a two-phase structure consisting of 90% B2 and 10% $Fe_{13}Ga_9$ intermetallic phases. The alloy sample was then subjected to continuous heating at a rate of 2 °C/min up to a temperature of 420 °C. Measurements were carried out in high-intensity mode. Within the 350–380 °C range, a sharp increase in the volume fraction of the $Fe_{13}Ga_9$

intermetallic phase was observed (Fig.1a), accompanied by a decrease in the lattice parameter of the B2 phase (see Fig. 1b). At 375 °C, a phase transition B2 → $Fe_{13}Ga_{13}$ also occurs. A detailed analysis of the peak shapes revealed that, at a temperature of ~250 °C, the full width at half maximum (FWHM) begins to increase. We believe this is associated with the spinodal decomposition process, given that no other changes in phase composition were observed within this temperature range. The FWHM then levels off at ~310 °C and a sharp increase begins again at 350 °C, which is associated with the formation of the $Fe_{13}Ga_9$ intermetallics.

To confirm that a spinodal decomposition process occurs in the 250–310 °C range, an *in situ* experiment was conducted in high-resolution mode (Fig. 2). A sample of the $Fe_{66}Ga_{34}$ alloy was heated to 270 °C at a rate of 10 °C/min and then held at that temperature for 30 hours. As can be seen from Fig. 2b, upon reaching the set temperature, satellites had already formed to the right and left sides of (200) peak, corresponding to the formation of BCC phases with lower (BCC_I) and higher (BCC_{II}) gallium content, respectively. Subsequently, as the holding time increases, the intensity of the satellites grows, confirming the continued progression of the spinodal decomposition process.

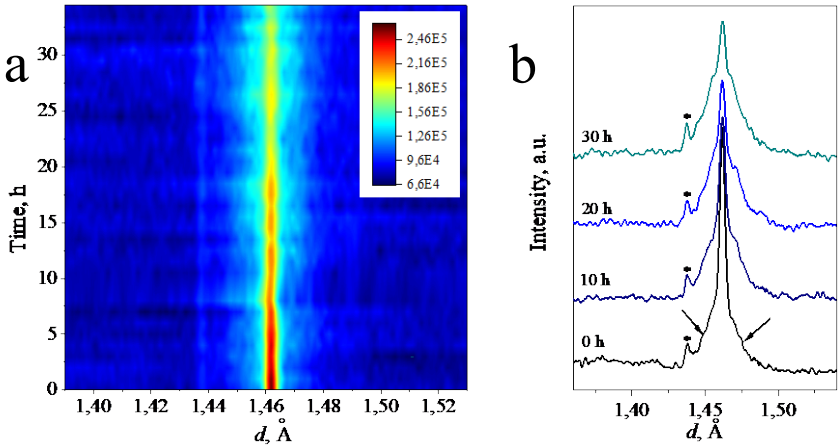

Figure 2. 2D visualization of the evolution of (200) peak of B2 phase of $Fe_{66}Ga_{34}$ alloy in a quenched state measured upon slow heating up to 270 °C (a) and profiles of (200) peak of B2 phase obtained at different temperatures. The arrows indicate the satellites. The peak from the furnace is marked with a sticker.

Since continuous heating results in a significant reduction in the B2 lattice parameter when the $Fe_{13}Ga_9$ intermetallic compound forms, it can be inferred that the gallium-rich phase with a BCC-based lattice structure transforms into the $Fe_{13}Ga_9$ intermetallic compound.

Experiments have thus confirmed that a spinodal decomposition process BCC → BCC_I + BCC_{II} occurs in Fe-Ga alloys, followed by a transition BCC_{II} → $Fe_{13}Ga_9$.

[1] A. M. Balagurov et. al. (2021) In-grain phase separation and structural ordering in Fe-Ga alloys seen from reciprocal space, Intermetallics 128, 107016 (1-4).
[2] A. Leineweber (2026) Monoclinic ω-phase related $Fe_{13}Ga_9$ as precipitate in Fe-≈27 at%Ga Galfenol-type alloys, Materials Today Communications, 50, 114105.
[3] M. Nakagawa et.al. (1987) Electron microscopic observation of omega-like phase in an Fe-26.9 at%Ga alloy, Scripta Materialia, 21, 461-464.
[4] C. Guan et.al. (2021) Atomic-scale insights into ω-variants in galfenol triggered by displacive-diffusive transformation, Materials Design, 205, 109745.
[5] T. N. Vershinina et.al. (2025) Influence of initial state and heating rate on phase transformation in $Fe_{66}Ga_{34}$ alloy, Journal of Alloys and Compounds, 1039, 182962.

FERRITIN-BASED HYBRIDS FOR VACCINES, DRUG DELIVERY AND IMAGING PLATFORMS

A.V. Vlasov[1,2], O.M. Tilinova[1], A.I. Yusova[1], R.K. Gretskiy[1], D.A. Galiguzov[1], S.D. Osipov[1], Yu.L. Ryzhykau[1,2], A.I. Kuklin[1,2]

[1] *Research Center for Molecular Mechanisms of Aging and Age-Related Diseases, Moscow Institute of Physics and Technology, Dolgoprudny, Russia*
[2] *Frank Laboratory of Neutron Physics, Joint Institute for Nuclear Research, Dubna, Russia*

E-mail: vavplanet@gmail.com

Ferritin is a 24-subunit protein nanocage that combines high stability, biocompatibility, and a well-defined hollow architecture, making it an attractive platform for recombinant vaccines, targeted drug delivery, and multimodal imaging. In this contribution, we summarize recent progress in ferritin-based hybrid nanoparticles, i.e. cages assembled from distinct ferritin subunits or subunit-conjugates that enable modular control of surface occupancy, ligand density, cargo loading, and circulation properties [1], [2]. Natural heteropolymers, including mammalian H/L ferritins and several non-mammalian hybrids, show that successful cage formation depends not only on sequence identity but also on conserved structural form factor and conformational flexibility of the protomers. Engineered hybrids extend this principle to multifunctional systems for mosaic vaccines, theranostic carriers, and neutron capture therapy.

Special attention will be paid to structural studies by small-angle scattering. Time-resolved SAXS has shown that ferritin reassembly proceeds through folded dimeric and higher oligomeric intermediates and is strongly influenced by electrostatic screening and solution conditions [3]. Complementary SAXS/SANS studies of apoferritin provide low-resolution shell parameters, reveal concentration-dependent interparticle effects, and offer a convenient benchmark for validating hollow-cage integrity in solution. For hybrid ferritins, these approaches are especially valuable because they allow one to verify whether antigen fusion, PEGylation, peptide targeting, or cargo encapsulation preserves the cage geometry. In addition, SANS at pulsed neutron sources such as YuMO/IBR-2 is well suited for the analysis of ferritin-based supramolecular assemblies because ferritin behaves as a structurally well-defined hollow shell with characteristic scattering features. Thus, SAXS/SANS can serve not only as mechanistic tools for studying self-assembly, but also as a practical layer of structural quality control for biomedical ferritin constructs [4].

Finally, we conclude that ferritin hybrids are among the most promising modular protein nanoplatforms for immunology and theranostics, and that their further translation will depend on combining rational subunit engineering with routine SAXS/SANS characterization of assembly pathways, cage integrity, and structural heterogeneity.

This work was supported by the Ministry of Science and Higher Education of the Russian Federation (agreement 075-03-2025-662, project FSMG-2025-0003).

[1] V.V.Sudarev, S.M.Dolotova, S.M.Bukhalovich, S.V.Bazhenov, Y.L.Ryzhykau, V.N.Uversky, N.A.Bondarev, S.D.Osipov, A.E.Mikhailov, D.D.Kuklina, T.N.Murugova, I.V.Manukhov, A.V.Rogachev, V.I.Gordeliy, I.Y.Gushchin, A.I.Kuklin, A.V.Vlasov (2023). Ferritin self-assembly, structure, function, and biotechnological applications. *Int. J. Biol. Macromol.* 224, 319-343.

[2] M.S.Gette, V.V.Sudarev, S.D.Osipov, E.V.Laptenkova, S.V.Bazhenov, Y.A.Zagryadskaya, O.M.Tilinova, E.A.Dronova, D.D.Kuklina, R.Al Ebrahim, D.M.Fedorov, T.S.Kurkin, Y.S.Semenov, N.A.Bondarev, V.V.Skoi, I.S.Okhrimenko, N.Li, A.I.Kuklin, I.V.Manukhov, Y.L.Ryzhykau, V.N.Uversky, A.V.Vlasov (2025).

Ferritin-based hybrid macromolecules experience unusual shift of stoichiometry distribution. *Int. J. Biol. Macromol.* 293, 139335.
[3] D.Sato, H.Ohtomo, Y.Yamada, T.Hikima, A.Kurobe, K.Fujiwara, M.Ikeguchi (2016). Ferritin Assembly Revisited: A Time-Resolved Small-Angle X-ray Scattering Study. *Biochemistry* 55, 287-293.
[4] T.N.Murugova, A.I.Kuklin, V.I.Gordeliy, A.V.Rogachev, A.K.Islamov, I.V.Manasiev, Y.L.Ryzhykau, A.V.Vlasov (2015). Low resolution structural studies of apoferritin via SANS and SAXS: The effect of concentration. *J. Optoelectron. Adv. Mater.* 17, 1397-1402.

FUNDAMENTALS OF SMALL-ANGLE SCATTERING IN THE STUDY OF THE STRUCTURE OF DISORDERED SYSTEMS

V. Volkov[1]

[1] *National Research Center "Kurchatov Institute", 119333 Moskow, Leninski Prospekt, 59*

E-mail: volkicras@mail.ru

Small-angle scattering of X-rays and neutrons has become a standard part of studying the structural organization of various nanomaterials and the morphology of nanoparticles in amorphous matrices and solutions, as it allows for the study of the structure of samples in their natural, undisturbed state. Using neutrons offers a number of significant advantages over X-rays, opening up wide possibilities for varying contrast both in the study of organic and biological systems by replacing protons in structures (which scatter predominantly incoherently) with deuterium atoms, and in the study of inorganic samples by exploiting the magnetic properties of nuclei. X-ray and neutron scattering effectively complement each other.

This report presents the technical features of modern X-ray and neutron stations. After reviewing the theoretical foundations of data interpretation methods, the report will present practical application examples:

– for monodisperse systems (particles of the same size and shape), how to determine integral structural parameters from scattering data—the radius of gyration, maximum size, volume, and shape of nanoparticles;

– for polydisperse systems (particles of different sizes), several methods for reconstructing size distribution functions are presented.

Particular attention is given to the reliability and ambiguity of such calculations. The latter issue is particularly critical when attempting to determine the shape and internal structure of nanoparticles from low-resolution data.

This paper was prepared in the frame of a state assignment of the National Research Center "Kurchatov Institute".

[1] L.A. Feigin, D.I. Svergun. Structure Analysis by Small-Angle X-ray and Neutron Scattering // Plenum Press: New York. - 1987. – 321 p.

[2] O. Glatter, O. Kratky. Small–Angle X–ray Scattering. – London: Academic Press Inc. (1982) – 515 p.

[3] K. Manalastas-Kantos, P. V. Konarev, et al., J. Appl. Cryst. **54**, 343 (2021). https://doi.org/10.1107/S1600576720013412

NEUTRON OPTICS INSPIRED BY PHOTONIC AND PHONONIC CRYSTALS: BRAGG FILTERING, DEFECT MODES AND TOPOLOGICAL EDGE STATES IN PERIODIC AND QUASI PERIODIC MULTILAYERS

I. Zaky[1,2], V.D. Zhaketov[2]

[1] *Physics Department, Faculty of Science, Beni-Suef University, Beni Suef 62514, Egypt*
[2] *Frank Laboratory of Neutron Physics, Joint Institute for Nuclear Research, Dubna, 141980, Russia*

Neutron scattering at modern pulsed sources increasingly relies on engineered multilayers and superlattices, which are formally analogous to one-dimensional photonic and phononic crystals. In this contribution, we discuss how key concepts developed in electromagnetic and acoustic wave crystals, Bragg band gaps, defect modes, and topological edge states, can be systematically transferred to neutron optics using periodic and quasi-periodic multilayer structures.

First, We outline the mapping between the neutron optical potential in stratified media and the refractive-index or elastic-contrast profiles in photonic and phononic crystals, emphasizing the similar band-structure and transfer-matrix formalisms used to describe wave propagation and Bragg scattering. Second, we show that introducing controlled defects or interfaces between different "topological phases" of multilayers enables narrowband neutron transmission or reflection resonances, directly mirroring defect modes and topological edge states known from optical and acoustic systems.

As a concrete example, we present our recent simulation study on periodic superlattices composed of ferromagnetic and paramagnetic layers, originally proposed as tunable neutron filters and waveguides. These structures realize neutron band-gap engineering via magnetic contrast and can be extended towards quasi-periodic and topological designs for robust, spectrally selective neutron control. The approach suggests new possibilities for IBR-2 instruments, including compact neutron filters, waveguides and radiation detectors based on multilayer structures.

FERROMAGNETIC-SUPERCONDUCTING FIBONACCI LAYERED QUASICRYSTALS: NEUTRON-OPTICAL MODELING AND PROSPECTS FOR STUDYING STRONGLY CORRELATED STATES

V.D. Zhaketov[1,2,3], E.D. Kolupaev[2], A. Zaky[2,4], D.A. Tatarsky[5], R.N. Sadradze[6], D.A. Norov[2,7], S.E. Boguslavsky[7], A.A. Kamashev[8], D.A. Arbuzov[8]

[1] *Moscow Institute of Physics and Technology, Dolgoprudny, Russia*
[2] *Joint Institute for Nuclear Research, Dubna, Russia*
[3] *National Research University Higher School of Economics, Moscow, Russia*
[4] *Beni-Suef University, Beni-Suef 62521, Egypt*
[5] *Lobachevsky State University of Nizhny Novgorod, Nizhny Novgorod, Russia*
[6] *Dubna State University, Dubna, Russia*
[7] *Lomonosov Moscow State University, Moscow, Russia*
[8] *Kazan Physical-Technical Institute, Kazan, Russia*

E-mail: zhaketov@jinr.ru

Quasicrystals exhibit long-range order without translational periodicity, which gives rise to unusual electronic phenomena such as fractal superconductivity [1] and the potential coexistence of superconducting and ferromagnetic order parameters [2-4]. Here we propose the design of artificial layered quasicrystals consisting of alternating superconducting and ferromagnetic films arranged according to the Fibonacci rule. Such heterostructures are ideal for investigation by polarized neutron reflectometry, a technique sensitive to both nuclear and magnetic scattering-length densities. Neutron-optical simulations have been carried out for Fibonacci sequences of orders from F_6 to F_{12}. It is shown that starting from F_{10} the neutron reflectivity coefficient becomes essentially stable, indicating the formation of a robust quasiperiodic structure. The reflectivity spectra display distinct “quasi-Bragg” peaks arising from hidden long-range order, in contrast to disordered systems. Remarkably, under certain conditions the quasiperiodic arrangement can absorb more neutrons than its periodic counterpart. Stability simulations reveal that the quasi-Bragg peaks are insensitive to missing layers and thickness inaccuracies, which is important for experimental feasibility. Of special interest is the low-temperature phase ($T < 1$ K), where competition and possible coexistence of superconductivity and ferromagnetism are anticipated in the absence of translational invariance. Quasiperiodicity may induce a spatial modulation of the order parameter, which will affect the shape and intensity of neutron peaks detected by polarized reflectometry. The obtained results provide a foundation for experimental searches of fractal superconductivity and long-range magnetic order in quasiperiodic systems, as well as for the study of quantum critical phenomena in strongly correlated layered nanoheterostructures.

[1] K. Kamiya et al. // Nature Communications 9, 154 (2018).
[2] V.D. Zhaketov et al. // Physics of the Solid State 65, 1123 (2023).
[3] Yu.N. Khaydukov et al. // Physical Review B 99, 140503(R) (2019).
[4] V.L. Aksenov et al. // Physics of Elementary Particles and Atomic Nuclei 54, 898 (2023).

MAGNETIC ORDER AND DYNAMICS IN FRUSTRATED MAGNETS: THE INDISPENSABLE ROLE OF LOCAL NMR MEASUREMENTS IN COMBINATION WITH NEUTRON SCATTERING

S.V. Zhurenko[1,2,3], A.V. Tkachev[1], N.E. Gervits[1] and A.A. Gippius[1,2]

[1] *P.N. Lebedev Physical Institute of the Russian Academy of Science, Moscow, Russia*
[2] *Faculty of Physics, M. V. Lomonosov Moscow State University, Moscow, Russian*
[3] *Russian Medical Academy of On-going Professional Education, Moscow, Russia*

E-mail: Zhurenko.Sergey@gmail.com researchgate.net/profile/Sergei_Zhurenko

Frustrated magnetic materials are extensively studied in condensed matter physics due to their potential to realize exotic states such as spin liquids, disproportionate structures, and phases with hidden order. In the investigation of such systems, information obtained from neutron techniques (which primarily focus on elastic processes and rapid fluctuations) may be insufficient. In these cases, it becomes essential to employ local methods that are sensitive to local magnetic fields and slow spin fluctuations. Nuclear Magnetic Resonance (NMR) spectroscopy and Nuclear Quadrupole Resonance (NQR) spectroscopy emerge as crucial techniques in this context.

Their key strengths include isotope-specific sensitivity, enabling selective probing of distinct crystallographic sites, and, in the case of NQR, the ability to operate in zero external field – a critical feature for determining the ground state of frustrated magnets. Measurements of the temperature dependence of spin-lattice and spin-spin relaxation rates yield valuable information on spin dynamics in the kHz–MHz range, which is challenging to access by conventional neutron scattering.

Among frustrated lattices, the kagome lattice is regarded as one of the most promising platforms for realizing a spin-liquid state in solids. In this geometry, magnetic ions form a network of regular hexagons and corner-sharing triangles. Natural copper-rich minerals such as herbertsmithite, volborthite, francisite, avdoninite, and averievite provide realizations of such arrangements [1]. Additional magnetic ions located above or below the triangles can complete tetrahedral motifs, leading to a so-called decorated (capped) kagome lattice. This modification introduces extra magnetic exchange interactions within the tetrahedra, thereby altering the magnetic properties and the quantum ground state.

Among frustrated lattices, the kagome lattice is regarded as one of the most promising platforms for realizing a spin-liquid state in solids. In this geometry, magnetic ions form a network of regular hexagons and corner-sharing triangles. Natural copper-rich minerals such as herbertsmithite, volborthite, francisite, avdoninite, and averievite provide realizations of such arrangements. Additional magnetic ions located above or below the triangles can complete tetrahedral motifs, leading to a so-called decorated (capped) kagome lattice. This modification introduces extra magnetic exchange interactions within the tetrahedra, thereby altering the magnetic properties and the quantum ground state.

An example of such a system is the copper-rich natural mineral averievite, (CsCl)Cu5V2O10. This work presents a detailed analysis of the structural features, magnetic interactions, and thermodynamic properties of spin systems with a two-dimensional kagome lattice, focusing on synthetic analogs: (CsCl)Cu5As2O10 [2] and Zn-substituted (Cs,Br)Cu5-xZnxV2O10 (x = 0, 1, 2), studied by NMR spectroscopy.

The experimental results were obtained at the Solid-State NMR Laboratory, Department of Low Temperature Physics and Superconductivity, Faculty of Physics, M.V. Lomonosov Moscow State University, and the P.N. Lebedev Physical Institute of the Russian Academy of Sciences.

The combined use of NMR and neutron methods represents a powerful approach for investigating frustrated magnetic systems. This approach enables a more comprehensive understanding of complex magnetic interactions and dynamics in such systems, opening new avenues for fundamental research in condensed matter physics.

[1] L. V. Shvanskaya and A. N. Vasiliev (2024). Diverse magnetic chains in inorganic compounds. Accounts of Materials Research, 5(7):836–845. DOI: 10.1021/accountsmr.4c00083

[2] I. V. Kornyakov, M. V. Likholetova, I. E. Lezova, S. V. Krivovichev, H. O. Jeschke, Y. Iqbal, A. V. Tkachev, S. V. Zhurenko, A.A. Gippius, L.V. Shvanskaya, and A.N. Vasiliev (2026). Crystal structure, magnetic and resonant properties of decorated spin kagome system (CsCl)Cu5As2O10. Journal of Materials Chemistry C, 14, 3749-3758. DOI: 10.1039/d5tc03217b

NEUTRON ACTIVATION ANALYSIS AT THE IBR-2 REACTOR

I. Zinicovscaia[1,2]

[1] *Joint Institute for Nuclear Research, 6 Joliot-Curie Str., 1419890, Dubna, Russia*
[2] *Horia Hulubei National Institute for R&D in Physics and Nuclear Engineering, 30 Reactorului Str., MG-6, Bucharest - Magurele, Romania.*

E-mail: zinikovskaia@mail.ru

Neutron activation analysis (NAA), owing to its high accuracy, reproducibility, and non-destructive nature, is a widely employed analytical technique in environmental, material, archaeological, geological, and nanotoxicological studies. The presentation will highlight the key favorable features of NAA and describe the principles of its implementation on the Regata facility at the IBR-2 reactor. Examples of NAA applications will be presented, including its use for the assessment of heavy metal deposition through active and passive moss biomonitoring, water biomonitoring, the development of wastewater treatment approaches, analysis of medicinal plants, archeological objects and extraterrestrial materials. In addition, the effects of metal nanoparticles on various living organisms will be discussed. This information is addressed to researchers interested in the applications of NAA, as well as to those seeking an analytical technique suitable for environmental, biomedical, geological, and related studies.

SYNCHROTRON RADIATION FACILITY SKIF: A NEW-BORN MEMBER IN THE RUSSIAN MEGASCIENCE FAMILY

Y.V. Zubavichus[1], A.V. Bukhtiyarov[1]

[1] *Synchrotron Radiation Facility SKIF, Koltsovo, Novosibirsk region, Russia*

E-mail: ya.v.zubavichus@srf-skif.ru

The presentation reports on the Synchrotron Radiation Facility SKIF, its construction is on the final stage of implementation in Koltsovo, Novosibirsk region. Commissioning of the complex is expected by the end of 2026. The normal user operation should start in 2027.

Detailed technical specifications of the accelerator complex as well as seven first-priority beamlines are given. X-ray techniques implemented at the first-priority beamlines of SKIF are discussed within the context of complementarity with neutron beamlines installed at the reactor IBR-2.

Principles of the SKIF user policy are briefly outlined, including the system for the submission and expert evaluation of beamtime proposals. Infrastructure development program of SKIF aimed at the construction of second-priority beamlines is envisaged.

POSTER SESSION

CRYSTAL STRUCTURE OF Bi/Mn CO-DOPED STRONTIUM ALUMINATE PHOSPHORS

B.A. Abdurakhimov[1,2,3], S.E. Kichanov[1], D.P. Kozlenko[1], Y. Bokshyts[4]

[1] *Joint Institute for Nuclear Research, Dubna, Russia*
[2] *Denov Institute of Entrepreneurship and Pedagogy, Denau, Uzbekistan*
[3] *Institute of Nuclear Physics, Academy of Sciences of the Republic of Uzbekistan, Tashkent, Uzbekistan*
[4] *Research Institute for Physical Chemical Problems of the Belarusian State University, Minsk, Belarus*

E-mail: bekhzod@jinr.ru

Strontium aluminate-based compounds have gained much attention due to their outstanding optical properties, high chemical and thermal stability, and wide possibilities for obtaining both bulk and nanostructured highly effective optical phosphors. Recently, research on the activation of aluminates by bismuth and manganese ions has intensified. The luminescence of Bi^{3+} and Mn^{4+} ions in various crystal environments can cover almost the entire visible range, which is important for white LEDs and optoelectronic devices. Of special interest is the sensitization of Mn^{4+} luminescence by Bi^{3+} ions, where the energy transfer efficiency strongly depends on the phase composition and the distribution of activators between the crystalline phases. However, X-ray methods cannot reliably determine the positions of oxygen atoms nor distinguish between neighbouring cations (Sr, Bi, Mn).

In the present work, a set of 16 powder samples of strontium aluminates with systematic variation of dopants (pure matrix, Bi, Mn, and Bi/Mn) and annealing temperatures (1200, 1300, 1400, 1500 °C) was synthesised. The samples were characterised by X-ray diffraction (XRD), Raman spectroscopy, and scanning electron microscopy (SEM). It was found that all samples contain a mixture of monoclinic $SrAl_2O_4$ (space group $P2_1$) and cubic $Sr_3Al_2O_6$ (space group Pa-3) phases, with the phase ratio depending strongly on the annealing temperature. The average grain size of both phases is in the nanometre range, as confirmed by SEM and X-ray line broadening analysis. Raman spectroscopy confirmed the incorporation of Bi^{3+} and Mn^{4+} ions into both phases through shifts of the characteristic vibration modes.

Subsequently, a detailed neutron diffraction study was performed at room temperature and ambient pressure using the DN-6 diffractometer at the IBR-2 reactor (Dubna, Russia). Rietveld refinement of the neutron data allowed us to determine the phase fractions, unit cell parameters, atomic coordinates, and site occupancies for both phases. The results show that the cubic phase fraction increases with annealing temperature, while the incorporation of Bi and Mn leads to measurable changes in the Sr–O and Al–O bond lengths. In the co-doped samples, the distribution of Mn is significantly affected by the presence of Bi, providing a structural basis for the Bi→Mn energy transfer mechanism. Luminescence measurements confirm the sensitization of Mn^{4+} emission by Bi^{3+} ions, with the energy transfer efficiency varying systematically with synthesis temperature.

Thus, the combination of XRD, Raman, SEM, and neutron diffraction establishes a direct correlation between the crystal structure and the sensitization efficiency in Bi/Mn co-doped strontium aluminates. These findings enable rational design of high-performance phosphors for white light-emitting diodes and other optoelectronic applications.

NEUTRON DIFFRACTION STUDY OF GAMMA- AND NEUTRON-IRRADIATED W-Ni HEAVY ALLOY

A.S. Abiyev[1] and V.A. Turchenko[1,2]

[1] *International Intergovernmental Organization Joint Institute for Nuclear Research, Dubna 141980, Russia*

[2] *National University of Science and Technology "MISIS", Moscow 119049, Russia*

E-mail: afsunabiyev@gmail.com

W-Ni heavy alloys are promising radiation-resistant materials for nuclear and plasma-facing applications, where phase stability and bulk lattice response are decisive for long-term performance. In the present work, neutron diffraction was used as the main structural method to compare the irradiation-induced changes in a W-rich W-Ni heavy alloy after gamma irradiation and neutron irradiation. The initial alloy was identified as a two-phase system consisting of dominant cubic W with space group Im-3m and secondary tetragonal WNi_4 with space group I4/m. Because neutron diffraction probes the sample volume rather than only the near-surface region, it provides a more reliable basis for evaluating bulk phase stability and lattice-parameter evolution in irradiated heavy alloys.

Neutron diffraction measurements were performed at room temperature at the Frank Laboratory of Neutron Physics, Joint Institute for Nuclear Research, using the Real-Time Neutron Diffractometer installed on beamline 6a of the IBR-2M pulsed reactor. The diffraction profiles were treated by the Rietveld method using the FullProf suite. For the gamma-irradiated series, samples exposed to 620, 1239, 2712, and 3566 kGy were analyzed. For the neutron-irradiated series, the corresponding fluence range was from 9.7×10^{12} to 3.2×10^{14} n/cm². In both irradiation series, the refined diffraction patterns confirmed preservation of the same W + WNi_4 phase composition, without evidence of a radiation-induced crystalline phase transition.

The gamma-irradiated samples demonstrated a phase-specific structural response. The main W phase showed a gradual lattice contraction, with the cubic parameter decreasing from 3.1698 Å in the initial state to 3.1681 Å at 3566 kGy, while the unit-cell volume decreased from 31.85 to 31.798 Å³. This indicates comparatively stable behavior of the W matrix and suggests that the gamma-induced structural response is mainly accommodated by point-defect formation, local relaxation, and redistribution of internal strain. In contrast, the WNi_4 phase exhibited non-monotonic and anisotropic behavior: the a and c parameters changed in different directions, and the unit-cell volume varied from 116.224 Å³ in the initial state to 116.547 Å³ at the highest gamma dose.

A different trend was revealed after neutron irradiation. The W phase expanded rapidly after the first irradiation step: the lattice parameter increased from 3.1699 Å to 3.1716 Å at 9.7×10^{12} n/cm² and then approached a quasi-saturated value of about 3.1721 Å at the highest fluence. The corresponding unit-cell volume increased from 31.85 to 31.919 Å³. The WNi_4 phase was again more sensitive, with the unit-cell volume increasing from 116.224 to 117.045 Å³, while its tetragonal axes changed anisotropically. These results show that gamma and neutron irradiation affect the W matrix differently, producing lattice contraction in the gamma-irradiated series and lattice expansion in the neutron-irradiated series, whereas the secondary WNi_4 phase remains the most structurally sensitive component in both cases.

Overall, neutron diffraction proves that the irradiation response of W-Ni heavy alloy is governed mainly by phase-dependent lattice-strain evolution and defect accumulation rather than by phase transformation. The comparative analysis also shows that the type of irradiation strongly influences the direction and magnitude of lattice-parameter changes in the W matrix,

while the WNi_4 phase and phase-boundary regions act as more responsive structural zones under both gamma and neutron exposure.

Keywords: Neutron diffraction; W-Ni heavy alloy; gamma irradiation; neutron irradiation; Rietveld refinement; lattice parameters; phase stability.

[1] R. Cury, J.M. Joubert, S. Tusseau-Nenez, E. Leroy and A. Allavena-Valette (2009). Intermetallics. 17, 174-178.
[2] D. Neov, A.I. Beskrovnyi, A.S. Abiyev, D.M. Mirzayeva, E. Demir, A.H. Valizade et al. (2023). Advanced Physical Research. 5, 95-102.
[3] E. Demir, M.N. Mirzayev, E.P. Popov, P. Horodek, I.G. Genov, K. Siemek et al. (2021). Vacuum. 184, 109934.

THERMAL DECOMPOSITION OF ACETYLACETONATE PRECURSORS AS A ROUTE TO MONODISPERSE SUPERPARAMAGNETIC $NiFe_2O_4$ NANOCRYSTALS

Lj. Andjelković[1], M. Balasoiu[2], M. Šuljagić[1], A. Sknepnek[3], and D. Jeremić[4]

[1] *University of Belgrade-Institute of Chemistry, Technology and Metallurgy, Department of Chemistry, Njegoševa 12, Belgrade, Republic of Serbia*
[2] *Frank Laboratory of Neutron Physics, Joint Institute for Nuclear Research, 141980 Dubna, Russia*
[3] *University of Belgrade, Faculty of Agriculture, Nemanjina 6, Belgrade, Serbia*
[4] *University of Belgrade, Innovation Center of the Faculty of Chemistry, Studentski Trg 12-16, Belgrade, Serbia*

E-mail: ljubica.andjelkovic@ihtm.bg.ac.rs

Phase-pure nickel ferrite ($NiFe_2O_4$) nanocrystals were obtained *via* an optimized thermal decomposition route employing acetylacetonate precursor complexes. The structural, morphological, and magnetic properties of the resulting powder were examined by X-ray powder diffraction (XRPD), Fourier-Transform Infrared Spectroscopy (FT-IR), and Transmission Electron Microscopy (TEM). Single-phase spinel formation was confirmed, and TEM analysis revealed polygonal nanoparticles with a mean diameter of approximately 7.5 nm. The close agreement between crystallite sizes derived from XRPD and grain sizes from TEM imaging is consistent with the monocrystalline character of the particles, pointing to a highly controlled nucleation and growth process. Magnetic measurements demonstrated superparamagnetic behavior under ambient conditions, with the magnetic response showing marked sensitivity to external fields and measurement conditions — a direct consequence of the narrow size distribution achieved through this synthetic approach. These findings establish organic-phase thermal decomposition as an efficient strategy for producing monodisperse $NiFe_2O_4$ nanoparticles with well-defined superparamagnetic properties, positioning them as promising candidates for magnetically responsive biomedical applications.

To advance the understanding of the structural and magnetic properties of the nickel ferrite system, Small-Angle Neutron Scattering (SANS) experiments have been planned to be performed.

This research has been financially supported by the Ministry of Science, Technological Development and Innovation of Republic of Serbia (Contract No: 451-03-136/2025-03/200026, 451–03–136/2025–03/200116, and 451–03–13/2025–03/200288), as well as by Science Fund of the Republic of Serbia, #7551, Development of epsilon-iron oxide-based nanocomposites: Towards the next-generation rare-earth-free magnets – DOMINANTMAG, and Ministry of Science, Technological Development, and Innovation of the Republic of Serbia under Grant No. 676/04.08.2025 with JINR (Next-Generation MRI Contrast Agents: Exopolysaccharides - Functionalized Ferrite Nanoparticles for Enhanced Safety and Performance).

NEUTRON ACTIVATION ANALYSIS FOR ELEMENTAL CHARACTERISATION OF COLLOCATED SOIL, LEAF LITTER AND CENTIPEDE SAMPLES

M. Aničić Urošević[1], B. Mitić[2], D. Stojanović[2], M. Popović[1], O. Chaligava[3], P. Nekhoroshkov[3] and I. Zinicovscaia[3]

[1] *Institute of Physics Belgrade, University of Belgrade, Belgrade, Serbia*
[2] *Institute of Zoology, University of Belgrade – Faculty of Biology, Belgrade, Serbia*
[3] *Frank Laboratory of Neutron Physics, Joint Institute for Nuclear Research, Dubna, Russia*

E-mail: mira.anicic@ipb.ac.rs

In temperate deciduous forests, centipedes (members of the arthropod class Chilopoda) can occur at densities exceeding 100 individuals per square metre and play an important role in soil ecosystem functioning and in transferring PTEs to higher-level carnivores in the food chain [1]. In this study, the concentrations of PTEs were determined in centipedes with hemiedaphic *Cryptops anomalans* Newport, 1844 (Can) and euedaphic *Clinopodes flavidus* C. L. Koch, 1847 (Cfl) lifestyles, collected from two woodlands in Serbia: one site near the Smederevo Ironworks, heavily contaminated with red dust (Fe) enriched with As, Cd, Cr, Ni, Pb, and other elements; the other site in an isolated rural area on Mt Vršačke Planine. The centipedes were starved for five days in individual plastic boxes lined with filter paper to allow their gut contents to be voided, while damaged specimens were immediately placed in vials containing 70% alcohol in the field. The aim was to investigate whether these and other PTEs can be detected in the centipedes, as well as in collocated topsoil and leaf litter samples, in measurable quantities and in proportion to their presence in the habitat — that is, the surrounding environment — indicating the level of environmental disturbance. Due to the low sample weights, elemental characterisation (Al, As, Ba, Br, Ca, Ce, Co, Cr, Cs, Cu, Eu, Fe, Ga, Hf, K, La, Mg, Mn, Nd, Ni, P, Pb, Rb, S, Sb, Sc, Sm, Sr, Ta, Tb, Ti, Th, U, V, W, Yb, Zn, and Zr) of centipede samples was performed by inductively coupled plasma optical emission spectrometry (ICP-OES), while soil and leaf litter samples were analysed by instrumental neutron activation analysis (INAA). The preliminary results (Fig. 1) suggest that PTEs accumulated in the samples in measurable quantities, with much higher levels in non-starved centipede samples compared to those starved after collection. The likely reason why the concentrations of PTEs were much higher in non-starved samples is that these elements may be bound in the prey in a form that is insoluble in digestive fluids. A large proportion of the diet of centipedes consists of worms, springtails and woodlice, which store heavy metals in highly insoluble intracellular granules within their digestive tissues. Thus, much of the metal that enters the centipedes through food may remain bound in this form in the gut lumen and be voided in the feces. In addition, both starved centipede samples from the polluted site accumulated approximately the same levels of elements identified as heavy metal pollutants. The exceptions were Cd, which accumulated in significantly higher quantities in Cfl, while Cr was found, to some extent, in higher amounts in Can. Differences in Cd and Cr accumulation between centipede species are mainly due to variations in their physiology, lifestyle, and detoxification efficiency. Some species are high accumulators, while others maintain significantly lower concentrations, even in the same environment. Finally, the centipede samples from the unpolluted site, which were non-starved, had PTE concentrations at the same level as the starved samples from the polluted site.

[1] B.Mitić, S.Borković-Mitić, A.Stojsavljević, D.Stojanović, S.Pavlović, L.Vasiljević, N.Ristić (2022). Metal and metalloid bioaccumulation in three centipedes (Chilopoda). Arch. Biol. Sci. 74, 207-215.

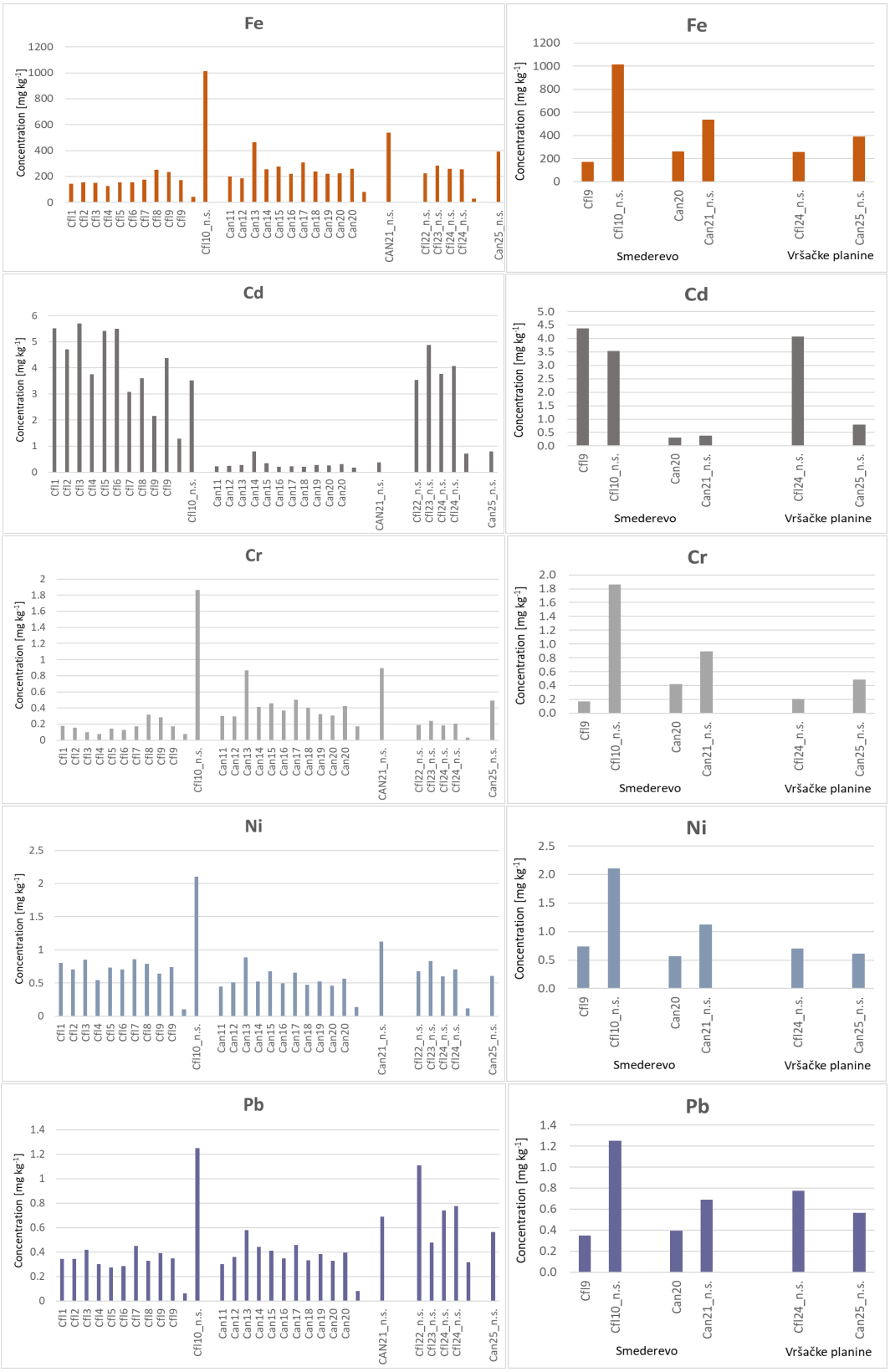

Figure 1. Left: Concentrations (mg kg-1) of heavy metals Fe, Cd, Cr, Ni, and Pb in two centipede species: Clinopodes flavidus (Cfl) and Cryptops anomalans (Can). Right: Average concentrations of the elements per species at polluted (Smederevo) and unpolluted sites (Mt Vršačke Planine). n.s. — non-starved specimens.

FROM STRUCTURE TO STRENGTH: ANALYSIS OF POLYMER COMPOSITES FILLED WITH HYBRID FILLERS

E.A. Lebedeva[1], E.V. Ivanova[1], D.K. Trukhinov[1], T.S. Istomina[1], M. Balasoiu[2,3,4], A.H. Elmekawy[2,5], Yu.E. Gorshkova[2], S.E. Kichanov[2] and S.A. Astaf'eva[1]

[1] *"Institute of Technical Chemistry of UB RAS" – Affiliation of Perm Federal Research Centre of Ural Branch of Russian Academy of Sciences, Perm, Russia*
[2] *Joint Institute for Nuclear Research, Dubna, Russia*
[3] *"Horia Hulubei" National Institute of Physics and Nuclear Engineering, Magurele, Romania*
[4] *R&D CSMBA, Faculty of Physics, West University of Timişoara, Timişoara, Romania*
[5] *Department of Experimental Nuclear Physics, Nuclear Research Center, Egyptian Atomic Energy Authority, Cairo, Egypt*

E-mail: svetlana-astafeva@yandex.ru

Recently, the development of polymer composites has become a relevant direction in modern materials science. To ensure functional properties and optimize the structure of products, fillers with different dispersities, i.e., hybrid fillers, are introduced into them. The key challenge in designing polymer composites with such fillers is selecting the concentration to achieve the expected synergistic effect and uniform distribution of the dispersed phase.

One of the common methods for producing polymer composites is solution casting. Obtaining materials by this method helps to solve the problem of non-uniform filler distribution; however, in practice, this potential often remains unrealized due to uncontrolled agglomeration caused by complex solvent evaporation kinetics and ambiguous interfacial interactions, which leads to distortion of the initial filler morphology [1]. In this regard, the task of comprehensively studying changes in the morphology of the hybrid filler with increasing its concentration in the polymer matrix becomes particularly relevant.

The aim of this work is to establish the relationship between the mass content of the hybrid filler (recycled carbon fiber and boehmite/magnetite in a 1:1 ratio, total concentration of 1-5 wt.%) in acrylonitrile–butadiene–styrene (ABS), its morphological parameters (aggregate size, type of structural organization according to SAXS data), and the maximum tensile strength of polymer composites obtained by solution casting. This will make it possible to predict the strength of composites depending on the concentration and type of filler.

The table presents the fitting parameters of the SAXS results of polymer composites with hybrid fillers. The figure shows a histogram of the dependence of maximum tensile strength on filler concentration for two systems: ABS/rCF/AlOOH and ABS/rCF/Fe_3O_4.

Table - Fitting parameters of polymer composite samples

Sample	Type of function	Correlation length (nm)	Porod coefficient
ABS	1	6,7	4,01
ABS/rCF/AlOOH (0,5/0,5)	1	1386,8	~5
ABS/rCF/AlOOH (1,5/1,5)	2	35,3 1341,7	2,73
ABS/rCF/AlOOH (2,5/2,5)	2	42,5 1697,8	2,88
ABS/rCF/Fe3O4 (0,5/0,5)	2	44,7 1103,8	3,42

ABS/rCF/Fe3O4 (0,5/0,5)	2	43,04 1270,1	2,95
ABS/rCF/Fe3O4 (0,5/0,5)	2	42,6 1366,8	2,87

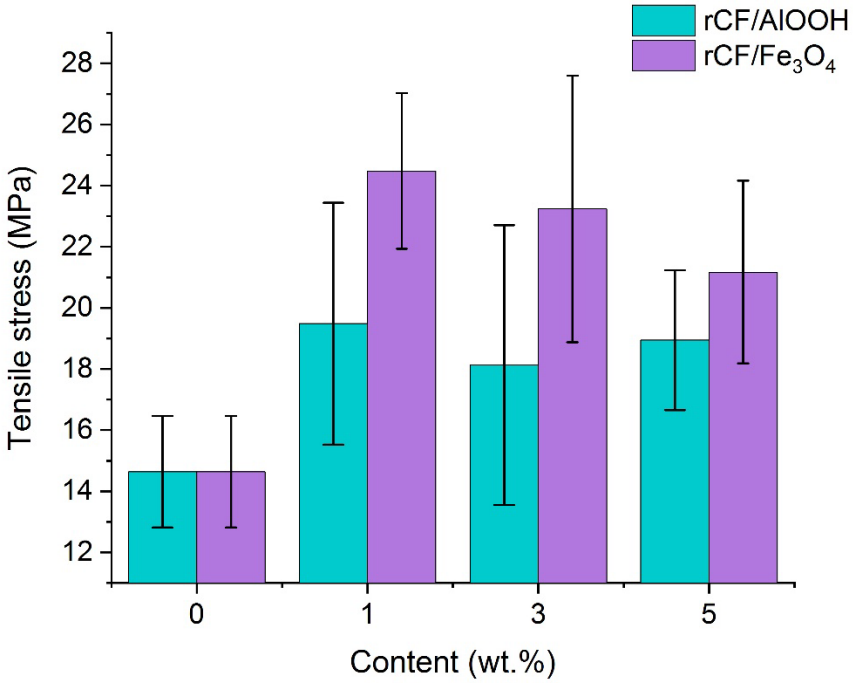

Figure 1 - Dependence of maximum tensile strength on filler concentration for the ABS/rCF/AlOOH and ABS/rCF/Fe_3O_4 systems.

SAXS results and tensile strength tests show that with an increase in the concentration of the hybrid filler, the correlation length increases, meaning the size of the filler aggregates grows, which correlates with a decrease in strength at high concentrations of the hybrid filler. It was also noted that the hybrid filler with magnetite provides a greater increase in strength at all concentrations (up to +67 %) than the hybrid filler with boehmite (+33 %). The standard error of strength is higher at medium concentrations (3 % total), which may reflect non-uniform filler distribution or variability in agglomeration.

For a better understanding of the morphology and size of the detected nanostructures, the polymer composites were studied by small-angle neutron scattering using the YuMO instrument operating at the IBR-2 reactor.

This work was financially supported by the framework of the State Assignment (State Registration No. 124022100088-6). This work was carried out using the equipment of the Research of Materials and Substances Center for Collective Use of the Perm Federal Research Center of the Ural Branch of the Russian Academy of Sciences.

[1] E. Ziv, D. Attia, G. Vasilyev, O. Mendelson, E. Zussman, R. Yerushalmi-Rozen (2019). The role of polymer–solvent interactions in polyvinyl-alcohol dispersions of multi-wall carbon nanotubes: from coagulant to dispersant. Soft Matter. 15, 47-54.

STRUCTURAL STUDIES OF SURFACTANT MICELLES INTERACTING WITH POLYMERS IN BULK AND AT INTERFACES BY NEUTRON SCATTERING

M.M. Avdeev[1,2], V.S. Molchanov[1], O.I. Ivankov[2], A.Kh. Islamov[2], A.I. Kuklin[2,3], M. Yerdauletov[2,4], K. Nazarov[2,4,5], Yu.E. Gorshkova[2,6], O.E. Philippova[1]

[1] *Lomonosov Moscow State University, Moscow, Russia*
[2] *Joint Institute for Nuclear Research, Dubna, Russia*
[3] *Moscow Institute of Physics and Technology (National Research University), Dolgoprudny, Russia*
[4] *Institute of Nuclear Physics, Almaty, Kazakhstan*
[5] *Al-Farabi Kazakh National University, Almaty, Kazakhstan*
[6] *Institute of Physics, Kazan Federal University, Kazan, Russia*

E-mail: avdeev@polly.phys.msu.ru

The interaction of surfactants and polymers in solutions, including the adsorption of surfactants and surfactant micelles on polymers, is characterized by a wide variety of structures, offering extensive opportunities for controlling the properties of colloidal systems. Identification of the structural features of such systems enables more effective development of their scientific and industrial applications, particularly those related to their unique viscoelastic properties. Neutron scattering methods are widely used for this purpose. The high penetration depth of neutron radiation allows for studies to be conducted in bulk solutions and for investigation of hidden interfaces modified for the adsorption of components from the solution. This paper presents aspects of structural studies using neutron scattering methods for a number of relevant surfactant-polymer systems, based on experiments conducted at the IBR-2 reactor at JINR (Dubna).

Small-angle neutron scattering (SANS) was used to study aqueous solutions of polymer-like worm-shaped micelles of the "traditional" surfactant potassium oleate and the gemini surfactant C18-4-C18 [1]. Surfactant solutions are widely used in the oil industry as smart thickeners that lose their viscoelasticity upon contact with oil. Their rheological properties can be improved by adding both inorganic and organic (including polymeric) nanoparticles, which act as cross-linking agents between the micelles. The improvement of the viscoelastic properties of solutions while maintaining sensitivity to hydrocarbons is possible by incorporating a self-organizing percolation network of cellulose nanocrystals. Nanocrystals have been shown to increase the viscosity and elastic modulus of a solution of potassium oleate micelles by an order of magnitude and ensure temperature stability of these properties. This phenomenon can be explained by the formation of a fused network consisting of worm-like micelles and of nanocrystals. SANS data showed that within this network, the shape and size of both micelles and nanocrystals remain unchanged, indicating that the micelle network structure is preserved in the presence of nanocrystals and that additional nanocrystal aggregation does not occur.

Surfactant-polymer interactions can also lead to significant changes in the structural parameters as determined by SANS, as in the case of the addition of polyethyleneglycol (PEG) to aqueous micellar solutions of dodecylbenzenesulfonic acid (DBSA)[2]. The interaction between DBSA and PEG molecules occurs primarily through hydrogen bonds, leading to the formation of lamellar structures. A mechanism also occurs due to the hydrophobic interaction of surfactant tails and the adsorption of individual micelles onto the polymer chain, forming "necklace"-type structures. The coexistence of free spherical micelles and surfactant-polymer complexes in a "necklace" structure was demonstrated using SANS. The influence of PEG molar mass on the formation of multimicellar complexes in these systems was observed.

The interaction of micelles and polymers near a flat quartz surface can be studied using polymer grafting. This approach chemically anchors densely packed polymer chains to the surface, forming a coating in the form of a polymer "brush." Polyacrylamide polymer brushes with thickness of tens of nanometers have been synthesized using the "grafting-through" technique [3]. This approach allows for the production of films with a relatively high grafting density, resulting in strong elongation of the polymer chains in the film compared to a free polymer coil. Reflectometry methods allow for obtaining the scattering length density profile of the film on the surface, followed by analysis of the thickness and structure of the internal layers. The "grafting-through" method demonstrated to be scalable to large substrates for neutron reflectometry. The proposed approach opens a relatively simple path for modifying the surface with polymer nanolayers of controlled thickness as a model surface, on which neutron methods can be used to analyze the adsorption of objects and their interaction with the polymer.

Using polyacrylamide polymer brushes, we analyzed the adsorption of surfactant micelles from aqueous solutions onto a surface. When a polymer brush comes into contact with water, it partially swells, effectively increasing its thickness and roughness compared to the dry state. When micelles are added to the solution, they interact with the polymer chains via one of the mechanisms previously described for the bulk case, initiating their adsorption. In neutron reflectometry, this interaction can be observed by constructing and analyzing a depth profile of the scattering length density, effectively changing the density, thickness, and roughness of the polymer layer. In the case of a polyacrylamide film, the addition of a surfactant increases the layer thickness and roughness comparable to the micelle diameter, thus detecting micelle adsorption.

Thus, based on the information obtained in neutron scattering experiments, studies of the structure of surfactant micelles interacting with polymers, which combine studies in the bulk and on the surface, are promising in the field of soft matter investigation.

[1] M.M. Avdeev, Y.M. Chesnokov, S.V. Kozlov, A.V. Shibaev, A.Kh. Islamov, O.E. Philippova (2024). New long tail gemini surfactant in aqueous solution: Self-assembly, rheological properties and responsiveness to hydrocarbon, Journal of Molecular Liquids. 403, 124930. https://doi.org/10.1016/j.molliq.2024.124930.

[2] O.P. Artykulnyi, A.V. Shibaev, M.M. Avdeev, O.I. Ivankov, L.A. Bulavin, V.I. Petrenko, O.E. Philippova (2020). Structural investigations of poly(ethylene glycol)-dodecylbenzenesulfonic acid complexes in aqueous solutions, Journal of Molecular Liquids. 308, 113045. https://doi.org/10.1016/j.molliq.2020.113045.

[3] M.M. Avdeev, A.V. Shibaev, K.I. Maslakov, S.V. Dvoryak, B.V. Lokshin, Y.E. Gorshkova, T.V. Tropin, O.E. Philippova (2024). Polymer Brushes Synthesized by the “Grafting-through” Approach: Characterization and Scaling Analysis, Langmuir. 40, 23918–23929. https://doi.org/10.1021/acs.langmuir.4c03088.

PRESSURE-INDUCED PHASE TRANSITION IN NANOSTRUCTURED CATION-DEFICIENT $ZN_{0.34}FE_{2.53}\square_{0.13}O_4$ FERRITE

N.M. Belozerova[1,2], O.N. Lis[2], A.V. Rutkauskas[2], E.V. Lukin[2], D.P. Kozlenko[2], B.N. Savenko[2], N.T. Nguyen[2], S.E. Kichanov[2]

[1] *Center for Photonics and 2D Materials, Moscow Institute of Physics and Technology, 141701, Dolgoprudny, Russia*

[2] *Frank Laboratory of Neutron Physics, Joint Institute for Nuclear Research, 141980, Dubna, Russia*

E-mail: nmbelozerova@jinr.ru

Cation-deficient spinel ferrite nanoparticles are of strong interest because point defects and nanoscale strain can markedly tune electronic, magnetic, and transport properties. In particular, cation vacancies modify local bonding and the compressibility of oxygen polyhedra, potentially altering pressure-induced transformation pathways compared with stoichiometric $ZnFe_2O_4$, whose high-pressure behavior is better established [1,2].

Nanostructured cation-deficient zinc ferrite $Zn_{0.34}Fe_{0.53}\square_{0.13}O_4$ (□ - denotes cation vacancies) with mean particle size ~14 nm were prepared by thermal decomposition of metal acetylacetonates in a high-boiling solvent under inert atmosphere. High-pressure measurements including X-ray diffraction (XRD) up to 34 GPa and Raman spectroscopy up to ~29 GPa were conducted in a diamond anvil cell using an alcohol-based pressure medium.

At ambient conditions the sample crystallizes in the cubic spinel structure (space group Fd–3m) with lattice parameter a ≈ 8.331 Å. With increasing pressure, cubic reflections shift smoothly up to ~18 GPa. Above ~18 GPa, new diffraction features appear and characteristic cubic peak intensities are suppressed, indicating the onset of a structural transformation. Among tested post-spinel models, an orthorhombic Bbmm ($CaTi_2O_4$-type) phase provides the best fit to high-pressure XRD patterns. The transformation is strongly broadened: the orthorhombic fraction is already detectable near the onset (~12% at ~18 GPa) and rises to ~43% at ~32–34 GPa, consistent with extended phase coexistence typical for nanomaterials with internal strain and defect-related local distortions.

Equation-of-state analysis yields a bulk modulus $B_0 \approx 185$ GPa for the cubic phase (with fixed $B' \approx 4$) and $B_0 \approx 210$ GPa for the orthorhombic phase, consistent with densification in the post-spinel structure. The orthorhombic lattice compresses anisotropically (the b axis is more compressible than a and c). In the spinel phase, octahedral (B-site) Fe–O bonds contract more strongly than tetrahedral (A-site) Fe–O bonds, consistent with vacancies predominantly affecting octahedral environments.

Raman spectra show the expected spinel modes ($A_{1g} + E_g + 3F_{2g}$). Above ~18 GPa, a clear splitting/restructuring of the A_{1g} band (~ 620–675 cm^{-1}) is observed, in agreement with XRD evidence for the emergence of the orthorhombic component and indicating modified local coordination/force constants, similar in spirit to high-pressure Raman signatures in $ZnFe_2O_4$ [2].

This work was financially supported by the Ministry of Science and Higher Education of the Russian Federation (FSMG2024-0014).

[1] D. Levy, et al. (2000). Phase transition of synthetic zinc ferrite spinel ($ZnFe_2O_4$) at high pressure, from synchrotron X-ray powder diffraction. Physics and Chemistry of Minerals. 27, 638-344.

[2] Z. Wang, et al. (2003). High pressure Raman spectroscopy of spinel-type ferrite $ZnFe_2O_4$. Journal of Physics and Chemistry of Solids. 64(12), 2517-2523.

CHEMICAL ACTIVATION OF *tert*-BUTYL HYDROPEROXIDE BY Et_4NBr. NOTE ON INTRAMOLECULAR DYNAMICS

N.A. Turovskij[1], Yu.V. Berestneva[2] and E.V. Raksha[3]

[1] *Federal State Budget Educational Institution of Higher Education "Donetsk State University" Donetsk, Russia*
[2] *Federal State budgetary Institution "V.K. Gusak Institute of Emergency and Reconstructive Surgery" of the Ministry of Health of the Russian Federation, Donetsk, Russia*
[3] *International Intergovernmental Organization "The Joint Institute for Nuclear Research," Dubna, Russia*

E-mail: berestnevayuv@mail.ru

Organic hydroperoxides (RO-OH) are key intermediates in radical-chain oxidation processes occurring in the biosphere. Establishing the mechanism of chemically activated radical-pair decomposition of hydroperoxide compounds is an important priority task in the study of the complex metabolic processes of living cells both in health and in disease. The molecular recognition stage of the supramolecular catalytic decomposition reaction of RO-OH in the presence of tetraalkylammonium bromides was studied by complementary methods of chemical kinetics, NMR spectroscopy and molecular modeling [1-2].

The chemical activation features of *tert*-butyl hydroperoxide by tetraethylammonium bromide (Et_4NBr), including the structural models features of complex intermediates RO-OH – Et_4NBr are discussed (Fig. 1). Models that assume the combined action of the cation (Et_4N^+) and the anion (Br^-) of the salt in the process of hydroperoxide chemical activation are proposed. The specific solvation of the anion is taken into account by the supermolecule approximation. Structural reorganization of the hydroperoxide molecule along with changes in its molecular dynamics are discussed.

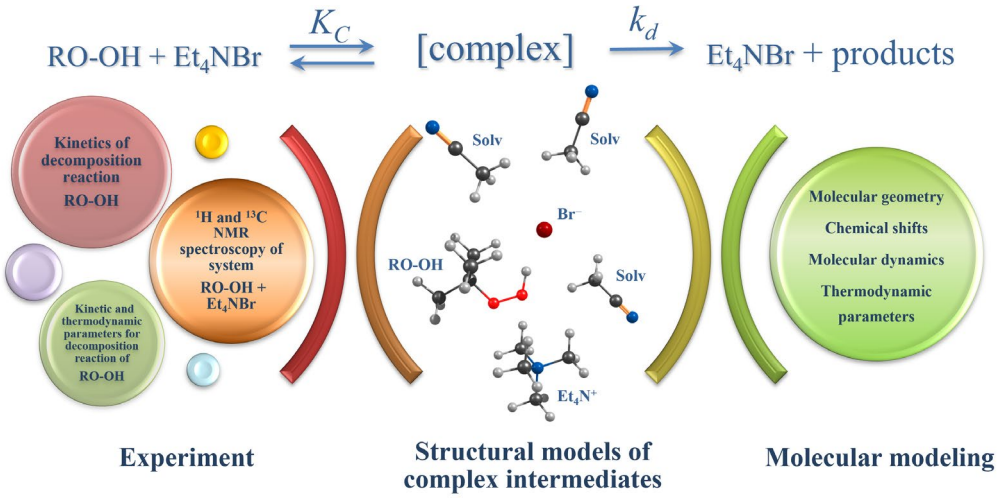

Fig. 1. Complementary methods in the study of chemical activation of tert-butyl hydroperoxide by Et_4NBr.

[1] N.A. Turovskij, Yu.V. Berestneva, E.V. Raksha, M.Yu. Zubritskij, S.A. Grebenyuk (2014). NMR study of the complex formation between *tert*-butyl hydroperoxide and tetraalkylammonium bromides. Monatsh. Chem. 145, 1443-1448.

[2] N.A. Turovskij, E.V. Raksha, Y.V. Berestneva (2020). Chemically activated decomposition of arylalkyl hydroperoxides in the presence of tetraalkylammonium bromides (Chapter). In: Hydroperoxide Properties, Uses and Reactions, Ed. Voleta Aubin, New York: Nova Science Publishers Inc. 4, 89-122.

SANS STUDY OF NATIVE HORSE SPLEEN FERRITIN AT DIFFERENT CONTRAST VARIATION

I.O. Bezruchko[1], T.N. Murugova[2], O.I. Ivankov[2], A.I. Kuklin[1,2], Yu.L. Ryzhykau[1,2]

[1] *Research Center for Molecular Mechanisms of Aging and Age-Related Diseases, Moscow Institute of Physics and Technology, Dolgoprudny, Russia*
[2] *Frank Laboratory of Neutron Physics, Joint Institute for Nuclear Research, Dubna, Russia*

E-mail: bezruchko.ivan.olegovich@gmail.com

Horse apoferritin has been studied with small-angle scattering techniques for a long time [1]. At the same time, native ferritin has been less characterized [2]. Here we present results of SANS study of native horse spleen ferritin with the use of contrast variation.

Ferritin was purchased from Sigma-Aldrich. Experiments were conducted at YuMO spectrometer of IBR-2 reactor [3] (JINR, Dubna). SAS curves were processed in BioXTAS RAW software [4], and *ab initio* model was built in MONSA [5] (here we also used SAXS data of apoferritin from the previous experiments (SASBDB ID: SASDWV6)).

The final structure demonstrated several interesting features: the cage were underloaded, and the mineral core was positioned at the part of inner surface of protein cage; a part of core pseudoatoms was out of the cage, this fact can be interpreted as presence of mineral structures on the outer surface of the protein shell. These outcomes could be compared with curious results of anomalous SAXS study of native ferritin [2] — the mineral core also intersected with the protein shell, albeit in a different way, and, unlike our model, there was an iron overload.

Yu. Ryzhykau acknowledges Federal scientific and technical program for the development of synchrotron and neutron research and research infrastructure of the Ministry of Science and Higher Education of the Russian Federation (agreement No. 075-15-2025-512)

[1] D.V. Zabelskii et al. (2018). Ambiguities and completeness of SAS data analysis: investigations of apoferritin by SAXS/SANS EID and SEC-SAXS methods. Journal of Physics: Conference Series. 994, 012017.
[2] D.C.F. Wieland, M.A. Schroer, A.Y. Gruzinov, C.E. Blanchet, C.M. Jeffries, and D.I. Svergun (2021). ASAXS measurements on ferritin and apoferritin at the bioSAXS beamline P12 (PETRA III, DESY). Journal of Applied Crystallography. 54, 830-838.
[3] A.I. Kuklin et al. (2021). Small-Angle Neutron Scattering at the Pulsed Reactor IBR-2: Current Status and Prospects. Crystallography Reports. 66, 231–241
[4] J.B. Hopkins (2024). BioXTAS RAW 2: new developments for a free open-source program for small-angle scattering data reduction and analysis. Journal of Applied Crystallography. 57, 194-208.
[5] M.V. Petoukhov, and D.I. Svergun (2006). Joint use of small-angle X-ray and neutron scattering to study biological macromolecules in solution. European Biophysics Journal. 35, 567-576.

MODERNISATION OF DATA REDUCTION ALGORITHMS FOR SMALL-ANGLE NEUTRON SCATTERING USING NUMERICAL SIMULATION

R.D. Borisov[1,2], L.A. Azarova[1,2]

[1] *St. Petersburg State University, St. Petersburg, Russia*
[2] *Petersburg Nuclear Physics Institute named by B.P. Konstantinov of National Research Centre «Kurchatov Institute», Saint Petersburg, Gatchina, Russia*

E-mail: st095754@student.spbu.ru

Small-angle neutron scattering (SANS) is widely used for non-destructive characterization of structural inhomogeneities in materials in the 1–1000 nm range, providing access to information on the size, morphology, and interactions of nano-objects, molecular assemblies, cluster systems, etc. [1]. Like other neutron scattering facilities, a SANS instrument requires careful design and optimization, where numerical modeling plays a key role.

Simulation results enable evaluation of the instrument performance, including the momentum transfer resolution Q, intensity losses, and signal-to-background ratio. In addition, numerical modeling is also applicable to existing instruments. In particular, the Q-resolution obtained from simulations can be incorporated into SANS data reduction, i.e., the reconstruction of the scattering curve I(Q), which is a key step that determines the reliability of the subsequent analysis.

In this work, we present an approach to SANS data reduction using numerical modeling. We developed algorithms and a software module implementing a complete data processing workflow for two SANS experimental configurations. A monochromatic setup with a multi-disc velocity selector and a time-of-flight (TOF) setup with a “blind pair” chopper system [2] require fundamentally different approaches to normalization and binning. In TOF mode, the neutron wavelength is reconstructed from the time of detection, introducing an additional degree of freedom and preventing the direct application of standard data reduction procedures used for monochromatic SANS.

The input data were obtained from Monte Carlo simulations performed with the McStas package for a model system of monodisperse solid spheres with radii of 10–100 nm. This model system is advantageous because the analytical expression for I(Q) is known, providing a reference for assessing the accuracy of the data processing.

The developed software module enables reconstruction of scattering curves while preserving the statistical significance of the data points. Validation using the model system shows good agreement with the analytical solution, confirming the applicability of the proposed algorithms to real experimental data analysis.

[1] Schmatz, W., Springer, T., Schelten, J. T., & Ibel, K. (1974). Neutron small-angle scattering: experimental techniques and applications. Applied Crystallography, 7(2), 96-116.
[2] Van Well, A. A., & Fredrikze, H. (2005). On the resolution and intensity of a time-of-flight neutron reflectometer. Physica B: Condensed Matter, 357(1-2), 204-207.

STUDY OF PHOSPHOLIPID LAYERS ADSORPTION ON PLANAR SOLID INTERFACES BY SPECULAR NEUTRON REFLECTOMETRY

V.A. Chausova[1], M.A. Kiselev[1,2], V.V. Sadilov[1] and M.V. Avdeev[1,2]

[1] *Joint Institute for Nuclear Research, Dubna, Russia*
[2] *Physics Department, Lomonosov Moscow State University, Moscow, Russia*

E-mail: varvara@jinr.ru

Studying model lipid layers is the first and important step in understanding biological membranes and their permeability to biologically active compounds. A phospholipid bilayer can be considered as a model membrane. Studies of the structure of a planar phospholipid bilayer deposited at a solid-water interface using specular neutron reflectometry have demonstrated the high efficiency of this method for both studying the structure of the phospholipid bilayer and investigating the kinetics of its formation *in situ* [1, 2]. Time-of-flight neutron reflectometry is the most effective method for such studies [3].

This report will present data from reflectometry experiments focusing on:

- the deposition of a single phospholipid bilayer,
- the potential for interaction between a phospholipid transport nanosystem (PhTNS) containing a drug and the precipitated bilayer,
- as well as the deposition of a bilayer consisting of PhTNS.

A special consideration is also given regarding the comparison of neutron experiments on the adsorption of lipids in horizontal and vertical sample geometries.

A phospholipid transport nanosystem developed at the Orekhovich Institute of Biomedical Chemistry was chosen as the target for interaction. These aggregates are relatively small in size (approximately 50 nm) and consist of soy phospholipids and maltose (in a ratio of 1:4) and may also contain a medicament. Using PhTNS as a delivery system is promising, as it leads to increased efficacy of medicinal compounds [4,5].

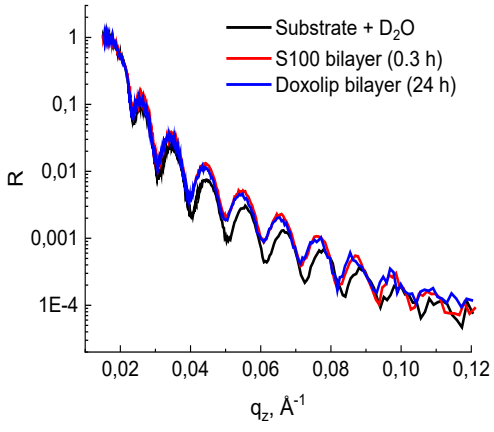

Fig.1 Reflectometric curves from substrate and soy phospholipid bilayer (S100)

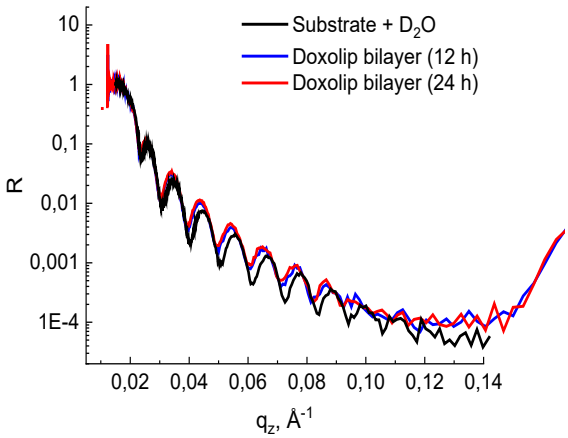

Fig.2 Reflectometric curves from precipitated PhTNS bilayer

For the experiment, we used a cell with a wash function, which allows us to remove unsettled particles from the cell and observe only the settled bilayer. A crystal with a nickel 'support'

layer was used as a substrate (Si/Ni 50 nm/Si 10 nm). Solutions were prepared in heavy water with a phospholipid concentration of 0.1%.

During the experiment, we were able to achieve a precipitated phospholipid bilayer [Fig.1]. We also precipitated the phospholipid transport systems themselves, containing the antitumor drug doxorubicin [Fig.2].

The hypothesis that PhTNS would interact with the precipitated bilayer and possibly even penetrate it was not confirmed [Fig.1]. We hypothesize that maltose, which is part of the PhTNS, may have acted as a barrier to interaction.

[1] Schoenborn, B.P. Neutron Scattering for the Analysis of Membranes. Biochim. Biophys. Acta - Rev. Biomembr. 1976, 457, 41–55, doi:10.1016/0304-4157(76)90013-7..

[2] Gutberlet, T.; Klösgen, B.; Krastev, R.; Steitz, R. Neutron Reflectivity as Method to Study In-Situ Adsorption of Phospholipid Layers to Solid-Liquid Interfaces. Adv. Eng. Mater. 2004, 6, 832–836, doi:https://doi.org/10.1002/adem.200400093.

[3] Gupta, M.; Gutberlet, T.; Stahn, J.; Keller, P.; Clemens, D. AMOR - The Time-of-Flight Neutron Reflectometer at SINQ/PSI. Pramana - J. Phys. 2004, 63, 57–63, doi:10.1007/BF02704051.

[4] Medvedeva, N.V.; Prosorovskiy, V.N.; Ignatov, D.V.; Druzilovskaya, O.S.; Kudinov, V.A.; Kasatkina, E.O.; Tikhonova, E.G.; Ipatova, O.M. Pharmacological Agents and Transport Nanosystems Based on Plant Phospholipids. Biomeditsinskaya Khimiya 2015, 61, 219–230, doi:10.18097/PBMC20156102219.

[5] Medvedeva, N.V.; Torkhovskaya, T.I.; Kostryukova, L.V.; Zakharova, T.S.; Kudinov, V.A.; Kasatkina, E.O.; Prozorovskiy, V.N.; Ipatova, O.M. Influence of Doxorubicin Inclusion into Phospholipid Nanoparticles on Tumor Accumulation and Specific Activity. Biomeditsinskaya Khimiya 2017, 63, 56–61, doi:10.18097/PBMC20176301056.

NEUTRON DIFFRACTION STUDIES OF AL-SUBSTITUTED HEXAFERRITES WITH GIANT COERCIVITY

L.A. Trusov[1], E.A. Gorbachev[1], J. Chen[1], V.A. Lebedev[2], V.A. Turchenko[3]

[1] *Shenzhen MSU-BIT University, Shenzhen, China*
[2] *Faculty of Chemistry, Moscow State University, 119991, Moscow, Russia*
[3] *Joint Institute for Nuclear Research, 141980, Dubna, Russia*

High-coercivity magnetic materials are indispensable for applications spanning permanent magnets to high-frequency electromagnetic filters; however, the scarcity and high cost of rare-earth and noble-metal-based benchmarks necessitate the development of cost-effective alternatives. While M-type hexaferrites (MFe12O19) offer a sustainable platform, their coercivity (Hc) is typically constrained by high saturation magnetization (Ms) compared to the traditional hard magnetic materials. Recent studies have demonstrated that Fe^{3+} substitution, in particular Al^{3+}, Cr^{3+}, Mn^{3+}, will significantly enhance magnetic property of strontium hexaferrite. Recently we report a systematic study on SrFe*12-xAlxO*19 (x = 0∽8) synthesized via a modified citrate-nitrate auto-combustion method, which produces highly porous precursors that effectively suppress grain growth below the single-domain limit (≈100 nm). In this work, the coercivity (Hc) and natural ferromagnetic resonance (NFMR) frequencies of strontium hexaferrite ($SrFe_{12}O_{19}$) have been significantly enhanced after Al-substitution in Fe^{3+} sites, a fundamental understanding of the site-specific substitution mechanism is critical for property optimization.

In this study, neutron powder diffraction (NPD) was employed to resolve the cation distribution across the five distinct crystallographic sublattices (2a, 2b, $4f_1$, $4f_2$, 12k). In contrast to transition metal dopants (Mn, Cr), NPD reveals that Al^{3+} ions exclusively occupy the octahedral 2a and 12k sites, while rigorously avoiding the trigonal bipyramidal 2b site—the primary locus of magnetocrystalline anisotropy. This selective occupancy of uncompensated spin-up sublattices triggers a rapid reduction in saturation magnetization (Ms) relative to the anisotropy constant (K1), thereby significantly elevating the effective anisotropy field (Ha).

Magnetic characterization correlates these structural findings with record-breaking performance: at x = 5.5, the compounds exhibit a giant room-temperature coercivity of 40 kOe and an NFMR frequency of 280 GHz. Temperature-dependent analysis further identifies a characteristic coercivity maximum at T ≈Tc/2. These results underscore the efficacy of neutron diffraction in elucidating the microscopic origins of macroscopic magnetic hardening, providing a robust framework for the development of rare-earth-free permanent magnets and high-stability components for next-generation terahertz communications.

ANTIBIOTIC-DRIVEN CHANGES IN THE ELEMENTAL STATUS OF CULTIVATED SOILS

O.-A. Culicov[1,2], I. Lung[3], M.-L. Soran[3], A. Stegarescu[3], O. Opriș[3], M. Shvetsova[1], P. Nekhoroshkov[1], V. Galustov[1]

[1] *Joint Institute for Nuclear Research, Dubna, Russia*
[2] *National Institute for Research and Development in Electrical Engineering ICPE-CA, Bucharest, Romania*
[3] *National Institute for Research and Development of Isotopic and Molecular Technologies, Cluj-Napoca, Romania*

E-mail: otilia.culicov@jinr.int

Antibiotics represent a real advance in medicine, and their discovery has led to the modification of old therapeutic concepts in human and animal health care. Their overuse and wrong application have led to contamination with antibiotics, with large quantities of them being present in manure, soils, wastewater, and water basins. Among the most widely used antibiotics are fluoroquinolones and β-lactam antibiotics.

Soil microbiota—bacteria, fungi, and archaea is crucial for the soil health including cycling of essential elements into plant-available forms. They decompose organic matter, release inorganic compounds, aggregate soil particles, and regulate nutrient bioavailability, effectively acting as the belowground engine for nutrient cycling and carbon sequestration.

Antibiotics in the soil environment may induce its degradation by impacting microbial activity and diversity. It is known that the occurrence and accumulation characteristics of antibiotics in soil may affect the carbon and nitrogen cycles, but there is a lack of information about their impact on the elemental content of the soil.

For the present study two representative antibiotics were selected: ampicillin, a β-lactam antibiotic, one of the most consumed antibiotics for the treatment of infections with Gram-negative and -positive bacteria and ciprofloxacin, a synthetic fluoroquinolone antibiotic, globally used for the management of bacterial infections in both humans and animals.

The antibiotics were dissolved in 200 mL of ultrapure water and used for the cultivation of lettuce under controlled laboratory conditions. Three concentrations were used: 7.5 mg kg^{-1}; 15 mg kg^{-1}; 30 mg kg^{-1} for ampicillin; 5 mg kg^{-1}; 10 mg kg^{-1} and 20 mg kg^{-1} for ciprofloxacin.

The soil samples, including noncontaminated ones, was taken for analysis when the lettuce was harvested 6 weeks after planting. Control soil was not contaminated with antibiotics. The elemental content was determined by Neutron Activation Analysis at IBR-2 reactor.

Gradual increases in the concentration of applied penicillin in soil did not reveal significant changes in the elemental composition, while changes in ciprofloxacin content correlated to varying degrees with the levels of 10 elements in the soil. Aluminum show the highest strength of association with the antibiotic content in soil, but while Al has a positive association, K, Ca and Br show antagonism.

MEASUREMENT OF NEUTRON TRANSMISSION FACTOR AND TOTAL CROSS SECTION OF VANADIUM IN THE WAVELENGTH RANGE 0.5–10 Å AT THE YuMO FACILITY

T.V. Cuong[1,2], O.I. Ivankov[1], A.Kh. Islamov[1], A.H.A. Elmekawy[1], A.I. Kuklin[1,3]

[1] *Joint Institute for Nuclear Research, Dubna, Russia*
[2] *Dalat Nuclear Research Institute, Dalat, (Viet Nam)*
[3] *Moscow Institute of Physics and Technology, Moscow, Russia*

E-mail: cuongtv@dnri.vn, alexander.iw.kuklin@gmail.com

We report measurements of the neutron transmission factor through high-purity (99.4%) vanadium over the wavelength range 0.5–10 Å to evaluate its suitability as a reference material for small-angle neutron scattering (SANS). The experiments were performed at the YuMO instrument [1] at the IBR-2 reactor, where a direct-beam detector was used to record the transmitted neutron spectrum at the beam center. Five vanadium samples with thicknesses of 0.15, 0.45, 0.53, 3.02 and 3.3 mm were investigated. The total neutron cross sections were derived from the measured transmission data and compared with the evaluated nuclear data libraries, including ENDF/B-VIII.0[2] and ROSFOND-2010[3]. Good agreement within the experimental error was observed, confirming the reliability of the measurements. Based on the transmission behavior, an optimal thickness range for vanadium reference standards in SANS experiments at the IBR-2 facility is identified.

[1] A. I. Kuklin, et al (2012). Past and present of time-of-flight small-angle neutron scattering at IBR-2, Journal of Physics: Conference Series, vol. 351, no. 1, p. 012001, 2012, doi: 10.1088/1742-6596/351/1/012001.
[2] M. Chadwick and et al (2018). ENDF/B-VIII.0: The 8th major release of the nuclear reaction data library, vol. 148, Nuclear Data Sheets, Feb 2018, pp. 1-142.
[3] S. Zabrodskaya and et al (2007). ROSFOND—Russian national library of evaluated neutron data, Vols. Nuclear Constants 1-2, VANT, 3 (2007).

INVESTIGATION OF CRYSTAL STRUCTURE OF EPITAXIAL THIN FeRh FILMS DURING AFM-FM PHASE TRANSITION

D.I. Devyaterikov[1], G.E. Zhezlyaev[1]

[1] *IMP UB RAS, Ekaterinburg, RussiaE-mail:*

E-mail: devidor@yandex.ru

The equiatomic compound FeRh exhibits an unusual magnetostructural phase transition from the antiferromagnetic (AFM) to the ferrimagnetic (FM) phase upon passing through a critical temperature of ~380 K. In bulk samples, this transition is accompanied by an isotropic expansion of the bcc FeRh lattice by 1% [1]. In epitaxial thin FeRh films, a similar phase transition is accompanied by a tetragonal distortion of the FeRh unit cell with an increase in the lattice parameter c in the direction normal to the sample surface [2]. Moreover, the coexistence of FM and AFM phases, characterized by different lattice parameters, is observed in the sample over a certain temperature range. This work is devoted to studying the processes occurring with both the lattice parameter c in the out-of-plane direction and the lattice parameter a in the in-plane direction during the phase transition.

The work was performed on a PANalytical Empyrean X-ray diffractometer. During the experiment, the temperature dependence of the positions of three out-of-plane reflections was measured: FeRh(003), FeRh(103), and FeRh(222). FeRh(003) was measured in symmetric geometry, while FeRh(103) and FeRh(222) were measured in asymmetric beam geometry. Separation of the contributions to the diffraction maximum of the FM and AFM phases in the temperature range of their coexistence was accomplished by fitting the reflection to Pearson (VII) and Voigt distribution functions.

Assuming that each phase has a tetragonally distorted unit cell with its own set of lattice constants (aAFM, cAFM, aFM, cFM), we obtained the temperature dependences of these lattice constants and estimated the change in the quantity of FM and AFM phases. Use of polarized neutron reflectometry is proposed to obtain depth resolved concentration profiles of FM and AFM phases in the sample during phase transition.

[1] A. I. Zakharov, A. Kadomtseva, R. Levitin, and E. Ponyatovskii, Zh. Eksp. Teor. Fiz. 46, 2003 (1964).

[2] M. A. de Vries, M. Loving, M. McLaren, R. M. D. Brydson, X. Liu, S. Langridge, L. H. Lewis, and C. H. Marrows, Appl. Phys. Lett. 9 June 2014; 104 (23): 232407

ALBUMIN COMPLEXES WITH AMYLOIDOGENIC PROTEINS: A SANS STUDY

N.A. Grudinina[1], O.I. Ivankov[2], T.N. Murugova[2] and V.V. Egorov[1]

[1] *Instutute of Experimental Medicine*
[2] *Joint Institute of Nuclear Research*

E-mail: sondyn@yandex.ru

Early diagnosis of conformational diseases such as Alzheimer's, Parkinson's, and transthyretin-induced cardioamyloidosis is essential for timely treatment. Treatment is only possible in the early stages, when symptoms have not yet manifested, and the concentration of misfolded marker proteins in patients' biological fluids (e.g., by the CAMP method [1]) is insufficient for detection. Therefore, the development of biochemical and biophysical methods for early detection of misfolded amyloidogenic proteins low concentrations in the blood is an actual issue, and its solution is essential for the treatment of amyloidoses.

For a number of proteins, it is known that when misfolded, exposed hydrophobic regions can bind to serum albumin [2]. But there is a little known about prefibrillar oligomers ability to form complexes with serum albumin. If such oligomers form complexes with serum albumin *in vivo*, it allows us to search proteins oligomers associated with conformational diseases in the albumin-containing blood fraction. In this case, this fraction will be enriched in proteins of interest, which can significantly facilitate the detection of oligomers in the early stages of conformational diseases.

In this study, we examined the ability of monomers, oligomeric forms (prone to amyloidogenesis), and amyloid-like fibrils of model proteins (lysozyme and insulin) to form complexes with human serum albumin *in vitro* using electrophoresis under native conditions, fluorimetry of the hydrophobic probe ANS, and small-angle neutron scattering. It was demonstrated that prefibrillar oligomers of the studied proteins are capable of forming complexes with albumin in electrophoresis under native conditions. A change in the hydrophobic surface accessible to ANS upon the formation of such complexes was also demonstrated. The mass and (preliminary) morphology of these complexes in solution were characterized using small-angle neutron scattering.

The obtained data will be expanded with data on other amyloidogenic proteins and used to analyze the presence of albumin complexes with amyloidogenic proteins in patient biological fluids. The research was supported by the Institute of Experimental Medicine (project FGWG-2025-0021). The experiment were performed under IBR-2 User Program, proposal number 2025-04-29-14-32-50.

[1] G. P. Saborio, B. Permanne, and C. Soto, “Sensitive detection of pathological prion protein by cyclic amplification of protein misfolding,” Nature, vol. 411, no. 6839, pp. 810–813, 2001, doi: 10.1038/35081095.

[2] Nakajima K, Yamaguchi K, Noji M, Aguirre C, Ikenaka K, Mochizuki H, Zhou L, Ogi H, Ito T, Narita I, Gejyo F, Naiki H, Yamamoto S, Goto Y. Macromolecular crowding and supersaturation protect hemodialysis patients from the onset of dialysis-related amyloidosis. Nat Commun. 2022 Oct 3;13(1):5689. doi: 10.1038/s41467-022-33247-3. PMID: 36192385; PMCID: PMC9530240.

NANOPARTICLES OF REDUCED GRAPHENE OXIDE AND GRAPHENE NANOPLATELET – HOW AND THEY ORGANIZED IN POLYLACTIDE MATRIX?

L.V. Elnikova[1], S.Z. Rogovina[2], M.M. Gasymov[2], O.P. Kuznetsova[2], V.G. Shevchenko[3], A. Elmekawy[4], V.V. Skoi[4,5] and A.I. Kuklin[4,5]

[1] *NRC Kurchatov institute, Moscow, Russian Federation*
[2] *N.N. Semenov Federal Research Center of Chemical Physics, Russian Academy of Sciences, Moscow, Russian Federation,*
[3] *N.S. Enikolopov Institute of Synthetic Polymeric Materials, Moscow, Russian Federation*
[4] *Joint Institute for Nuclear Research, Dubna, Russian Federation*
[5] *Moscow Institute of Physics and Technology, Dolgoprudny, Russian Federation*

E-mail: elnikova@itep.ru

The polymer composites composed of biodegradable synthetic Polylactide (PLA) and carbon allotrope additives reduced graphene oxide (RGO) and graphene nanoplatelets (GNP) were studied with Small Angle Neutron Scattering (SANS) at the YuMO instrument located at the IBR-2, Dubna.

Filling PLA with nanosize particles (NPs) of RGO or GNP results in clusterization of nanoparticles in the bulk of the polymer matrix, decreases its segmental mobility, changes thermal, conductive and mechanical properties (strength, toughness), thereby improves their operational characteristics important for different industrial, economic and medical applications.

Recently, the PLA composites filled with RGO and GNP nanoparticles were carefully studied; in [1], [2], [3], synthesis of nanocomposites (by solid-phase- and liquid-phase mixing) and their characterization with thermogravimetrical analysis, thermophysical analysis for the original PLA (4043D manufactured by NatureWorks, USA, with a crystallinity of 30.8%,) and its compositions with RGO and GNPs (from 1 to 5 wt%) nanofillers were carried out, electrical and mechanical properties of the composites at 0.25-15wt% of RGO and GNPs in PLA were clarified. The percolation thresholds of PLA/RGO (2wt%) and PLA/GNP (7wt%) were found, as well as differential distributions of RGO and GNP particles sizes in the bulk. Aggregated carbon nanoparticles RGO and GNP have high polydispersity in the bulk of PLA, they reach the maximum sizes in plane from 0.34 to 80 μm and from 2.24 to 88.4 μm for RGO and GNP particles respectively, whereas original particles are of units to tens nm sizes; as the SEM data showed [1], [2], [3].

At the same time, at the filling PLA with NPs, obscure shifts were observed X-ray microtomography images of the composites, which have to be interpreted as formation of new functional groups or new unknown intermolecular interactions.

At the YuMO instrument, we obtained the SANS spectra $I(Q)$ for pure PLA and PLA compositions with RGO concentrations 0.05, 0.1, 0.15, 0.2, 0.25 wt% and GNPs concentrations 0.05, 0.1, 0.25, 1 and 5 wt% of solid-phase's and 0.1, 0.2, 0.25 wt% liquid-phase's method of synthesis. Theses spectra $I(Q)$ for pure PLA and 3 series with "PLA/GNPs from a solid-phase", "PLA/GNPs from a liquid-phase" PLA/RGO samples are shown in Figure 1.

We present the results of Guinier (at $Q<0.04$ Å^{-1}) and Porod (at $Q>0.04$ Å^{-1}) analysis of the experimental SANS curves: structure factor and formfactor of the nanofillers, such as the gyration radii R_g, fractal dimensionality of the RGO ($d_f \sim 2$) and GNP nanoparticles [4], [5]. For instance, we found out the organization of RGO in PLA matrix into ellipsoid-like sheets of ~0.5 nm thickness and confirmed high polydispersity of nanoparticles.

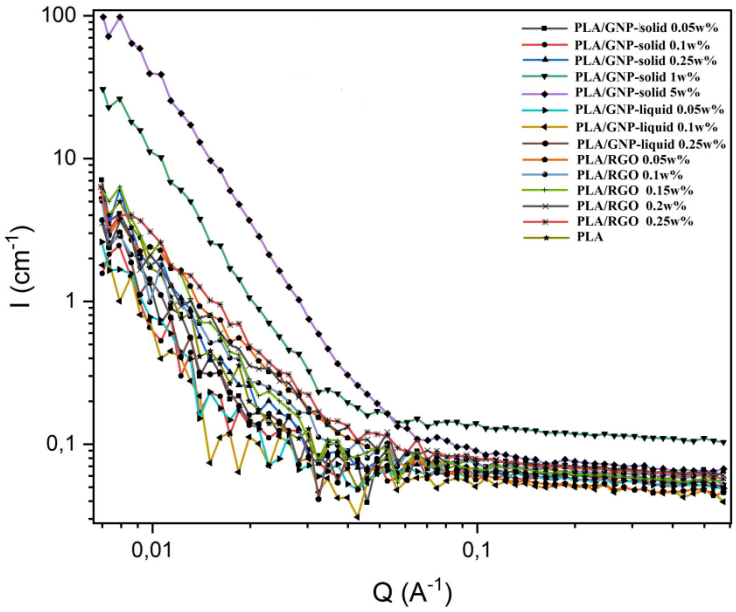

Fig.1. Experimental intensities $I(Q)$ SANS for PLA, PLA/RGO and PLA/GNP samples

Our SANS data analysis is useful for refined nondestructive evaluations of morphology of RGO and GNP particles in PLA and further scientific substantiation of unknown mechanisms of self-organization of carbon allotrope nanoparticles under various synthesis conditions.

The work was supported by the Government contract of the NRC Kurchatov Institute.

[1] M.M. Gasymov, S.Z. Rogovina, O.P. Kuznetsova, E.O. Perepelitsyna, V.G. Shevchenko, S.M. Lomakin, A.A. Berlin (2024). Investigation of the Influence of UV Radiation on Compositions of Polylactide with Graphite Nanoplatelets. Russian Journal of Physical Chemistry B. 18(2), 562.

[2] S.Z. Rogovina, O.P. Kuznetsova, M.M. Gasymov, S.M.Lomakin , V.G. Shevchenko, A.A. Berlin (2024) Composites of polylactide with carbon nanofillers: synthesis, structure, properties. Polymer Science, Series C. 66(1), 68.

[3] S. Rogovina, S. Lomakin, S. Usachev, M. Gasymov, Olga Kuznetsova, N. Shilkina, V. Shevchenko, A. Shapagin, E. Prut, and A. Berlin (2022). The Study of Properties and Structure of Polylactide–Graphite Nanoplates Compositions. Polymer Crystallization. Art. ID 4367582.

[4] A.G. Soloviev, T.M. Soloveva, A.V. Stadnik, A.H. Islamov and A.I. Kuklin. SAS. The Package for Small-Angle Neutron Scattering Data Treatment Version 2.4. Long Write-Up and User's Guide. Communic. of JINR P10-2003-86, Dubna.

[5] M.V. Petoukhov, D. Franke, A. V. Shkumatov, G. Tria, A.G. Kikhney, M. Gajda, Ch. Gorba, H.D.T. Mertens, P.V. Konarev and D. I. Svergun (2012) New developments in the ATSAS program package for small-angle scattering data analysis. J. Appl. Crystallogr. 45, 342–350.

PHASE COMPOSITION ANALYSIS OF WELDS IN AUSTENITIC STAINLESS STEELS

S.N. Petrov[1], M.L. Fedoseev[1], A.N. Dobrotvorskaya[2]

[1] *NRC "Kurchatov institute" – CRISM "Prometey", St. Petersburg, Russia*
[2] *JSC "NPO "Lenkor", St. Petersburg, Russia*

E-mail: ckp@crism.ru

Austenitic stainless steels are used for the manufacture of equipment and structures in fast neutron reactor plants (BN reactors). Long-term operation in the temperature range of approximately 500–550 °C leads to a reduction in plasticity, impact toughness, and crack resistance of the metal due to the formation of secondary phases at grain boundaries, special boundaries, and interphase boundaries [1]. Aging of austenitic chromium-nickel steels results in the formation of carbide phases such as $M_{23}C_6$ (where M = Cr, Fe) and intermetallic χ-, σ-, and η-phases (Laves phase). The formation of the σ-phase is a key problem in the operation of corrosion-resistant steels, as it causes a sharp loss of plasticity and long-term strength of the material, leading to premature failure of equipment. The stability of the metal's properties is related to structural and phase stability, since phase reactions occurring in the metal during operation can alter its properties.

Chromium-nickel-molybdenum austenitic stainless steel – AISI 316-type after operation for 195,000 hours at 515°C was studied. The method of differential physicochemical phase analysis (carbide analysis) was applied, which makes it possible to evaluate changes in the metal and predict the possibility of its safe operation.

The method of carbide analysis consists of the following main stages [1], [3]:

1. Electrochemical isolation of carbide and intermetallic phases under conditions of anodic dissolution of the metal sample (selectively extracting carbide and intermetallic phases from the metal matrix by dissolving the surrounding matrix electrochemically);
2. Investigation of the structure of the isolated phases by X-ray diffraction (XRD);
3. Investigation of the composition and quantity of phases by analytical chemistry methods.

The method of anodic dissolution described in [3] was used as the basis. The adaptation of the method consisted in selecting the electrolyte composition, current density *I*, dissolution time, and the material of the auxiliary electrode (cathode). The base electrolyte was a methanol solution of hydrochloric acid [3]. For all experimental series, the conditions were unified: the temperature in the electrochemical cell was maintained at –10°C using a cryothermostat, and the electrolysis duration was 2 hours.

Previous studies have been conducted on the phase composition changes in the weld metal of austenitic stainless steels of AISI 302 and AISI 316-type, whose welds were made using A-2 (A-1) electrodes (roughly corresponds to AWS E308-type electrodes) or ER316L-type welding wire, in the operating temperature range of approximately 500–550 °C. To evaluate phase changes in the material, impact bending tests at +20 °C were used, as well as both X-ray and neutron diffraction IBR-2 reactor (JINR, Dubna). In addition, small-angle neutron scattering was used to determine fine-dispersed precipitates in the weld samples. It was found that thermal embrittlement after accelerated laboratory aging of the metal of austenitized and non-austenitized welds at a temperature of 700 °C occurs due to the formation and growth of brittle intermetallic σ- and χ-phases.

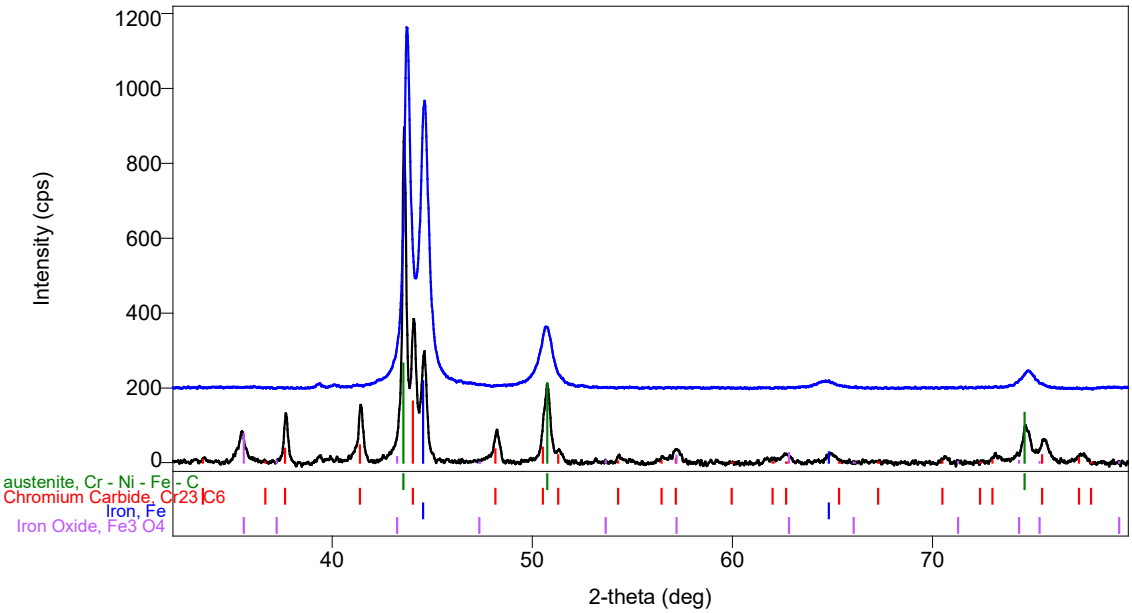

Figure 1 – Lower XRD pattern: phase composition of the carbide precipitate of steel AISI 316-type after operation for 195,000 hours at 515°C; upper XRD pattern: metallographic section of steel AISI 316L-type after operation for 170,000 hours at ~520°C.

The figure shows XRD patterns of samples after operation, where carbide analysis reveals BCC (Fe, Cr) and FCC (Fe, Ni) crystal lattices, an oxide of the M_3O_4 type, and a carbide of the $M_{23}C_6$ type, which is not detected in the metallographic sample surface. A similar pattern is observed in the weld with a noticeable amount of σ-phase: the carbide precipitate shows a carbide of the $M_{23}C_6$ type, while it is not detected in the metallographic section. The difficulties in detecting the carbide in the polished section by XRD can be attributed to the fine dispersion of the carbide and its small quantity.

This study makes it possible to focus on intermediate states with minor changes in the phase composition of fine-dispersed precipitates. This allows obtaining data on the kinetics of the transformation process as the aging time increases. The method of carbide precipitates allows obtaining data on dispersed phases in cases where diffraction from bulk samples did not reveal any other phases in the composition of the specimen.

[1] Pigrova, G.D. (Ed.) (2009). Phase Transformations in Materials for Power Engineering. Transactions of NPO CKTI (Scientific Production Association – Central Boiler and Turbine Institute). 297 p
[2] Popova, N.M. (1957). Carbide Analysis of Steel. State Publishing House of the Defense Industry. 100 p.
[3] Lashko, N.F., Zaslavskaya, L.V., Kozlova, M.N., et al. (1970). Physicochemical Methods of Phase Analysis of Steels and Alloys. Moscow: Metallurgiya Publishing House. 479 p.

CRYSTAL AND MAGNETIC STRUCTURE OF OXYGEN-DEFICIENT $La_{0.5}Sr_{0.5}FeO_{3-\delta}$ FERRITE AT ROOM AND LOW TEMPERATURE

K.A. Gavrilicheva[1], A.V. Rutkauskas[2], S.S. Nikitin[1] and O.I. Barkalov[1]

[1] *Osipyan Institute of Solid State Physics RAS, Chernogolovka, Russia*
[2] *Joint Institute for Nuclear Research, Dubna, Russia*

E-mail: xenia.gavrilicheva@issp.ac.ru

Perovskite-type ferrites ($R_{1-x}A_xFeO_{3-\delta}$, where R is a rare-earth element and A is Ca, Sr, or Ba) exhibit unique electrical, magnetic, and catalytic properties. These make them suitable for various applications, such as cathode materials for solid oxide fuel cells [1–3] and catalysts [4,5]. In substituted $La_{1-x}Sr_xFeO_{3-\delta}$ ferrite, an increase in the number of oxygen vacancies can be achieved by high-temperature vacuum annealing. Our previous work showed that this process was accompanied by a change in the oxidation state of iron ions from a mixed Fe^{3+}/Fe^{4+} state to a purely Fe^{3+} [6–9]. The resulting compositions can be described by the formula $La_{1-x}Sr_xFeO_{3-x/2}$. The equiatomic $La_{0.5}Sr_{0.5}FeO_{2.75}$ composition corresponds to the maximum oxygen vacancy concentration in the series and exhibits a cubic structure ($Pm\bar{3}m$ space group) for the metal sublattice[8]. Notably, these compounds have antiferromagnetic ordering, for instance, the $LaFeO_3$ and $SrFeO_{2.5}$ ferrites are antiferromagnets at room temperature (T_N ~750 K [10,11] and ~690 K [12], respectively).

Although the $La_{0.5}Sr_{0.5}FeO_{2.75}$ ferrite is considered a key composition for practical applications, it remains unexplored within the La-Sr ferrite system. Low-temperature behavior has been observed for La-Sr ferrites [13, 14]. We decided to study this ferrite using neutron diffraction as a direct method to investigate its crystal and magnetic structures.

A polycrystalline $La_{0.5}Sr_{0.5}FeO_{3-\delta}$ sample was synthesized by a glycine-nitrate combustion method and subsequently annealed at 1100°C for 10 h in air. Details of the preparation procedure are described in [6]. After synthesis, the as-prepared $La_{0.5}Sr_{0.5}FeO_{3-\delta}$ ferrite was annealed in vacuum (10^{-6} Torr) at 650°C for 10 h to reduce oxygen concentration.

Neutron diffraction data were acquired on the DN-12 diffractometer at the IBR-2 reactor with the detector rings positioned at 55° scattering angles. The powder bulk sample of $La_{0.5}Sr_{0.5}FeO_{2.75}$ in an aluminum container was cooled in a closed-cycle cryostat to about 14 K and diffraction patterns were collected at eight temperature points up to RT (292 K).

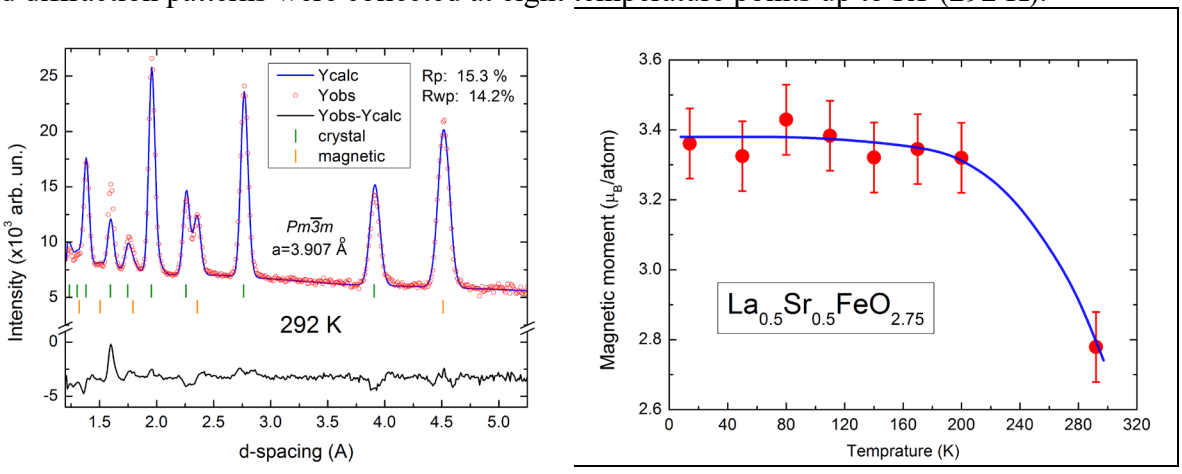

Fig. 1 Left: Neutron diffraction pattern of $La_{0.5}Sr_{0.5}FeO_{2.75}$ at 292 K. The bottom curve (Yobs-Ycal) represents the difference between the experimental data and calculated data. The vertical bars indicate the position of magnetic (bottom) and nuclear Bragg (top) peaks. Right: Temperature dependence of the magnetic moment values of Fe ions obtained by Rietveld refinement. The blue curve is a guide to the eye

Figure 1 (Left) presents the results of the Rietveld refinement of the room-temperature diffraction pattern performed using the FullProf program suite. The fit converged with R_p = 15.3% and R_{wp} = 14.2%. The lattice parameter a=3.907 Å are agrees with the cubic $Pm\bar{3}m$ structure reported recently [8] for the metal sublattice of the ferrite. The crystal phase Bragg R-factor is 11.5%. An excess intensity is observed in the difference curve for the (211) reflection. This reflection is purely crystallographic, with no magnetic contribution. This effect is likely due to higher oxygen content in these planes, since oxygen ions contribute significantly to the overall scattering. Consequently, the symmetry of the structural refinement should be lowered to resolve this discrepancy.

A magnetic reflection at 4.5 Å corresponding to the antiferromagnetic phase was observed. The magnetic contribution was fitted using a model with G-type antiferromagnetic ordering and a doubled lattice parameter. A magnetic R-factor of 3.61% was obtained.

The temperature dependence of the magnetic moment of the iron ions is shown in Fig. 1, Right. The variations of the magnetic moment below ~200 K are rather sluggish, while a small drop (~18%) is observed above ~200 K. Additional experiments planned in the near future will help to determine the exact temperature interval of this change and provide insights into its origin.

[1] A. Shaula, et al. (2006). Ionic conductivity of brownmillerite-type calcium ferrite under oxidizing conditions. *Solid State Ionics*. **177**, 2923.

[2] M. V. Patrakeev, et al. (2003). Electron/hole and ion transport in $La_{1-x}Sr_xFeO3-\delta$. *Journal of Solid State Chemistry*. **172**, 219.

[3] Y. Shin, et al. (2020). Effect of oxygen vacancies on electrical conductivity of $La_{0.5}Sr_{0.5}FeO_{3-\delta}$ from first-principles calculations. *J. Mater. Chem. A*. **8**, 4784.

[4] Z.-X. Wei, Y.-Q. Xu, H.-Y. Liu, and C.-W. Hu (2009). Preparation and catalytic activities of $LaFeO_3$ and Fe_2O_3 for HMX thermal decomposition. *Journal of Hazardous Materials*. **165**, 1056.

[5] S. N. Tijare, et al. (2012). Photocatalytic hydrogen generation through water splitting on nano-crystalline $LaFeO_3$ perovskite. *International Journal of Hydrogen Energy*. **37**, 10451.

[6] V. D. Sedykh, et al. (2019). Effect of the Oxygen Content on the Local Environment of Fe Atoms in Anion-Deficient $SrFeO_3$. *Phys. Solid State*. **61**, 1099.

[7] V. Sedykh, et al. (2022). Role of Fe atom valence states and oxygen vacancies in substituted lanthanum ferrite $La_{0.67}Sr_{0.33}FeO_{3-\gamma}$. *Journal of Physics and Chemistry of Solids*. **171**, 111001.

[8] V. Sedykh, et al. (2023). Fe ion valence states and oxygen vacancies in the $La_{0.5}Sr_{0.5}FeO_{3-\gamma}$ ferrite under vacuum annealing. *Ceramics International*. **49**, 25640.

[9] O. I. Barkalov, et al. (2022). Strontium ferrite $SrFeO_{3-\delta}$ ($2.50 \leq 3-\delta \leq 2.87$) studied by Raman and Mössbauer spectroscopy. *Solid State Communications*. **354**, 114912.

[10] J. B. Goodenough (1963). *Magnetism and the Chemical Bond*, Vol. 1.

[11] C. Boekema, et al. (1978). Super transfer in doped $LaFeO_3$. *Hyperfine Interactions*. **45**.

[12] M. Schmidt and S. J. Campbell (2001). Crystal and Magnetic Structures of $Sr_2Fe_2O_5$ at Elevated Temperature. *Journal of Solid State Chemistry*. **156**, 292.

[13] N. Sivakumar, et al. (2023). Crystal structure, dielectric and magnetic studies of pure and Sr substituted $LaFeO_3$ single crystal grown by optical floating zone technique. *Journal of Alloys and Compounds*. **943**, 169161.

[14] A. I. Dmitriev, et al. (2024). Effect of oxygen content variations on structural and magnetic features in $La_{0.5}Sr_{0.5}FeO_{3-\delta}$. *Physics of the Solid State*. **66**, 386–391.

STRUCTURE AND PROPERTIES OF MATERIALS FROM BiOX (X=Br, Cl, I, BrO3), WITH APPLICATION FOR PHOTOCATALYTIC WATER PURIFICATION AND NO2 GAS SENSORS

I.G. Genov[1], A.G. Bannov[2], S.A. Shpakova[2], E.V. Lukin[1], S.E. Kichanov[1], I.I. Vinogradov[1], N.A. Drozhzhin[1] and D.P. Kozlenko[1]

[1] *Joint Institute for Nuclear Research, Dubna, Russia*
[2] *Novosibirsk State Technical University, Novosibirsk, Russia*

E-mail: genov@jinr.ru

The emergence of novel environmental protection technologies based on the application of semiconductor photocatalytic materials for converting CO_2, splitting water to generate H_2, and eliminating pollutants, has stimulated extensive research in the field of photocatalytic chemistry. In addition the accurate detection of human hazardous gases, such as NO_2, using a low-cost gas sensing device is quite important.

The semiconductor photocatalysators can be used to treat degrading toxic organic pollutants in wastewater contaminated with dyes and antibiotics. They converting pollutants into simpler or non-toxic molecules, without the need for additional treatments using expensive oxidizing chemicals.

The materials containing bismuth show improved spontaneous polarization effects due to the stereochemical activity of the $6s^2$ lone pair of Bi^{3+} ions. The bismuth-based layered materials, present extended photooxidative ability in the splitting of various pollutants. The layered crystal structures provide the formation of an internal electric field through the diffusion of charges between the layers and the easier separation of electron-hole pairs.

The layered photocatalytic materials with the general formula BiOX (X = Cl, Br, I or BrO_3) and a silenite structure, has unique structural and physical properties, and a complex band structure. They exhibit an open layered structure with -Bi_2O_2- sheets inserted into double halogen atomic units. A stack of [X-Bi-O-O-Bi-X] layers is formed with weak Van-der-Waals interactions between each layer [1]. Moreover these materials has not been studied much in the realm of gas detection, especially NO_2 [2].

In our study were successfully synthesized Bi-based layered materials for use for photocatalysts and gas-sensing sensors, via a solution combustion method using $Bi(NO_3)_3x5H_2O$ as the starting material .

The phase and crystal structures analysis of the obtained samples were performed using powder X-ray (XRD) and neutron diffraction (ND). The XRD and ND data were analyzed using the FULLPROF package.The structural and morphologies of prepared samples were analyzed by scanning electron microscopy (SEM).

[1] X.Dong, Y. Zhang, Z.Zhao (2021) Role of the Polar Electric Field in Bismuth Oxyhalides for Photocatalytic Water Splitting, Inorg. Chem. 60 8461-8474.
[2] N.Dhariwal, P.Yadav, A.Sanger, S.B.Kang, M.S.Goyat, Y.K.Mishra, V.Kumar((2005). Fabrication of a room-temperature NO_2 gas sensor with high performance at the ppb level using an rGO/BiOCl heterostructure. Mater. Adv. 5, 4187-4199 .

STUDY OF NSAIDS MOLECULAR DYNAMICS BY INELASTIC NEUTRON SCATTERING AND COMPLEMENTARY METHODS

P.A. Gergelezhiu[1,2], E.V. Raksha[1], E.A. Goremychkin[1], A.B. Eresko[1], L.I. Savostina[3] and D.M. Chudoba[1]

[1] *Frank Laboratory of Neutron Physics, Joint Institute for Nuclear Research, Dubna, Russia*
[2] *Branch of Lomonosov Moscow State University in Dubna, Dubna, Russia*
[3] *Institute of Physics, Kazan Federal University, Kazan, Russia*

E-mail: gergelezhiu@jinr.ru

Ibuprofen and ketoprofen are well-known NSAIDs (propionic acid derivatives) that inhibit cyclooxygenase-II. They contain a chiral center and are used clinically as racemates, although only the S-enantiomers are biologically active (the R-forms are converted in vivo to S-enantiomers). Chemical structures of ibuprofen and ketoprofen include three key fragments: a hydrophilic carboxyl group, an aromatic ring, and a hydrophobic alkyl or keto-aryl substituent. Lability of these fragments will be one of the main factors ensuring dynamic complementarity in the formation of a complex with an enzyme. Combining experimental and computational methods for drug characterization is now common practice, but the choice of structural model critically affects result interpretation. Previous IR, Raman, and molecular modeling studies [1, 2] showed good correlation for most spectral parameters; however, data on carboxyl group vibrations remain inconsistent.

Here we report on the intra- and intermolecular dynamics of racemic ibuprofen and racemic ketoprofen using a combination of experimental methods: IR, Raman, and inelastic neutron scattering (INS) spectroscopy, complemented by DFT molecular modeling at the BP86/def2-TZVP level of theory. INS measurements were performed on the NERA spectrometer at the IBR-2 reactor (JINR, Dubna) over a temperature range of 5–200 K. The INS technique provides unique access to low-frequency vibrational modes, with spectra dominated by hydrogen atom motions and free from optical selection rules, thereby offering critical information that complements optical spectroscopy.

a b

Figure 1 – Equilibrium geometries of cyclic S-R dimers of ibuprofen (a) and ketoprofen (b), obtained at the BP86/def2-TZVP level of theory.

For computational modeling, cyclic dimers were used as a small-cluster representation of the ibuprofen and ketoprofen structures (Fig. 1), explicitly accounting for intermolecular hydrogen bonds. DFT calculations of vibrational frequencies based on these dimer models yielded good correlations with experimental data for both compounds. Key vibrational frequencies of the carboxyl group were identified, which can serve as reliable markers for investigating the molecular dynamics of these NSAIDs.

[1] K. Logacheva (2024). Vibrational spectroscopic features of ibuprofen and ketoprofen: IR and Raman spectroscopy combined with DFT calculations. Part. Nuclei Lett. 21, 839-842.
[2] P. Gergelezhiu (2025). Structure and Dynamics Investigation of Ibuprofen Dimers by DFT MethodPhys. Part. Nuclei Lett. 22, 1102-1105.

THEORETICAL DESCRIPTION OF NEW EFFECT SPACE OSCILLATION OF CORRELATION FUNCTION FOR ULTRA-THIN FERROMAGNETIC FILM IN ALGEBRAIC THEORY OF SYMMETRY BREAKING AND SUGGESTION OF ITS EXPERIMENTAL VERIFICATION

E.L. Gudkov[1]

[1] *Dubna State University, Russia*

E-mail: EugeneGoodok@gmail.com

Suggests new theory of symmetry breaking with using of algebraical methods , so indeed creating of C^*-algebra of observables this system. This theory reconstructed algebraically meaning of factornorm as physical order parameter. This theory successfully corresponding with experimental results of in a number of experimental examples, such as neutron scattering correlation functions and neutron scattering spectrum shapes.

Results

Proved general theorem

Let exists C^* algebra with unity. Lets I - closed double side ideal:

$$\pi: A \to B(H)$$

$\omega \in H$ cycling vector of unity norm $\|\omega\|=1$ corresponds to alpha-invariant state:

$$\{g_n\} \subset G$$

Thus difference between matrix element approximate as:

$$|\langle \omega, \pi(a), \omega \rangle| - |\langle \omega, \pi(\alpha(a)\omega) \rangle| \leq \|a\|_q$$

If $I=K(H)$- ideal of compact operators exists sequence which has reached limits equality:

$$lim_{n\to\infty} \left\| \pi(\alpha)_{g_n}(a) - \langle \omega, \pi(\alpha)(a)\omega \rangle I_H \right\| = 2\|a\|_q$$

For susch operator there is weak*-closed (in *- topology):

$$T_n(a) = \pi\left(\alpha_{g_n}(a)\right) - \langle \omega, \pi\left(\alpha_{g_n}(a)\right)\omega \rangle I_H$$

$$lim_{n\to\infty} \|T_n(a_m)\| = 2dist\left(\pi(a), CI + K(H)\right)$$

But completes the proof of the limit equality.

Weak convergence follows from the boundedness of the sequence and the Banach--Alaoglu theorem.

$$\lim_{m\to\infty} \lim_{n\to\infty} \langle \mu, T_n(a_m)\rho \rangle, \langle \mu, T(a)\rho \rangle$$

$$\{T_n(a)\}_{n\to\infty}$$

Consequence 1.

1. Factornorm is parameter of symmetry breaking – the measure for difference from general state (for paramagnetic system factorm is matches with magnetized ability.
2. Maximal ideal for symmetry is double sided ideal.

Predictions for the experiment:

1. Spatial oscillations in the correlation functions of magnetization for ferromagnetic materials (analogous to the Kapitza-Dirac effect for transmitted pulses.
2. Improvement of the accuracy of the magnetization calculation for thin films, estimated relative accuracy σ=0.2-0.001

$$\Delta q = \frac{2\pi}{Ld} = \frac{2\pi}{3 * 2.86} \approx 0.73A^{-1}$$

3.Broadening of the spectral function described as:

$$S(q_{||}, q_z) = A \cdot \frac{1}{\kappa_{II}^2 + q_{II}^2} \cdot F(q_z)$$

$$F(q_z) = \frac{\sin^2(Lq_z\frac{d}{2})}{\sin^2(q_z\frac{d}{2})}$$

For the first time, the consequence of the unified theory of symmetry breaking for magnetic systems is being tested. The result will either confirm the new formalism or set the limits of its applicability. The success of the experiment will pave the way for the application of algebraic methods to describe a wide class of phase transitions, there $F(q_z)$ it is the factor of causality. Based on these predictions we also can to construct oscillations for one-dimensional spin chain at asymptotics.

We constructed numerically simulation and predicted two new effects time-period oscillation for and spin wave oscillation for changing currents for thin surface. Statistical significance of the effect in cross-sectional pooled analysis.

p≈0.66 - good correspondence

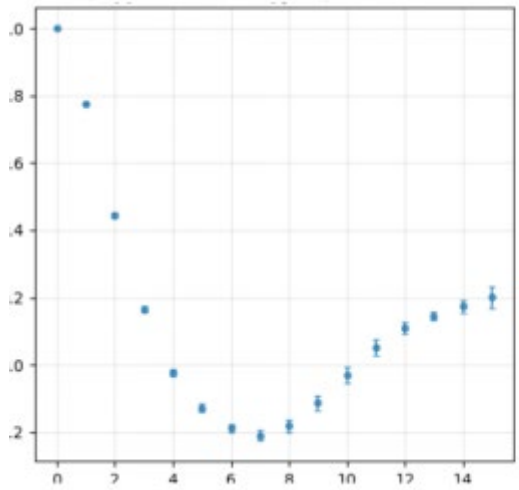

Fig 1. Fourier transformation for correlation function oscillation exchange integral for periodically oscillation for J=0.292 for absolutely estimate.

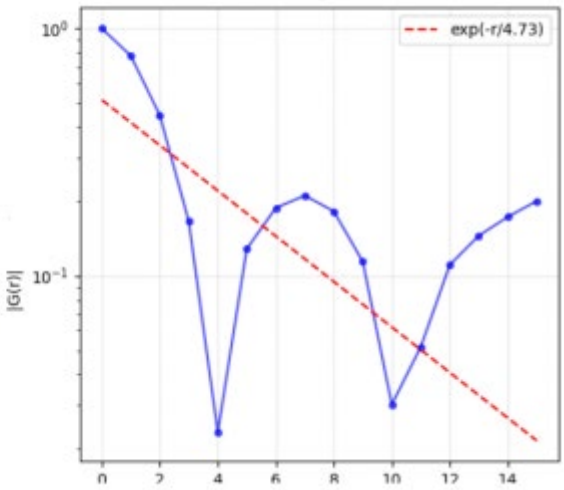

Fig 2. Correlation function oscillation for T=0.1(logariphmic scale)

[1] S.S. Khoruzhy, "Introduction to Algebraic Quantum Field Theory," 1986, Nauka Publishing House.

[2] R. Haag, "Local Quantum Physics: Fields, Particles, Algebras," Springer, 1996.

[3] G. Shirane, S.M. Shapiro, and J.M. Tranquada, "Neutron Scattering with a Three-Axis Spectrometer," Cambridge University Press, 2002.

STUDY OF RADIATION-THERMOSTIMULATED PROPERTIES IN MODIFIED COMPOSITE THERMOREGULATING COATINGS

V.V. Harutyunyan[1]

[1] *A.Alikhanyan National Science Laboratory, Yerevan, Armenia*

E-mail: vachagan,harutyunyan@aanl.am

The aim of this work is to study the radiation-thermostimulated properties of modified composite thermoregulating coatings by the method of hydrothermal microwave synthesis - zinc orthosilicate (willemite) and zirconium doped with cerium (Ce-Zn_2SiO_4 and Ce-$ZrSiO_4$) using X-ray diffraction analysis and optical spectroscopy (photoluminescence). Neutron activation analysis of the (NNAs) of the studied temperature-regulating coatings was performed, and the elemental composition of these materials was determined. It is known that in the luminescence spectra of some simple oxides (BeO, Al_2O_3) several bands of intrinsic luminescence are observed, and in complex crystals, such as TRC, there may be several sublattices and structural fragments of different types, and therefore defects formed as a result of heat treatment, radiation and the presence of impurity ions. Doping with cerium allows to obtain a highly crystalline nanosized structure. It also stabilizes the crystal structure due to the difference between the electric field of Ce_3^+/Ce_4^+ и Zn_2^+, Zr_2^+ cations. Such a difference can lead to a decrease in the total energy of the lattice, which will make it more stable when irradiated with high-energy electrons. The phase composition of TRC was investigated using X-ray diffraction analysis (XRD)[1]. Figure 1 shows the XRD patterns of Ce-$ZrSiO_4$ and Ce-Zn_2SiO_4 samples. The Ce-$ZrSiO_4$ sample has diffraction peaks of tetragonal structure with lattice parameters a=b=0.65989 nm, c=0.59857 nm. The average grain size is 19.1 nm (from the Scherrer equation), see Fig. 1a. The Ce-Zn_2SiO_4 sample exhibits broad diffraction peaks of α-Zn_2SiO_4 rhombohedral structure (the space group R–3, the cell constant a=b=1.395 nm, c=0.9312 nm). The average grain size is 20.2 nm (Fig. 1b).

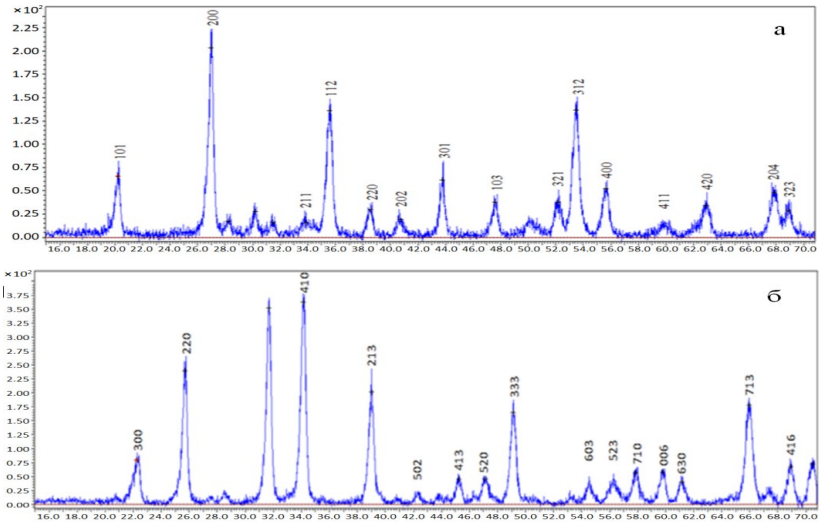

Fig. 1. X-ray diffraction patterns of Ce-$ZrSiO_4$ (a) and Ce–Zn_2SiO_4 (b) synthesized using microwave irradiation.

To further evaluate the radiation resistance of TRC, the optical properties of the samples were studied before and after electron irradiation. Point defects that arise during irradiation serve as traps for electrons and holes and become color centers. Electrons and holes fill these

centers, which leads to an increase in the optical density of silicates. The optical density depends on the irradiation dose rate, as well as on the isothermal annealing rate of the color centers

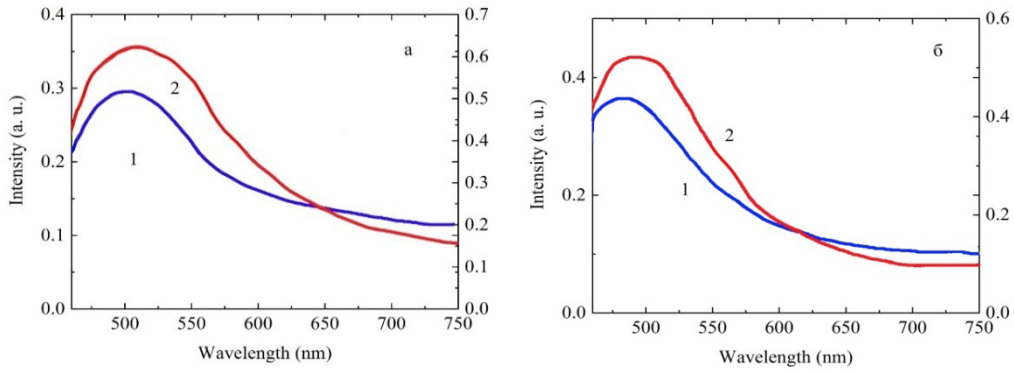

Fig. 2 . Photoluminescence spectra of termoregulating coatings: T = 300K, E_{exc} = 3.06 eV (1 - before irradiation, 2 - after irradiation with 4 MeV electrons at a dose of 10^{16} eV/cm^2), a)$ZrSiO_4$ (Ce_2O_3-5%), b) Zn_2SiO_4 (Ce_2O_3-5%)

480 nm (2.6 eV); 500 nm (2.5 eV) bands observed in the photoluminescence spectra of the studied samples (Fig. 2) characteristic of the luminescence of many silicates, are usually associated with the emission of, for example, defect $[SiO_4]^4$ centers caused by local distortions of silicon-oxygen tetrahedra [16]. Zirconium (zinc) ions can present in a tetrahedral environment in the form of groups (OH)-Zr-$(OSi)_3$ or Zr–$(OSi)_4$ and appear when the symmetry of the silicon-oxygen tetrahedron is violated due to a nearby defect. The irradiation bands are mainly associated with the creation of impurity defects as well as complex radiation defects: zinc, zirconium, oxygen vacancies, respectively with the formation of anion vacancies of the F, F^+ type as emission centers. The observed bands are possibly due to the intermediate stage of the formation of exciton-defect complexes or short-lived defects in the form of V_{Zr}^-, V_{Zn} vacancies and Zr^+, Zn^+ interstitial ions formed during bond rupture Thus, it can be assumed that when irradiated with 4 MeV electrons, the observed maxima in the photoluminescence spectra are due to the formation of point defects-anion vacancies. It follows from the X-ray spectra that TRC subjected to heat treatment at 220^0C have an amorphous phase. Therefore, the work presents TRC that had a crystalline structure after heat treatment at 1050^0C and 1200^0C [1].

[1] V.V. Baghramyan, A.A. Sargsyan, N.B. Knyzyan, V.V. Harutyunyan, A.H. Badalyan, N.E. Grigoryan, A. Aprahamian, K.V Manukyan, (2020), Pure and cerium-doped zinc orthosilicate as a pigment for thermoregulating coatings. Ceramics International, Volume 46, Issue 4 , pp. 4992-4997.

MINERAL PREFERRED ORIENTATION AND PROPERTIES OF ROCKS FROM SOURCE AREA OF EARTHQUAKES: COMPREHENSIVE STUDY BY NEUTRON DIFFRACTION AND ULTRASONIC ANALYSIS

T.I. Ivankina[1], A.V. Ponomarev[2] and I.Yu. Zel[1]

[1] *Joint Institute for Nuclear Research, Frank Laboratory of Neutron Physics, Dubna, Russia*
[2] *Schmidt Institute of Physics of the Earth RAS, Moscow, Russia*

E-mail: iti@jinr.ru

The elastic behaviour of rocks in the Earth's crust is generally anisotropic, with the degree of anisotropy mainly determined by the mineral textures (all minerals are anisotropic with respect to the propagation velocities of the P- and S waves) and the crack fabric (e.g., Ivankina et al., 1996). As rocks in the deep crust are not directly accessible, estimation of the elastic constants on surface equivalents in the laboratory can provide required information, e.g., to estimate the elastic wave velocities for the processing of geophysical data, to explain seismic structures, to verify velocity versus depth relationships or to describe the changing influence of the crack fabric in dependence on depth.

Although cracks may persist to great depths, their influence decreases rapidly with depth and the elastic constants largely depend on the crystal lattice and, therefore, on the mineral textures.

The study will be based on cores from Indian deep boreholes drilled to the source zone of the Koyna-Warna seismic area – classical area of induced earthquakes that recur regularly in this area for over 50 years. The great majority of the earthquakes are located in the granitic basement rocks underlying the Deccan flood basalt pile. These basalt and dominantly granite, granite-gneiss and migmatitic gneiss; cores are extracted from depths up to 1500 m (Fig.1).

Fig.1. Extracted core specimens of the depth of 477 m, 464 m and 314 m from the two boreholes PHAN and KHA.

The complex investigation was based on laboratory neutron diffraction and ultrasonic measurements. Neutron diffraction will be applied for the determination of the mineral crystallographic preferred orientations of samples and will be carried out using the time-of-flight texture diffractometer SKAT at the beamline 7A pulsed reactor IBR-2 at JINR (Dubna, Russia) (e.g., Fig.2).We have measured the degrees of crystallographic preferred orientation in basalts and granite, and determined the texture-related contribution to their acoustic anisotropies (P-waves) (Fig.3).

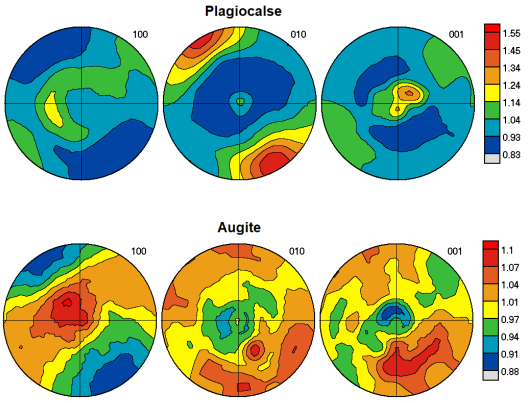

Fig, 2. Pole figures of major minerals obtained from neutron texture measurements of sample PHAN. Stereographic projection, pole density contours are in multiples of random distribution (m.r.d.).

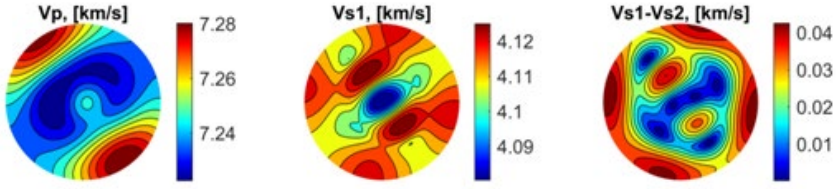

Fig 3. Calculated anisotropic distributions of elastic wave velocities in sample PHAN.

The experimental P-wave will be done using special equipment at the Institute of Geology Academy of Sciences of the Czech Republic (Prague, Czech Republic) (e.g., Fig.4).

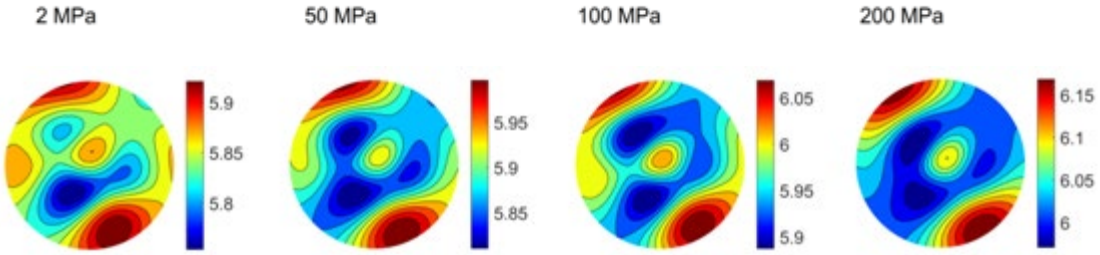

Fig. 4. 3D distributions of measured P-wave velocities in studied samples at different confining pressures. Stereographic projection.

As a result, elastic behavior of basalt PHAN and KHA2 samples are significantly differ from those of granite KHA1 sample. But commonly the elastic properties depend mainly on crystallographic textures of rock-forming minerals. Preferred orientations of plagioclase grains are almost the same for basalt samples what allows to permit the similar texture formation processes within basalt layer. As for the granite KHA1 sample, it is complex volume mineral composition evidences for the various deformation history of rocks below the basalt layer.

Authors thanks to Prof. K.Arora and Prof. R.K.Chadha (National Geophysical Research Institute, Hyderabad, India) for providing the samples for studies.

[1] T.I.Ivankina, I.Yu.Zel, T.Lokajicek et al. (2017) Elastic anisotropy of layered rocks: ultrasonic measurements of biotite gneiss versus texture-based theoretical predictions (effective media modeling). Tectonophysics. 712-713, 82-94.

COMPARATIVE ANALYSIS OF LIGAND AFFINITY TO THE C-RING OF ATP SYNTHASE

L.A. Kamalieva[1], S.D. Osipov[1], A.V. Minaeva[1], M.A. Semeno[1] and A.V. Vlasov[1]

[1] *Research Center for Molecular Mechanisms of Aging and Age-Related Diseases, MIPT, Dolgoprudny, Russia*

E-mail: kamalievalia@gmail.com

The F_OF_1 c-ring of ATP synthase represents a highly specific target for antimicrobial therapy and for overcoming existing mechanisms of bacterial antibiotic resistance. A striking example of the successful application of this strategy is bedaquiline, an anti-tuberculosis drug that specifically binds to the c-ring of ATP synthase from *Mycobacterium tuberculosis*, confirming the therapeutic potential of ATP synthase as a promising target [1].

Searching for new inhibitors using molecular docking requires knowledge of the protein's spatial structure. However, experimentally determining the structure of the F_OF_1 c-ring of ATP synthase is a labor-intensive task. Therefore, computer modeling methods represent a promising alternative for obtaining structural models. However, when using such methods, in particular AlphaFold, preliminary validation of the generated models for molecular docking tasks is required due to a number of limitations of this algorithm: inaccurate prediction of rotameric states of side chains, reduced accuracy when modeling large oligomers, and low quality of predictions for membrane proteins.

In this study, we assessed the suitability of the AlphaFold, Chai-1, and Boltz-2 models for molecular docking tasks and searched for ligands to the F_OF_1 c-ring of ATP synthases from various organisms. ATP synthases from *M. tuberculosis* and *Saccharomyces cerevisiae* were chosen as study objects due to the availability of experimental structures of their c-rings in complex with ligands. Combining pharmacophore and structural search methods against a database of known ligands allowed us to identify potentially active compounds. The affinity of ligands for the monomeric forms and c-ring complex from *M. tuberculosis* and *S. cerevisiae*, obtained experimentally and predicted using AlphaFold, was assessed. Clusters of ligands demonstrating a stable binding pattern independent of oligomerization and the conformational state of the target, were identified.

This work was supported by the Russian Science Foundation (RSCF) (project 25-24-00792).

[1] Andries, K., Verhasselt, P., Guillemont, J. et al (2005). A diarylquinoline drug active on the ATP synthase of Mycobacterium tuberculosis, Science. 5707, 223–227.

EFFECTS OF MN^{2+} DOPING ON MAGNETIC AND ELECTRONIC PROPERTIES OF $ZNFE_2O_4$: A FIRST-PRINCIPLES STUDY

B. Khongorzul[1], N. Jargalan[1], N. Tsogbadrakh[2], D. Sangaa[1]

[1] *Institute of Physics and Technology, Mongolian Academy of Sciences, Ulaanbaatar 13330, Mongolia*

[2] *Department of Physics, National University of Mongolia, Ulaanbaatar 14201, Mongolia*

E-mail: khongorzulb@mas.ac.mn

The structural parameters, magnetic properties (M_s, H_c), and heat generation ability (SAR) of Cu^{2+} and Ni^{2+} substituted $MgFe_2O_4$ spinel ($Mg_{1-x}M_xFe_2O_4$, M = Cu, Ni) have been systematically investigated as functions of temperature and composition using experimental methods and first-principles study [1-3].

In this study, we investigate the effects of Mn^{2+} concentration on the structural, magnetic, and electronic properties of $ZnFe_2O_4$ using first-principles calculations based on density functional theory (DFT). The Mn^{2+} concentration (x) is systematically varied from 0.0 to 1.0 to understand its influence on the key physical properties.

The results show that the saturation magnetization (M_s) increases gradually with increasing Mn^{2+} concentration, indicating enhanced magnetic ordering. In contrast, the magnetic anisotropy energy constant (K_u) decreases significantly and changes sign from positive to negative, indicating a transition of the magnetic easy axis (spin reorientation) due to the sign change of K_u.

The predicted unit cell (Figure 1) volume decreases with increasing Mn^{2+} concentration, implying lattice contraction due to ionic substitution. Furthermore, electronic structure calculations reveal that the band gap reduces dramatically with Mn doping, evolving from a semiconducting state (1.89 eV at x = 0.0) to a nearly metallic state at higher concentrations ($x \geq 0.5$).

These findings demonstrate that Mn^{2+} doping plays a crucial role in tuning both magnetic and electronic properties of the system. The combined analysis of magnetic parameters and electronic structure highlights the potential of Mn-doped materials for spintronic and multifunctional applications.

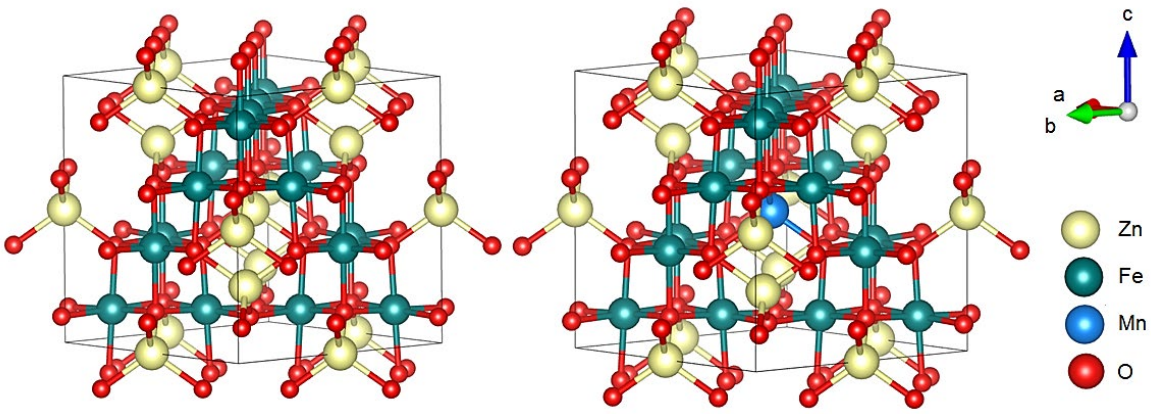

Figure 1. The crystal structures of $Zn_{1-x}Mn_xFe_2O_4$ phases for x = 0.00 and 0.25.

[1] E. Uyanga, I. Khishigdemberel, B. Khongorzul et al., (2024). Enhancing heat generation ability and magnetic properties of $MgFe_2O_4$ with Ni substitutes for biomedical applications, Materials Today Chemistry. 35, 101841.

[2] I. Khishigdemberel, E. Uyanga, H. Hirazawa et al., (2018). Influence of Cu dope on the structural behavior of $MgFe_2O_4$ at various temperatures. Physica B: Condensed Matter. 544, 73-78.
[3] B. Khongorzul, N. Jargalan, N. Tsogbadrakh et al., (2023). First-Principles and Experimental Studies of Structural, Electronic, and Magnetic Properties of Nickel Substituted Magnesium Ferrite Spinel. Journal of Surface Investigation: X-ray, Synchrotron and Neutron Techniques. 17, 518-522.

STRUCTURE OF IONOGELS BASED ON POLYMER AEROGELS OBTANIED FROM POLYAMIDE 6,6

S.Yu. Kottsov[1], G.P. Kopitsa[2,3], G.S. Taran[1], O.S. Lezova[3], Yu.E. Gorshkova[4,5], A.E. Baranchikov[1]

[1] *Kurnakov Institute of General and Inorganic Chemistry of the Russian Academy of Sciences, Moscow, Russia*
[2] *Konstantinov Petersburg Nuclear Physics Institute NRC KI, Orlova rosha, Gatchina, Leningrad District, Russia*
[3] *Grebenshchikov Institute of Silicate Chemistry PNPI NRC KI, St. Petersburg, Russia*
[4] *Joint Institute for Nuclear Research, Dubna, Russia*
[5] *Institute of Physics, Kazan Federal University, Kazan, Russia*

E-mail: kopitsa_gp@pnpi.nrcki.ru

Ionogels are soft-matter two-phase composites, synergising the properties of ionic liquids and solid porous matrices. In their composition, ionic liquids (IL) are the organic salts with a melting point below 100°C, which possess a set of unique properties including ionic conductivity, non-volatility, dissolving ability, as well as excellent chemical, thermal and electrochemical resistance. A solid component of ionogels endows them with a stable shape and valuable mechanical performance – mechanical strength or elasticity and flexibility. The interest to ionogel materials is related to their emerging properties, which are not inherent in both bare IL and a solid phase alone, such as self-healing or stimuli-responsive behaviour.

The most impressive ionogels' functionality were observed for the polymer-based ionogels. These include the design of switchable adhesives, ionic skins, thermoelectric devices, cuttable electric batteries, photo-, mechano- and thermochromic materials, etc.

These findings induced the structural research by small-angle scattering methods on ionic liquid-polymer systems including poly-ionic liquids, molecular or colloidal polymer-in-IL solutions, liquid crystals, IL-impregnated membranes. At the same time, the SAXS/SANS studies of polymer-based ionogels are mostly focused on the characterisation of the structure of a solid (polymer) component of ionogels, while the assessment of the confinement-dependent structure of ionic liquids is virtually ignored.

In the authors' previous work [1], a very strong distortion of the structure of the confined C8MIm BF_4 ionic liquid was shown in highly porous silica. Most probably, this effect was due to the specific sorption of BF_4 anions onto the silica surface thus resulting in chemically-driven confinement effect. It was hypothesised that such an effect could be far less pronounced for the ionogels obtained on base of polyamide 6,6 aerogels which is relatively inert towards ionic fluorine-containing species. In this view, the current work was aimed at the comparison of the structural parameters in the bare 1-methyl-3-octyl-imidazolium-tetrafluoroborate (C_8MIm BF_4) and 1-butyl-3-methylimidazolium bis(trifluoromethylsulfonyl)imide (C_4MIm TFSI) confined in porous polyamide 6.6, obtained by dissolution polymer in dimethylacetamide in the presence of lithium chloride and subsequent critical drying in CO_2 [2].

For the preparation of ionogels, the polyamide 6,6 aerogels were carefully cut into ~100 mg tablet-shaped fragments and placed into the excess volume (~5 ml) of ionic liquids C_8MIm BF_4 and C_4MIm TFSI, respectively. Next, the samples were left overnight at 50°C to ensure the IL uptake by the porous solids. After the impregnation, ionogels were removed from the IL and the liquid was dabbed away with paper towel. The structure of obtained ionogels was studied using helium pycnometry, low-temperature nitrogen adsorption, WAXS and SAXS.

The analysis of experimental data showed that ionogels based on polyamide 6,6 aerogels and ionic liquids C8MIm BF4 and C4MIm TFSI are two-phase systems in which the structure

of the solid phase remains unchanged upon impregnation with ILs, which sequentially fill the micro- and mesopores of porous polyamide 6,6. Unlike silica-based ionogels [1], the structure of ionic liquids enclosed in porous polyamide 6,6 remains practically unchanged, meaning no confinement effect is observed.

The work was supported by the Russian Science Foundation (grant 23-73-00028).

[1] S. Yu. Kottsov, G.P. Kopitsa, A.E. Baranchikov, A.A. Pavlova, T.V. Khamova, A.O. Badulina, Yu.E. Gorshkova, N.A. Selivanov, N.P. Simonenko, M.E. Nikiforova, and V.K. Ivanov. Langmuir, 2024, vol. 40, N. 44.
[2] A.E. Baranchikov, S.A. Lermontov, S.Y. Kottsov G.S. Taran, A.N. Malkova, E.A. Trufanova, A.S. Badulina, G.P. Kopitsa, Yu.E. Gorshkova. Journal of Polymer Research, 2025, Vol. 32, 385.

CRYOGENIC INSERT FOR STUDYING KAPITZA JUMP AND TURBULENT HEAT TRANSFER IN SUPERFLUID HELIUM AT TEMPERATURES BELOW 1 K

Y.S. Korshikov[1,2], V.B. Efimov[3], A. Sabidolda[1], D.E.Yerezhep[4], G.N. Kryzhevskiy[5]

[1] *Institute of Nuclear Physics, Agency of the Republic of Kazakhstan for Atomic Energy, Almaty 050032, Kazakhstan*
[2] *Al-Farabi Kazakh National University, Almaty 050040, Kazakhstan*
[3] *Osipyan Institute of Solid State Physics RAS (ISSP RAS), Chernogolovka, Russian Federation*
[4] *Technology Commercialization Center, Almaty Management University, Almaty 050060, Kazakhstan*
[5] *Almaty branch of the National Research Nuclear University MEPhI, Almaty050040, Kazakhstan*

E-mail: e.s.korshikov@physics.kz

The development of high-power ultracold neutron (UCN) sources using superfluid helium (He II) requires efficient removal of 5–15 W of heat power from the converter chamber at temperatures below 1 K. [1] The key factors limiting the achievable temperature are (i) the Kapitza resistance at the He II boundaries with construction materials (copper, stainless steel, nickel) and (ii) the thermal resistance due to turbulent counterflow of the normal and superfluid components in the heat conductor. Experimental data for these phenomena in the range $T < 1$ K are practically absent, and theoretical models yield discrepancies of 2–3 orders of magnitude. [2]

This paper presents a detailed design of a cryogenic insert intended for direct measurements of:

— The thermal resistance of capillaries made of CuNi and stainless steel with diameters of 1.2, 2.6 and 11 mm, filled with He II, in the heat flux range of 0.01–100 mW and temperatures of 0.5–1.5 K;

— The Kapitza resistance at the He II interface with flat samples (Cu, SS, SS+Ni) at heat flux densities.

The insert uses a standard liquid ^{4}He cryostat and an additional ^{3}He pumping system providing a base temperature of ~0.5 K. Drawings of the vacuum jacket, the ^{3}He unit, and the measuring cells are presented. Thermometry based on RuO_2 resistors with a sensitivity of ~1 mK is described. Calculations of parasitic heat loads through capillary walls, wires, radiation, and the superfluid film are performed; it is shown that these are 2–4 orders of magnitude smaller than the measured powers. Estimates of the contributions of laminar and turbulent heat transfer regimes are made. The setup is currently under construction. The obtained results will enable, for the first time, systematic measurements of the Gorter–Mellink constant and the viscosity of the normal component at $T < 1$ K, as well as determination of the Kapitza jump for materials relevant to UCN sources.

[1] Sakhiyev, S.; Turlybekuly, K.; Shaimerdenov, A.; Sairanbayev, D.; Sabidolda, A.; Kurmanaliyev, Z.; Almukhametov, A.; Bayakhmetov, O.; Kiryanov, R.; Korobkina, E.; et al. Concept of UCN Source at WWR-K Reactor (AlSUN). *Physics* **2025**, *7*, 64. https://doi.org/10.3390/physics7040064

[2] Efimov, V.B. Heat Flux in the Storage Plant of Ultracold Neutrons. *J. Surf. Investig.* **18**, 1634–1639 (2024). https://doi.org/10.1134/S1027451024701647

MAIN DIRECTIONS OF YUMO SPECTROMETER DEVELOPMENT

A.I. Kuklin[1,2], O.I. Ivankov[1], A.Kh. Islamov[1], A.H.A. Elmekawy[1,3], A. Rogachev[1,2], T.N. Murugova[1], V. Skoi[1], T.V. Cuong[1,4], A.V. Vlasov[1,2], Y.L. Ryzhykau[1,2], A.G. Solovjev[1], V.I. Gordeliy[1,2]

[1] *Joint Institute for Nuclear Research, Dubna, Russia*
[2] *Moscow Institute of Physics and Technology, Dolgoprudny, Russia*
[3] *Nuclear Research Centre, Egyptian Atomic Energy Authority, Cairo, Egypt.*
[4] *Dalat Nuclear Research Institute, Lam Dong, Viet Nam*

E-mail: alexander.iw.kuklin@gmail.com

Small-angle neutron scattering (SANS) is one of the most widely used neutron diffraction techniques due to its broad applicability across scientific field. Its instrumentation requires high neutron flux at the sample, low background, a wide momentum-transfer range (Q range), versatile sample environments, and an automation. The neutron flux depends on the source power, moderator, setup configuration, and collimation system, while the dynamic Q range is defined mainly by the multi-detector system and modular detector configuration.

The evolution of the experimental setup has been closely linked to instrument development. A multi-detector system for the SANS spectrometer was first proposed and implemented as described in Ref. [1], and subsequent detector designs were adapted to this configuration. The development of a position-sensitive detector (PSD) with a central aperture followed from this approach [2-4]. Current spectrometer development is focused on two main directions: firstly, expanding the detector base through small angle scattering (SAS), ring detectors, advanced PSDs, and direct-beam detectors; and secondly, developing normalization methods to overcome invariant-related limitations and enable determination of both the small-angle scattering cross section on an absolute scale and the total scattering cross section of samples.

This report presents results on neutron flux stability, transmission studies of materials used in YuMO spectrometer components, and measurements obtained in a non-standard configuration employing an original PSD design. The main directions for the spectrometer's near- and medium-term modernization are also discussed.

[1] A.I. Kuklin, A.Kh. Islamov, V.I. Gordeliy, and et al (2005). Scientific Reviews: Two-Detector System for Small-Angle Neutron Scattering Instrument. Neutron News, 16(3), 16–18. https://doi.org/10.1080/10448630500454361
[2] A.I. Kuklin, D. Zabelskii, V.I. Gordeliy, and et al (2020). On the Origin of the Anomalous Behavior of Lipid Membrane Properties in the Vicinity of the Chain-Melting Phase Transition. Sci Rep 10, 5749. https://doi.org/10.1038/s41598-020-62577-9
[3] A. Zeleňáková, P. Hrubovčák, A.I. Kuklin, and et al (2019). Size and distribution of the iron oxide nanoparticles in SBA-15 nanoporous silica via SANS study. Sci Rep 9, 15852 (2019). https://doi.org/10.1038/s41598-019-52417-w
[4] B. Balasoiu, A.I. Kuklin, and et al (2010). Rom. Journ. Phys., Vol. 55, Nos. 7–8, P. 782–789, Bucharest.

SPACER-DEPENDENT SELF-ASSEMBLY OF UREA-BASED GEMINI SURFACTANTS AND THEIR APPLICATION IN TEMPLATING ORDERED MESOPOROUS SILICA

S. Kurbonov[1,2], Zs. Czigány[3], Z. Kovács[3], L. Péter[4], M. Pisárčik[5], M. Lukáč[5], M. Kriechbaum[6], V. Ryukhtin[7], A.-M. Lacrămă[8] and L. Almásy[1]

[1] *Institute for Energy Security and Environmental Safety, HUN-REN Centre for Energy Research, Budapest, Hungary*
[2] *Doctoral School of Physics, Faculty of Natural Sciences, Eötvös Loránd University, Budapest, Hungary*
[3] *Institute of Technical Physics and Materials Science, HUN-REN Centre for Energy Research, Hungary*
[4] *HUN-REN Wigner Research Centre for Physics, Budapest, Hungary*
[5] *Department of Chemical Theory of Drugs, Faculty of Pharmacy, Comenius University, Bratislava, Slovakia*
[6] *Nuclear Physics Institute, Czech Academy of Sciences, Czech Republic*
[7] *Institute of Inorganic Chemistry, Graz University of Technology, Austria*
[8] *"Coriolan Drăgulescu" Institute of Chemistry, Bv. Mihai Viteazul, Timisoara, Romania*

E-mail: sarvarjon@student.elte.hu

Urea-based cationic gemini surfactants with polymethylene spacers of two to ten methylene units were investigated for their micellization behavior and their role as pore-forming agents in the synthesis of mesoporous silica nanoparticles. The micellar structure was characterized using small-angle neutron scattering (SANS) with multi-model form factor analysis, employing a core–shell ellipsoid and two homogeneous ellipsoid models. All models consistently showed that spacer length critically governs micellar geometry, aggregation number, and hydration. The surfactant with four methylene groups in the spacer formed the largest micelles with the highest aggregation number, while longer spacers yielded progressively smaller and more compact aggregates. Shell hydration decreased systematically with increasing spacer length due to enhanced hydrophobicity of the headgroup-spacer region. Intermicellar interactions, modeled via the rescaled mean spherical approximation (RMSA) as screened Coulomb repulsion, were strongest for the four-methylene spacer, corresponding to the highest micellar charge and largest interparticle spacing.

Mesoporous silica nanoparticles were subsequently synthesized through sol–gel processing under basic conditions using these surfactants as structure-directing agents. The effect of spacer length on particle morphology and pore structure was examined by nitrogen porosimetry, small-angle X-ray scattering (SAXS), ultra-small-angle neutron scattering, and electron microscopy (SEM, TEM). Depending on the spacer length, spherical and cylindrical nanoparticles formed in varying proportions. All materials exhibited the hexagonal pore arrangement characteristic of MCM-41 molecular sieves, with the exception of the sample prepared with the shortest spacer. SAXS and TEM analysis revealed that spacer length influences the lattice parameter and the size of ordered domains, with a lattice parameter spread of 10–20% across crystalline domains attributed to finite domain size effects and lattice parameter variance [1]. Despite the spacer-dependent variation in micelle morphology, no direct correlation was found between micelle shape and size and the resulting pore dimensions, indicating that gemini surfactants across a broad range of spacer lengths are equally suitable for MCM-41 synthesis.

These findings advance the understanding of how molecular-level surfactant architecture governs both self-assembly behavior and the structural properties of templated nanomaterials.

[1] Kurbonov, S.; Czigány, Z.; Kovács, Z.; Péter, L.; Pisárčik, M.; Lukáč, M.; Kriechbaum, M.; Ryukhtin, V.; Lacrămă, A.-M.; Almásy, L. Structural Characterization of Ordered Mesoporous Silica Prepared by a Sol–Gel Process Using Urea-Based Cationic Gemini Surfactants. Gels 2025, 11, 804. doi:10.3390/gels11100804.

STRUCTURE OF THE COMPLEXES OF RecA AND DprA PROTEINS WITH SHORT SINGLE STRANDED DNA

D.M. Baitin[1,2], D.V. Lebedev[1,3], I.V. Bakhlanova[1], M.G. Petukhov[1,3]

[1] *Petersburg Nuclear Physics Institute Named by B.P. Konstantinov of National Research Center «Kurchatov Institute», Orlova Roscha 1, 188300 Gatchina, Russia*
[2] *Research Center of Nanobiotechnologies, Peter the Great St. Petersburg Polytechnic University, Polytechnicheskaya, 29, 195251 St. Petersburg, Russia*
[3] *National Research Center «Kurchatov Institute», Akademika Kurchatova pl. 1, 123182 Moscow, Russia*

E-mail: lebedev_dv@pnpi.nrcki.ru

RecA protein is an enzyme that plays the central role in the process of homologous recombination in prokaryotic cells. DprA is a bacterial protein that directly interacts with RecA and single-strand binding proteins to facilitate natural chromosomal transformation. The molecular mechanisms of homologous DNA recombination in bacteria were investigated in order to find molecular targets for combating bacterial antibiotic resistance.

Presynaptic complex formation by RecA protein on a ssDNA was investigated by biochemical methods and small-angle scattering for a set of oligonucleotides between 21 and 102 bases in length. The ability to induce formation of the active RecA-ssDNA complex capable of ATP hydrolysis was demonstrated for the oligonucleotides 34 bases in length and larger. Starting with the length of 68 nucleotides and above formation of the full-length filament of extended geometry was shown. In contrast, RecA and DprA protein complex with single-stranded DNA was shown to have ATPase activity with short poly-dT substrates with a length of only 21 nucleotides. Based on these experimental data, using methods of molecular modeling and protein ligand docking, we obtained a model for the spatial structure of the RecA–DprA–ssDNA complex of the smallest possible size [1].

Contrary to previously accepted view, in this model of the RecA–DprA–onDNA complex, only one DNA binding site of the DprA dimer interacts with ssDNA, while the binding site of the second DprA subunit can be used to search for and bind ssDNA with high homology to DNA associated with the first DprA subunit. These results not only radically change modern concepts in this field, but also create the necessary basis for a practically important problem for designing new means of combating the adaptation of bacteria to the action of antibiotics.

[1] Bakhlanova I., Carrasco B., Alekseev A., Yakunina M., Morozova N., Khodorkovskii M., Petukhov M., Baitin D. A Single DNA Binding Site of DprA Dimer Is Required to Facilitate RecA Filament Nucleation // International Journal of Molecular Sciences. - 2025. - Vol. 26. - P. 7873.

PRESSURE EFFECT ON CRYSTAL, MAGNETIC STRUCTURE AND VIBRATIONAL PROPERTIES OF VAN DER WAALS MATERIALS

O.N. Lis[1], D.P. Kozlenko[1], S.E. Kichanov[1], E.V. Lukin[1], I.Yu. Zel[1]

[1] *Frank Laboratory of Neutron Physics, Joint Institute for Nuclear Research, Dubna, Russia*

E-mail: olis@jinr.ru

The discovery of long-range magnetic order in van der Waals materials down to the monolayer limit has established a new platform for the development of all-spintronic devices based on these structures and opened up new opportunities for studying physical properties of quasi-two-dimensional systems and low-dimensional magnetism, which holds significant fundamental and technological importance. The structural features of these compounds lead to a significant sensitivity of the physical properties to external influences, which can cause many unusual phenomena: charge, orbital and spin ordering, superconductivity, various phase transitions etc., which leads to special, exotic phenomena in them. In the last few years, Cr trihalides have been widely investigated, and a series of exciting phenomena are revealed in this family of materials. In this regard, further in-depth research and understanding of emerging properties in $CrBr_3$ and $CrCl_3$ becomes an essential objective, especially with variations in thermodynamic parameters.

This work focuses on the study of crystal, magnetic structure and vibrational properties of $CrBr_3$ and $CrCl_3$ in wide temperature and pressure ranges using neutron, X-ray powder diffraction and Raman spectroscopy. Neutron experiments were performed on the DN-6 diffractometer at the high-flux pulsed reactor IBR-2 (FLNP, JINR, Dubna, Russia).

In $CrCl_3$, a structural phase transition is observed under high pressure above ~2.3 GPa from the initial monoclinic $C2/m$ phase to the rhombohedral $R\bar{3}$ phase [1]. Anomalous behavior of some vibrational modes is also observed in the vicinity of the structural transition. Initial A-type AFM order in $CrCl_3$ is rapidly suppressed at high pressures of about 1 GPa. Instead, the FM state with a Curie temperature of $T_C \approx 19$ K is formed under high pressure. With further increase in pressure up to 2 GPa no evidence of magnetic contribution is observed.

Our results demonstrate that high pressure effectively drives a structural dimensionality crossover in $CrBr_3$ from a quasi-two-dimensional van der Waals system to a three-dimensional-like arrangement at $P \approx 15$ GPa [2]. Below this pressure, a strongly anisotropic compression is observed, with the interlayer distance decreasing rapidly while the layer thickness varies less markedly. Above 15 GPa, the compressibility becomes nearly isotropic and the interlayer distance reduces significantly more slowly, reflecting the onset of strong interlayer coupling. As a result, at high pressures the interlayer distance becomes smaller than the layer thickness, indicating a transformation from the weak interlayer coupling typical of van der Waals materials to a much denser three-dimensional bond. In addition, anomalies in the pressure dependence of several vibrational modes in the vicinity of the crossover were observed.

[1] O.N. Lis, D.P. Kozlenko, E.V. Lukin, S.E. Kichanov et. al. (2025) Pressure-induced ferromagnetism and structural phase transition in the van der Waals material $CrCl_3$, Phys. Rev. B. 112, 104105.

[2] D.P. Kozlenko, O.N. Lis, N.T. Dang, S.E. Kichanov, E.V. Lukin, et. al. (2025) Pressure induced crossover from 2D-like to 3D structural arrangement in van der Waals magnet $CrBr_3$, ChemPhysMater. 4, 280-288.

ARCHITECTURE AND FEATURES OF THE DATA ACQUISITION SYSTEM BASED ON THE DT5560 DIGITIZER FROM CAEN FOR THE DETECTOR SYSTEM OF THE FOURIER STRESS DIFFRACTOMETER FSD

E.I. Litvinenko[1] and A.A. Bogdzel[1]

[1] *Joint Institute for Nuclear Research, Dubna, Russia*

E-mail: litvin@nf.jinr.ru

The report describes the architecture and characteristics of a newly developed data acquisition system for the upgraded detector system of the Fourier stress diffractometer operating on the beam 11a of the IBR-2 neutron reactor [1]. The upgraded FSD detector system includes a backscatter detector assembled from 16 ^{6}Li scintillation elements and two ASTRA detectors, each containing 7 ZnS(Ag) scintillation elements, designed according to the principles of combined electronic and geometric focusing proposed in [2]. New data acquisition system (DAQ) is based on CAEN's 32-channel DT5560 digitizer, part of the Open FPGA family [3], whose distinguishing feature is the ability for the developer to quickly create custom firmware designed and compiled from an extensive list of ready-made firmware components. The digitizer-based DAQ system operates successfully on the beam 11a, replacing the previous MPD240-based system in the fall of 2025. A description of developed firmware and software of the DAQ system is presented.

[1] Bokuchava, G. (2018) “Neutron RTOF Stress Diffractometer FSD at the IBR-2 Pulsed Reactor,” Crystals, 8(8). Available at: https://doi.org/10.3390/cryst8080318.
[2] Kudryashev, V.A., Trounov, V.A. and Mouratov, V.G. (1997) “Improvement of Fourier method and Fourier diffractometer for internal residual strain measurements,” Physica B: Condensed Matter, 234–236, pp. 1138–1140. Available at: https://doi.org/https://doi.org/10.1016/S0921-4526(97)89271-X.
[3] https://www.caen.it/families/open-fpga-digitizers/

HIGH-PRESSURE NEUTRON AND X-RAY DIFFRACTION FACILITIES AT FLNP JINR: CAPABILITIES AND APPLICATIONS

E.V. Lukin[1], S.E. Kichanov[1], D.P. Kozlenko[1], O.N. Lis[1], A.V. Rutkauskas[1]

[1] *Frank Laboratory of Neutron Physics, Joint Institute for Nuclear Research, Dubna, Russia*

E-mail: lukin@jinr.ru

Structural studies of condensed matter under extreme conditions are a key research area at the Frank Laboratory of Neutron Physics, JINR. High pressure serves as a precise tool for tuning interatomic distances and lattice configurations, enabling a direct probe into the fundamental links between crystal/magnetic structures and physical properties.

This work presents the experimental capabilities of the DN-12 and DN-6 diffractometers at the IBR-2 pulsed reactor, which are optimized for high-pressure neutron diffraction using various high-pressure cells, including diamond anvil cells (DAC). To complement these studies, the laboratory utilizes a high-brightness Xeuss 3.0 X-ray source, specifically configured for small-sample diffraction in DAC environments. We describe the design features, technical parameters, and a unified experimental approach for conducting comprehensive neutron and X-ray diffraction studies under extreme pressure, supported by recent experimental results.

STUDY OF THE HYDROGEN-INDUCED MAGNETIC PROPERTIES OF THE FE/GD SUPERLATTICE USING POLARIZED NEUTRON REFLECTOMETRY

M.V. Makarova[1,2], D.I. Devyaterikov[1], V.V. Matyukhov[1] and E.A. Kravtsov[1,2]

[1] *Institute of Metal Physics, Ural Branch of the Russian Academy of Sciences, Ekaterinburg, Russia*

[2] *Ural Federal University, Ekaterinburg, Russia*

E-mail: makarova@imp.uran.ru

Superlattices (SL), which are formed by alternating layers of transition (Fe, Ni, Co) and heavy rare-earth (RE) (from Gd to Tm) metals, have complex types of intralayer and interlayer magnetic order can be realized. Such nanostructures are of high interest both from the fundamental viewpoint and in view of possible applied use of them in materials for the next-generation spintronics. The magnetic structure of such SLs is determined by the competition of different mechanisms, namely, intralayer and interlayer exchange interactions, the size and proximity effects, epitaxial stresses, structural peculiarities, etc. The magnetic ordering of the system is determined by strong antiferromagnetic Gd–Fe exchange interaction, strong Fe–Fe ferromagnetic exchange interaction, and relatively weak Ruderman–Kittel–Kasuya–Yosida Gd–Gd interaction, which result in the existence of the complex magnetic phase diagram plotted in accordance with the temperature and magnetic field [1].

It is known that, in contrast to the ferromagnetic 3d metals (Fe, Ni, Co), the rare-earth metals easily absorb hydrogen from the surrounding atmosphere even at low hydrogen pressures [2]. By varying the hydrogen pressure and temperature, it is possible to controllably change the hydrogen concentration in the layers of rare-earth metals, changing their structural, magnetic, and electronic properties. It has been recently shown that hydrogenation could enhance the Curie temperature of Gd. Moreover, the processes of hydrogen absorption in thin RE films with a thickness of 1-50 nanometers remain unexplored. An increased concentration of hydrogen can be expected both in the center of the layers and near the interlayer boundaries. The scientific novelty of the proposed research lies in conducting studies on the effect of hydrogenation on the magnetic properties of Fe/Gd SL, as well as exploring opportunities for controlled modifications to their atomic and magnetic structures. For investigation of magnetic structure we used polarized neutron reflectometry (PNR). PNR is a powerful technique which is able to estimate concentration of hydrogen in Gd, Nb layers and determine chemical and magnetic depth profiles and the evolution with temperature.

A series of Nb(10 nm)[Gd (t Å)/Fe (3.5)]$_{20}$/Ni(10 nm) (t=10, 20, 40 nm) SLs were fabricated on single-crystal substrates of Si(100) by DC magnetron sputtering. To enhance the hydrogenation efficiency, the structure was covered with a catalytic nickel layer 10 nm. Structural characterization of the samples was performed by X-ray diffraction (XRD) and X-ray reflectometry (XRR) using a laboratory PANalytical Empyrean Series 2 diffractometer, Co radiations. Polarized neutron reflectometry (PNR) experiment was conducted on the Multi-Purpose Reflectometer at the China Spallation Neutron Source.

The combined application of X-ray structural, magnetometric, and PNR (Fig.1) methods has been investigated the effect of hydrogenation on the atomic and magnetic structure of Fe/Gd superlattices. Hydrogen accumulates in the center of the Gd layers, forming the crystalline phases GdH_2 and GdH_3. Near the interfaces, the hydrogen content is reduced to a depth of up to 12 Å. A proximity magnetic effect is observed between the Fe layers, leading to the formation of an induced magnetic moment near the interfaces in the GdHx layers at all temperatures up to room temperature. At low temperatures, the layers exhibit GdHx ferromagnetism, with both

the magnetic moment and Curie temperature being lower than those in the unhydrogenated Gd layers but significantly higher than those in bulk and thin-film gadolinium hydrides.

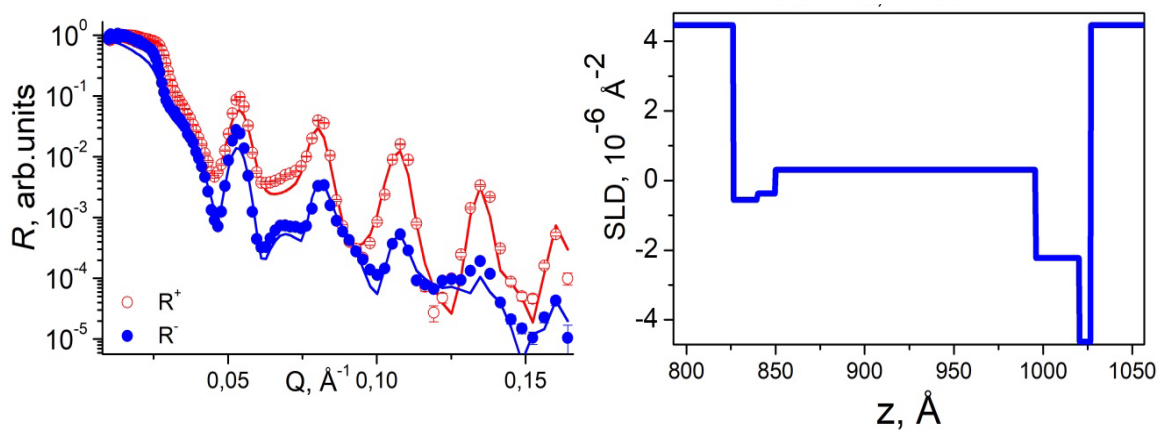

Fig. 1 Polarized neutron reflectivity of fully hydrogenated sample at 3.5 K in magnetic field of 1 kOe (left). The magnetic scattering length profile this sample (right).

This work has been supported by the grants the Russian Science Foundation, RSF 24-12-20024.

[1] A. B. Drovosekov, A. O. Savitsky, D. I. Kholin, N. M. Kreines, V. V. Proglyado, M. V. Makarova, E. A. Kravtsov, and V. V. Ustinov (2019). J. Magn. Magn. Mater. 475, 668-674.
[2] V. Leiner, M. Ay, and H. Zabel (2004), Phys. Rev. B 70, 104429.

NEUTRON SCATTERING IN SOLID SOLUTIONS $Mn_{1-x}Rh_xSi$ WITH TEMPERATURE-BLURRED PHASE TRANSITION

I.D. Manko[1], A.A. Povzner[1], D.A. Stoler[1]

[1] *Ural Federal University named after the First President of Russia B.N. Yeltsin*

E-mail: i.d.manko@urfu.ru

In compounds of group B20 with a non-centrosymmetric crystal structure characterized by the absence of an inversion center and the presence of a Dzialoshinsky-Moriya interaction, high magnetic phase transition temperatures (over 100 K) were observed both for isostructural FeGe and MnGe, and for solid solutions based on them, for example, in (Mn1-xFex Ge) and (Mn1-xRhxSi) [1,2]. Moreover, in the solid solution of Mn1-xRhxSi, an increase in the concentration of rhodium (starting from x = 0.05) causes a sharp increase in the temperature of the phase transition [2]. In addition, in solid solutions of Mn1-xRhxSi with a low concentration of rhodium (less than x = 0.05), in the absence of an external magnetic field, a diffuse ring of small-angle neutron scattering was observed, which is characterized by wave vectors directed towards stochasticity [3].

In this work, using the first-principle DFT modeling, the electronic structure of Mn1-xRhxSi was studied for concentrations x = 0.25, 0.50 and 0.75. An analysis performed using the Ginzburg-Landau functionality [4] showed that the increase in the phase transition temperature is due to a decrease in the value of the intermode interaction parameter (κ) with an increase in x, which, in turn, is associated with features of the fine density structure of electronic states. The calculated temperature dependences of magnetization and magnetic susceptibility are in good agreement with the experimental data [4,5]. The analysis of the contribution of triple correlations arising in the energy region characterized by negative κ values makes it possible to describe the features of neutron scattering intensity, such as the appearance of diffuse "rings" on neutron scattering maps at low rhodium concentrations. In addition, analysis of the fine structure of electronic states Mn1-xRhxSi indicates a sharp increase in the upper temperature limit of triple correlations up to the values indicated earlier in the work [2] as the temperature of the phase transition.

The results were obtained within the framework of the assignment of the Ministry of Science and Higher Education, contract No. FEUZ-2026-0013.

[1] J.D. Bocarsly, R.F. Need, R.Seshadri, S.D. Wilson. // Phys. Rev. B 97, 100404(R) (2018).
[2] Demishev, S.V., Krasnorussky, V.N., Os'kin, A.E. et al. Record Increase in the Curie Temperature up to Room Values in the Noncentrosymmetric Magnet Mn1 – xRhxSi. Jetp Lett. 121, 111–118 (2025).
[3] V.N. Krasnorussky, A.V. Bokov, Z.N. Volkova, A.P. Gerashchenko, N.M. Chtchelkatchev, M.V. Magnitskaya, D.O. Skanchenko, E.V. Altynbaev, I.V. Alferev, D.A. Salamatin, V.A. Sidorov, A.V. Semeno, V.V. Brazhkin, A.V. Tsvyashchenko. // Phys. Rev. Mat. V. 8. N. 12. P. 124405.
[4] Povzner A. A., Nogovitsyna T. A., Lopatko E. I. // Physics of the Solid State, 2024, Vol. 66, No. 8
[5] Yamauchi, H., Sari, D.P., Watanabe, I. et al. // Commun Mater 1, 43 (2020).

CHANGES IN THE STRUCTURAL PROPERTIES OF THIN FILMS OF RARE-EARTH METALS DURING HYDRATION

V.V. Matyukhov[1], M.V. Makarova[1], Yu.A. Salamatov[1], G.E. Zhezlyaev[1], D.I. Devyaterikov[1], E.A. Tolmacheva[1], E.A. Kravtsov[1]

[1] *M.N. Mikheev Institute of Metal Physics UB RAS, Yekaterinburg, Russia*

E-mail: vvmatyukhovimpuran@yandex.ru

One promising area of nanospintronics is the study of magnetic nanostructures in which the magnetic ordering can be controllably changed without applying a magnetic field. Such nanostructures include thin films and superlattices of rare-earth metals, whose properties change upon controlled saturation with hydrogen. [1]

This work presents results on the growth of gadolinium and dysprosium thin films and a systematic study of changes in their structural properties during hydrogenation.

The growth of gadolinium and dysprosium thin films with platinum or palladium catalytic layers was carried out using magnetron sputtering and pulsed laser deposition. Thin films were hydrogenated using a chemical vapor deposition system at hydrogen pressures ranging from 25 mTorr to 750 Torr. Samples were analyzed using X-ray diffraction and reflectometry.

For the gadolinium sample, gadolinium dihydride GdH_2 was found to be present in the initial state. Increasing the hydrogen pressure to 2 Torr leads to the complete conversion of metallic gadolinium to GdH_2. At 2.4 Torr, a mixture of GdH_2 dihydride and gadolinium trihydride GdH_3 forms in the sample. Further increases in pressure lead to the complete conversion of GdH_2 to GdH_3.

In a dysprosium thin film at a pressure of 10 Torr, the metallic phase completely converts to DyH_2 dihydride. Dysprosium trihydride DyH_3 forms at a pressure of 50 Torr. With further pressure increases, dysprosium dihydride DyH_2 gradually transforms into dysprosium trihydride DyH_3.

In the hydrogenation process of metal films, accompanied by the formation of solid solutions of hydrogen in metals and the subsequent formation of hydride phases, a significant change in the magnetic characteristics is possible. These changes are due to variations in the interatomic distances, and the hydride phases influence on the electron and spin subsystems. The X-ray diffraction analysis performed in this work confirmed the presence of these structural modifications. In this regard, it is logical to study the magnetic state evolution during hydrogenation. The solution of this problem requires the use of polarized neutron reflectometry, which can be performed on the neutron instruments of the IBR-2 research reactor.

This research was supported by grants from the Russian Science Foundation (Project No. 24-12-20024) and the Sverdlovsk Region (Project No. 2-25-OG).

[1] I.Aruna, L.K.Malhotra, B.R.Mehta (2006) Switchable metal hydride films, Handbook on The Physics and Chemistry of Rare Earths, Elsevier.

SIMULATION OF EPITHERMAL NEUTRON FLUX SPATIAL DISTRIBUTION FROM 1 TO 200 EV AT PHOTONEUTRON SOURCE

I.V. Meshkov[1], V.N. Ponomarev[2] and S.I. Potashev[2]

[1] *Lebedev Physical Institute of Russian Academy of Sciences, 119991 Moscow, Russia*
[2] *Institute for Nuclear Research of Russian Academy of Sciences, 117312 Moscow, Russia*

E-mail: meshkoviv@*lebedev.ru*

Simulation of epithermal neutron spatial distribution were carried out for 10x10x10 cm^3 beryllium target placed in bremsstrahlung. Tungsten target in electron accelerator beam was proposed to generate bremsstrahlung. Distribution is considered at 1 m distance from beryllium target. The neutron spectra and their coordinate distribution have uniform distribution for 3-mm polyethylene plate in energy between 1 to 200 eV.

STRUCTURE AND CRYSTALLIZATION KINETICS IN SODIUM MONTMORILLONITE-CONTAINING POLYPROPYLENE NANOCOMPOSITES: INTEGRATION OF SAXS AND DSC ANALYSES OF DISPERSION, FRACTAL STRUCTURE, AND INTERFACIAL PROPERTIES

A.A. Nabiyev[1,2], R.L. Mammadova[3] and O.I. Ivankov[2]

[1] *Ministry of Science and Education Republic of Azerbaijan, Institute of Physics, Baku, Azerbaijan*

[2] *International Intergovernmental Organization, Joint Institute for Nuclear Research, Dubna, Russia*

[3] *Karabakh University, Khankendi, Azerbaijan*

E-mail: asifnebi@gmail.com

Sodium montmorillonite-based PP nanocomposites are used as model systems in the fields of polymer physics, surface phenomena, rheology, and nanomaterials. Research conducted on them seeks to answer fundamental questions such as the self-assembly of low-dimensional fillers in a polymer matrix, the influence of interfacial interactions on properties, and the dynamics of polymer chains under nanoconfinement. For this reason, they have become a classic example in both fundamental and applied aspects of materials science. That may provide high performance at low filler content. From a scientific perspective, they reveal fundamental mechanisms such as nanoconfinement, interfacial interactions, and self-assembly of fillers. They also serve as a superior alternative to conventional polypropylene in industries requiring lightweight properties, mechanical strength, thermal resistance, barrier performance, and flame retardancy—including automotive, packaging, electronics, construction, and agriculture. Thus, this material contributes to deepening scientific understanding to providing the lightweight resources needed by industry [1-4].

This study investigates the effect of sodium montmorillonite (Na-MMT) incorporation on the supramolecular structure, thermal behavior, and crystallization kinetics of syndiotactic polypropylene (sPP) using a multi-method SAXS and DSC approach. Three complementary analyses – low-q power-law, high-q broad-peak modeling, and one-dimensional correlation function – were applied to neat sPP and a series of **sPP + %Na^+ MMT** composites (0–7 wt% Na-MMT). For neat sPP, the low-q region ($q<0.046$ Å^{-1}) power-law exponent was p=4.07, indicating a diffuse interface (fuzzy boundary) of large morphological entities such as spherulites. Upon Na-MMT addition, pp decreased monotonically from 4.01 (2 %) to 3.78 (7 %), i.e. the surface fractal dimension $D_s=6-p$ increased from 2.00 to 2.22. This demonstrates that at low clay loadings the aggregate interfaces remain relatively smooth, while higher loadings lead to progressive roughening due to particle agglomeration.

For neat sPP, the broad-peak model applied to the high-q region (**$q>q_{peak}$**) revealed a mass-fractal structure with exponent p=1.48 (fractal dimension D_m=1.48), indicating an open, branched lamellar organization. The correlation function gave an average long period of 7.83 nm, a crystalline lamellar thickness of 2.76 nm, an amorphous layer thickness of 5.07 nm, an interphase thickness of 0.82 nm, and a local crystallinity of 35.2 %.

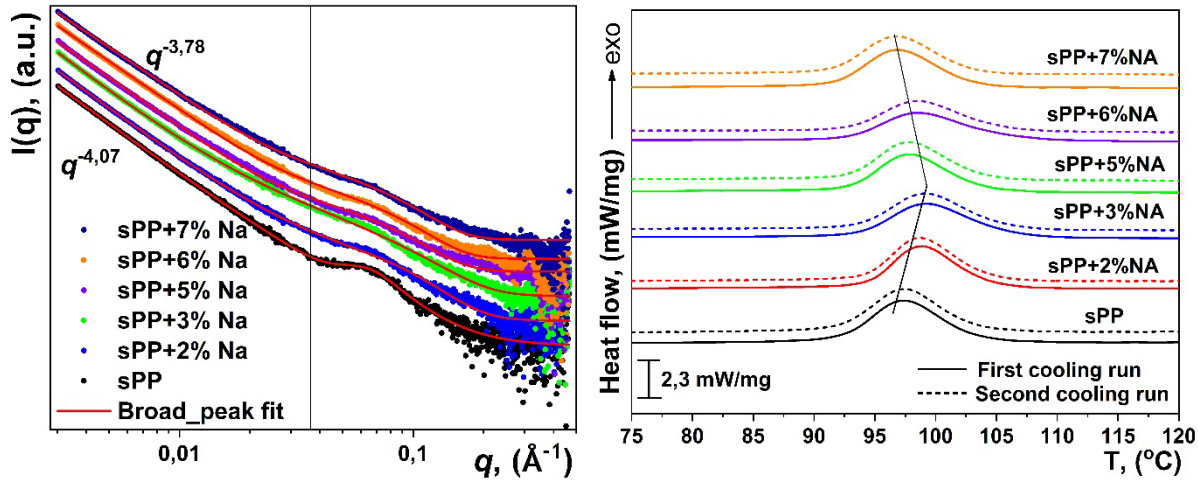

Figure 1. SAXS plots (left) and DSC thermograms (right) of PP+Na^+MMT nanocomposite films

From another hand results of DSC showed that the melting temperature (T_m) increased from 138.6 °C (0 %) to 140.9 °C (7 %). The crystallization temperature (T_c) first rose from 97.4 °C to a maximum of 99.3 °C at 3 % and then decreased to 96.9 °C at 7 %. Consequently, the supercooling degree ($\Delta T = T_m - T_c$) initially decreased from 41.2 °C to 39.5 °C (3 %) and later increased to 44.0 °C (7 %). This non-monotonic behavior reflects the dual role of Na-MMT: at low loadings (≤ 3 %) it acts as a heterogeneous nucleating agent, facilitating chain ordering and reducing supercooling; at higher loadings (≥ 5 %) particle agglomerates create a physical confinement effect that hinders chain mobility, increasing supercooling.

We may conclude that, the low-q power-law analysis for SAXS results, captures the progressive roughening of large-scale structures (spherulites/aggregates) with increasing Na-MMT content, in full agreement with the DSC-derived transition from nucleation-dominated to confinement-dominated crystallization. The high-q and correlation function results provide the detailed lamellar parameters of neat sPP, while the composites exhibit a clear shift from mass to surface fractal behavior on both size scales. This integrated SAXS/DSC approach offers a comprehensive framework for correlating hierarchical structural changes – from the lamellar to the aggregate level – with the crystallization kinetics and nucleation efficiency in sPP/clay nanocomposites, enabling tailored design of their mechanical and barrier properties.

[1] Dimitri D.J. Rousseaux, et al., (2010). Carboxylate clays: A model study for polypropylene/clay nanocomposites, Polymer Degradation and Stability. 95, 7, 1194-1204.

[2] Shipeng Zhu, et al., (2011). Montmorillonite/polypropylene nanocomposites: Mechanical properties, crystallization and rheological behaviors. Applied Clay Science, 52,171-178.

[3] Li, S., Zheng, et al., (2025). Interfacial Engineering of Hydrophobic Montmorillonite for High-Energy-Capability Polypropylene Nanocomposite Dielectrics. Crystals, 15(9), 786.

[4] Yong Tang, et al., (2003). Preparation and thermal stability of polypropylene/montmorillonite nanocomposites, Polymer Degradation and Stability, 82, 127-131.

HIGH-DOSE GAMMA IRRADIATION EFFECTS ON HDPE/SiO_2 NANOCOMPOSITE FILMS: STRUCTURE, CRYSTALLINITY, AND INTERFACIAL BEHAVIOR

A.A. Nabiyev[1,2], O.I. Ivankov[2], A.H.A. Elmekawy[2,3,4] and A.I. Kuklin[2]

[1] *Ministry of Science and Education Republic of Azerbaijan, Institute of Physics, Baku, Azerbaijan*
[2] *International Intergovernmental Organization, Joint Institute for Nuclear Research, Dubna, Russia*
[3] *Experimental Nuclear Physics Department, Nuclear Research Center, Egyptian Atomic Energy Authority, Cairo, Egypt*
[4] *Cyclotron Facility, Nuclear Research Center, Egyptian Atomic Energy Authority, Cairo, Egypt*

E-mail: asifnebi@gmail.com

The presence of nano-SiO_2 particles in a polymer matrix can influence the behavior of the polymer under ionizing radiation by altering radical formation, recombination dynamics, and structural efficiency. In particular, the addition of inorganic nanoparticles such as silicon dioxide (SiO_2) can improve the crystallinity, thermal stability, and mechanical strength of the polymer matrix. These types of nanocomposites have potential applications in electronics, coatings, optics, and space technologies [1–5]. In this study, HDPE nanocomposites reinforced with nano-SiO_2 particles were fabricated and exposed to high-dose gamma irradiation. The objective of this work is to analyze changes in structural integrity, crystallinity, defect formation, radiation resistance, nanoparticle dispersion, and interfacial interactions within these nanocomposites, as well as to assess their long-term suitability for use in radiation-intensive environments.

Here we presented the effects of gamma radiation on the structural and thermal characteristics of high-density polyethylene nanocomposite films. These thin films consist of a combination of high-density polyethylene (HDPE) and nano-SiO_2 particles prepared by hydrostatic thermal pressing a mixture of HDPE powder and nano-SiO_2 in various volume concentrations (ω = 1%, 5%, 10%, and 20%). Radiation-induced defects and microstructural changes in HDPE nanocomposite films containing embedded nano-SiO_2 particles were investigated under high-dose gamma irradiation (100–500 kGy). DBAS analysis revealed that SiO_2 nanoparticles effectively suppress radiation-induced defect formation and positronium formation across most doses through void-filling and interfacial positron trapping mechanisms [6]. Defect evolution showed a transition from chain scission-dominated behavior (increasing defects up to 300 kGy) to crosslinking dominance at 500 kGy, with SiO_2 significantly mitigating both processes. However, at the critical dose of 300 kGy, where crystallinity (66.2%) and structural reorganization peak, anomalous defect behavior was observed for 1% and 20% SiO_2 loadings, attributed to insufficient structural constraint and interfacial stress concentration, respectively. Electron momentum distribution (EMD) analysis confirmed carbonyl group (C=O) formation during oxidative degradation. Optimal radiation resistance was achieved with 5–10 vol% SiO_2 at doses up to 300 kGy, in consistent with SAXS and WAXS findings, where the lamellar long period and crystallite thickness decreased, indicating a more ordered structural arrangement, while at 500 kGy chain scission and oxidative degradation became dominant.

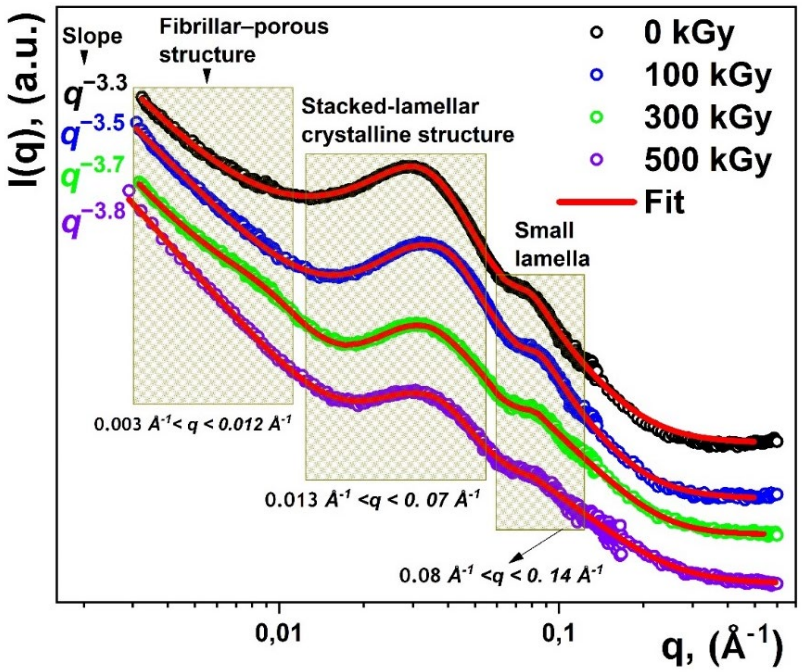

Fig. 1. Small-angle X-ray scattering plots of high dose gamma-ray irradiated pure HDPE films

These results provide fundamental insights into radiation resistance mechanisms and support the design of HDPE/SiO_2 nanocomposites for use in high-dose radiation environments.

[1] S. Mallakpour, M. Naghdi, (2018). Polymer/SiO_2 nanocomposites: Production and applications, Progress in Materials Science, 97 409-447.

[2] D.W. Lee, B.R. Yoo, (2016). Advanced silica/polymer composites: Materials and applications, J. Ind. Eng. Chem. 38 1–12.

[3] A.A. Nabiyev, et al., (2021). Composite films of HDPE with SiO_2 and ZrO_2 nanoparticles: The structure and interfacial effects, Nanomaterials 11 2673.

[4] A.A. Nabiyev, et al. (2020). Nano-ZrO_2 filled high-density polyethylene composites: Structure, thermal properties, and the influence γ-irradiation, Polymer Degradation. Stability 171

[5] A.A. Nabiyev, et al. (2025), Post-γ-irradiation effects in nano-SiO_2 particle reinforced high-density polyethylene composite films: Structure–property relationships, thermal stability and degradation, Polymer Composites, 46(S3)) S44–S62.

[6] A.A. Nabiyev, O.I. Ivankov, et al., (2026). High-dose gamma irradiation effects on HDPE/SiO_2 nanocomposite films: Structure, crystallinity, defects, radiation endurance, dispersion, and interfacial behavior, Polymer Degradation and Stability, 245, 111851.

EFFECT OF HIGH-DOSE GAMMA RADIATION AND WS_2 NANOSHEETS ON THE SUPRAMOLECULAR STRUCTURE, FRACTAL MORPHOLOGY, AND INTERFACIAL BEHAVIOR OF PVDF BY SAXS

A.A. Nabiyev[1,2], O.I. Ivankov[2], M.A. Nuriyev[1], N.Sh. Aliyev[1], A.H.A. Elmekawy[2,3,4] and A.I. Kuklin[2]

[1] *Ministry of Science and Education Republic of Azerbaijan, Institute of Physics, Baku, Azerbaijan*
[2] *International Intergovernmental Organization, Joint Institute for Nuclear Research, Dubna, Russia*
[3] *Experimental Nuclear Physics Department, Nuclear Research Center, Egyptian Atomic Energy Authority, Cairo, Egypt*
[4] *Cyclotron Facility, Nuclear Research Center, Egyptian Atomic Energy Authority, Cairo, Egypt*

E-mail: asifnebi@gmail.com

In this study, PVDF nanocomposites reinforced with WS_2 nanosheets were fabricated and exposed to high-dose gamma irradiation. The objective of this work is to analyze changes in structural integrity, crystallinity, defect formation, radiation resistance, nanoparticle dispersion, and interfacial interactions within these nanocomposites, as well as to assess their long-term suitability for use in radiation-intensive environments. PVDF/WS_2 nanocomposite films are highly promising materials for a wide range of applications, including flexible energy storage devices, sensors, and energy harvesting systems [1]. By combining the piezoelectric properties of PVDF with the high surface area and electrochemical properties of WS_2, these composites show enhanced performance in energy storage and conversion, as well as mechanical flexibility for wearable and flexible electronics. In this work, the effect of high-dose ionizing gamma radiation (0–700 kGy) and WS_2 nanosheets at different concentrations (1%, 3%, 5%, 10%) on the supramolecular structure, crystal/amorphous interface, and fractal morphology of PVDF was systematically studied using SAXS (broad peak, two-power-law, correlation function) method [2-3].

It was established that the roughness of neat PVDF thin films of surface fractal ($p=3.21$, $D_s=2.79$) transforms into a diffuse interface ($p>4$), with increasing radiation dose, while interlamellar distance decreases monotonically from 9.57 nm to 8.33 nm (densification), with short-range order ($\xi\approx4.4–4.6$ nm) is preserved and the degree of crystallinity increases (WAXS: 36.2% → 44.6%). At the same time, it was found that PVDF is resistant to radiation and no destruction occurs in the bulk structure. Furthermore, it was determined that at 1–3% WS_2 concentration, the WS_2 nanosheets exhibit good dispersion and a nucleating effect in the polymer matrix. This leads to a sharp smoothing of the polymer crystal/amorphous interface ($D_s=2.79 \rightarrow 2.05$) and increment in lamellar spacing ($d=9.57 \rightarrow 10.12$ nm). At 5% WS_2 – the onset of aggregation, return of the surface to moderate roughness ($D_s\approx2.30$), lamellar densification ($d=9.22$ nm) and maximum correlation length ($\xi=46.6$ Å) – this concentration is optimal for piezoelectric applications. At 10% WS_2 – formation of large aggregates (crossover size ~113 nm), two-level fractal structure: large aggregates very rough ($D_s\approx2.92$), small structures moderately rough ($D_s\approx2.44$). The PVDF matrix is constrained, and its own lamellar structure weakens (Fig. 1.).

Additionally, it was found that in low-concentration composites WS_2 nanosheets delays the radiation-induced interface diffusion (e.g., in 5% WS_2 the diffuse interface appears at 500 kGy, whereas in neat PVDF it appears at 300 kGy). Despite the presence of agglomeration, the relatively homogeneous distribution of nanosheets around 10 wt% filler concentration leads to

more effective absorption and scattering of radiation energy. This shields the PVDF matrix from direct radiation damage, limiting crosslinking and chain scission, and thereby significantly enhances the radiation resistance of the nanocomposite. The SAXS results directly confirm this protective effect, as the fractal parameters remain stable over the 0–700 kGy dose range in this highly filled system.

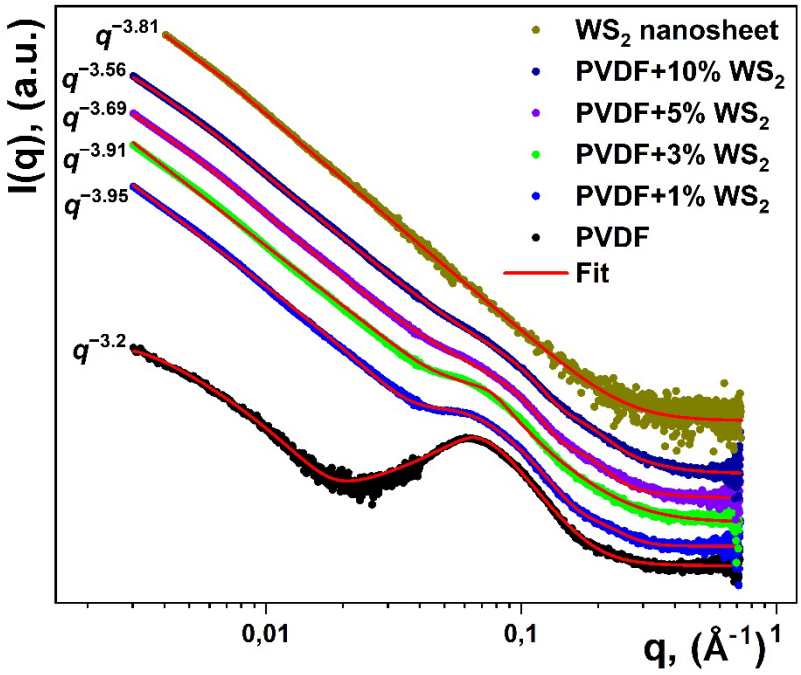

Fig. 1. Small-angle X-ray scattering plots of WS_2 nanosheets and PVDF+%WS_2 nanocomposite films

PVDF+5%WS_2 composite is recommended for optimal piezoelectric response, while 10% WS_2 is recommended for structural stability in radiation environments (sterilization, nuclear technology, aerospace industry). Nevertheless, several unsolved problems remain for the practical application of PVDF/WS_2 composites: potential increase in dielectric loss due to the diffuse interface, instability caused by aggregates, strong temperature dependence, and the difficulty of combining multiple functions (high piezoelectric response + low loss + radiation stability) in the same material. This work makes important contributions to both fundamental science (polymer physics, radiation chemistry) and practical materials science by quantitatively describing, through fractal analysis, the structural behavior of PVDF/WS_2 nanocomposites under radiation. The research provides a scientifically based guide for optimizing the WS_2 concentration and radiation dose according to the intended application area. Future work should focus particularly on determining the interface thickness, conducting in-situ studies, and establishing correlations with macroscopic properties. This approach will pave the way for the design of a new generation of multifunctional polymer nanocomposites.

[1] Arun Mondal, et al., (2024). High-performance flexible piezoelectric nanogenerator assisted by a three-phase PVDF/WS2/rGO nanocomposite, Nanotechnology 395401.

[2] A.A. Nabiyev, et al. (2020). Nano-ZrO_2 filled high-density polyethylene composites: Structure, thermal properties, and the influence γ-irradiation, Polymer Degradation. Stability 171

[3] A.A. Nabiyev, O.I. Ivankov, et al., (2026). High-dose gamma irradiation effects on HDPE/SiO_2 nanocomposite films: Structure, crystallinity, defects, radiation endurance, dispersion, and interfacial behavior, Polymer Degradation and Stability, 245, 111851.

PHASE RECOVERY IN POLARIZED NEUTRON REFLECTOMETRY USING DY AND ITS HYDRIDES AS REFERENCE LAYERS

E.S. Nikova[1,2], Yu.A. Salamatov[1], E.A. Kravtsov[1,2]

[1] *M.N.Miheev Institute of Metal Physics UB RAS, Ekaterinburg, Russia.*
[2] *Ural Federal University, Ekaterinburg, Russia.*

E-mail: e.nikova@mail.ru

Polarized neutron reflectometry (PNR) is a powerful experimental technique to probe layered metal nanostructures. Special methods for setting up experiments and methods for processing the obtained results are being intensively developed. One of these methods is the reference layer method, proposed independently by V.O. de Haan and C.F. Majkrzak [1, 2] to solve the phase problem for non-magnetic systems. This method has been modernized and successfully applied by us to the study of magnetic systems using PNR. The gadolinium layer is used as a reference layer in this approach. Previously, experiments on neutron reflectometry were carried out at the reflectometers REFLEX and REMUR of the IBR-2 reactor, which showed the usefulness of the gadolinium reference layer method in the study of both non-magnetic and magnetic nanoheterostructures using polarized neutrons [3, 4].

However, in experiments with the gadolinium reference layer, it is necessary to change the incident angles in order to vary gadolinium scattering characteristics. This variation makes it more difficult to bond the different q-ranges. Gadolinium's resonance effects are most noticeable in the wavelength range 0.5 – 2 Å. But not every reflectometer is capable of providing sufficient intensity in this wavelength range. Therefore, we suggest new an approach with changing the chemical properties of the reference layer itself. To do this, we propose using dysprosium, pure and saturated with hydrogen and deuterium, so that there are 3 experiments.

The mathematical formalism for calculation the reflection amplitude is similar to that used in the case of a gadolinium reference layer. Successful numerical calculations were performed for the test layered systems Si//Cr(500 Å)/***RL*(50 Å)**/Pd(30 Å) and Si//Cr(200 Å)/***RL(50 Å)***/Cr(30 Å)/Pd(30 Å). Here ***RL*** is reference layer: Dy, DyH_3, DyD_3. (Figure 1).

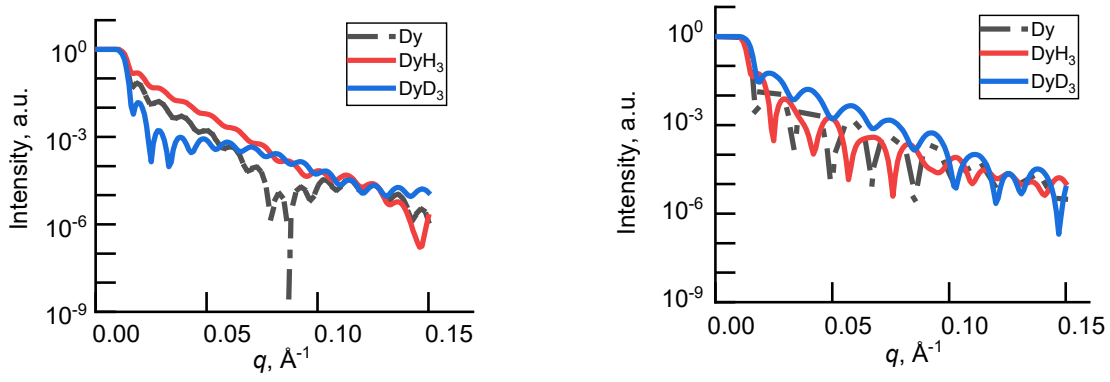

Figure 1 - Numerical calculations for the test layered systems: a - Si//Cr(500 Å)/RL(50 Å)/Pd(30 Å); b - Si//Cr(200 Å)/RL(50 Å)/Cr(30 Å)/Pd(30 Å) for tree different reference layer RL: Dy, DyH_3, DyD_3

Neutron reflectivity was carried out on the neutron reflectometer REFLEX at the pulsed reactor IBR-2 (JINR, Dubna). Reflectivity was measure in the region of total external reflection (approximately up to q=0.05 Å^{-1}) with high-energy resolution and good statistics at room

temperature. The angles of incidence were 4 and 9 mrad. Beam polarization and external magnetic fields were not applied.

The work was carried out with the support of the Ministry of Science and Higher Education of the Russian Federation, agreement № 075-15-2022-830 of June 5, 2025.

[1] C. F. Majkrzak and N. F. Berk (1995). Exact determination of the phase in neutron reflectometry. Phys. Rev. B. 52, 10827
[2] V.O. de Haan, A. A. van Well, P. E. Sacks, S. Adenwalla (1996) Toward the solution of the inverse problem in neutron reflectometry. Physica B Condens. Matter. 221, 524–532.
[3] E.S. Nikova, Yu.A. Salamatov, E.A. Kravtsov, M.V. Makarova, V.V. Proglyado, V.V. Ustinov, V.I. Bodnarchuk, A.V. Nagorny (2019) Experimental approbation of reference layer method in resonant neutron reflectometry. Physics of metals and metallography. 120, 838-844.
[4] E. S. Nikova, Yu. A. Salamatov, E. A. Kravtsov, V. V. Proglyado, V. D. Zhaketov, M. A. Milyaev (2022). Gd-Reference-Layer Method in Polarized Neutron Reflectometry. Journal of Surface Investigation. X-ray, Synchrotron and Neutron Techniques. 16. 939—942.

PROXIMITY EFFECTS IN HETEROSTRUCTURES OF SUPERCONDUCTING NIOBIUM AND RARE EARTH METALS WITH HELIMAGNETIC ORDERING

D.A. Norov[1,2], V.D. Zhaketov[2,3]

[1] *Lomonosov Moscow State University, Moscow, Russia*
[2] *Frank Laboratory of Neutron Physics, JINR, Dubna, Russia*
[3] *Moscow Institute of Physics and Technology, Dolgoprudny, Russia*

E-mail: dmitriynorov@yandex.ru

The rare earth metals holmium (Ho) and dysprosium (Dy) are of particular interest due to their ability to form complex magnetic structures, including helical magnetic ordering. This magnetic structure provides a good platform for studying proximity effects, since weak magnetic ordering can bring the energies of magnetic and superconducting interactions into proximity. Studies of heterostructures and thin films based on rare earth metals and superconductors are of interest both for fundamental physics and for applications, for example, in spintronics [1].

Polarized neutron reflectometry is one of the best methods for studying such effects in layered structures. The measurements described here were carried out on the REMUR reflectometer at the IBR-2 reactor (JINR, Dubna).

In a previous study on a periodic structure Nb(25nm)/[Dy(6nm)/Ho(6nm)]$_{34}$, partial suppression of the transition to the fan-shaped magnetic state and restoration of the spiral state at temperatures below the superconducting transition temperature of niobium were demonstrated. This work presents a more detailed analysis of the reflectometry curves, in particular of the Bragg peaks arising from the magnetic spiral.

A magnetic helix in a simpler three-layer structure Nb(40nm)/Dy(200nm)/V(10nm) was modeled first. Comparison of the calculated and experimental reflectometry curves indicates that the magnetic helix in this structure propagates coherently over approximately 10 helical periods (~330A), with a period deviation from the mean of approximately 8%. A more complex periodic structure Nb(25nm)/[Dy(6nm)/Ho(6nm)]$_{34}$ was then modeled. The magnetic helix in such a superlattice propagates coherently over approximately 6 layers of dysprosium and holmium (~600A). This means that even when transitioning from one substance to another, the period deviation from the average value is approximately 10%. Calculations were performed for experimental data at 100 K. Future studies are planned to examine the data at lower temperatures in more detail to obtain information on changes in the parameters of the helimagnetic structure under the influence of superconductivity.

[1] N.G. Pugach et al. (2022). Superconducting Spin Valves Based on a Single Spiral Magnetic Layer**.** Phys. Rev. Appl. **18**,5, 054002.
[2] V.D. Zhaketov et al. (2023). Structural Properties of Nb/Dy and Nb/Ho Superlattices. Physics of the Solid State, 65,7,1076-1080.

CHARACTERIZATION OF INTERLAYER CORRELATIONS IN SPECIAL PLANAR STRUCTURES BY SPECULAR NEUTRON REFLECTOMETRY

R. Nurulin[1,2], R. Safonov[1,3], M.V. Avdeev[3], V.A. Matveev[4], B. Mukhametuly[3,2]

[1] *Faculty of Physics and Technology, Al-Farabi Kazakh National University, Almaty, Kazakhstan*
[2] *Institute of Nuclear Physics, Almaty, Kazakhstan*
[3] *Joint Institute for Nuclear Research, Dubna, Russia*
[4] *Petersburg Nuclear Physics Institute named by B.P. Konstantinov of the National Research Centre «Kurchatov Institute», Gatchina, Russia*

E-mail: rasim.nurulin.99@inbox.ru

Both periodic and aperiodic structures are the basis for development of neutron optical devices, such as supermirrors [1], as well as special structures for advanced reflectometry experiments [2-4]. They consist of a system of multilayers composed as a set of bi/multilayers of materials possessing high and low optical potentials. Roughness and homogeneity control at layer interfaces is a subject of special consideration when such systems are made on extended substrates using magnetron deposition according to special algorithms. There is a general problem how to reliably characterize interlayer correlations in a multiparameter system with a greate number of inner interfaces.

In this work, we consider this problem regarding experimental possibilities of specular neutron reflectometry for periodic and aperiodic structures based on $Ni_{1-x}Mo_x$/Ti bilayers in special cases. For periodic structures with equal sublayer thickness, the observation in practice the peaks corresponding to systematic extinctions gives the direct information on the depth correlation length of the multilayered structure. Smearing effects due to inhomogeneities at the inner interfaces in aperiodic structures with equal sublayer thickness in each bilayer are modulated by the algorithm used in the deposition.

Here, the analysis is given for samples produced in NRC KI - PNPI by dc magnetron sputtering on float glass. Two series of periodic and aperiodic (linier growth thickness growth) multilayered structures based on $Ni_{0.9}Mo_{0.1}$/Ti bilayers were prepared for NR experiments in the specular mode. The NiMo alloy was used to avoid magnetic scattering of neutrons. Measurements were done at the neutron reflectometer GRAINS with a horizontal sample geometry at the IBR-2 reactor, FLNP JINR.

The experiment aimed at testing the application of specular neutron reflectometry for characterizing the quality of a model system (e.g. neutron supermirror) imitating aperiodic structure in a step-by-step manner regarding several deposition stages.

[1] J.B. Hayter, H.A. Mook, Discrete thin-film multilayer design for X-ray and neutron supermirrors, J. Appl. Cryst. 1989, 22, 35
[2] I. Carron, V.K. Ignatovich, Algorithm for preparation of multilayer systems with high critical angle of total reflection, Phys. Rev A 2003, 67, 043610
[3] T. Veres, L. Cser, V. Bodnarchuck, V. Ignatovich, Z.E. Horváth, B. Nagy, Investigation of periodic Ni–Ti multilayers, Thin Solid Films 2013, 540, 69–72
[4] M. V. Avdeev, I. V. Gapon, D. Merkel, M. S. Yerdauletov, D. M. Djanseitov, T. V. Tropin, Low-Period Multilayer Ti/Ni_xMo_y Films with Variable Quasi-Homogeneous Structure for Neutron Reflectometry, Journal of Surface Investigation 2023, 17 (4), 886–891

STUDY AND OPTIMIZATION OF VIRAL RHODOPSINES 1

E.A. Petrova[1], V.V. Sudarev[1], S.M. Bukhalovich[1]

[1] *Research Center for Molecular Mechanisms of Aging and Age-Related Diseases, Moscow Institute of Physics and Technology, Dolgoprudny, Russia*

E-mail: petrova.ekaterina@phystech.edu

Rhodopsins are light-sensitive 7-α-helical membrane proteins that comprise the retinal molecule as a prosthetic group. They are used as a main optogenetic tool. The optogenetic approach allows to control cells' activity using light, ionic composition of cells with high spatiotemporal precision. Recently explored channel rhodopsins from genome of giant viruses (homological proteins VirChR1 and OLPVR1) [1] might become a perspective optogenetic tool. Recently it has been shown that OLPVR1 generate light-induced calcium current from ER of mammalian cells [2], paving the way to direct calcium optogenetics. Despite of the interest in viral rhodopsins, their intracellular localization during heterological expression in mammalian cells is ambiguously understood, which makes it difficult to use viral rhodopsins in optogenetics.

We studied intracellular localization of VirChR1 and OLPVR1 in mammalian cell lines and possibility of generating calcium current by these proteins. We conducted experiments with transfected HEK293T cells to determine intracellular localization using confocal microscopy and shown their preferable localization in ER. Using genetically encoded fluorescent sensors, we observed light-dependent calcium currents both for OLPVR1 and VirChR1. For the VirChR1 protein, we optimized the genetic construct in order to increase the proportion of protein localized in cytoplasmic membrane and shown its light-dependent currents using patch-clamp. Our data suggest that combined use of OLPVR1 and VirChR1 with different localization might be used to control intracellular calcium signals and, in the future, lead to the creation of novel optogenetic tools.

The work was supported by the Russian Science Foundation (project No. 25-24-00786).

[1] Zabelskii D. et al. Viral rhodopsins 1 are an unique family of light-gated cation channels. // Nature communications. 2020. V. 11. № 1. P. 5707.

[2] Eria-Oliveira, A.-S. et al. Hijacking of internal calcium dynamics by intracellularly residing viral rhodopsins. // Nature Communications. 2024. V. 15. № 1. P. 65.

EPITHERMAL NEUTRON FLUX MEASUREMENTS AT PHOTONEUTRON SOURCE USING POSITION-SENSITIVE DETECTOR WITH DOUBLE-LAYER ^{10}B

V.N. Ponomarev[1], S.I. Potashev[1], K.Yu. Burmistrov[1], A.L. Polonski[1] and A.N. Sakharov[1]

[1] *Institute for Nuclear Research of Russian Academy of Sciences, 117312 Moscow, Russia*

E-mail: vasnikpon@rambler.ru

Spatial distribution neutron measurements in energy range from 40 to 200 eV were performed by using gas-filled position-sensitive detector with two ^{10}B layers. Neutron energy in flux of value ~ 10^7 c^{-1} $см^{-2}$ was determined by using time-of-flight method. Beryllium target in bremsstrahlung from tungsten target in electron accelerator beam was used to generate neutrons. The neutron spectra and their coordinate distribution depending on polyethylene plate moderator thickness were studied to increase epithermal neutron yield in selected energy range.

DESIGN AND ANALYSIS OF THE LATENT SPACE FOR VAE-BASED NEUTRON DIFFRACTION DATA

A.I. Popov[1,2], N.O. Antropov[1,2], E.A. Kravtsov[1,2], A.A. Smirnov[2] and I.N. Ogorodnikov[2]

[1] *M.N. Mikheev Institute of Metal Physics of the Ural Branch of the Russian Academy of Sciences (IMP UB RAS),620108, Ekaterinburg, st. S. Kovalevskaya, 18, Russia.*

[2] *Federal State Autonomous Educational Institution of Higher Education Ural Federal University named after the first President of Russia B.N.Yeltsin, 620002, 19 st. Mira, Ekaterinburg, Russia*

E-mail: AI.Popov@urfu.me

Variational autoencoders with a spatially structured latent space, combined with a geometric push-pull regularization mechanism, offer a powerful framework for analyzing and generating neutron diffraction data under high-noise conditions. The proposed VAE architecture introduces intra-class compactness (Pull) and inter-class separation (Push) losses alongside the standard reconstruction and KL divergence terms. This design enables the latent space to maintain both global connectivity and class-wise structure, which is particularly challenging for unconditional models. Quantitative experiments show that the conditional VAE, incorporating class information, achieves significantly better clustering metrics (Silhouette Score, Calinski-Harabasz Index) and linear separability compared to its unconditional counterpart, while also demonstrating nonlinear sensitivity to the push component weight.

The generative capabilities of the conditional VAE extend beyond simple reconstruction, producing physically meaningful and visually "idealized" diffraction patterns even from severely corrupted inputs. Using domain-specific evaluation metrics such as PSNR, SSIM, a modified Inception Score, FID, and physically motivated distortion measures (integral intensity divergence and peak shape divergence via the Wasserstein distance), the model successfully learns canonical features of diffraction patterns—including reflection positions, shapes, and spatial organization—from clean classes (Cr, Cu, Fe, Ni, Ti) and generalizes them to noisy data. As a result, the generated patterns exhibit enhanced peak clarity, reduced noise, and preserved crystallographic fidelity, demonstrating robust denoising and generative performance rooted in a well-structured latent space.

A MULTIMODAL DUAL-BRANCH SWIN TRANSFORMER NETWORK FOR NEUTRON 2D DIFFRACTION POST-PROCESSING

A.I. Popov[1,2], N.O. Antropov[1,2], E.A. Kravtsov[1,2], A.A. Smirnov[2] and I.N. Ogorodnikov[2]

[1] *M.N. Mikheev Institute of Metal Physics of the Ural Branch of the Russian Academy of Sciences (IMP UB RAS), 620108, Ekaterinburg, st. S. Kovalevskaya, 18, Russia.*

[2] *Federal State Autonomous Educational Institution of Higher Education Ural Federal University named after the first President of Russia B.N.Yeltsin, 620002, 19 st. Mira, Ekaterinburg, Russia*

E-mail: ai.popov@urfu.me

Neutron diffraction is a powerful but challenging technique due to low beam intensity, difficult detection, and hardware limits. Detectors (gas, semiconductor, or scintillator) each have drawbacks like low efficiency, high voltage needs, or poor resolution. Inspired by ML the authors propose using deep learning (e.g., Swin transformer networks) to post-process 2D time-of-flight (TOF) neutron diffraction images, improving quality despite physical and technological constraints.

This paper presents a new approach to the post-processing of time-of-flight neutron diffraction data. The data being processed are two-dimensional images of time-of-flight neutron diffraction. The authors employed deep learning tools traditionally used in computer vision. The solution is aimed at supporting and optimizing neutron experiments by improving data quality and accessibility.

The authors propose an original method for refining and post-processing two-dimensional neutron diffraction (TOF diffraction) images. They developed the SwinWnet model for segmentation, filtering, noise reduction, and intensity enhancement of the neutron signal (see Fig.1). Experiments have shown that the proposed approach effectively increases signal intensity, improves the separation of diffraction peaks, and reduces noise levels.

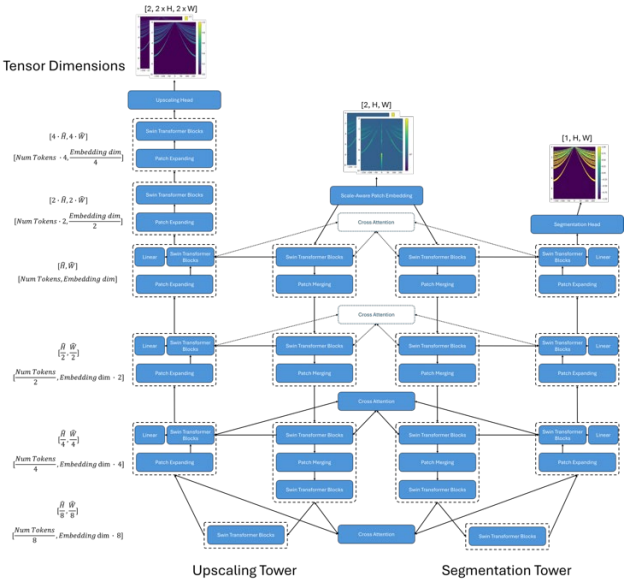

Fig.1 SwinWnet model architecture

NONLINEAR LASER SCANNING MICROSCOPY FOR LABEL-FREE POLYMER (MICROPLASTIC) DETECTION IN A BIOLOGICAL MATRIX

M. Popović[1], M. Aničić Urošević[1], A. Popović[2], M. Ćurčić[1], T. Pajić[3], M.D. Rabasović[1], A. Krmpot[1]

[1] *Institute of Physics Belgrade, University of Belgrade, Belgrade, Serbia*
[2] *University of Belgrade – Faculty of Chemistry, Belgrade, Serbia*
[3] *University of Belgrade – Faculty of Biology, Belgrade, Serbia*

E-mail: pmilica@ipb.ac.rs

Microplastics (MPs) are detected across environmental and biological systems, yet reliable screening in heterogenous matrices remains challenging. Conventional optical microscopy is widely used after particle isolation, but visual inspection becomes unreliable for nano-scale, transparent, or irregularly shaped particles, motivating alternative label-free imaging strategies. In this study, we evaluate nonlinear laser scanning microscopy (NLSM) modalities focusing on third-harmonic generation (THG; excitation at 1040 nm, detection at 347 nm) as a label-free screening approach and two photon excitation fluorescence (TPEF; excitation at 730 nm, detection at 400-700 nm) as a secondary signal to assess intrinsic fluorescence. Three laboratory-grade polymer standards: high-density polyethylene (HDPE) granules (size 2-4 mm), polystyrene (PS) granules (size 3-5 mm), and polypropylene (PP) granules (size 3-4 mm) were compared with consumer-derived MPs mechanically generated from representative plastic items used in laboratory and cosmetic packaging: a transparent HDPE bottle, a transparent PP centrifuge tube, and a PS disposable cup. Particle sizes ranged from a few nanometers to several hundred micrometers. Nonlinear imaging revealed strong THG contrast for all three polymers in both reference and consumer-derived MPs enabling straightforward localization and plane selective imaging of the particles. In contrast, no detectable autofluorescence was observed upon two photon excitation at the wavelength of 730 nm for any of the reference polymers, whereas consumer-derived MPs exhibited weak and heterogenous autoTPEF that varied across particles and may require high excitation powers to become detectable which can damage the sample. To assess applicability in a biologically complex matrix, consumer-derived MPs were imaged with *Phycomyces blakesleeanus* hyphae, a filamentous fungal model previously established for THG imaging of intracellular lipid droplets [1]. THG enabled simultaneous visualization of hyphal structures and associated MPs, and z-stacks provided to show particle size and three-dimensional morphology in relationship to the hyphae. In conclusion, THG provides robust, label-free contrast for MP screening across reference polymers, consumer-derived MPs, and hyphae which supports THG microscopy as a reliable pre-selection tool to guide targeted downstream chemical identification and future studies on hyphal responses to prolonged MP exposure.

[1] Pajić T., Todorović N., Živić M., Nikolić S., Rabasović M. D., Clayton A. H., Krmpot A. (2022). Label-free third harmonic generation imaging and quantification of lipid droplets in live filamentous fungi. *Sci Rep* 12, 18760.

INTRA- AND INTERMOLECULAR DYNAMICS OF AZA-AROMATIC SYNTHONS: A CASE STUDY OF THE 4,4′-BIPYRIDINE

E.V. Raksha[1], D. Zagorac[2,3], E.A. Goremychkin[1], A.B. Eresko[1], S. Dabylova[4], J. Zagorac[2,3], M. Pejić[2,3], T. Škundrić[2,3], S. Butulija[2], B. Matović[2], D.M. Chudoba[1]

[1] *Joint Institute for Nuclear Research, Dubna, Russian Federation*
[2] *Institute of Nuclear Sciences "Vinča", University of Belgrade, Belgrade, Serbia*
[3] *Center for synthesis, processing and characterization of materials for application in extreme conditions "CextremeLab", Belgrade, Serbia*
[4] *Institute of nuclear physics, Almaty, Republic of Kazakhstan*

E-mail: elenaraksha@jinr.ru

This study systematically investigates the intra- and intermolecular dynamics of aza-aromatic synthons for MOFs, which have a wide range of potential applications, including the production and use of functional materials for spintronics and microelectronics, as well as the development of highly effective catalysts. The torsion energy profile in aza-aromatic molecules is primarily influenced by two opposing trends: π-conjugation between the aza-phenyl rings, which favors a coplanar conformer, and steric repulsion, which stabilizes a nonplanar structure. We use a multidisciplinary approach that has previously been shown to be effective in studying the molecular dynamics of the 4,4′-bipyridine synthon (Fig. 1) [1-4].

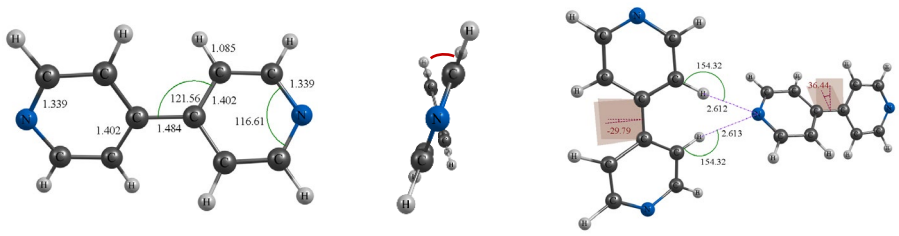

Fig. 1. Equilibrium geometries of the 4,4'-bipyridine (a) and its dimer (b) (B3LYP/6-31G(d,p) theory level)

Experimental studies of 4,4'-bipyridine using inelastic neutron scattering were performed in the energy transfer range of 0-160 meV at 5 K (NERA inverse geometry spectrometer at IBR-2, JINR, Dubna). DFT methods were used to study the molecular dynamics of 4,4'-bipyridine and its dimer, which are stabilized by non-valent C-H-N interactions (Fig. 1). The dimer's 4,4'-bipyridine molecules have varying torsion angles (φ), indicating the relative orientation of the pyridine fragments. This is consistent with the results of X-ray structural analysis [5]. The vibrational spectrum of 4,4'-bipyridine in the low-wavenumber region is characterized by non-valent C-H-N interactions. A comparison of experimental and DFT results contributes to our understanding of 4,4'-bipyridine dynamics and flexibility, as well as their potential applications in MOF design.

[1] D. Zagorac, M. Fonović, S. Butulija, et al. (2025) Journal of Alloys and Compounds, 1010, 178343.
[2] D.T.Teppala, M.Pejić, D. Zagorac, et al. (2026) International Journal of Applied Ceramic Technology, 23 (1), e70120.
[3] P. Gergelezhiu, E. Raksha, L. Savostina, et al. (2025) Phys. Part. Nuclei Lett., 22, 1102.
[4] Ł. Hetmańczyk, E.A. Goremychkin, J. Waliszewski, et al. (2021) Molecules. 26(16), 5043.
[5] N.M. Boag, K.M. Coward, A.C. Jones, M.E. Pemble, J.R. Thompson (1999) Acta Crystallographica, Section C: Crystal Structure Communications. 55, 672.

PRESSURE-INDUCED PHASE TRANSITIONS IN MAGNETITE NANOPARTICLES DOPED WITH Sm AND La IONS

A.V. Rutkauskas[1], O.N. Lis[1], S.E. Kichanov[1], E.V. Lukin[1] , D.P. Kozlenko[1], G.S. Rymski[2] and A.L. Zhaludkevich[2]

[1] *Frank Laboratory of Neutron Physics, Joint Institute for Nuclear Research, Dubna, Russia*
[2] *Scientific-Practical Materials Research Centre of the National Academy of Sciences of Belarus, Minsk, Belarus*

E-mail: ranton@nf.jinr.ru

Bulk and nanostructured ferrites with a spinel-type crystal structure (AFe_2O_4) have been actively studied for many decades due to their attractiveness from both fundamental and practical points of view. Such compounds exhibit a wide range of physical phenomena: high electrical resistivity, low electrical losses, high chemical stability, magnetic phase transitions of various types, geometric frustration effects, and much more. This makes possible the wide technological application of ferrites as materials for transformers, solar cells, biomedicine, magnetic sensors, catalysts, drug delivery systems, electronic and magnetic components.

Depending on the chemical composition and size of nanoparticles, ferrites with a spinel structure have different distributions of cations in tetrahedral (A) and octahedral (B) oxygen coordination. In particular, the case can be realized when Fe^{3+} ions are in positions A, and there is also a mixture of Fe^{3+} and Fe^{2+} ions located in positions B. When doping with transition metals or alkali elements in positions A or B or creating vacancies in the cubic spinel structure, magnetic interactions between iron ions change. This leads to significant changes in the physical properties of these ferrites.

In our work we have studied the crystal structure of $R:Fe_3O_4$ nanostructured ferrites (where R is Sm, La and R= 5%) under high pressure.

The $Sm:Fe_3O_4$ compound has been studied in the pressure range of 0-26 GPa. At pressures above 17 GPa, a structural phase transition has been detected from the initial cubic phase with space group $Fd\bar{3}m$ to the orthorhombic structure Bbmm.

The $La:Fe_3O_4$ compound has been studied in the pressure range of 0-25 GPa. For this compound the structural transition from cubic phase $Fd\bar{3}m$ to the orthorhombic structure Bbmm has been observed at pressure 8 GPa.

For both compounds the phase transition is a wide range of phase coexistence pressures. Under pressure there is a gradual suppression of the initial cubic phase and an increase in the volume fraction of the orthorhombic phase. The lattice parameters, bond lengths, and bulk modulus have been determined for both the cubic and orthorhombic phases in this ferrite.

This work has been supported by the joint grants of the Russian Science Foundation (RSF) № 24-42-10003, https://rscf.ru/project/24-42-10003/ and the Belarusian Foundation for Basic Research, BFBR T23RNFM-023.

DEVELOPMENT OF COMPLEX FIBONACCI SYSTEMS WITH MIXED SUPERCONDUCTIVITY AND ARTIFICIAL ANTIFERROMAGNETISM

R.N. Sadradze[1], V.D. Zhaketov[2]

[1] *Dubna State University, Dubna, Russia*
[2] *Joint Institute for Nuclear Research, Dubna, Russia*

E-mail: srn.22@uni-dubna.ru

Fibonacci systems involve the following sequence of layers during nanostructure deposition: A→B, B→BA. As a result, the total number of structural layers forms a Fibonacci sequence (1, 1, 2, 3, 5, 8, 13, 21, 34, 55, 89) with increasing order. The layer marked as A has a different thickness and density of the neutron coherent scattering length (SLD) compared to the layer marked as B.

Unlike periodic structures, Fibonacci structures lack translational symmetry [1], which may enable the observation of mixed superconductivity effects and the asymmetry of the critical temperature T_c for structures made of superconducting materials such as Nb, V, Pb, In, Sn, Ta, and high-temperature superconductors like the Pb/Bi alloy [2].

Fibonacci structures with artificial antiferromagnetism, based on ferromagnetic materials like Co, Fe, and diamagnetic materials like Cu, Ru, Cr, exhibit perpendicular magnetic anisotropy, differing from the in-plane magnetization found in periodic structures [3].

It is proposed to manufacture and study Fibonacci structures with layer thicknesses on the order of tens of angstroms and complex magnetic structures at REMUR after determining the optional thicknesses, materials, and number of layers. Theoretical calculations of the neutron reflection coefficient R and a comparison of the Fibonacci structure with a periodic structure have been preliminarily carried out.

[1] Vekilov Y. K., Chernikov M. A. Quasicrystals // Physics-Uspekhi. 2010. T. 53. № 6. C. 537-560 // DOI: 10.3367/ufne.0180.201006a.0561

[2] B. W. Roberts // Survey of Superconductive Materials and Critical Evaluation of selected properties // General Electric Research and Development, Box 8, Schenectady N. Y. 12301

[3] agnetization dynamics of a Fibonacci-distorted kagome artificial spin ice // Ali Frotanpour, Justin Woods, Barry Farmer, Amrit P. Kaphle, and Lance E. De Long Loris Giovannini, Federico Montoncello // Phys. Rev. B 102, 224435 // DOI: https://doi.org/10.1103/PhysRevB.102.224435

NEUTRON-DIFFRACTION STUDY OF ANISOTROPY IN GAS-ATOMIZED Nd-Fe-B MAGNETS POWDERS

V.V. Savin[1], V.K. Semina[2], I.V. Barinov[1] and E.K. Poghosyan[1]

[1] *Immanual Kant Baltic Federal University, Kaliningrad, Russian Federation*
[2] *Joint Institute for Nuclear Research, Dubna, Russian Federation*

E-mail: vvsavin@kantiana.ru

A modern high-energy permanent magnet of the Nd-Fe-B system is a complex physicochemical system in which the magnetic properties depend on the orientation of the grains, the presence of foreign phases (including non-metallic inclusions and intermetallic compounds), surface modified layers of grains of the main phase $Nd_2Fe_{14}B_1$ (T_1), intergranular layers, grain scattering fields and many other features of the structural-phase state of the material at the nano- and microlevels. The maximum magnetic hardness and the magnetic energy correlating with it of a classical permanent magnet are determined by the chemical composition of the alloy and its structural-phase state, including those associated with the features of the technological process and the quality of the initial charge materials. For anisotropic sintered magnets, improved functional properties are achieved by optimizing the size and shape of the grains of the T_1 phase (L×H×T ≈ 6×3×3 μm), their high crystallographic wear (texture), the presence of a uniform intergranular boundary (with a thickness of ≈ 1 μm) and minimizing the contacts of other phases (primarily intermetallic compounds) with the main magnetic phase (T_1). The textured state increases the free energy of the magnet, which is compensated by the development of a domain structure within the grains. The process of magnetization reversal (demagnetization) of the domain structure can be slowed down by creating a certain microstructure of the alloy, which prevents the nucleation of domains of the opposite sign and hinders the movement of domain walls, thereby increasing the coercive force of the magnet.

Nonequilibrium crystallization under conditions of quenching from the liquid state or, in English terminology, Melt Quenching (MQ) can significantly affect the structural-phase state of the alloy (up to its amorphization) and opens up technological possibilities for controlling the magnetic properties of the material and products made from it. In the work, the MQ is implemented using the technology of spraying a jet of melt with a flow of inert gas, or Gas Atomization (GA). This produces a powder material (GAP) with a fractional composition that meets the requirements of both classical processing (mechanical crushing and grinding of the ingot to particles 6÷10 μm in size; compaction in a magnetic field; sintering and heat treatment in a protective atmosphere) and modern additive technologies of direct growth (60÷120 μm). In fact, the additive process involves the melting of an individual powder particle and the subsequent crystallization of a drop of comparable size under conditions of directed heat removal through a gaseous medium in a protective atmosphere.

Between the classical technology of producing sintered anisotropic magnets and the additive technology of direct growth of magnetic microsystems of complex shape, there is a large area of applied problems when the dimensions of the permanent magnet approach the dimensions of the GAP and the spherical shape of the magnet is a functional requirement.

At the same time, remelting of a separate GAP (heating above Tm ≥1250°C), as an independent technological operation for the production of a finished product (in the cycle of a single technological process) is often not allowed. Moreover, the implementation of such a micrometallurgical process requires significant correction of the alloy composition to achieve the required level of functional magnetic properties. In this work, a solution is proposed by

implanting a separate GRP with surface melting (technological soldering) and volumetric recrystallization of T_1 phase grains [1].

In the academic aspect, the solution comes down to proving that in any individual GAP there is always an average anisotropy of the spatial orientation of T_1 grains due to the random nucleation of crystallization centers in the volume of an individual drop of supercooled melt and the spherical symmetry of the heat sink of the solidifying (crystallizing) melt.

In the materials science aspect, such random heterogeneity can be enhanced by recrystallization (by analogy with primary recrystallization) during special heat treatment: 1) thermal cycling in the Curie temperature region (T_c≈310°C), when the volumetric changes of an individual grain of the T_1 phase reach 6%; 2) heating and holding above the melting point of the ternary eutectic (T_e≈510°C), when, under the conditions of a developed pseudo-capillary system of the intergranular space, an anomalous mass transfer of matter occurs and selective directional recrystallization is realized.

In this study, we investigated a series of Nd-Fe-B-based MQ-GA-alloys alloyed with various elements. The first case of recrystallization was realized: thermal cycling near $T_c \approx 310$°C (ΔT = 200÷400°C, 10 cycles). To enhance the effect and provide a reducing environment, thermal cycling was carried out in flowing hydrogen.

The features of the emerging grain anisotropy and its relationship with magnetic properties are illustrated in Fig. 1.

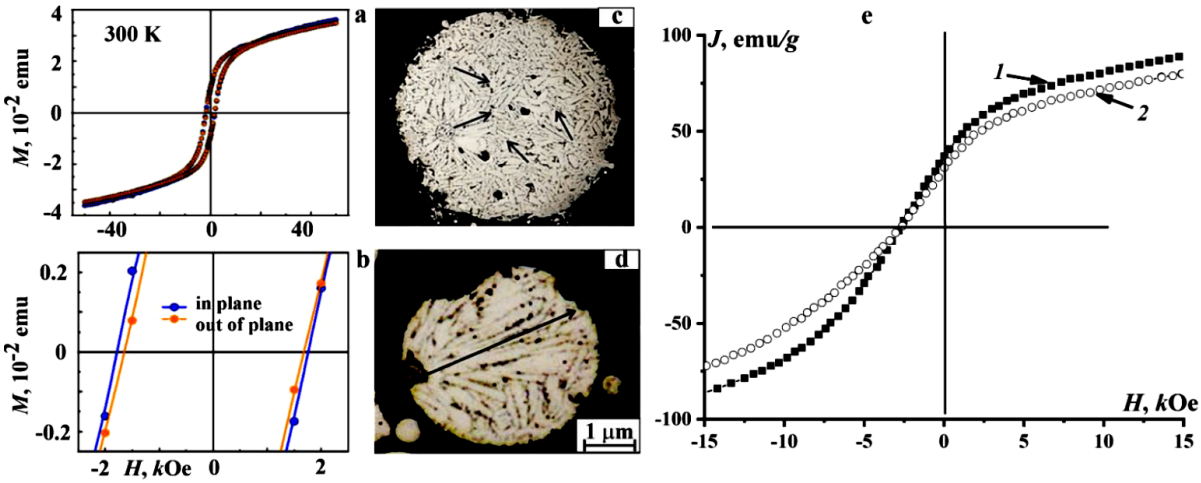

Fig. 1. Anisotropy of hysteresis properties of Fe-Nd-B GA-alloys: *a*, *b* - SQUID-magnetometry of $Fe_{78}Nd_{15}B_7$ alloy (No.4) in the longitudinal and transverse directions (*a* – powder on a silicon substrate obtained by laser cladding in a magnetic field perpendicular to the substrate surface; *b* – central part of the loop with color highlighting of property measurement data along and across the orientation of the powders); *c*, *d* – metallographic structure of the GAP alloy of the same composition; *e*, *f* – demagnetization curves of the sample (as a powder suspension, 20 g) on a vibrating magnetometer at room temperature: *e* – alloy No. 4, *f* - alloy No. 855 (identical to No. 4 in Nd and B), additionally alloyed (Mo+Ti+V+Al+In+Ga+Bi+Sc ≤ 2 at. %) [1]

Using X-ray and neutron diffraction methods, it was shown that the main phase in the studied GAP alloys is the $Fe_{14}Nd_2B$ boride (tetragonal phase T_1), space group $P4_2/mnm$ or $I4\bar{3}d$. Its quantity reaches 95±2 vol.%. Neutron diffraction analysis demonstrated the presence of magnetic, and therefore grain anisotropy in the GA-alloys. Thermal cycling in hydrogen environment near T_c increases this magnetic and grain anisotropy effect (by approximately 10%).

[1] V.V.SAVIN et al. (2025). Powder materials of REM-containing alloys obtained by gas atomization of the melt for laser surfacing technologies and additive processes. Materials Science Forum, 1151, 76-88.

INVESTIGATION OF LIPID MEMBRANES AND MEMBRANE-MIMETIC SYSTEMS BY SANS AT YUMO SPECTROMETER

A.Yu. Shishkin[1], I.O. Bezruchko[1], S.M. Bukhalovich[1], D.D. Kuklina[1], E.A. Dronova[1], A.E. Mikhailov[1], D.V. Sidorov[1], Yu.S. Semenov[1], O.I. Ivankov[2], A.I. Kuklin[1,2], Yu.L. Ryzhykau[1,2]

[1] *Research Center for Molecular Mechanisms of Aging and Age-Related Diseases, Moscow Institute of Physics and Technology, MIPT, Dolgoprudny, 141701, Russia*

[2] *Frank Laboratory of Neutron Physics, Joint Institute for Nuclear Research, Dubna, 141980, Russia*

E-mail: shishkin.aiu@phystech.edu

Small-angle neutron scattering (SANS) is one of the key methods for studying the structure of biological and materials science objects at the nanoscale (1-100 nm). In this work, we use it to study liposomes, vesicles from purple membranes, and detergent micelles.

Liposomes are microscopic vesicles consisting of one or more lipid bilayers that are used as model cell membranes for biophysical and biochemical studies of membrane proteins [1]. In our study, we present SANS results for azolectin liposomes containing the proton pumps MAR (marine actinobacterial rhodopsin) and *Mp*R (*Marinomonas posidonica* rhodopsin), as well as for empty liposomes. Based on the obtained data, conclusions are drawn regarding such liposomal properties as integrity, unilamellarity, and, where possible, overall size. In particular, it is shown that liposomes with incorporated protein are generally smaller than empty liposomes, as previously reported [2]. Verification of the above-mentioned characteristics is important for the subsequent use of liposomes in functional assays, for example, ΔpH and bilayer lipid membrane experiments. In turn, such assays will be applicable not only to proton pumps, but also to membrane proteins of other classes, for example, channelrhodopsins (ChR2, OLPVR1, etc.).

Purple membranes (PM) are specialized regions of the cell membrane of certain halophilic archaea and represent two-dimensional crystals of bacteriorhodopsin. This protein is a light-driven proton pump and is often used as a model system for studying the mechanism of proton transport [3]. Under certain conditions, PM can be transformed into spherical vesicles, which may subsequently be used to obtain bacteriorhodopsin crystals [4]. In our work, we present SANS data for such vesicles, which are used to determine their geometric dimensions.

We also use SANS to investigate the structure of detergent micelles, such as dodecyl maltoside and dodecyl phosphocholine. Previously, micelle models were obtained solely from SAXS data [5]; however, when their geometric parameters are fixed, it is not possible to fit the SANS data using any combination of scattering length densities (SLDs) of the individual model components. Therefore, obtaining accurate micellar models requires the simultaneous fitting of SAXS and SANS data. The experience gained from integrating these two methods may subsequently be applied to modeling the structure of protein-detergent complexes formed during the solubilization of membrane proteins.

A. Shishkin acknowledges the Russian Science Foundation (project no. 25-24-00786).

Yu. Ryzhykau acknowledges Federal scientific and technical program for the development of synchrotron and neutron research and research infrastructure of the Ministry of Science and Higher Education of the Russian Federation (agreement No. 075-15-2025-512).

E. Dronova acknowledges the Russian Science Foundation (project no. №25-24-00851).

[1] Routledge, S. J., Linney, J. A., & Goddard, A. D. (2019). Liposomes as models for membrane integrity. Biochemical Society Transactions, 47(3), 919-932.

[2] Okhrimenko, I. S. et al. (2023). Mirror proteorhodopsins. Communications chemistry, 6(1), 88.
[3] Stoeckenius, W., Lozier, R. H., & Bogomolni, R. A. (1979). Bacteriorhodopsin and the purple membrane of halobacteria. Biochimica et Biophysica Acta (BBA)-Reviews on Bioenergetics, 505(3-4), 215-278.
[4] Takeda, K. et al. (1998). A novel three-dimensional crystal of bacteriorhodopsin obtained by successive fusion of the vesicular assemblies. Journal of molecular biology, 283(2), 463-474.
[5] Oliver, R. C. et al. (2013). Dependence of micelle size and shape on detergent alkyl chain length and head group. PloS one, 8(5), e62488.

NEUTRON DIFFRACTION STUDY OF STRUCTURAL DISTORTIONS AND MAGNETIC STRUCTURE OF Bi-Sm-Fe-Ti-O MULTIFERROIC

V.V. Sikolenko[1], V.V. Efimov[1], R. Lanovsky[2], N. Tereshko[2], A. Sazonov[3] and D.V. Karpinsky[2,4]

[1] *Joint Institute for Nuclear Research, Dubna, Russia*
[2] *SSPA "Scientific-Practical Materials Research Centre of NAS of Belarus", Minsk, Belarus*
[3] *European Spallation Source, Lund, Sweden*
[4] *National Research University of Electronic Technology MIET, Moscow, Russia*

E-mail: vadim.sikolenko@jinr.int

We present the results of investigation the structural and magnetic properties of multiferroic $Bi_{1-x}Sm_xFe_{0.94}Ti_{0.06}O_3$ perovskites with compositions within the morphotropic phase boundary (x = 0.1 and 0.12). The combination of high-resolution neutron powder diffraction with complementary techniques has provided deeper insight into the temperature- and composition-dependent evolution and local distortions in the coexisting *R3c* and *Pbam* phases in the 1.5 to 300 K temperature range, and their correlation with the emergence of weak ferromagnetism and exchange bias effects. Our results demonstrate that the temperature-dependent magnetic response, including the enhancement of weak ferromagnetism and emergence of exchange bias at low temperatures for both samples, cannot be attributed to variations in the volume fractions of the structural phases, which remain nearly constant over the considered temperature range, specifically nearly 37/63 and 50/50 *Pbam*-to-*R3c* phase ratios for the x = 0.1 and x = 0.12, respectively. Instead, the key factor is the temperature-dependent evolution of the structural parameters within the orthorhombic *Pbam* phase, particularly the tilting, rotation, and distortion of FeO_6 octahedra. These distortions, accompanied by the complex dynamic of overlapped Fe^{3+} d- and O^{2-} p-orbitals due to the changes in Fe – O - Fe bond angles, directly affect the magnetic exchange interactions, enhance spin canting via increased Dzyaloshinskii-Moriya interactions, resulting in enhancement of weak ferromagnetism and complex magnetization behavior.

OPTIMIZATION OF PURIFICATION AND CRYSTALLIZATION CONDITIONS FOR OLPVR2

V.V. Sudarev[1], E.A. Dronova[1], D.V. Sidorov[1], E.D. Petrova[1], D.D. Kuklina[1] and Yu.L. Ryzhykau[1]

[1] *Research Center for Molecular Mechanism of Aging and Age-Related Diseases, Moscow Institute of Physics and Technology, MIPT, Dolgoprudny, Russia*

E-mail: sudarev.vv.research@gmail.com

Microbial rhodopsins are a diverse subfamily of light-sensitive membrane proteins extensively utilized across various fields of biology. Their distinctive feature is sensitivity to light, which induces conformational changes, thus enabling protein function. One of the new classes of microbial rhodopsins are viral rhodopsins identified in the genome of giant viruses [1]. Considering that the host of such viruses is phytoplankton, the function, physiological and biological role of viral rhodopsins can be of great interest for global ecology and climate.

OLPVR2 (Organic Lake Phycodnavirus Rhodopsin 2) exhibits a distinct structural architecture and oligomerization state compared to other known rhodopsins [2]. It assembles into a stable pentamer, forming a central pore that is structurally analogous to those found in pentameric ligand-gated ion channels. This unique arrangement suggests that OLPVR2 may function as a pentameric light-gated ion channel, a hypothesis that has not yet been experimentally validated. To investigate this mechanism, determining the open-state structure of OLPVR2 is essential, as has been accomplished for other viral rhodopsins [3]. However, existing purification and crystallization protocols have yielded insufficient quantities of high-quality crystals, necessitating further optimization.

In this study, we systematically optimized the OLPVR2 production pipeline by modifying the conditions for recombinant expression, protein solubilization, and crystallization. Our modified protocol resulted in an approximately fivefold increase in protein yield and enabled the successful formation of crystals.

This work was supported by the Federal Scientific and Technical Program for the Development of Synchrotron and Neutron Research and Research Infrastructure of the Ministry of Science and Higher Education of the Russian Federation (agreement No. 075-15-2025-512).

[1] T.Yutin, E.V.Koonin (2012). Proteorhodopsin genes in giant viruses. Biology direct. 7, 34.

[2] D. Bratanov et al. (2019). Unique structure and function of viral rhodopsins. Nature Communications. 10, 4939.

[3] D. Zabelskii et al. (2025). Ion-conducting and gating molecular mechanisms of channelrhodopsin revealed by true-atomic-resolution structures of open and closed states. Nature Structural & Molecular Biology. 32, 1347-1357.

PHASE-PURE COBALT FERRITE NANOPARTICLES WITH TUNABLE MAGNETIC PROPERTIES *VIA* MILD THERMAL TREATMENT AND CONTROLLED PRECIPITATION

M. Šuljagić[1], Lj. Andjelković[1], M. Tadić[2], D. Miletić[3] and V. Pavlović[3]

[1] *University of Belgrade-Institute of Chemistry, Technology and Metallurgy, Department of Chemistry, Njegoševa 12, Belgrade, Republic of Serbia*
[2] *"VINČA" Institute of Nuclear Sciences - National Institute of the Republic of Serbia, University of Belgrade, Belgrade, Serbia*
[3] *University of Belgrade, Faculty of Agriculture, Nemanjina 6, Belgrade, Serbia*

E-mail: marija.suljagic@ihtm.bg.ac.rs

Cobalt ferrite ($CoFe_2O_4$) nanoparticles were obtained through two coprecipitation strategies — conventional and reverse — and subsequently subjected to low-temperature annealing between 100 and 300 °C. This study explores how the order of reagent addition and mild thermal processing collectively shape the structural, morphological, and magnetic behavior of the resulting nanomaterials. The samples were characterized by X-ray powder diffraction (XRPD), Fourier-transform infrared spectroscopy (FTIR), scanning electron microscopy and transmission electron microscopy (SEM/TEM). Phase-pure spinel $CoFe_2O_4$ was confirmed across all conditions, demonstrating that high-temperature calcination is not a prerequisite for single-phase formation. While crystallite dimensions remained stable in the 10–12 nm range throughout the annealing series, lattice contraction toward bulk values indicated progressive strain relaxation and cation redistribution. Room-temperature ferrimagnetic behavior was observed in all samples, with saturation magnetization in the range 47–54 emu/g; both saturation magnetization (*M*s) and coercivity (*H*c) decreased with annealing temperature, attributed to surface oxidation effects rather than microstructural coarsening. Notably, the two synthesis routes produced nanoparticles with comparable structural characteristics, yet the reverse coprecipitation route without any post-synthesis thermal treatment stood out as the most efficient strategy — yielding phase-pure $CoFe_2O_4$ with the highest *M*s (54.39 emu/g) and well-defined coercivity (459.1 Oe) in a single, low-temperature step. These findings highlight precipitation sequence as an underexplored yet powerful handle for achieving targeted magnetic properties in ferrite-based nanomaterials.

Small-Angle Neutron Scattering (SANS) is a powerful technique uniquely suited for investigating ferrite-based nanomaterials, enabling the determination of particle size, size distribution, and morphology, as well as providing insight into magnetic microstructure, domain formation, and spin correlations. Therefore, SANS experiments are planned to gain deeper insight into the structural and magnetic properties of cobalt ferrite systems.

This research has been financially supported by the Ministry of Science, Technological Development and Innovation of Republic of Serbia (Contract No: 451-03-136/2025-03/200026, 451–03–136/2025–03/200116, and 451–03–13/2025–03/200288), as well as by Science Fund of the Republic of Serbia, #7551, Development of epsilon-iron oxide-based nanocomposites: Towards the next-generation rare-earth-free magnets – DOMINANTMAG, and Ministry of Science, Technological Development, and Innovation of the Republic of Serbia under Grant No. 676/04.08.2025 with JINR (Next-Generation MRI Contrast Agents: Exopolysaccharides - Functionalized Ferrite Nanoparticles for Enhanced Safety and Performance).

A NEW MODEL OF PRIMARY RADIATION DAMAGE IN MATERIALS

N.T.H. Trung[1,2], H.S.M. Phuong[1]

[1] *Dalat Nuclear Research Institute, VINATOM, Dalat, Vietnam*
[2] *Frank Laboratory of Neutron Physics, JINR, Dubna, Russia*

E-mail: trung@jinr.ru

Accurate quantification of radiation-induced damage is critical for advancing nuclear, ion implantation and semiconductor technologies [1]. The current international standard, the Norgett-Robinson-Torrens displacements per atom (NRT-dpa) model, exhibits significant limitations in physical accuracy [2]. Specifically, in metals, the NRT-dpa model overestimates the number of surviving point defects by a factor of three due to athermal recombination during the picosecond thermal spike phase. Conversely, it underestimates the extent of atomic mixing (replacements) by a factor of up to thirty [3]. To resolve these profound discrepancies, in 2015 the expert group of Nuclear Energy Agency OECD proposed two physically realistic models that complement the existing NRT-dpa standard: the athermal recombination-corrected dpa (arc-dpa) and replacements per atom (rpa) [4, 5]. Although these two models provide accurate predictions of surviving stable defects and reliably quantify the true extent of atomic mixing, they are fundamentally limited in their ability to describe the essential qualitative features of radiation damage. In particular these models yield no insight into the dynamic, spatial distribution of defects, the morphology of surviving clusters, or the influence of crystal lattice symmetry on the radiation damage.

In this work, we introduce a novel approach that overcomes these limitations. Our methodology relies on Voronoi tessellation analysis for identification and classification of defects and atomic mixing, followed by adaptive kernel density estimation to precisely map their distribution. Contrary to the conventional view that the distribution of defects in irradiated solids is random and unpredictable, our results demonstrate that while primary radiation damage is a highly stochastic and complex process, the final distribution of defects follows a specific pattern uniquely defined by crystal symmetry. This behavior persists until the accumulated radiation damage is large enough to break the underlying symmetry, ultimately leading to the radiation-induced amorphization of the material. Our findings provide new insights into the mechanisms of radiation damage in materials, which can be leveraged in the search for advanced radiation-resistant materials.

Keywords: *radiation damage, lattice and molecular dynamics of materials under extreme conditions*

Acknowledgment: We thank the HPC Center at the Dalat Nuclear Research Institute and the HybriLIT computing platform at MLIT, Joint Institute for Nuclear Research for providing computational resources.

[1] B.D. Wirth, How Does Radiation Damage Materials?, Science 318 (2007) 923–924.
[2] M.J. Norgett, M.T. Robinson, I.M. Torrens, A proposed method of calculating displacement dose rates, Nuclear Engineering and Design 33 (1975) 50–54.
[3] K. Nordlund et al., Primary radiation damage: A review of current understanding and models, Journal of Nuclear Materials 512 (2018) 450–479.
[4] NEA report, Primary Radiation Damage in Materials, OECD Publishing, 2015
[5] K. Nordlund et al., Improving atomic displacement and replacement calculations with physically realistic damage models, Nature Communication 9 (2018) 1084.

SOFTWARE FOR TRANSFORMING NEUTRON SCATTERING DATA FROM INSTRUMENTAL COORDINATES INTO Q-SPACE FOR TIME-OF-FLIGHT INSTRUMENTS BASED ON IBR-2

G.E. Zhezlyaev[1], D.I. Devyaterikov[1], E.A. Kravtsov[1], V.D. Zhaketov[2,3], E.D. Kolupaev[2]

[1] *Institute of Metal Physics of the Ural Branch of the RAS, Ekaterinburg, Russia*
[2] *Joint Institute for Nuclear Research, Dubna, Russia*
[3] *Moscow Institute of Physics and Technology, Dolgoprudny, Russia*

E-mail: g.e.zhezlyaev@mail.ru

Essential part of polarized neutron reflectivity experiment is a conversion of neutron scattering data from instrumental coordinates into q-space. A simple approach involves cutting out the specular reflection area and then integrating with respect to the angle within the cutting out angle range. This method is actual if you need to extract only specular reflectivity, but if you want to see diffuse part of reflection it can't be used. In this case you should make a q-space map. Purpose of this work is to create software for correct transforming neutron scattering data from instrumental coordinates into reciprocal space for time-of-flight instruments based on IBR-2. The importance of this work is in the opportunity to observe and analyze not only the effects affecting specular reflection, but also the effects affecting diffuse scattering.

The program utilizes following equation [1] for converting raw instrumental data into q-space:

$$\begin{cases} q_x = \left(\frac{2\pi}{\lambda}\right)\left(cos\alpha_f cos\varphi - cos\alpha_i\right), \\ q_y = \left(\frac{2\pi}{\lambda}\right)\left(cos\alpha_f sin\varphi\right), \\ q_z = \left(\frac{2\pi}{\lambda}\right)\left(sin\alpha_f + sin\alpha_i\right), \end{cases} \quad (1)$$

where q_i – coordinates in q-space, α_i – glancing angle of incidence, α_f – polar angle of reflection, φ – azimuthal angle of reflection.

The main problem that was tackled in this work is that coordinate grid in instrumental coordinates is irregular when transformed into reciprocal space. The problem is solved by calculating density maps using custom function created in python. The software divides the q-space into pixels and counts the number of neutrons that have entered a single pixel. This program accounts for three components of q-space, it allows visualization not only of off-specular mode, but also GISANS mode.

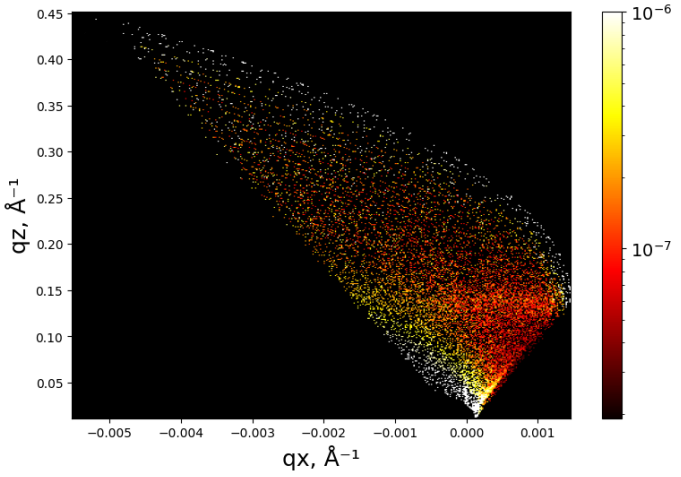

Fig. 1 – The 2D scattering map for Tb thin film

Additionally, transforming from 2D map into 1D dependence by summarizing along selected axis in q-space was implemented in program.

The software has already been used to transform neutron data obtained from scattering on the Tb thin film. This sample exhibits helicoid magnetic ordering in a narrow temperature range. Since it has a large period of approximately 4 nm, we expect that the reflection will be located at relatively small q values. However, due to the low Bragg intensity, it is difficult to detect it and determine the period of the magnetic structure using only specular reflectivity. Nevertheless, magnetic Bragg extends into diffuse scattering regions. With the latter, it is possible to detect and determine q values. 2D scattering map of Tb thin film was obtained using developed program. As Fig. 1 shows, thanks to the transformation into q-space, diffuse scattering is observed at a certain temperature, and it is possible to determine the parameters of the magnetic structure.

[1] Korolkov D. (2012). Analysis of randomly oriented structures by grazing-incidence small-angle neutron scattering. Journal of Applied Crystallography. 45, 245–254.

EPSILON AS A TEXTURE DIFFRACTOMETER: FIRST RESULTS

I.Yu. Zel[1], S.E. Kichanov[1], B. Altangerel[1], D.P. Kozlenko[1] and E.V. Lukin[1]

[1] *Joint Institute for Nuclear Research, Dubna, Russia*

E-mail: zel@jinr.ru

As part of the current upgrade of the EPSILON diffractometer (channel 7A1, IBR-2), the ability to measure pole figures was implemented to study crystallographic texture in polycrystalline materials. Modifications to the detector system made it possible to obtain a quasi-regular 15-degree grid on the pole figure by performing 24 sample rotations. A Jupyter Notebook script was created for data processing and analysis. Measurements performed on a highly textured aluminum alloy showed good agreement between the experimental pole figures obtained with EPSILON and the SKAT texture diffractometer (channel 7A2, IBR-2).

CONCENTRATION OF METALS IN MOSS SAMPLES FROM FIVE DIFFERENT ENVIRONMENTS IN SERBIA: COMPARISON AND ANALYSIS

M. Živković[1], N. Sarap[1], I. Lazović[1], I. Zinicovscaia[2], O. Chaligava[2], D. Grozdov[2]

[1] *Vinča Institute of Nuclear Sciences, National Institute of the Republic of Serbia, University of Belgrade, Belgrade, Serbia*

[2] *Joint Institute of Nuclear Research, Dubna, Russia*

E-mail: marijaz@vin.bg.ac.rs

Mosses are widely recognized as effective bioindicators of atmospheric metal pollution due to their ability to accumulate heavy metals from the surrounding environment. This study investigates metal concentrations in moss samples collected from five different locations across Serbia, representing diverse environmental settings, from urban and industrial to rural and mountainous areas.

This study presents the results of metal concentration analysis in moss samples collected from five distinct environments in Serbia: 1 (Bor city, industrial area with a copper smelter complex), 2 (recreational complex Ada Ciganlija on the Sava River, near busy roads), 3 (area influenced by the Obrenovac Thermal Power Plant), 4 (urban area near the Šabac city), and 5 (Kopaonik mountain, background site). The collected samples were analyzed using neutron activation analysis at Regata facility of the IBR-2 reactor. The concentrations of 33 elements (Na, Mg, Al, Cl, K, Ca, Sc, Ti, V, Cr, Mn, Fe, Co, Ni, Zn, As, Br, Rb, Sr, Sb, Cs, Ba, La, Ce, Sm, Tb, Yb, Hf, Ta, W, Au, Th, U) were measured in ppm.

The results demonstrate significant variability in metal accumulation depending on the sampling site and local environmental conditions. The highest levels of Al (7580 ppm), Fe (4680 ppm), and Mn (106 ppm) were found in moss from site 2, likely due to combined effects of road traffic and proximity to the Sava River. Site 1, as an industrial zone with a copper smelter, showed elevated concentrations of Cu-related and heavy metals, including As (6.17 ppm) and Ni (3 ppm), reflecting industrial emissions. Site 3, under the influence of the thermal power plant, exhibited increased levels of Cr (56 ppm) and Ni (37.1 ppm), indicating possible combustion related pollution. The urban site (sample 4) had moderate metal levels, with notable Zn (136 ppm) and Br (5.19 ppm), possibly associated with urban activities and traffic. In contrast, the mountainous site of Kopaonik (sample 5) showed the lowest overall metal concentrations, serving as a background reference for atmospheric deposition in Serbia.

These results demonstrate that mosses are effective biomonitors for assessing spatial patterns of atmospheric metal deposition and can distinguish between industrial, urban, traffic-related, and natural background influences. The findings are discussed in the context of biomonitoring potential of mosses for assessing atmospheric metal deposition in Serbia and compared with similar studies in neighboring regions.

List of Authors

Oral Session

Alruqeishi M.	17	Lychagina T.A.	52
Aničić Urošević M.	18	Maksimov P.A.	54
Arslanov T.R.	20	Manukovskaya D.V.	55
Asadov A.G.	21	Martyanov D.E.	58
Azarova L.A.	22	Minaeva A.V.	60
Bakirov A.V.	23	Molchanov V.S.	61
Bakirov B.A.	25	Nashaat M.	62
Balagurov A.M.	15	Nguyen N.T.	63
Balasoiu M.	27	Nikolayev D.I.	64
Belozerova N.M.	29	Pakhnevich A.V.	66
Borshchevskiy V.	31	Petrova M.O.	68
Elmekawy A.H.A.	32	Ryazanov V.V.	69
Grigoriev S.V.	35	Ryzhykau Yu.L.	71
Harutyunyan V.V.	33	Saprykina I.	73
Ivankov O.I.	36	Shvetsova M.	74
Ivashchenko S.D.	38	Sterkhov E.V.	75
Karavaeva I.A.	40	Tilinova O.M.	76
Kichanov S.E.	39	Ushkov A.A.	77
Kolupaev E.D.	42	Vershinina T.N.	79
Kozhevnikov S.V.	44	Vlasov A.V.	81
Kravtsov E.A.	46	Volkov V.V.	83
Kurilkin A.K.	47	Zaky I.	84
Kurkin T.S.	48	Zhaketov V.D.	85
Kwiatkowski A.L.	49	Zhurenko S.V.	86
Lebedev O.V.	50	Zinicovscaia I.	88
Litvinenko E.I.	51		

Poster Session

Abdurakhimov B.A.	91	Kurbonov S.	133
Abiyev A.S.	92	Lebedev D.V.	135
Andjelković Lj.	94	Lis O.N.	136
Aničić Urošević M.	95	Litvinenko E.I.	137
Astaf'eva S.A.	97	Lukin E.V.	138
Avdeev M.M.	99	Makarova M.V.	139
Belozerova N.M.	101	Manko I.D.	141
Berestneva Yu.V.	102	Matyukhov V.V.	142
Bezruchko I.O.	103	Meshkov I.V.	143
Borisov R.D.	104	Nabiyev A.A.	144
Chausova V.A.	105	Nikova E.S.	150
Chen J.	107	Norov D.A.	152
Culicov O.-A.	108	Nurulin R.	153
Cuong T.V.	109	Petrova E.A.	154
Devyaterikov D.I.	110	Ponomarev V.N.	155
Egorov V.V.	111	Popov A.I.	156
Elnikova L.V.	112	Popović M.	158
Fedoseev M.L.	114	Raksha E.V.	159
Gavrilicheva K.A.	116	Rutkauskas A.V.	160
Genov I.G.	118	Sadradze R.N.	161
Gergelezhiu P.A.	119	Savin V.V.	162
Gudkov E.L.	120	Shishkin A.Yu.	164
Harutyunyan V.V.	122	Sikolenko V.V.	166
Ivankina T.I.	124	Sudarev V.V.	167
Kamalieva L.A.	126	Šuljagić M.	168
Khongorzul B.	127	Trung N.T.H	169
Kopitsa G.P.	129	Zel I.Yu.	172
Korshikov Y.S.	131	Zhezlyaev G.E.	170
Kuklin A.I.	132	Zinicovscaia I.	173

Alphabetical Authors List

-A-

Abdurakhimov B.A. 91
Abiyev A.S. 92
Aleksanyan E.M. 33
Aliyev N.Sh. 148
Almásy L. 133
Alruqeishi M. 17
Alsalmi N. 17
Alshumi H. 17
Altangerel B. 64, 172
Andjelković Lj. 94, 168
Aničić Urošević M. 18, 95, 158
Antropov N.O. 156, 157
Arbuzov D.A. 85
Aricu A. 74
Arsenin A.V. 29, 77
Arslanov T.R. 20
Asadov A.G. 21
Astaf'eva S.A. 27, 97
Avdeev M.M. 61, 99
Avdeev M.V. 105, 153
Aydanov G.M. 64
Azarova L.A. 22, 104

-B-

Baitin D.M. 135
Bakhlanova I.V. 135
Bakirov A.V. 23
Bakirov B.A. 25
Balagurov A.M. 15, 79
Balasoiu M. 27, 94, 97
Bannov A.G. 118
Baranchikov A.E. 129
Barinov I.V. 162
Barkalov O.I. 116
Belozerova N.M. 29, 77, 101
Berestneva Yu.V. 102
Bezruchko I.O. 71, 103, 164
Bobreva L.A. 57
Bodnarchuk V.I. 47, 68
Bogdzel A.A. 47, 51, 68, 137
Boguslavsky S.E. 85
BokshytsY. 91
Borisov R.D. 22, 104
Borshchevskiy V. 31, 36
Bukhalovich S.M. 71, 154, 164
Bukhtiyarov A.V. 89
Bulaeva A.S. 79
Burmistrov K.Yu. 155
Butulija S. 159

-C-

Chaligava O. 18, 74, 95, 173
Chausova V.A. 105
Chen J. 107
Chesnokov Yu.M. 49
Chudoba D.M. 119, 159
Chvalun S.N. 23
Ciocarlan A. 74
Ciocarlan N. 74
Culicov O.-A. 108
Cuong T.V. 36, 109, 132
Ćurčić M. 158
Czigány Zs. 133

-D-

Dabylova S. 159
Dang N.T. 39, 63
Dat T.N. 63
Daulbaev O. 64
Daulbayev O. 47
Devyaterikov D.I. 46, 110, 139, 142, 170
Dobrotvorskaya A.N. 114
Dolmatov V.Yu. 48, 50
Dronova E.A. 71, 164, 167
Drozdov V.A. 47
Drozhzhin N.A. 118
Dyubo D.V. 29, 77

-E-

Efimov V.B. 131
Efimov V.V. 166
Egorov V.V. 111
Elmekawy A.H.A. 27, 32, 35, 36, 97, 109, 112, 132, 146, 148
Elnikova L.V. 112
Eresko A.B. 119, 159

-F-

Fedoseev M.L. 114
Frontasyeva M.V. 18

-G-

Galiguzov D.A. 76, 81
Galustov V. 108
Gasymov M.M. 112
Gavrilicheva K.A. 116
Genov I.G. 118
Gerasimov E.G. 35
Gergelezhiu P.A. 119
Gervits N.E. 86
Gippius A.A. 86

Golovin I.S. 79
Golubev E.K. 48, 50
Gorbachev E.A. 107
Gordeliy V.I. 36, 132
Goremychkin E.A. 119, 159
Gorshkova Yu.E. 97, 99, 129
Goryainova Z. 18
Gretskii R.K. 76
Gretskiy R.K. 81
Grigoriev S.V. 22, 35
Grigoryan N.E. 33
Grigoryeva N.A. 35
Grozdov D. 74, 173
Grudinina N.A. 111
Gudkov E.L. 120

-H-

Harutyunyan V.V. 33, 122

-I-

Ilić M. 18
Islamov A.Kh. 32, 35, 36, 99, 109, 132
Istomina T.S. 97
Ivankina T.I. 124
Ivankov O.I. 27, 32, 36, 49, 71, 99, 103, 109, 111, 132, 144, 146, 148, 164
Ivanova E.V. 27, 97
Ivashchenko S.D. 38

-J-

Jargalan N. 127
Jeremić D. 94
Jovanović G. 18

-K-

Kamalieva L.A. 60, 126
Kamashev A.A. 85
Karavaeva I.A. 40
Karpinsky D.V. 166
Kashkarov E.B. 40
Khongorzul B. 127
Kichanov S.E. 21, 27, 39, 63, 64, 75, 91, 97, 101, 118, 136, 138, 160, 172
Kirilov A.S. 64
Kiselev M.A. 105
Klimov S.V. 77
Kolesnikov A.G. 47
Kolesnikov A.O. 47
Kolupaev E.D. 42, 44, 85, 170
Kopitsa G.P. 129
Korshikov Y.S. 131
Kottsov S.Yu. 129
Kovács Z. 133
Kozhevnikov S.V. 44
Kozlenko D.P. 20, 21, 39, 64, 91, 101, 118, 136, 138, 160, 172
Kravtsov E.A. 46, 139, 142, 150, 156, 157, 170
Kriechbaum M. 133
Krmpot A. 158
Krotkevich D.G. 40
Kryzhevskiy G.N. 131
Kučerka N. 36
Kuklin A.I. 32, 35, 36, 49, 58, 61, 71, 76, 81, 99, 103, 109, 112, 132, 146, 148, 164
Kuklina D.D. 71, 164, 167
Kurbonov S. 133
Kurilkin A.K. 47
Kurkin T.S. 48, 50
Kuznetsova O.P. 112
Kwiatkowski A.L. 49, 61

-L-

Lacrămă A.-M. 133
Lanovsky R. 166
Lazović I. 173
Lebedev D.V. 135
Lebedev O.V. 48, 50
Lebedev V.A. 107
Lebedev V.T. 58
Lebedeva E.A. 27, 97
Lezova O.S. 129
Likhacheva A.Yu. 20, 75
Lis O.N. 21, 39, 101, 136, 138, 160
Litvinenko E.I. 51, 68, 137
LukáčM. 133
Lukin E.V. 21, 39, 64, 75, 101, 118, 136, 138, 160, 172
Lung I. 108
Lychagina T.A. 52, 64, 66

-M-

Makarova M.V. 46, 139, 142
Maksimov P.A. 54
Mammadova R.L. 144
Manko I.D. 141
Manukovskaya D.V. 55, 57
Martyanov D.E. 58
Matović B. 159
Matveev V.A. 153
Matyukhov V.V. 46, 139, 142
Meshkov I.V. 143
Mikhailov A.E. 71, 164

Miletić D. 168
Milićević T. 18
Milkov V.M. 47, 51, 64
Minaeva A.V. 60, 126
Mitić B. 18, 95
Molchanov V.S. 49, 61, 99
Mukhametuly B. 153
Murashkevich S.M. 64
Murugova T.N. 36, 103, 111, 132
Mushnikov N.V. 35
Muzafarov A.M. 23

-N-

Nabiyev A.A. 36, 144, 146, 148
Nashaat M. 62
Nazarov K. 99
Nekhoroshkov P. 95, 108
Nguyen N.T. 63, 101
Nikitenko Yu.V. 42
Nikitin S.S. 116
Nikolayev D.I. 52, 64, 66
Nikova E.S. 150
Norov D.A. 44, 85, 152
Novikov S.M. 29, 77
Nuriyev M.A. 148
Nurulin R. 153

-O-

Ogorodnikov I.N. 156, 157
Opriș O. 108
Osipov S.D. 60, 81, 126
Ostrovnaya T. 18
Ozerin A.N. 48, 50

-P-

Pajić T. 158
Pakhnevich A.V. 66
Palatnikov M.N. 55
Pavlov S.S. 18
Pavlović V. 168
Pejić M. 159
Péter L. 133
Petrov S.N. 114
Petrova E.A. 154
Petrova E.D. 167
Petrova M.O. 68
Petukhov M.G. 135
Petukhova T.B. 64
Philippova O.E. 49, 61, 99
Phuong H.S.M. 169
Pisárčik M. 133
Poghosyan E.K. 162
Polonski A.L. 155
Ponomarev A.V. 124
Ponomarev V.N. 143, 155
Popov A.I. 156, 157
Popović A. 18, 158
Popović M. 18, 95, 158
Potashev S.I. 143, 155
Povzner A.A. 141
Pschenichniy K.A. 22

-R-

Rabasović M.D. 158
Raksha E.V. 102, 119, 159
Rashchenko S.V. 20
Ril A.I. 20
Rogachev A.V. 36, 132
Roganović J. 18
Rogovina S.Z. 112
Rutkaukas A.V. 63
Rutkauskas A.V. 20, 101, 116, 138, 160
Ryazanov V.V. 69
Rymski G.S. 160
Ryukhtin V. 133
Ryzhykau Yu.L. 36, 71, 76, 81, 103, 132, 164, 167

-S-

Sabidolda A. 131
Sadilov V.V. 68, 105
Sadradze R.N. 85, 161
Safonov R. 153
Sahakyan A.A. 33
Sakharov A.N. 155
Salamatov Yu.A. 46, 142, 150
Sangaa D. 127
Saprykina I. 73
Sarap N. 173
Savenko B.N. 64, 101
Savin V.V. 162
Savostina L.I. 119
Sazonov A. 166
Semeno M.A. 60, 126
Semenov Yu.S. 71, 164
Semina V.K. 162
Shevchenko V.G. 112
Shishkhanova K.B. 61
Shishkin A.Yu. 71, 164
Shpakova S.A. 118
Shukrinov Yu.M. 62
Shvetsov V.V. 64
Shvetsova M. 74, 108
Sidorov D.V. 38, 71, 164, 167
Sidorov N.V. 55

Sidorov V.A. 20, 75
Sikolenko V.V. 166
Sknepnek A. 94
Skoi V.V. 36, 58, 112, 132
Škundrić T. 159
Smirnov A.A. 156, 157
Solovjev A.G. 36, 132
Son L.V.T. 63
Soran M.-L. 108
Stegarescu A. 108
Sterkhov E.V. 75
Stojanović D. 95
Stoler D.A. 141
Strelkova L.P. 18
Sudarev V.V. 154, 167
Suharev A.A. 47
Šuljagić M. 94, 168
Sumnikov S.V. 51, 79
Syuy A.V. 29, 77

-T-

Tadić M. 168
Taran G.S. 129
Tatarsky D.A. 85
Tekić J. 62
Tereshko N. 166
Thinh P.D. 63
Tien D.P.T. 63
Tilinova O.M. 76, 81
Titov R.A. 55
Titova S.G. 75
Tolmacheva E.A. 142
Tomašević M. 18
Trukhinov D.K. 27, 97
Trung N.T.H. 169
Truong-Tho N. 63
Trusov L.A. 107
Tselikov G.I. 29, 77
Tsogbadrakh N. 127
Turchenko V.A. 92, 107
Turovskij N.A. 102

-U-

Ushkov A.A. 29, 77
Utesov O.I. 22
Uzhinskiy A. 18

-V-

Vergel K. 18
Vershinina T.N. 79
Vinogradov I.I. 118
Vlasov A.V. 36, 38, 60, 76, 81, 126, 132
Volkov V. 83
Vul A.Ya. 58

-Y-

Yerdauletov M. 99
Yerezhep D.E. 131
Yerzhanov B. 79
Yushin N. 18
Yusova A.I. 76, 81

-Z-

Zabanov Zh.G. 40
Zagorac D. 159
Zagorac J. 159
Zaky A. 85
Zaky I. 84
Zavyalov A.P. 20
Zel I.Yu. 64, 124, 136, 172
Zhaketov V.D. 42, 44, 84, 85, 152, 161, 170
Zhaludkevich A.L. 160
Zhezlyaev G.E. 46, 110, 142, 170
Zhurenko S.V. 86
Zinicovscaia I. 18, 74, 88, 95, 173
Živković M. 173
Zubavichus Y.V. 89